Cloning and expression of virus-like particles (VLPs) in microalgal expression systems

Fuyao Li

A thesis submitted for the degree of
Doctor of Philosophy
to
University College London

The Advanced Centre for Biochemical Engineering
Department of Biochemical Engineering
University College London

2018

Declaration

I, Fuyao Li, confirm that the work presented in this thesis is my own. Where information has been derived from other sources, I confirm that this has been indicated in the thesis.

Signature: _____ Date: _____

I dedicate this PhD thesis to
my mum and dad

Abstract

Virus-like particles (VLPs) can be constructed from self-assembled viral capsid proteins. While preserving structural and antigenic similarities to the authentic native viruses, they are non-infectious and non-replicating molecules due to the lack of genetic material. Additionally, the highly repetitive and organised display of epitopes on the VLP surface promotes strong immunogenic responses. Some VLPs can also serve as particulate carriers with linked heterologous epitopes, forming so-called chimeric VLPs.

Hepatitis B core antigen (HBcAg) VLPs are one of the most promising and well-documented particulate carriers for heterologous epitope presentation. The formation of HBcAg VLPs has previously been demonstrated in various prokaryotic and eukaryotic hosts. However, the development of chimeric HBcAg VLP-based vaccine candidates will require an inexpensive, safe and robust production platform. The transgenic green alga *Chlamydomonas reinhardtii* is examined here as an alternative expression system due to its ability to fold complex protein structures, relatively low production costs and the absence of viral toxins or human pathogens giving it GRAS (Generally Recognised as Safe) status.

In this work, the codon-optimised nucleotide sequence of the truncated HBcAg monomer (HBc150_HA) was inserted into the *C. reinhardtii* chloroplast genome and HBc150_HA expression was confirmed by western blot analysis. Subsequently, both bioprocess and genetic engineering strategies were assessed to boost HBc150_HA production. These resulted in a 26-fold increase in HBc150_HA production which accumulated up to 2.34% (w/w) of total soluble protein (TSP) mainly as consequence of using a stronger 16S ribosomal RNA (rRNA) promoter. Based on the densitometric analysis, the yield of HBc150_HA (4.9 mg per g $_{\text{dry cell weight (DCW)}}$) was almost four-fold higher than the yeast-derived tandem-core HBcAg (1.3 mg per g $_{\text{DCW}}$) in which two monomers were genetically fused. Despite low abundancy, isometric particles of 25-30 nm in diameter and with a morphology typical of HBcAg VLPs were observed in transmission electron microscopy (TEM) after partial purification by either sucrose gradient ultracentrifugation or size exclusion chromatography (SEC). The results of

immunogold labelling further confirmed the presence of capsid assembly in the HBc150_HA-expressing microalgal samples.

This is the first study to show that HBcAg VLPs can be synthesized and correctly assembled in microalgal chloroplasts. It therefore enables further exploration of the potential of *C. reinhardtii* as a versatile platform for low-cost production of recombinant therapeutic proteins.

Impact statement

This research has demonstrated the capability of microalgal chloroplast to synthesize and assemble complex protein structures such as HBcAg VLPs. It serves as a solid foundation of using *C. reinhardtii* as a potential platform for low-cost production of recombinant therapeutic proteins. There are various benefits arising from this work that can potentially impact both inside and outside academia.

Within academia, this is the first study to demonstrate the feasibility of VLP formation in microalgal chloroplasts to date. These findings can be published for wider knowledge dissemination and may be included in taught material related to algal research. In addition, the concept of a bio-encapsulated oral vaccine derived from the dried algal biomass has attracted much attention in recent years. Therefore, future research projects can be designed and carried out for the continued exploration of algal-derived VLP-based vaccine candidates suitable for oral delivery.

Moreover, this research could have potential benefits to the biopharmaceutical industry. Transgenic microalgae have considerable potential as an alternative to conventional protein expression platforms. This is mainly due to the absence of viral toxins or human pathogens, the cost-effectiveness of protein production and the rapid scalability of production processes. Therefore, with successful production of VLPs in this work, the microalgal chloroplast has potential to become a prime VLP-based vaccine expression platform for the cost-effective manufacturing of oral vaccines in the future. This will greatly reduce costs and complexity associated with downstream processing purification steps and may also facilitate the regulatory approval for biopharmaceuticals.

Furthermore, there is currently an urgent need to produce cost-effective vaccines in a form suitable for storage and delivery in developing countries. Algal-based oral vaccines provide a promising route forward due to improved shelf life at elevated temperatures and needle-free delivery to patients. From a broader perspective, this technology will enable wider patient coverage for certain vaccine uses. It will not only

reduce the financial burden of local governments but also improve the quality of life of patients in the long run.

Overall, the results generated in this work have a variety of impacts on academia, the biopharmaceutical industry and society over varying timescales. In order to realize the benefits of this research, it is essential to disseminate these research findings in publications, conferences and in taught programme material.

Acknowledgement

First and foremost, I would like to express my sincerest gratitude to my parents for their endless love, genuine encouragement and never-ending patience. I am very grateful for the important values they have passed down to me-particularly perseverance and honesty.

My sincere gratitude also goes to my supervisors, Prof. Gary Lye, Dr. Tarit Mukhopadhyay and Prof. Saul Purton, who have supported and guided me with great patience and immense knowledge throughout my doctoral journey. With Gary's trust and support, I was able to get the scholarships to start my PhD in the first place. Thanks for all the time, efforts and in-depth expertise he put in every meeting, thesis structuring, thesis correction and manuscript preparation. In addition, I have learnt so much form Tarit about the techniques and knowledge in the vaccine field. I am also very grateful for him to introduce me to Ben and Steve who shared so much valuable knowledge in the VLP field. My sincere thanks also go to Saul for letting me use the lab and office space. I am truly amazed by the deep expertise he has in the microalgal biotechnology field and have learnt so much from him. I am also very grateful for his great efforts in thesis correction and manuscript preparation.

I am truly indebted to Dr. Steve Morris who shared so much useful knowledge and experiences in the VLP field. I am also very grateful to his tremendous help in sucrose gradient preparation, gel filtration as well as TEM and his genuine advice in Chapter 5 and manuscript. I would also like to thank Dr. Mark Turmaine for his great support in TEM analysis and immunogold labelling. Without his timely arrangement in TEM booking, I would not be able to finish the work in time. I am grateful to Dr. Vernon Skinner, who helped me with the use of ultracentrifuge and sonicator. I would also like to extend my appreciation to Elaine Briggs who helped me for numerous consumables ordering. Great thanks also go to Dr. Brian O'Sullivan, Dr. Gareth Mannall and Dr. Mike Sulu for their generous help, advice and technical support in ACBE. Also, special thanks to Jana, Paula, Kate and others in the departmental office who helped me with numerous administrative matters.

I thank all the members in Purton lab, who not only helped me in research but also shared so much fun together. Thanks for all the celebration lunch/dinner, afternoon tea breaks and boat trip that made my time during study so much more enjoyable and memorable. I am also grateful to Thushi Sivagnanam for her great effort in managing the lab to ensure there is a safe and nice environment for everyone to work in. I want to thank Dr. Priscilla Rajakumar, for being my first teacher in microalgal research. I really appreciate her patience and kindness. I also want to thank Dr. Laura Stoffels for her tremendous support and countless experience-sharing sessions in the lab. My gratitude also goes to Dr. Rosie Young for being a great molecular biology teacher and helping me to get Gibson assembly worked in the first try. I thank Dr. Janet Waterhouse for giving me useful suggestions in thesis writing and sharing interesting stories. I would also like to thank Dr. Max Blanshard for sharing experiences not only in research but also in job hunting. My sincere thanks also go to Dr. Alice Lui, Dr. Henry Taunt, Dr. Marco Alvarez, Juliana Ramos, Saowalak Changko, Dr. Steffi Braun Galleani, Dr. Umaima Hoqani, and Xenia Spencer for being very helpful and kind to me and giving me useful advice in experiments and thesis writing.

I am also very grateful to Baolong Wang, Chris Wayne, Haoran Yu and Yang Lu for being such good friends to me and sharing so much valuable knowledge in the molecular biology and bioprocessing fields. I really appreciate their patience and kindness. I also want to thank Zhongdi Song for sharing useful knowledge in algal research. My sincere gratitude also goes to Dr. Hadiza Auta, Dr. Nurashikin Binti Suhaili, Dr. Ebenezer Ojo and Dr. Kane Miller who have taught me useful laboratory techniques and shared valuable experiences in research and writing. I would also like to thank Dr. Brenda Parker for her great support in algae research in the department.

Table of contents

List of figures

List of tables

Nomenclature

Symbol		Unit
μ	Specific growth rate	h^{-1}
R^2	Coefficient of determination	-
T	Temperature	°C
t	Time	s
w/v	Weight by volume	-
v/v	Volume by volume	-

Abbreviations

Amp^R	ampicillin resistant
AP	Antarctic phosphatase
APC	antigen-presenting cell
B/IC	Baculovirus/insect cell
bp	base pair
BSA	bovine serum albumin
CCM	carbon concentration mechanism
CDS	chromatography data system
cGMP	current Good Manufacturing Practice
CHO	Chinese hamster ovary
CRE	*cis*-RNA element
CSP	circumsporozoite protein
CTB	cholera toxin B subunit
CTL	cytotoxic T lymphocyte
CUO	codon usage optimiser
DCW	dry cell weight
DHA	docosahexaenoic acid
DNA	deoxyribonucleic acid
DTT	dithiothreitol
ECL	electrochemiluminescence
EDIII	third domain of the envelope protein of Dengue virus
EDTA	ethylenediaminetetraacetic acid
ELISA	enzyme-linked immunosorbent assay
FDA	Food and Drug Administration
FMDV	foot-and-mouth disease
Gag	group-specific protein
GFP	green fluorescent protein
GOI	gene of interest
GRAS	Generally Recognised as Safe
HA	hemagglutinin
HBcAg	hepatitis B core antigen
HBV	hepatitis B virus
HEPES	4-(2-hydroxyethyl)-1-piperazineethanesulfonic acid
HPLC	high performance liquid chromatography
HPV	human papillomavirus
HRP	horseradish peroxidase
HSM	high salt minimal
IAV	influenza A virus
IPTG	isopropyl β-D-1-thiogalactopyranoside
kb	kilobase
kDa	kilodalton
LB	Lysogeny broth
M	molar
M2e	ectodomain of the M2 protein

Min	minute
MIR	major immunodominant region
M-SAA	mammary-associated serum amyloid
NCBI	National Centre for Biotechnology Information
NIR	near-infrared
OD	optical density
PBS	phosphate buffered saline
PCR	polymerase chain reaction
PEG	polyethylene glycol
PSII	photosystem II
PTMs	post-translational modifications
RBS	ribosome binding site
rRNA	ribosomal RNA
RLP	rotavirus-like particle
SDS	sodium dodecyl sulphate
SDS-PAGE	sodium dodecyl sulphate-polyacrylamide gel electrophoresis
SEC	size exclusion chromatography
TAP	tris acetate phosphate
TB	terrific broth
TBE	tris-borate-EDTA
TBS	tris buffered saline
TBS-T	tris buffered saline-Tween^{TM} 20
TEM	transmission electron microscopy
TFA	trifluoroacetic acid
TFF	cross-flow filtration
TSP	total soluble protein
UTR	untranslated region
UV	ultraviolet
VEGF	vascular endothelial growth factor
VLP	virus-like particles
WHO	World Health Organisation

1 Introduction

1.1 Background to virus-like particles (VLPs)

1.1.1 VLP-based technology in the vaccine industry

Following the first demonstration of vaccination by Edward Jenner in the late 18th century, vaccine development has revolutionised modern medical history. Originally, inactivated or live-attenuated viruses were administered but this led to the fear of real virus outbreaks. In the late 19th century, scientists discovered that the use of protein subunits, which were part of the microorganisms that were used to provoke an immune response, could provide effective protection. With the advancement of recombinant DNA technology, the world's first genetically modified subunit vaccine for the prevention of foot-and-mouth disease (FMDV) was produced in 1981 (Kleid *et al.*, 1981). Five years later, the first recombinant VLP-based hepatitis B virus (HBV) vaccine, Recombivax HB®, containing the surface protein HBsAg was approved (Michel and Tiollais, 2010).

VLPs are constructed from the self-assembled viral envelope and/or capsid proteins (Tagliamonte *et al.*, 2017). While preserving structural and antigenic similarities to the authentic native viruses, they are non-infectious and non-replicating molecules due to the lack of genetic materials (Tagliamonte *et al.*, 2017). They are highly immunogenic due to the repetitive and organised display of epitopes on the surface. Moreover, with a size around 40-50 nm they are preferentially recognised by the dendritic cells of the immune system (Fifis *et al.*, 2004). As a result, a number of VLP-based vaccines are already commercialised with great success. In addition to the HBV vaccines, the human papillomavirus (HPV) vaccine Gardasil® was also licensed in 2006. The details of some commercial VLP-based vaccines are described in Table 1.1.

Table 1.1: Details of the commercial VLP-based vaccines in the market (non-exhaustive list). Table modified from Lua *et al.*, (2014).

	Compositions per dose		
Vaccine	**Protein**	**Adjuvant**	**Others**
Gardasil® human papillomavirus vaccine (0.5 mL/dose)	HPV 6 L1 (20 μg) HPV 11 L1 (40 μg) HPV 16 L1 (40 μg) HPV 18 L1 (20 μg)	Aluminum hydroxyphosphate sulphate (225 μg)	Sodium chloride (9.56 mg) L-histidine (0.78 mg) Polysorbate 80 (50 μg) Sodium borate (35 μg)
Cervarix® human papillomavirus vaccine (0.5 mL/dose)	HPV 16 L1 (20 μg) HPV 18 L1 (20 μg)	AS04 adjuvant system	Sodium chloride (4.4 mg) Sodium dihydrogen phosphate dehydrate (0.624 mg)
Hecolin® hepatitis E vaccine (0.5 mL/dose)	HE antigen (30 μg)	Aluminum hydroxide (800 μg)	Buffered saline

Another important and promising application of VLPs is the incorporation of heterologous antigen epitopes by either genetic manipulation or chemical conjugation, forming so-called chimeric VLPs (Chackerian, 2007; Roldão *et al.*, 2011). Such vaccine candidates overcome the problems that the heterologous epitopes do not possess optimal immunogenicity or cannot self-assemble into particulate forms to elicit strong immune responses (Grgacic and Anderson, 2006). Notably, several chimeric VLP-based vaccines are already at the clinical trials stage, including the anti-influenza A M2-HBcAg VLP vaccine and two anti-malaria vaccines (Roldão *et al.*, 2010). Among various particulate carriers, hepatitis B virus core antigen (HBcAg) is believed to be one of the most promising and well-documented carriers for the presentation of foreign antigens (Arora *et al.*, 2012; Roose *et al.*, 2013).

1.1.2 Characteristics of HBcAg VLPs

Hepatitis B virus can cause both acute and chronic liver infection that is a truly global disease burden. According to a World Health Organisation (WHO) census in 2017, around 257 million people are living with HBV infection (World Health Organization, 2017). In 2015 alone, the disease led to 887,000 deaths, mainly due to complications such as cirrhosis and hepatocellular carcinoma (World Health Organization, 2017). The HBV virion produced by infected hepatocytes is a double-shelled spherical virus with

a diameter of 42-47 nm (Shepard *et al.*, 2006). The virally encoded polymerase and the partially double-stranded viral genome are protected by an inner nucleocapsid and an outer lipid envelope, which are composed of core proteins (HBcAg) and surface proteins (HBsAg), respectively (Liang, 2009). As a result, the initial use of HBcAg is as a serological marker for HBV infection (Shepard *et al.*, 2006).

The full-length HBcAg monomer is composed of two domains, the N-terminal assembly domain (1-140 a.a.) and the C-terminal protamine domain (150-183 a.a.) that are connected by the nanopeptide STLPETTVV (Roose *et al.*, 2013). Previous studies have proved that the N-terminal assembly domain is necessary but also sufficient for monomer dimerization and subsequent capsid formation (Böttcher *et al.*, 1997; Wynne *et al.*, 1999). However, it is suspected that HBcAg stability, as evidenced by the thermal stability and capsid assembly integrity, is reduced in the absence of the C-terminal protamine domain (Vogel *et al.*, 2005; Sominskaya *et al.*, 2013). The stability is mainly attributed to intermolecular disulphide bond formation between C-terminal Cysteine residues (Vogel *et al.*, 2005) and the encapsulation of nucleic acids by the C-terminal arginine blocks (Sominskaya *et al.*, 2013).

The structure of HBcAg was confirmed by high resolution cryo-electron microscopy (cryo-EM) with each HBcAg monomer containing five α-helices that are connected by loops (Böttcher *et al.*, 1997). However, this structure is unusual for the icosahedral capsid proteins/viral particles that are mostly composed of β-sheets (Böttcher *et al.*, 1997). Two amphiphilic α-helical hairpins from two monomers associate to form the four-helix bundle as the major central feature containing the major immunodominant region (MIR) (76-82 a.a.) (Wynne *et al.*, 1999) (Figure 1.1). Although the dimer is stabilized by the disulphide bond at Cysteine-61, the mutation of Cysteine into Serine or Alanine does not impede particle formation. Instead, residues Arginine-127, Proline-129, Tyrosine-132 and Isoleucine-139 were discovered to be critical in dimer formation and thus VLP self-assembly (Wynne *et al.*, 1999; Pumpens and Grens, 2001).

Figure 1.1: Folding of the truncated HBcAg monomer (a) and the formation of dimer (b). Figure reproduced from Pumpens and Grens, (2001).

As shown in Figure 1.2, the HBcAg VLPs consisting of either 180 or 240 HBcAg polypeptide subunits with triangulation number T=3 or T=4 icosahedral symmetry (Prasad and Schimid, 2012) have sizes of 27 nm or 33 nm, respectively (Wynne *et al.*, 1999). Both forms are detectable in the liver of HBV-infected patients (Dryden *et al.*, 2006). Not surprisingly, HBcAg VLPs can also be produced and correctly assembled in heterologous expression systems outside of the natural context, including most prokaryotic and eukaryotic platforms (Lanford and Notvall, 1990; Tey *et al.*, 2006; Freivalds *et al.*, 2011).

Figure 1.2: HBcAg VLP assembly with T=3 or T=4 symmetry. Figure reproduced from Belnap *et al.*, (2003).

1.1.3 HBcAg VLPs as antigen-presenting platforms

According to clinical results, HBcAg induces the strongest B-cell, T-cell and cytotoxic T lymphocyte (CTL) responses among different HBV polypeptides (Pumpens and Grens, 2001). Importantly, this antigen acts both in a T-cell dependent and a T-cell independent manner due to its organised and repetitive icosahedral structure (Pumpens and Grens, 2001). This feature can be transferred to covalently-linked heterologous antigen epitopes as long as the HBc VLP structure remains undisturbed.

Due to the diversity of the primary structure of HBcAg, the protein sequence can be easily manipulated without damaging its ability to self-assemble into VLPs. Various research results have demonstrated its great flexibility for incorporating foreign epitopes at the N-terminus, C-terminus or the MIR. Schodel et al. (1992) have compared three positions of the heterologous epitopes inserted into HBcAg and concluded that the MIR is the preferred insertion site in terms of antigen-specific antibody induction.

Following the first chimeric HBcAg VLP-based FMDV vaccine (Clarke *et al.*, 1987), many antigens and epitopes have been fused to this particulate carrier and used in vaccination studies. Table 1.2 shows some examples of HBcAg fusion vaccine candidates that have subsequently been investigated. It should be highlighted that the HBcAg VLP-based universal influenza A vaccine developed by Sanofi-Pasteur has passed Phase I clinical trials, demonstrating promising results in term of safety and immunogenicity (Fiers *et al.*, 2009).

Table 1.2: Summary of the chimeric HBcAg VLP-based vaccine candidates (non-exhaustive list). Table modified from Roose *et al.*, (2013).

Pathogen	Antigen/epitopes	HBcAg fusion position
FMDV	Capsid protein VP1	N-terminal
	Capsid proteins VP1 and VP4	MIR
HIV	Gag	N-terminal
	Envelope protein V3 region	MIR
Dengue virus	EDIII	MIR
Hantavirus	Nucleocapsid protein	MIR
HPV	E7 oncoprotein	C-terminal
Plasmodium falciparum	CSP B-cell epitope, T-cell epitopes	N-terminal
IAV	M2e	N-terminal
HBV	Pre-S1	C-terminal MIR

Notes: CSP: circumsporozoite protein; EDIII: third domain of the envelope protein of Dengue virus; Gag: group-specific protein; HIV: human immunodeficiency virus; IAV: influenza A virus; M2e: ectodomain of the M2 protein.

However, if the size of the insertion is too large, then the dimerized polypeptide will fall apart. As a result, a genetically engineered artificial linker was created between two monomers to reinforce the VLP structure (Holmes *et al.*, 2015). This so-called 'tandem core' technology not only stabilises the particle formation with larger insertions but also ensures the original immunogenicity of VLPs. This modified VLP has been successfully expressed in both bacterial and plant systems (Peyret *et al.*, 2015).

1.1.4 Expression systems for HBcAg production and their features and drawbacks

The ability to clone a foreign gene and thus to express a recombinant protein in a heterologous host has made possible the production of almost any protein required for industrial, therapeutic or diagnostic applications. With years of exploration in the genetic engineering field, there are a variety of expression systems available to produce VLPs. Based on 174 VLP constructs, the majority are produced in bacterial (28%) and Baculoviruses and insect cells (B/IC) (28%) systems, followed by yeast (20%). The remainder are produced either in mammalian hosts (15%) or transgenic plants (9%) (Zeltins, 2013). Examples of HBcAg and HBsAg production in various expression systems with estimated yields are summarised in Table 1.3.

Table 1.3: Production of VLP-based vaccine candidates for the Hepatitis B virus. Table modified from Roldão *et al.*, (2010).

Expression system	Cells	Recombinant proteins	Yields
Bacteria	*Escherichia coli*	HBcAg	372 μg mL^{-1}
	E. coli	HBcAg	200 μg mL^{-1}
Yeast	*Pichia pastoris*	HBsAg	400 μg mL^{-1}
	Saccharomyces cerevisiae	HBsAg	100 μg mL^{-1}
B/IC	*Spodoptera frugiperda*	HBcAg and HBsAg	0.425 μg mL^{-1}
Mammalian cells	Chinese hamster ovary (CHO)	HBsAg	3.4 μg mL^{-1}
Transgenic plants	Tobacco	HBcAg	800 ng mg^{-1} fresh weight leaf
	Potato	HBsAg	15 ng mg^{-1} TSP of tuber

One of the most widely employed bacterial expression systems is *E. coli* due to the thorough understanding of its genetics, physiology and the availability of the complete genomic sequence (Rai and Padh, 2001). Not only can *E. coli* grow rapidly to high densities in inexpensive and defined media, it can also express heterologous proteins to levels as high as 50% (w/w) of TSP (Sivashanmugam *et al.*, 2009; Francis and Page, 2010). As a result, several *E. coli*-derived VLP-based vaccine candidates are undergoing pre-clinical or clinical development (Roldão *et al.*, 2010). However, as a prokaryotic host, lacking post-translational modifications (PTMs) such as glycosylation, and disulphide-bond formation, *E. coli* is not ideal for the production of complex and functional VLPs (Walker *et al.*, 2005; Roldão *et al.*, 2010). This is the reason that only structurally simple VLPs involving less than two coat proteins are typically expressed in *E. coli* and none of the *E. coli*-derived VLP-based vaccine candidates has entered the market to-date (Zeltins, 2013).

In contrast, yeast is widely acceptable for the production of recombinant proteins since it is a food-grade organism (Hitzeman *et al.*, 1981). Compared to mammalian cells, this lower eukaryotic system grows faster with a higher cell density on simpler media. In addition, heterologous proteins expressed in yeast can be post-translationally modified. However, the N-linked glycosylation is restricted to a high mannose pattern which is

largely different from the mammalian counterpart (Schillberg *et al.*, 1999; Potvin and Zhang, 2010). It should be noted that one of the most commonly used yeast strains is the methylotrophic *P. pastoris*. However, the use of methanol for protein induction may cause potential safety concerns and a fire hazard at industrial scale (Várnai *et al.*, 2014).

In recent years, a two-stage process involving Baculoviruses and insect cells has been intensively studied. The first step is to grow the insect cells to a desired concentration, followed by infection with recombinant Baculoviruses carrying the VLP gene of interest. The complexity of the proteins being produced by the B/IC system is comparable to those produced by mammalian cell lines (Roldão *et al.*, 2010; Zeltins, 2013) However, one of the critical drawbacks of this system is the co-production of recombinant Baculoviruses, which are enveloped viruses, during the infection process (Vicente *et al.*, 2011). This requires either an additional chemical inactivation step or multiple purification steps to remove the Baculoviruses, which complicate the downstream processing. One (GSK, Cervarix® HPV VLP vaccine) out of 151 licensed protein-based biopharmaceuticals is produced from the B/IV system (Ferrer-Miralles *et al.*, 2009).

Recombinant proteins requiring mammalian PTMs are preferably expressed in mammalian cells due to the greatest degree of product fidelity. This is demonstrated by the fact that 59 out of 151 licenced biotechnology products are manufactured using mammalian cell systems (Ferrer-Miralles *et al.*, 2009). In addition, half of the top ten selling protein-based biopharmaceuticals in 2014 were produced in mammalian cells with a total sales of more than $43 billion (Sanchez-Garcia *et al.*, 2016). However, the mammalian cell lines are expensive and comparably difficult to culture (Chu and Robinson, 2001). Furthermore, they grow slower compared to *E. coli* and yeast cultures and require more expensive media, which significantly impacts the cost-effectiveness of the production procedure. It is worth noting that N-linked glycosylation is species- and cell type-dependent among mammalian cells and should be taken into consideration when expressing different types of VLPs (Rai and Padh, 2001).

Transgenic plants offer several advantages over the expression systems mentioned above. It is cheaper to produce safe and functional recombinant proteins in crop plants on an agricultural scale, and production can be scaled easily and quickly, especially when compared to mammalian cell lines (Walker *et al.*, 2005). In addition, protein products are free from toxins and viral agents that may be present in preparations from microbial- or animal-based expression systems (Rasala *et al.*, 2010). Plant cells also have similar cellular pathways of protein synthesis, folding and PTMs to animal cells, although differences in protein processing, especially glycosylation, are observed (Walker *et al.*, 2005). However, there are several shortcomings associated with transgenic plants (Mayfield and Franklin, 2005; Manuell *et al.*, 2007; Specht *et al.*, 2010): (i) potential transgene flow (via pollen) to the surrounding ecosystem that may contaminate food crops; (ii) the need for large areas of arable land; (iii) the long growth time (2-3 years) of higher plants such as tomatoes or tobacco.

Overall, the various VLP expression systems have distinct features and drawbacks. There is thus an opportunity to find a new expression system that not only possesses the advantages of existing platforms but also overcomes the drawbacks they may have. As a result, transgenic microalgae have been investigated as an alternative expression system to produce recombinant proteins (Yan *et al.*, 2016; Dyo and Purton, 2018).

1.2 Genetic engineering of microalgae to express heterologous proteins

1.2.1 Background of microalgae

Microalgae are eukaryotic photosynthetic microorganisms, with many species being small, single cells containing one or a few chloroplasts. They are typically aquatic organisms, and their ability to convert solar energy into chemical energy by photosynthesis (and subsequently into algal biomass) is relatively efficient compared to land plants owing to their simple structures (Harun *et al.*, 2010). Microalgal biotechnology has been established for several commercial applications, and continued to be explored for new applications (Rosenberg *et al.*, 2008; Leu and Boussiba, 2014).

The existing successful applications involve the production of low-volume, high-value products such as human nutritional supplements, cosmetics and antioxidants. Table 1.4 demonstrates the present stage of commercial products derived from microalgae.

Table 1.4: Details of the commercial products from microalgae. Table modified from Brennan and Owende, (2010).

Microalgae	Annual production	Producer country	Application and product	Price (€)
Chlorella	2000 tonnes dry weight	Taiwan, Germany, Japan	Human nutrition	36 kg^{-1}
Dunaliella salina	1200 tonnes dry weight	Australia, Israel, USA, Japan	β-carotene	215-2150 kg^{-1}
Haematococcus pluvialis	300 tonnes dry weight	USA, India, Israel	Astaxanthin	7150 kg^{-1}
Crypthecodinium cohnii	240 tonnes DHA oil	USA	DHA oil	42 g^{-1}

Apart from the commercialised products, the investigation of biofuels produced from microalgae has grown and become a priority of the algal industry in recent years. Biodiesel and bioethanol are two common types of biofuels that can replace diesel and gasoline, respectively, and require little or no modifications of vehicle engines (Mata *et al.*, 2010). Microalgae are now a promising host for the generation of biodiesel due to their relatively fast growth rate, high lipid productivity and less arable land needed for growth (Mata *et al.*, 2010). For instance, the heterotrophic cultivation of *Chlorella protothecoides* has resulted in the accumulation of lipid content as high as 55% (w/w) and subsequently a great amount of microalgal oil was efficiently extracted using *n*-hexane (Miao and Wu, 2006). Meanwhile, bioethanol is produced either by fermentation (biochemical process) or gasification (chemical process) of algal biomass. Algal species generally contain large amounts of carbohydrates and proteins that can be used as a carbon source during fermentation. As a result, research work has focused on the production of bioethanol from microalgae. For example, different hydrolysis strategies and fermentation processes of bioethanol production were investigated by Ho et al. (2013) who showed that the enzymatic hydrolysis of the green alga *Chlorella vulgaris* gave a glucose yield of as high as 90.4% (w/w).

Microalgae also have environmental applications, mainly for flue gas CO_2 mitigation and wastewater treatment. Since conventional chemical-based CO_2 mitigation is energy-intensive and expensive, the biological method has attracted much attention in recent years. Using industrial flue gas (e.g. from power stations) as a carbon source for microalgal growth not only achieves CO_2 bio-fixation but also facilitates algal biomass accumulation. Wang et al. (2008) have shown that the green alga *Chlorophyta* is able to fix CO_2 10-50 times more efficiently than terrestrial plants. Moreover, microalgae are a promising system for wastewater treatment. Sewage effluent usually contains organic compounds such as nitrogen (N) and phosphorus (P) that are essential for microalgal growth. Experimental results have demonstrated that *Chlorella vulgaris* was able to remove up to 21.1 mgL^{-1} ammonia-nitrogen concentration with 100% efficiency (Aslan and Kapdan, 2006). Figure 1.3 illustrates a conceptual microalgae biomass refinery which combines the environmental applications with biofuel production.

Figure 1.3: A conceptual microalgal system for combined biofuels production, CO_2 bio-mitigation and N/P removal from wastewater and effluent. Figure reproduced from Wang *et al.*, (2008).

Furthermore, transgenic microalgae have been investigated as an alternative expression system to bacterial, yeast or mammalian hosts for the production of recombinant proteins. They have many of the advantages that transgenic plants possess as described in Section 1.1.4. However, they can be grown in an enclosed bioreactor, thus reducing

the possibility of gene flow and eliminating the need for large quantities of fertile land. Moreover, they have much faster growth rate and higher productivity compared to traditional agricultural crops, and usually take around 24 h to double their biomass (Chisti, 2007).

Due to these advantages, a transformed microalgal line can be generated and scaled to production within a short time frame. Heterologous protein production can be elevated to multi-litre volumes in as little as six weeks, with the potential to scale up to 64,000 L in another eight weeks as described in Figure 1.4 (Mayfield and Franklin, 2005). In addition, rapid advances in the development of genetic tools for genome engineering is facilitating recombinant protein technology in microalgae. Importantly, it has been reported that the green alga *C. reinhardtii* possesses the endogenous sialylated N-glycans, meaning that their glycosylation pattern is similar to their mammalian counterparts (Mamedov and Yusibov, 2011).

Figure 1.4: Large-scale production process of recombinant proteins in *C. reinhardtii*. Figure reproduced from Mayfield and Franklin, (2005).

Figure 1.5 demonstrates the simplified cellular pathways that are crucial for the generation of various algal products (Rosenberg *et al.*, 2008). Although the nucleus is key to metabolic control (dotted red line), the chloroplast is another important organelle, especially for the production of hydrogen and recombinant proteins (solid blue line). This is due to the fact that both organelles contain individual genomes, making independent transgene incorporation possible (dashed blue and red lines) (Rosenberg *et al.*, 2008).

Figure 1.5: Simplified diagram demonstrating the commercially important metabolic pathways in microalgae. Figure reproduced from Rosenberg *et al.*, (2008).

1.2.2 Genetic transformation of *C. reinhardtii*

A key requirement in the exploitation of microalgae as light-driven cell platforms is well-established transformation methodologies for both the nuclear and chloroplast genomes (Boynton *et al.*, 1988; Kindle, 1990). Due to the wide range of molecular genetic tools available for *C. reinhardtii,* this green alga is the best characterized candidate for protein production among the microalgal species to date (Walker *et al.*, 2005; Specht *et al.*, 2010). The schematic diagram of a *C. reinhardtii* cell is illustrated in Figure 1.6. Many eukaryotic microalgae are small cells with a thick cell wall which prevents DNA uptake during transformation experiments. *C. reinhardtii* has a relatively

thin proteinaceous cell wall and is larger in size than most other strains, as such the penetration of the cell wall and transfer of foreign DNA are easier. Furthermore, in order to improve the transformation efficiency, it is possible to exploit existing cell wall-deficient *C. reinhardtii* mutants, among which *cw15* is the most popular strain (Wannathong *et al.*, 2016).

Figure 1.6: Schematic diagram of a *C. reinhardtii* cell with the annotated internal structures. Figure reproduced from Cronodon, (n.d.).

Among the various methods of introduction foreign DNA into microalgae, agitation with glass beads, microparticle bombardment and electroporation are commonly performed for nuclear transformation (Mussgnug, 2015). One of the first methods used to transform the *C. reinhardtii* nucleus was agitation with glass beads and has been employed widely since then due to its simplicity and reproducibility (Kindle, 1990). Transient permeabilization can be achieved by vortexing which facilitates the entry of exogenous DNA while maintaining cell viability. However, this method is only efficient when using the cell wall-deficient mutants or with cells previously treated with autolysin to disrupt the cell walls (Kindle, 1990; Economou *et al.*, 2014). Electroporation is another method for nuclear transformation of *C. reinhardtii* in which parameters such as the intensity, duration and number of electric pulses are manipulated

to control the transformation efficiency (Coll, 2006). According to Brown et al. (1991), 10-50% of a cell wall-deficient mutant and 15-40% of a wild type strain were viable after transfection by electroporation.

The earliest chloroplast transformation was carried out with *C. reinhardtii* in 1988 using microparticle bombardment (Boynton *et al.*, 1988). This method usually involves the use of high helium pressure to introduce DNA-coated gold or tungsten microparticles into algal chloroplasts. This is effective for transforming *C. reinhardtii* with intact cell walls as little or no pre- or post-bombardment treatment is required. Recently, there is a considerably simpler and more cost-effective way to perform chloroplast transformation with *C. reinhardtii* in which a cell/DNA mixture is agitated with glass beads as has been described for nuclear transformation. The basic principle remains the same where the two membranes of the chloroplast are oppressed against the cell membrane, providing the opportunity for the entry of exogenous DNA directly into the chloroplast (Economou *et al.*, 2014; Braun Galleani *et al.*, 2015).

Although nuclear transformation enables regulated and tissue-specific expression and PTMs, there are several drawbacks associated with targeting transgenes to the nuclear genome compared to the chloroplast genome. Mainly, nuclear expression can be unstable resulting in transgene silencing, and expression levels are typically much lower compared to those in the chloroplast (Sun *et al.*, 2003). In contrast, chloroplast transformation offers several advantages (Sun *et al.*, 2003; Su *et al.*, 2005; Rosales-Mendoza *et al.*, 2012): (i) the absence of gene silencing; (ii) targeted transgene integration by homologous recombination; (iii) possible expression of multiple genes from polycistrons and thus reconstitution of multi-subunit proteins in a single transformation event.

1.2.3 Factors affecting protein expression in *C. reinhardtii*

In order to facilitate the use of the microalgal chloroplast as an economically viable production platform, it is critical to ensure high and robust heterologous protein expression. This can not only reduce the production costs but also alleviate the burden

for downstream processing. Despite the advantages of transgenic microalgae described in Section 1.2.1, its current advancement is hindered by the relatively low protein yields compared to conventional systems such as bacteria and yeast. Therefore, recent efforts have focused on the understanding of factors that influence protein expression and finding potential solutions in microalgae (Surzycki *et al.*, 2009; Potvin and Zhang, 2010; Michelet *et al.*, 2011). These factors include but are not limited to: (i) codon optimisation of transgenes; (ii) endogenous regulatory elements; (iii) sensitivity to proteases.

Early attempts at chloroplast transformation in *C. reinhardtii* failed to result in the accumulation of heterologous proteins in spite of the stable accumulation of recombinant mRNAs (Blowers *et al.*, 1989, 1990). This was most likely due to the lack of codon optimisation of transgenes. The overabundance in the number of codons means that one amino acid can be encoded by different triplets of codons. Different species often show preferences for one of the several codons that encode the same amino acid (Gustafsson *et al.*, 2004). It has been shown that *C. reinhardtii* displays such codon bias, with codons containing adenine or uracil in the third position favoured over those with guanine or cytosine (Nakamura *et al.*, 2000). This preference was investigated by Franklin et al. (2002) who synthesized a gene for green fluorescent protein (GFP) reporter gene to reflect such codon bias in the *C. reinhardtii* chloroplast genome. The results demonstrated an 80-fold increase in GFP accumulation with codon-optimised transformed strains over the non-optimised counterparts. Since then, it has become a standard practice for recombinant protein production in *C. reinhardtii* (Yang *et al.*, 2006; He *et al.*, 2007; Dreesen *et al.*, 2010; Stoffels *et al.*, 2017).

It is known that chloroplast gene expression is controlled at the transcriptional and post-transcriptional levels in which several *cis*-RNA elements (CREs) within promoters and untranslated regions (UTRs) are found to be essential (Eberhard et al. 2002; Zou et al. 2003; Barnes et al. 2005). The relative impacts of promoters, 5' and 3' UTRs in chloroplast translation were investigated using a combinatorial approach and gene reporter technology (Barnes *et al.*, 2005). This study has demonstrated that promoters and 5' UTRs are crucial in transcription efficiency, mRNA accumulation and protein

expression. In contrast, 3' UTRs have minimal functions in regulating transcription and translation, as long as a 3' UTR is present (Barnes *et al.*, 2005). In addition, Rasala et al. (2011) have demonstrated the importance of promoters on heterologous protein expression by fusing a stronger 16S rRNA promoter with the existing 5' UTR.

The net accumulation of recombinant proteins within the chloroplast is a balance between protein synthesis and degradation. Although some studies on plants or plant cell cultures have suggested that the environment in chloroplasts is more protective for recombinant proteins than that of the cytosol (Doran, 2006), it is inevitable that these 'foreign' proteins are still subjected to proteolytic degradation as various proteolytic enzymes responsible for protein quality control are present in chloroplasts (Adam *et al.*, 2002; Nair and Ramaswamy, 2004; Nishimura *et al.*, 2016). In fact, Birch-Machint et al. (2004) have suggested that rotavirus VP6 protein accumulation was subjected to rapid proteolytic degradation in the transgenic tobacco chloroplasts. In addition, Surzycki et al. (2009) have shown that proteolytic degradation is one of the principal factors affecting vaccine production in microalgal chloroplasts. It has been found that the addition of protease inhibitors directly into the liquid cell culture reduces the rate of protein degradation (Michelet *et al.*, 2011). However, more work needs to be done in order to understand the specific proteolytic sites that endogenous chloroplast proteases target and modify transgene sequences during sequence design.

1.2.4 Production of commercially relevant proteins in the *C. reinhardtii* chloroplasts

Based on previous studies and current knowledge of molecular cloning, researchers have started to transform the *C. reinhardtii* chloroplasts to produce recombinant proteins for therapeutic purposes. Table 1.5 summarises the recent development in biopharmaceutical production in *C. reinhardtii*, together with the expression techniques, expression levels and specific functions. It has been suggested that the expression levels of 2-3% (w/w) TSP are sufficient for purification and commercial production (Rasala *et al.*, 2010).

Table 1.5: Biopharmaceuticals produced in the *C. reinhardtii* chloroplasts (non-exhaustive list). Table modified from Rosales-Mendoza *et al*., (2012); Specht *et al.,* (2010); Dyo & Purton, (2018).

Biopharmaceutical	Type of biopharmaceutical	Transformation technique	Expression level % (w/w) TSP	Assessed properties of the recombinant protein	Reference
Fusion protein comprising FMDV VP1 protein fused to the cholera toxin B subunit (CTB)	Vaccine against FMDV	Biolistic	3 - 4	Display of antigenic determinants from both components	Sun *et al.*, 2003
Mammary-associated serum amyloid (M-SAA)	Protein found in the mammalian colostrum acts in the prophylaxis of bacterial and viral infections	Biolistic	5	Stimulation of mucin production in human gut epithelial cell lines	Manuell *et al.*, 2007
Human vascular endothelial growth factor (VEGF) isoform 121	Treatment of pulmonary emphysema and possible for erectile dysfunction and depression	Biolistic	2	Active in a VEGF receptor-binding assay	Rasala *et al.*, 2010
D2 fibronectin-binding domain of *Staphylococcus aureus* fused to the CTB	Whole-cell oral vaccine against *Staphylococcus aureus*	Biolistic	0.7	Animal tests (induction of specific mucosal and systemic immune responses)	Dreesen *et al.*, 2010
Plasmodium falciparum surface protein (Pfs25) fused to the CTB	Whole-cell oral vaccine against from malaria	Biolistic	0.09	Animal tests (induction of CTB-specific serum IgG antibodies and both CTB- AND Pfs25-specific	Gregory *et al.*, 2013

				secretory IgA antibodies)	
Human Papillomavirus 16 E7	Attenuated form of HPV E7-based vaccine	Biolistic	0.12	Animal tests (induction of immune responses and protection of mice against E7-expressing tumours)	Demurtas *et al.*, 2013
Variable domain of camelid heavy chain-only antibodies	Antibodies targeting botulinum neurotoxin	Biolistic	1.4-4.6	V_HH proteins were shown to bind with high affinity to the toxin, and to survive in the gut of mice fed fresh whole algae	Barrera *et al.*, 2014
Hemagglutinin of avian influenza virus H5	Vaccine against avian influenza	Biolistic	*770 µg per gram dried biomass*	Ocular administration of the recombinant HA to broiler chickens resulted in an immunogenic response	Castellanos-Huerta *et al.*, 2016
Endolysins identified from *Streptococcus pneumoniae*-infecting phages: Cpl-1, a lysozyme hydrolyzing the polysaccharide chains in the bacterial cell wall; Pal, an amidase cleaving the linker peptides in the peptidoglycan network	Endolysins against *S. pneumoniae*	Glass bead	0.9-1.2	Algal cell lysates and purified endolysins showed effective anti-bacterial activity against various serotypes of S. pneumoniae	Stoffels *et al.*, 2017

1.3 Bioprocess engineering of microalgae

Currently, most effort is being put into the genetic manipulation of *C. reinhardtii*, including DNA construct design and recombinant protein expression as described in Sections 1.2.2 and 1.2.4. However, a standard cultivation process has yet to be established for the commercial production of recombinant proteins in *C. reinhardtii* complying with current Good Manufacturing Practice (cGMP). This section outlines the recent status of the bioprocessing of *C. reinhardtii* such as cultivation methods, harvesting techniques and cell disruption processes.

1.3.1 Cultivation of microalgae

Microalgae such as *C. reinhardtii* exhibit three types of metabolism (photoautotrophic, heterotrophic, mixotrophic) as shown in Table 1.6, and can undergo a metabolic shift in response to the changing environmental conditions (Chojnacka and Marquez-Rocha, 2004).

Table 1.6: Summary of energy and carbon sources of different metabolisms in microalgae. Table reproduced from Chojnacka & Marquez-Rocha, (2004).

Metabolism	Energy source	Carbon source
Photoautotrophic	Light	Inorganic
Heterotrophic	Organic	Organic
Mixotrophic	Light and organic	Inorganic and organic

Given the potential cost saving of light-driven production of recombinant products, a large number of studies have been carried out to explore efficient and robust techniques for phototrophic cultivation of microalgae. Broadly, there are two widely employed cultivation methods: open raceway pond systems and closed photobioreactor systems as demonstrated in Figure 1.7. For production of high-value products, the former system is less favourable due to the limitations of control over contaminations and cultivation parameters, especially for applications in biopharmaceutical and vaccine production. In contrast, photobioreactor technologies provide a contained environment for algal growth, precisely controlled operational factors such as light, temperature, nutrient

concentration, pH and CO_2 concentration (Mata *et al.*, 2010). For example, there is a range of light intensity that is suitable for microalgal growth and product production, normally above the compensation point but below the light saturation point (Zhu *et al.*, 2016). Moreover, temperature is another important cultivation parameter since it affects metabolic rates such as the photosynthetic rate and the specific growth rate in microalgae (James *et al.*, 2013). These key operational parameters have been extensively investigated to improve microalgal growth and, in the case of biodiesel production, yield of neutral lipids (Cheirsilp and Torpee, 2012; Moon *et al.*, 2013; Zhu *et al.*, 2016; Severes *et al.*, 2017).

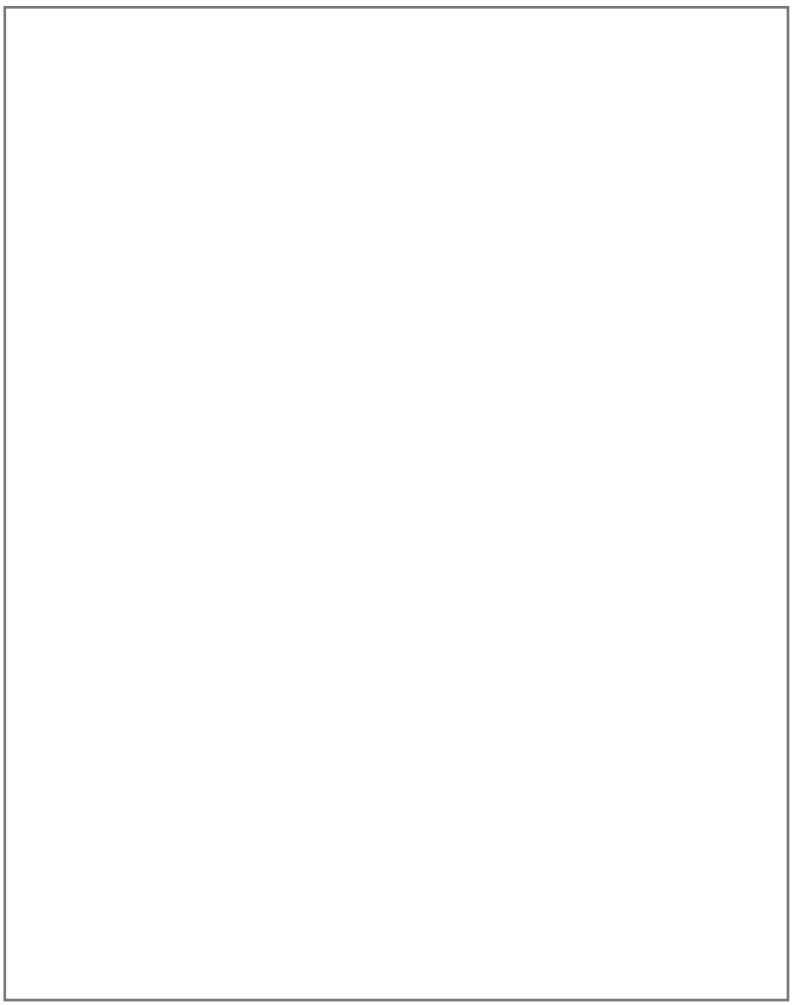

Figure 1.7: Examples of (a) raceway pond and (b) inclined tubular photobioreactors for microalgal cultivation. Figure reproduced from Bitog *et al.*, (2011).

Heterotrophic cultivation of microalgae has also been successfully applied for the production of algal biomass and metabolites due to faster growth rates and higher lipid

productivity (Zheng *et al.*, 2013). In this case, microalgae are grown on organic carbon sources such as acetate, glucose and glycerol in stirred-tank bioreactors where operational parameters are tightly controlled. Since the algal growth is not subjected to light limitation or photoinhibition, the scale-up process becomes much simpler. In fact, large-scale (11,000 L) biodiesel production from *Chlorella protothecoides* was achieved using heterotrophic cultivation (Li et al. 2007). However, few studies have been conducted to investigate the effects of heterotrophic cultivation of *C. reinhardtii* to express recombinant proteins. This may be due to the fact that heterotrophic metabolism mainly contributes to the accumulation of high lipid content instead of protein accumulation.

However, *C. reinhardtii* can also be grown mixotrophically with the addition of acetate as an organic carbon source. It has been demonstrated that acetate can directly down-regulate photosynthetic activity. Consequently, mixotrophic cultures produce less O_2 due to photosystem II (PSII) activity compared to that of the photoautotrophic counterparts. In addition, it is believed that the production of O_2 induces photoinhibition, thus acetate can reduce the photoinhibition phenomenon of *C. reinhardtii* (Roach *et al.*, 2013). These findings were consistent with the previous study in which they reported improved mixotrophic growth rates over both photoautotrophic and heterotrophic cultures (Brennan and Owende, 2010). In fact, Moon et al. (2013) have demonstrated that the initial concentration of acetate under mixotrophic conditions has great impacts on the growth kinetics and lipid accumulation profile of *C. reinhardtii*.

C. reinhardtii used for recombinant protein production is mainly grown mixotrophically using tris-acetate phosphate (TAP) medium expect for one case as demonstrated in Table 1.7. However, strains are typically cultivated in multi-litre shake flasks where growth parameters such as pH and CO_2 are difficult to monitor and control. By 2010, the largest scale achieved was the production of a fusion protein consisting of the D2 fibronectin-binding domain of *Staphylococcus aureus* and the CTB in a 20 L Cellbag^{TM} within a Wave Bioreactor^{TM} (Dreesen *et al.*, 2010). The same scale was achieved in a photobioreactor constructed from Nalgene^{TM} Carboys for the production of malaria

transmission-blocking vaccine candidate (Gregory *et al.*, 2013). Despite the stable expression and effective protection of mice, the 20 L system was only sufficient but not cost-effective for animal tests to be conducted. It should also be noted that cultivation of microalgae expressing transgenic M-SAA (Table 1.5) has been successfully demonstrated at pilot greenhouse scale (100 L) (Gimpel *et al.*, 2015). Figure 1.8 illustrates the set-up of the hanging bags for phototrophic cultivation in the greenhouse. Moreover, Zedler et al. (2016) have also demonstrated the feasibility of cultivating cell wall-deficient transgenic *C. reinhardtii* at pilot-scale (100 L) under mixotrophic conditions.

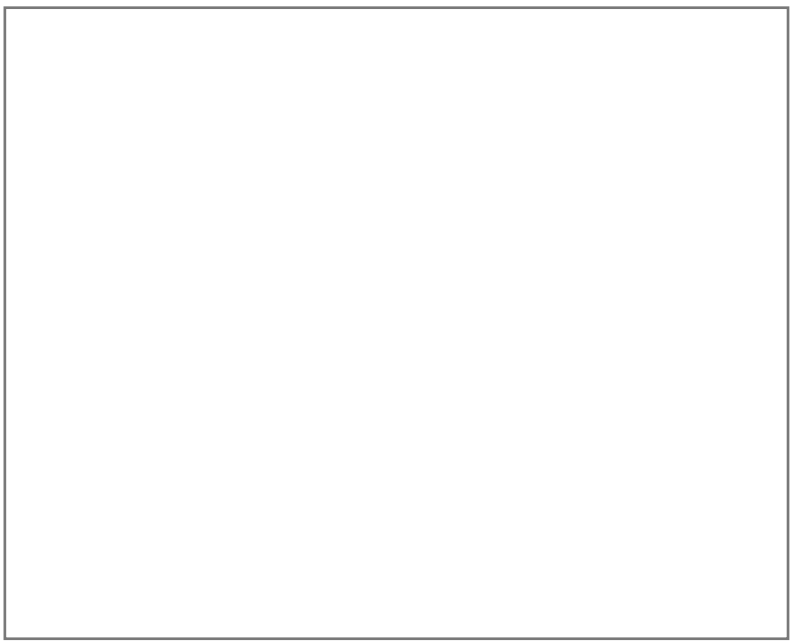

Figure 1.8: Cultivation of microalgae in hanging polybags in the greenhouse. Figure reproduced in Gimpel *et al.*, (2015).

Table 1.7: Summary of mixotrophic cultures of different *C. reinhardtii* transgenic strains for recombinant protein production.

Strain	Volume	Light intensity (µmol $m^{-2}s^{-1}$)	Temperature (°C) (Rotational speed)	Media	References
137C (mt+)	N/A	54 under continuous illumination	23 (100 rpm)	TAP with 40 mM 5-Fluorodeoxyuridine	Franklin *et al.*, 2002; Mayfield and Schultz, 2004; Barnes *et al.*, 2005
137C	N/A	30 under 16 h light/8 h dark cycle	25	TAP	Su *et al.*, 2005
CC-125 (mt+)	100 mL in 500 mL Erlenmeyer flask 14L working volume in 20L Cellbag™	54 under 12 h light/12 h dark cycle (30)	25 (100rpm)	TAP	Dreesen *et al.*, 2010
137C (mt+)	N/A	58 under continuous illumination	23	TAP with 40 mM 5-Fluorodeoxyuridine	Rasala *et al.*, 2010
N/A	100 mL in 250 mL Erlenmeyer flask 200 mL in 500 mL Erlenmeyer flask (15L Biocoil)	120 under continuous illumination (220 under continuous illumination)	25±1	Artificial and wastewater culture	Kong *et al.*, 2010
Cell wall-deficient strain *cw15*	N/A	120 under continuous illumination	25	TAP	Demurtas *et al.*, 2013
137C (mt+)	N/A	16 h light/8 h dark cycle	25	TAP	Soria-Guerra *et al.*, 2013
137C (mt+) psbA mutant strain (W1.1) non-photosynthetic psbH	N/A	N/A	29	TAP	Jones *et al.*, 2013

mutant strain (*psbH-)*					
W1.1	N/A	N/A	23	TAP	Gregory *et al.*, 2013
137C	100 L in hanging polybags	Natural sunlight	23.1±4.7 (constant air/CO_2 bubbling)	HSM	Gimpel *et al.*, 2015
Cell wall-deficient strain *cw15*	100 L in photobioreactor	Natural sunlight	25 (constant air/CO_2 bubbling)	TAP	Zedler *et al.*, 2016
Cell wall-deficient strain *cw15*	400 mL in 1L Erlenmeyer flask	100-200 under continuous illumination	25 (120 rpm)	TAP	Stoffels *et al.*, 2017

Notes: mt+: mating type plus; N/A: data not available; TAP: tris-acetate phosphate medium; HSM: high salt minimal medium

1.3.2 Harvesting microalgae

Despite promising results from genetic engineering of microalgae such as *C. reinhardtii*, few studies have reported the feasibility of downstream processing at large-scale for recombinant protein production. Nevertheless, it has been reported that 20-30% of total algal biomass production costs come from the primary harvesting of the algae (Harun *et al.*, 2010), and numerous studies have been carried out to investigate the cost-effectiveness of different methods to recover microalgal biomass for biodiesel production.

Centrifugation, which involves using centripetal force to achieve liquid-solid separation, is the gold standard in the biopharmaceutical industry for clarification (Vicente *et al.*, 2011) and thus the preferred method of harvesting algal cells (Molina Grima *et al.*, 2003). Since the current scale of recombinant protein production is in the range of litres, laboratory centrifuges are employed in almost every study for primary recovery (Kong *et al.*, 2010; Rasala *et al.*, 2010; Demurtas *et al.*, 2013; Jones *et al.*, 2013). In addition, continuously operating centrifuges are often recommended to process algal biomass at larger-scale, especially for the application of high-value protein products such as vaccines. Such recovery methods have a relatively high harvesting efficiency (95-100%) and reliability as the algal cells are fully contained during processing.

However, centrifugal recovery requires a large initial capital cost and is energy intensive when operating at large scale. Since centrifugation relies on the Stoke's Law to separate algal cells from media (Brennan and Owende, 2010), a large density difference between liquid and solid phases is favourable. Algal cells are usually small in size (2-10 μm) and low in density (close to water), particularly if they have a high lipid content (Uduman *et al.*, 2010; Vandamme *et al.*, 2012), thus a large centrifugal force needs to be applied in order to achieve efficient separation. This was proved by Heasman et al. (2000), who reported that cell recovery dropped from more than 95% to only 40% when the centrifugal acceleration was reduced from 13,000 g to 1300 g. Despite having strong cell walls, the algal cells may still be damaged, or the recombinant proteins can even be accidentally released, leading to product loss at an

early stage. Moreover, some researchers prefer to transform cell wall-deficient strains (e.g. *cw15*) due to the ease of genetic manipulation (Demurtas *et al.*, 2013). These mutants are likely to be more fragile and shear-sensitive during the centrifugation process.

Flocculation can be used as a pre-concentration step, in conjunction with centrifugation for commercial algal harvesting systems, to reduce the high energy demand of centrifugation and facilitate final dewatering (Vandamme *et al.*, 2012). Flocculation refers to the process in which cells or particles can be conjoined with the help of flocculation agents, namely flocculants (Scholz *et al.*, 2011). Since algal cells carry an identical charge, they repel each other and prevent coagulation. Since flocculants can neutralise the surface charge of the cells, this reduces repulsion and allows them to adhere to each other (Schlesinger *et al.*, 2012). In general, flocculants can be classified into three groups (Harun *et al.*, 2010) and the optimal dose and pH are listed in Table 1.8. Although the detailed list of algal species tested was not disclosed, it was suggested that the predominant species was of the *Chlorophyta*.

Table 1.8: Different type of flocculants with their optimal dose and pH for microalgal flocculation. Table reproduced from Uduman *et al.*, (2010).

Type	Flocculant	Optimal dose (mg L^{-1})	Optimal pH
Inorganic	Alum	80-250	5.3-5.6
	Ferric sulphate	50-90	3.0-9.0
	Lime	500-700	10.55-11.5
Organic	Purifloc	35	3.5
	Zetag 51	10	>9
	Dow 21M	10	4.0-7.0
	Dow C-31	1-5	2.0-4.0
Biological	Chitosan	100	8.4

Despite the fact that no flocculation has yet been applied for algal recovery in recombinant protein production, several *C. reinhardtii* strains typically used for protein expression were tested with inorganic and organic flocculants. Scholz et al. (2011) reported that flocculation was particularly efficient for a cell wall-deficient mutant. After nitrogen starvation, recovery was 83±3% for mutants while only 24±2% for

wild-type cells following the addition of 15 mM calcium chloride at pH 8.4. Another study demonstrated the effectiveness of cationic starches as flocculants for *C. reinhardtii* cells and concluded that algal cell density, flocculant concentration and medium condition were all crucial factors in maximizing flocculation efficiency (Gerde *et al.*, 2014).

Alternatively, filtration employs a permeable medium in which solids are retained while liquid is forced through due to the pressure drop (Uduman *et al.*, 2010). Grima et al. (2003) have suggested that a conventional dead-end filtration method is effective when recovering relatively large microalgal species (>70 μm) but are inadequate when processing microalgae that have diameters in the range of several micrometres (Brennan and Owende, 2010). This is because small algal cells tend to block the filter pores easily, leading to a large increase of pressure drop and damage to the filtration system (Schlesinger *et al.*, 2012). Small green algae such as *C. reinhardtii* (10-20 μm diameter) are often favoured for recombinant protein production but are not well suited to recovery by conventional filtration.

In contrast, tangential or cross-flow filtration (TFF) is a promising mode of operation to harvest small microalgae. Various micro- or ultra-filtration membranes with different pore sizes or molecular cut-offs can be selected and operated in a TFF mode, depending on the size and morphology of the microalga (Petrusevski *et al.*, 1995). It was reported that 5 to 40 fold concentration was achieved using a 0.45 μm pore size membrane when harvesting several green algal species (Petrusevski *et al.*, 1995). A comprehensive study has compared the performances of centrifugation, flocculation and membrane microfiltration (TFF mode) which are listed in Table 1.9 (Ahmad et al. 2014).

Table 1.9: Comparison of microalgae harvesting methods. Table reproduced from Ahmad *et al.*, (2014).

Harvesting method	Percentage of recovery (%)	Duration (min)	Relative energy required	Reliability	Efficiency	Maintenance required	Remarks	Reference
Centrifugation	Very high	Short	High	Good	High	High	One-step harvesting	Heasman et al. 2000
Membrane filtration	High	Medium	Low	Good	High	Low	Continuous method	Vandamme et al. 2013
Flocculation	Low	Long	Very low	Poor	Low	Low	Flocculant required	Scholz et al. 2011

At this point in time, centrifugation appears to be a more suitable method of commercial recovery of high-value products derived from microalgae. A pre-concentration step by flocculation is also recommended to reduce energy consumption and improve recovery efficiency for centrifugation. In contrast, microfiltration operating in TFF mode may become a preferred alternative if cells are fragile and shear-sensitive (Molina Grima *et al.*, 2003). Overall, different metrics such as capital investments, running costs, processing time, recovery efficiency, and protein degradation need to be investigated before making any decision.

1.3.3 Cell disruption methods for microalgae

A range of cell disruption methods have been investigated for microalgae including sonication, homogenisation, microwave heating, bead-beating and ball-milling. Even though these techniques have demonstrated positive results on recovery yield, only a few methods are applicable and cost-effective to operate at commercial scale (Yap *et al.*, 2015). This section highlights two widely used methods, sonication and homogenisation, that have important implications for the extraction of intracellular recombinant proteins from microalgae.

To date, the cell disruption method exclusively used for the extraction of recombinant proteins is sonication, especially the use of an ultrasonic probe. The sonicator probe vibrates vigorously, causing microscopic vacuum bubbles to quickly form and collapse. This process is called 'cavitation' which generates tremendous energy to break the cells open (Patchett *et al.*, 1989). In general, the higher the amplitude, the greater the cavitation intensity. However, sonication also generates a considerable amount of heat which is undesirable for the extraction of proteins. In order to reduce the heat effect, an alternating on/off system is recommended during the process. Despite the prevalent use of sonication, it is not applicable to large-scale processes.

Adapted from the dairy industry, homogenisation has become a well-established downstream unit operation in the biopharmaceutical industry. Compared to sonication,

homogenisation is widely used in large-scale recovery of recombinant proteins from *E. coli* and *S. cerevisiae* (Diels and Michiels, 2006). Yap et al. (2014) have demonstrated that the performances including processing capability, power and cell disruption efficiency of high-pressure homogenisation were insensitive to the feed concentration (for *Nannochloropsis sp.*) up to 25% (w/w). Since the same extent of algal cell breakage can be achieved when processing biomass at 25% (w/w) and 0.25% (w/w), respectively, the energy consumption is subsequently reduced one hundred fold per ruptured cell (Yap *et al.*, 2015). This refutes the drawback of homogenisation of being energy intensive as long as a high feed concentration is used.

1.4 Purification and characterisation of VLPs

1.4.1 Purification of VLPs

Since the approval of the first HBV vaccines, commercial VLP-based vaccines have been on the market for more than three decades. Hence, there is an established downstream process flowsheet to purify VLPs, although it should be noted that the process is also dependent on the production system employed (Zeltins, 2013). In general, the purification steps after fermentation include (Zeltins, 2013): (i) cell disruption (if the recombinant VLP proteins accumulate within the cells); (ii) initial clarification; (iii) concentration (iv) capture and polishing; (v) final sterile filtration.

After initial clarification and concentration steps, ultracentrifugation is the most widely applied laboratory-based technique to purify VLPs from host cell proteins and DNA based on the distinct physical properties of VLPs. This technique is also called rate-zonal centrifugation in which a narrow layer of sample is loaded onto a density gradient of sucrose or caesium chloride solutions as illustrated in Figure 1.9 (a) and (b) (Majekodunmi, 2015). The sedimentation speed in this case depends on the size and mass of the particles instead of the density (Zborowski and Chalmers, 1988). During centrifugation, each subcellular component will move up or down until it reaches a position where its buoyant density matches its surroundings (Figure 1.9 (c)) (Zborowski

and Chalmers, 1988). A series of distinct bands will eventually be produced and the partially purified VLPs can be collected at certain fractions depending on their specific structural characteristics.

Figure 1.9: Schematic diagram of the rate-zonal centrifugation with density gradient. (a): before centrifugation; (b): sample loading; (c): after centrifugation. Figure reproduced from Majekodunmi, (2015).

However, the ultracentrifugation-based method is limited to laboratory-based purification. It is time-consuming, labour-intensive and non-scalable for industrial applications (Zeltins, 2013). In contrast, special chromatographic steps such as ion-exchange, affinity and size exclusion chromatography are scalable and effective for the commercial purification of VLPs. For example, Vicente et al. (2007) have successfully demonstrated the applicability of anion-exchange membrane chromatography for the purification of rotavirus-like particles (RLPs) in terms of scalability and robustness. Moreover, as demonstrated in Figure 1.10, the key purification step of the commercial HPV vaccine Gardasil® is cation-exchange chromatography in which the L1 protein is captured and then polished through two chromatographic passes (Josefsberg and Buckland, 2012).

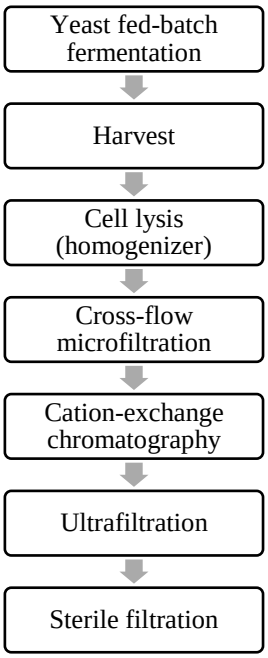

Figure 1.10: Simplified schematic diagram of the purification process for the Gardasil® HPV VLP-based vaccines. Figure modified from Josefsberg and Buckland, (2012).

1.4.2 Identification and characterisation of VLPs

Routine biochemical techniques such as western blotting and the enzyme-linked immunosorbent assay (ELISA) with the use of mono- or poly-clonal antibodies against denatured and/or native proteins can prove the presence of target VLP proteins. In addition, purification techniques such as sucrose gradient ultracentrifugation or size exclusion chromatography can also demonstrate the particulate nature of the protein samples and identify the higher order molecular structures of VLPs. Moreover, mass spectrometry can be used to determine the molecular weight of the assembled proteins. This technique facilitates the determination of proteolytic degraded and/or post-translationally modified VLP proteins during the production process (Zeltins, 2013).

However, these indirect methods mentioned cannot differentiate between correctly assembled VLPs and non-structured protein aggregates. Therefore, electron microscopic observations are necessary as a visual proof of VLP assembly. In fact, TEM has become the gold standard to visually confirm the production of VLPs. TEM

operates on the same basic principles as light microscopy but reveals macromolecular structures with higher magnification and higher resolution due to the much lower wavelength of electrons (Thompson *et al.*, 2013). Negative staining is typically performed in TEM in which the background is stained with charged heavy salts, leaving the specimen untouched (Newman *et al.*, 2003). The very high image contrast can help to reveal the structural characteristics of VLPs such as shape, size and the particle integrity. Figure 1.11 demonstrates the structures of *E. coli*-produced VLPs formed by truncated HBcAg monomers revealed in TEM analysis. In general, sample preparation in negative staining is relatively simple and quick to perform.

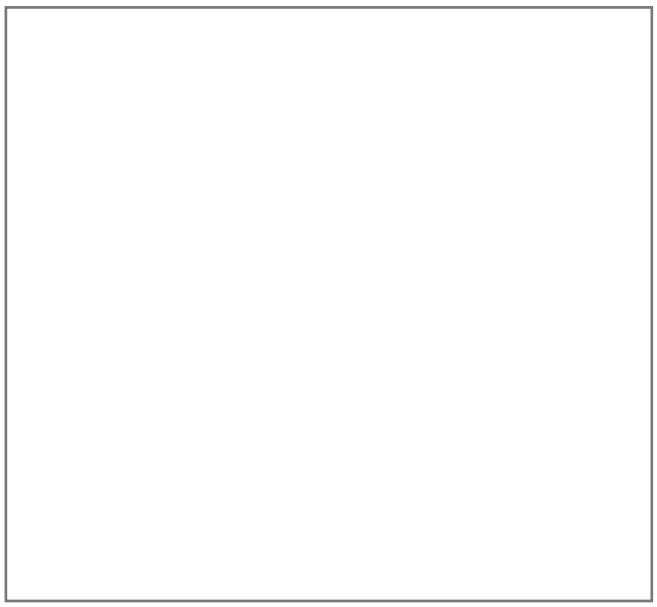

Figure 1.11: Example TEM micrograph of VLPs formed by truncated HBcAg monomer (1-149 a.a.) expressed in *E. coli*. Figure reproduced from Peyret *et al.*, (2015). Size bar, 100 nm. White arrow indicates smaller (T = 3) particles.

In complicated cases, such as the presentation of foreign antigens/epitopes on chimeric VLPs, immunogold labelling is a useful technique to confirm the immunoreactivity of the linked antigens/epitopes. As shown in Figure 1.12, the staining procedure is similar to that of the immunoblotting in which the antigen is recognised by a specific primary antibody. Then, the primary antibody is attached by a gold-conjugated secondary antibody. Therefore, the success of this technique mainly relies on the specificity and sensitivity of the antigen-antibody reaction. Gold is the most reliable choice for detection due to its excellent electron scattering property, biocompatibility as well as the minimal steric hindrance due to the small sizes (2 or 5 nm) available (Murtey, 2016).

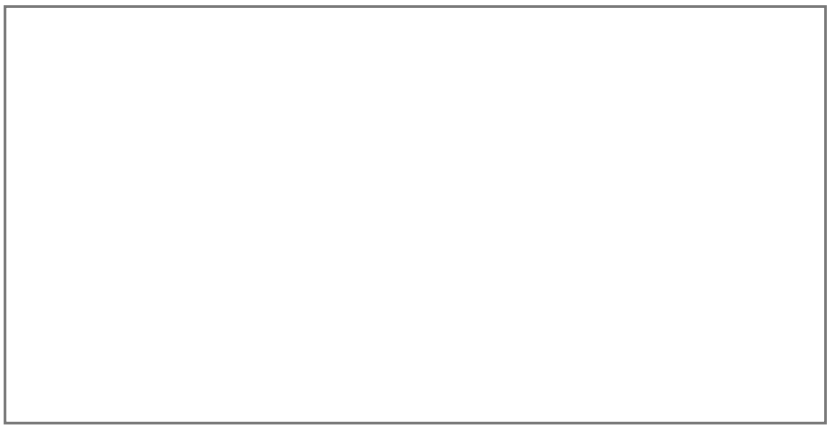

Figure 1.12: Simplified schematic diagram representing the immunogold labelling after secondary antibody incubation. Figure modified from Murtey, (2016).

Cryo-EM is another powerful technique to reveal the morphological characteristics and structural details of VLPs. During cryo-EM, the protein sample is cooled to around −190 °C. Thousands of electron micrographs can be taken for the random oriented protein samples and similar ones are grouped to generate the high-resolution two-dimensional (2D) images using sophisticated image processors. Then, the three-dimensional (3D) structures can be reconstructed at near atomic resolution based on these 2D images (Bai *et al.*, 2015). This so-called cryo-EM single particle analysis is an invaluable tool when assessing the structural details of the VLP-based vaccines especially when absorbed onto aluminium adjuvants (Zhao *et al.*, 2014).

1.5 Aims and objectives

VLPs are made of self-assembled viral envelope and/or capsid proteins and resemble the native viruses with similar structural and antigenic characteristics. In contrast, they are non-infectious and non-replicating molecules due to the lack of viral genetic materials (Tagliamonte *et al.*, 2017). Additionally, the highly repetitive and organised display of the epitopes on the VLP surface promotes strong immunogenic responses (Grgacic and Anderson, 2006). As a result, a handful of VLP-based vaccines have been successfully commercialised (Table 1.1). More importantly, some VLPs can serve as particulate carriers and thereby convey their strong immunogenic properties to linked heterologous epitopes. Such vaccine candidates overcome the problems that

heterologous epitopes do not possess optimal immunogenicity or cannot self-assemble into particulate forms to elicit strong immune responses. Due to the structural flexibility and intrinsic particle stability, HBcAg VLP is believed to be one of the most promising particulate carriers (Roose *et al.*, 2013). The formation of HBcAg VLP has been successfully demonstrated in various prokaryotic and eukaryotic expression systems. However, no such work has been reported in microalgae to date.

As discussed in Section 1.2.1, transgenic microalgae have considerable potential as an alternative to conventional protein expression platforms. This is mainly due to the absence of viral toxins or human pathogens, the cost-effectiveness of protein production and the rapid scalability of production processes. *C. reinhardtii* is chosen in this study as it is currently the best characterized candidate for protein production among microalgal species (Walker *et al.*, 2005; Specht *et al.*, 2010). Commercially relevant products derived from the *C. reinhardtii* chloroplasts include full-length human antibodies, oral vaccine candidates and immunotoxins (Tran *et al.*, 2009, 2013; Demurtas *et al.*, 2013; Specht and Mayfield, 2014). Therefore, the **aim** of this work is to investigate the capability of the *C. reinhardtii* chloroplast to synthesize and assemble HBcAg VLPs. This will further explore the potential of *C. reinhardtii* chloroplast as a versatile platform for low-cost production of recombinant therapeutic proteins. Key **objectives** to achieve the overall project aim are as follows:

- The first objective will be to synthesize HBcAg in the chloroplast of *C. reinhardtii*. This will involve the design and incorporation of transgenes encoding both full-length and truncated HBcAg monomers into the *C. reinhardtii* chloroplast genome. Short affinity tags will also be included to facilitate protein detection (Section 3.3 and Section 3.4). Once transgenic lines are established, HBcAg expression will be assessed by western blot analysis. In addition, the stability of the algal-based HBcAg will be assessed by a time-course study in which *de novo* protein synthesis in the chloroplast is blocked by the addition of chloramphenicol (Section 3.5). The results of this work are discussed in Chapter 3.
- The second objective will be to attempt to increase HBcAg levels in the algal

chloroplast through two different approaches. From the bioprocessing aspect, the effects of cultivation modes (phototrophy, heterotrophy and mixotrophy) and operational conditions (initial acetate concentration, light intensity and temperature) on algal growth kinetics and HBcAg accumulation levels will be investigated (Section 4.2). From the molecular biology aspect, the genetic modification of the transgene construct introduced into the chloroplast genome will be explored to potentially increase the transcriptional rate or the steady-state mRNA level of the transcripts (Section 4.3). Moreover, the final HBcAg production yield will be estimated by densitometric analysis and compared to that of the yeast-derived HBcAg (Section 4.4). The results of this work are presented in Chapter 4.

- The third objective will be to verify the assembly of HBcAg VLPs in the *C. reinhardtii* chloroplasts by TEM analysis. Initial work will involve the generation of suitable control samples for TEM analysis. The positive control will be expressed in *E. coli* (Section 5.2) whereas the negative control will be generated in two microalgal transgenic lines without HBcAg accumulation (Section 5.3). In addition, a standard clarification protocol for the isolation and visualization of the algal-based HBcAg VLPs will be established. Subsequently, all protein samples will be subjected to electron microscopic observations to confirm the presence of HBcAg VLPs in microalgal chloroplasts. Furthermore, the immunogold labelling technique will be applied to further support the evidence of capsid assembly in microalgal protein samples (Section 5.4). The results of this work are elaborated in Chapter 5.

Finally, the overall conclusions from this work and recommendations for future research are discussed in Chapter 6.

2 Materials and Methods

2.1 Materials

2.1.1 Microorganisms

For bacterial cultures, One Shot^{TM} TOP10 and BL21 (DE3) chemically competent *E. coli* cells (Thermo Fisher Scientific, Paisley, UK) were used for plasmid amplification and protein expression, respectively. For algal cultures, the *C. reinhardtii* stains used or created in this study are listed in Table 2.1. In this study, all microorganisms were handled aseptically, and all equipment was sterilised with 70% (v/v) ethanol before and after use.

Table 2.1: *C. reinhardtii* stains used or created in this study.

Strain	Genotype/phenotype	Reference
TN72	mt+, *cw15* (cell-wall deficient), *psbH* partly replaced by the *aadA* cassette, photosynthesis-incompetent mutant	Wannathong et al. 2016
TNE	TN72 transformed with the empty pSRSapI vector, carrying the *psaA* promoter/5' UTR, *psbH* rescued	Young & Purton 2014
TN72_SR_pal-HA	TN72 carrying pal with HA-tag sequence under the control of the *psaA* promoter/5' UTR, *psbH* rescued	Stoffels et al. 2017
TN72_HBc183	TN72 carrying HBc183 under the control of the *psaA* promoter/5' UTR, *psbH* rescued	This study
TN72_HBc150_Strep	TN72 carrying HBc150_Strep with Twin-Strep-Tag sequence under the control of the *psaA* promoter/5' UTR, *psbH* rescued	This study
TN72_HBc150_HA	TN72 carrying HBc150_HA with HA-tag sequence under the control of the *psaA* promoter/5' UTR, *psbH* rescued	This study
TN72_16S_HBc150_HA	TN72 carrying HBc150_HA with HA-tag sequence under the control of the 16S rRNA promoter/*psaA* 5' UTR, *psbH* rescued	This study
psaA strain	TN72_HBc150_HA_T3	This study
16S fusion strain	TN72_16S_HBc150_HA_T5	This study

All bacterial expression plasmids (pJ201, pJ241 and pD454-SR) were synthesized *de novo* by ATUM (Neward, California, USA). All chloroplast expression plasmids used or created in this study are listed in Table 2.2.

Table 2.2: Chloroplast expression plasmids used or created in this study.

Plasmid	Details	Reference
pSRSapI	Carries an expression cassette with the *psaA* exon1 promoter/5'UTR and *rbcL* 3'UTR, the *C. reinhardtii psbH* gene as selectable marker together with regions upstream and downstream flanking regions for homologous recombination during transformation	Young & Purton 2014
pHBc183	pSRSapI carrying HBc183 sequence under the control of the *psaA* promoter/5' UTR	This study
pHBc150_Strep	pSRSapI carrying HBc150_Strep with Twin-Strep-Tag sequence under the control of the *psaA* promoter/5' UTR	This study
pHBc150_HA	pSRSapI carrying HBc150 with HA-tag sequence under the control of the *psaA* promoter/5' UTR	This study
p16SHA	pSRSapI carrying HBc150 with HA-tag sequence under the control of the 16S rRNA promoter/*psaA* 5' UTR	This study

2.1.2 Media and buffer composition

The growth media used for routine *E. coli* cultivation are shown in Table 2.3 and Table 2.4. The growth media for routine *C. reinhardtii* cultivation are shown in Table 2.5. All media components were sterilised by the autoclave at 121 °C for 20 minutes using a Denley autoclave (Thermo Fischer Scientific, Paisley, UK). In addition, antibiotics were sterilised by filtration using a 0.22 μm syringe filter and added separately into the media when needed.

Table 2.3: Composition of Lysogeny broth (LB)

For preparation of 1 L LB	Mass (g)
Tryptone	10.0
Yeast extract	5.0
NaCl	10.0

Table 2.4: Composition of Terrific broth (TB)

For preparation of 1 L TB	Mass (g)
Tryptone	12.0
Yeast extract	24.0
Glycerol	(4.0 mL)

Table 2.5: Composition of algal media (composition of stock solutions and buffers are presented in Appendix 1 (A1)*).

For preparation of 1L media	TAP medium (mL)	HSM medium (mL)
5 x Beijerincks*	10.0	10.0
Phosphate solution*	8.3	8.3
Tris-Acetate stock*	10.0	-
Trace elements stock solution*	1.0	1.0
Final pH	7.0	7.0

Table 2.6: The concentration of stock solution and final concentration of different antibiotics used in this study.

Antibiotic	Stock solution (mg mL^{-1})	Final concentration (µg mL^{-1})
Ampicillin	100.0 in H_2O	100.0
Kanamycin	100.0 in H_2O	50.0
Chloramphenicol	100.0 in ethanol	Various concentrations depending on the application. Concentrations used described in Section 3.5.2.

2.2 Molecular biology techniques

2.2.1 Bacterial plasmid isolation

For small quantity (< 20 µg) plasmid isolation, the QIAprep Spin Miniprep Kit (QIAGEN, Duesseldorf, Germany) was used as per the manufacturer's instructions. Briefly, ~4 mL *E. coli* cell culture was harvested by centrifugation and disrupted by alkaline lysis (using a NaOH and sodium dodecyl sulfate (SDS) solution). After centrifugation, the supernatant containing the plasmid of interest was loaded onto the silica spin column which captured the DNA molecules at high salt concentrations. The column was washed with an 80% (v/v) ethanol solution to remove contaminants while DNA samples were eluted using either 30 µL deionized water or elution buffer.

Larger amounts of plasmid (20-100 µg) were extracted using the QIAGEN Plasmid Midi Kit (QIAGEN, Duesseldorf, Germany) according to the manufacturer's instructions. 30 mL cell cultures were harvested and lysed by the alkaline solution. The principles were the same as those of the Miniprep kit with the additional steps of QIAfilter filtration and endotoxin removal.

2.2.2 Polymerase chain reaction

DNA fragments were amplified using the polymerase chain reaction (PCR) method. The sequences of the primers used with detailed melting points (Tm) are listed in Appendix 2 (A2). Reactions were performed in a final volume of 50 µL using a thermocycler (Techne, Staffordshire, UK). Typical PCR conditions are as shown here unless otherwise stated: initial denaturation (98 °C, 30 s), 30 cycles of denaturation (98 °C, 10 s), annealing (varying temperatures depending on the melting points of primers, 30 s) and extension (72 °C, 60 s), final extension (72 °C, 10 min) and hold (4 °C). The PCR components are listed in Table 2.7.

Table 2.7: Components of PCR mix.

Component	Volume	Final concentration
DNA	Variable	50.0-100.0 ng
Forward primer (10µM)	2.5 µL	0.5 µM
Reverse primer (10µM)	2.5 µL	0.5 µM
dNTPs	1.0 µL	200.0 µM
5X Phusion HF buffer	10.0 µL	1X
dH_2O	Top up to 50 µL	-
Phusion polymerase	0.5 µL	1 U/50.0 µl PCR
Total volume	50.0 µL	-

Colony PCR analysis was used to screen for homoplasmic transformant lines when using the expression vector pSRSapI as the backbone for transformation. The strategy is displayed in Figure 2.1 where specific primers (FLANK1, rbcL.Fn and RY-psaR) were used (Economou *et al.*, 2014). The recipient strain TN72 and TNE were used as the negative and positive control, respectively. Primers Flank1 and rbcL.Fn can bind the parental sequence and generate a band of 850 bp. In contrast, successful integration

of the transgenic gene construct is verified by a band of 1135 bp when primers FLANK1 and RY-psaR are used. Homoplasmy is inferred if no 850 bp band is observed in transgenic lines.

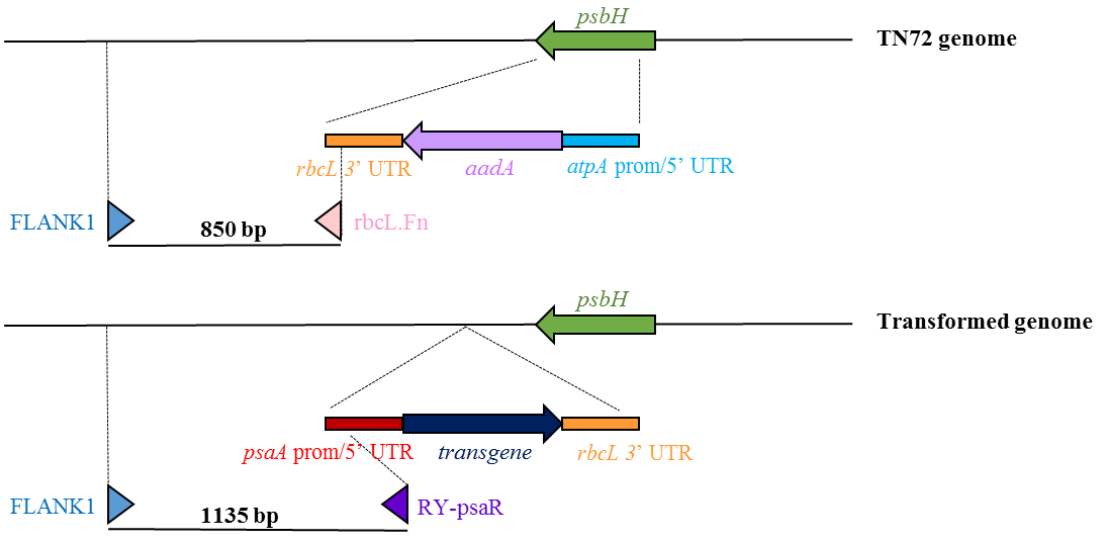

Figure 2.1: PCR strategy for the verification of homoplasmy in chloroplast genomes with three primers (FLANK1, rbcL.Fn and RY-psaR).

2.2.3 Restriction endonuclease digestion

Both the GOI and the algal chloroplast plasmid (pSRSapI) were digested with SapI and SphI restriction enzymes to create compatible sticky ends. The mixture, as demonstrated in Table 2.8, was incubated at 37 °C for 1 hour. The enzymes were inactivated by heating up to 65 °C for 20 minutes to stop the digestion reaction.

Table 2.8: Components of the digestion reaction for the GOI and pSRSapI.

Component	Volume
pSRSapI/GOI	Variable
SapI	1.0 µL
SphI	1.0 µL
10X CutSmart® Buffer	5.0 µL
dH_2O	Top up to 50.0 µL
Total volume	50.0 µL

2.2.4 Removal of 5' phosphates

To prevent the self-ligation of linearized vector and reduce background, Antarctic phosphatase (AP) was used to remove 5' phosphates of the algal vectors (Stoffels, 2015). Digested pSRSapI samples were treated with 2 units (U) of AP and incubated at 37 °C for 30 minutes. Once the reaction was complete, the enzymes were inactivated by heating to 70 °C for 5 minutes.

2.2.5 Agarose gel electrophoresis

Agarose gels contained 0.6-1.2% (w/v) agarose (depending on the sizes of DNA fragments being analysed) dissolved in 1X TBE buffer with the addition of 0.5 μg mL^{-1} intercalating florescent dye GelRed Nucleic stain (Biotium, California, USA). 6X gel loading dye was used to ensure the samples sink to the bottom of the well and to provide visual tracking of DNA migration. Gels were run in 1X TBE buffer at 120 V for approximately 40 minutes and visualized by the AlphaImager® Mini System (ProteinSimple, Oxford, UK).

2.2.6 Gel extraction

Agarose gels were put inside an AlphaImager® Mini System and cut with sterile single-use blades. The gels were trimmed and then purified by the QIAquick Gel Extraction Kit (QIAGEN, Duesseldorf, Germany) as per the manufacturer's instructions. The concentrations of DNA samples were determined using a NanoDrop™ 2000 UV-Vis Spectrophotometer (Thermo Fisher Scientific, Paisley, UK) in order to prepare different vector to insert ratios during ligation.

2.2.7 Ligation

The purified DNA fragments were ligated using T4 DNA ligase with different molar ratios of vector to insert as described in Section 3.2.2. Ligation mixtures as detailed in Table 2.9 were incubated overnight at 4 °C.

Table 2.9: Components of ligation mixtures for the GOI and pSRSapI.

Component	Volume
GOI	Variable
pSRSapI	
10X Ligase buffer	2.0 µL
10mM ATP	1.0 µL
T4 DNA Ligase	20-500 U
Total volume	20.0 µL

2.2.8 Transformation

For the transformation of *E. coli*, one vial of One Shot® TOP10 (50 µL) or BL21 (DE3) (50 µL) chemically competent *E. coli* cells were thawed on ice and mixed with DNA samples (ligation mixtures or plasmids) by gently tapping. After incubation on ice for 30 minutes, the mixture was heat shocked for exactly 30 seconds in a 42 °C water bath. Afterwards, 250 µL of pre-warmed TB was added and incubated for exactly 1 hour at 300 rpm at 37 °C. The resulting transformation mixture was split into different volumes and spread onto LB agar plates containing suitable antibiotics. The plates were inverted and incubated at 37 °C overnight for colony development. Single colonies were picked and inoculated into 5 mL liquid LB or TB complemented with compatible antibiotics either for plasmid propagation or protein expression.

For the transformation of *C. reinhardtii*, the recipient strain TN72 was re-streaked on 2% (w/v) TAP agar plates several times over a week at 25 °C in the dim light (< 10 µmol $m^{-2}s^{-1}$) to ensure healthy growth. Then a large loop of healthy cells was inoculated into 20 mL liquid TAP medium in a 50 mL shake flask under continuous light at 120 rpm for three days. The cell culture was transferred into a 2 L shake flask containing 500 mL TAP medium under the same conditions. After harvesting by centrifugation, cells were re-suspended in HSM medium to a final concentration of ~2×10^8 cells mL^{-1}. Approximately 4 mL of cell suspension was divided equally and then transferred to 12 sterile test tubes, each containing 0.3 g sterile acid-washed glass beads (Sigma-Aldrich, Munich, Germany). 10 µg of plasmid DNA was transferred to each of ten tubes with an additional two tubes used as 'no DNA' controls. The test tubes were then

agitated at top speed for 15 seconds using a vortex mixer Vortex-Genie 2 (Scientific Industries, Inc, New York, USA). 3.5 mL 0.5% (w/v) molten HSM agar was added to each tube and the mixture was quickly poured onto the surface of 2% (w/v) HSM agar plates. The plates were covered in black cloth to prevent phototactic migration of cells (Economou *et al.*, 2014) with a setting time of 20 minutes. The plates were inverted and sealed with Parafilm® for transformant colony development.

2.2.9 Crude genomic DNA extraction from *C. reinhardtii*

A loopful of algal cells at logarithmic-growth phase was re-suspended in 10 µL sterile water, followed by the addition of 10 µL pure ethanol. After incubating for one minute at room temperature, 100 µL 5% (w/v) Chelex® 100 resin (Bio-Rad Laboratories, Hertfordshire, UK) was added. Then, the mixture was vortexed and heated at 99 °C for 5 minutes. The supernatant was collected by centrifugation (at 13,000 rpm, 2 minutes, 4 °C) and stored at -20 °C.

2.2.10 DNA sequencing and gene synthesis

DNA samples such as plasmids or PCR products were sent for sequencing (Source Bioscience, Nottingham, UK). The required concentrations for the plasmids and PCR products were 100 ngµL^{-1} and 10 ngµL^{-1}, respectively. In addition, the primers were provided at a concentration of 3.2 pmolµL^{-1}. The volumes required for all the samples per reaction were 5 µL. The sequencing results were aligned and analysed using Nucleotide BLAST and ApE v2.0.49.10, respectively. Codon-optimised genes were synthesized *de novo* by ATUM (Menlo Park, CA, USA).

2.2.11 Gibson assembly

Gibson assembly can efficiently join multiple overlapping DNA fragments in a single isothermal reaction (Gibson *et al.*, 2009, 2010). First, the purposely-designed overlapping DNA fragments are digested by T5 5' exonuclease to create complementary

sticky ends. Then, Phusion polymerase fills in gaps within annealed fragments. Last, *Taq* DNA ligase seals the nicks in the assembled DNA backbone.

For the construction of the plasmid p16SHA by Gibson assembly, the procedures are detailed below. First, the isothermal reaction buffer was made according to Table 2.10. After mixing, the mixture was briefly centrifuged and topped up to 1 mL. Then it was sterilized by filtering through a 0.22 µm syringe filter and stored at -20 °C. Second, the components of run tubes including the previously-prepared buffer mix (Table 2.10) were made according to Table 2.11. Each run tube contained 12.3 µL of the mixture. Third, the reaction mastermix was made according to Table 2.12. After calculating the amount of DNA needed for each DNA section based on Equation 1, the reaction mixture was run in the PCR machine at 50 °C for one hour and then subjected to *E. coli* transformation as described in Section 2.2.8.

$$\textbf{Amount of DNA needed for each fragment} = \frac{\textbf{9.075} \times \textbf{no.of base pair}}{\textbf{1000}} \qquad \text{[Equation 1]}$$

Table 2.10: Components of isothermal reaction buffer mix used to prepare run tubes.

Components	Volume/Mass
Tris-HCl (1 M)	500.0 µL
$MgCl_2$ (2 M)	25.0 µL
DTT (1 M)	50.0 µL
NAD (100 mM)	50.0 µL
PEG 8000	0.3 g
dH_2O	Top up to 1.0 mL
Total volume	1.0 mL

Table 2.11: Components of run tubes used to prepare Gibson assembly mixture.

Components	Volume
Isothermal Reaction Buffer mix	320.0 µL
T5 exonuclease (10 $U\mu L^{-1}$)	0.7 µL
dH_2O	667.3 µL
Total volume	998.0 µL

Table 2.12: Components of reaction mastermix to prepare Gibson assembly mixture.

Component	Volume
dNTPs mix (10 Mm each)	0.4 µL
Taq DNA ligase (40U/ µL)	2.0 µL
Phusion DNA polymerase (20U/ µL)	0.3 µL
Total volume	2.7 µL

Table 2.13: Components of Gibson assembly used to construct the plasmid p16SHA.

Components	Volume
Run tube	12.3 µL
Reaction mastermix	2.7 µL
Three DNA fragments with dH_2O	5.0 µL
Total volume	20.0 µL

2.2.12 Bioinformatics

A range of bioinformatics tools were used in this study as described in Table 2.14.

Table 2.14: Database and bioinformatics tools used in this study.

Peptide sequence database	
NCBI	http://www.ncbi.nlm.nih.gov
Bioinformatics tools	
Restriction endonuclease digestion	http://tools.neb.com/NEBcutter2/
Primer design	https://www.ncbi.nlm.nih.gov/tools/primer-blast/
Reverse translation	http://www.bioinformatics.org/sms2/rev_trans.html
Translation	http://web.expasy.org/translate/
Nucleotide BLAST	https://blast.ncbi.nlm.nih.gov/Blast.cgi?PROGRAM=blastn&PAGE_TYPE=BlastSearch&LINK_LOC=blasthome
Protein BLAST	https://blast.ncbi.nlm.nih.gov/Blast.cgi?PROGRAM=blastp&PAGE_TYPE=BlastSearch&LINK_LOC=blasthome
Codon Usage Optimiser (CUO)	http://www.ucl.ac.uk/algae/genetic_engineering_tools

2.3 Cultivation of microorganisms

2.3.1 Bacterial and yeast cell cultures

When grown in solid media, 2% (w/v) LB agar plates supplemented with suitable antibiotics were used to support colony isolation after transformation for bacterial cell cultures. For long-term storage, 25% (v/v) glycerol stocks of *E. coli* strains were prepared and stored in a -80 °C freezer.

For plasmid isolation or seed culture, glycerol stocks were inoculated into small volumes of LB medium (2-10 mL) in 50 mL Falcon™ conical centrifuge tubes. The culture was grown in a shaking incubator (SI60 Incubator, Stuart Scientific, UK) at 37 °C, 200 rpm. For protein expression, the seed culture was inoculated into 250 mL shake flasks with 100 mL LB medium and grown at 37 °C for three hours. 1 µM isopropyl β-D-1-thiogalactopyranoside (IPTG) was added to the cultures when they reached the exponential growth phase (OD_{600nm} at 0.6-0.8). After IPTG induction, cells were grown at 18 °C for 16-18 h and harvested for further analysis.

Yeast cultures expressing tandem-core HBcAg named K1.K1 (two HBcAg monomers were genetically fused together using a (GGS)*7 linker) were kindly provided by Prof. Tarit Mukhopadhyay.

2.3.2 Algal cell cultures

2% (w/v) TAP and HSM agar plates were used for short-term storage of algal strains and transformation, respectively. Plates were placed under different light intensities depending on the specific experiment. For example, TAP plates for strain maintenance were placed under dim light (< 10 µmol $m^{-2}s^{-1}$) in the storage room. HSM plates for transformation purposes were placed under bright light at around 150 µmol $m^{-2}s^{-1}$ for 4-6 weeks. Fresh TAP agar plates were supplemented every month to maintain the healthy growth of algal cells.

250 mL Erlenmeyer flasks were used to cultivate 50 mL and 100 mL cell cultures in TAP medium for pre-inoculation and growth investigations, respectively. Pre-inoculation cultures were initiated with a loop of healthy algal cells from the agar plate and were grown to mid-logarithmic phase before propagating to the next passage. A starting OD_{750nm} of 0.3 or 0.1 depending on the application was used for consistency of growth characterisation. Cell cultures were grown at 120 rpm, 25 °C with a light intensity of approximately 50 µmol $m^{-2}s^{-1}$ in a Kuhner incubator (Kuhner, Herzogenrath, Germany).

In addition, 1 L Erlenmeyer flasks with 500 mL working volume were used in the Algem® photobioreactors (Algenuity, Bedfordshire, UK) with a tight control of light intensity, temperature and rotational mixing speed. The standard conditions used were 120 rpm, 200 μmolm^{-2}s^{-1} (white light) and 25 °C. OD_{740nm} was automatically measured *in situ* every 30 min to monitor growth whereas OD_{750nm} was measured manually every day to calculate specific growth rates and maximum biomass accumulation. Samples were also harvested to monitor pH values by a benchtop pH meter (Thermo Fisher Scientific, Paisley, UK) and acetate consumption by HPLC (Section 2.5.1).

2.3.3 Biomass quantification and specific growth rate calculation

Three different methods to quantify algal biomass were used depending on the specific applications. Optical density (OD) and dry cell weight (DCW) were measured to monitor cell growth for specific growth rate and maximum biomass calculations. Cell count using haemocytometer was mainly used during algal transformation.

Table 2.15: Brief descriptions of three algal biomass quantification methods

Quantification methods	Brief description
OD	A Ultrospec 1100 Pro spectrophotometer (Amersham Biosciences, New Jersey, USA) was used to measure the OD at the wavelengths of 750 nm and 600 nm to monitor the growth of algal and bacterial cells, respectively.
Cell count	A haemocytometer (Hausser Scientific, West Sussex, UK) and a bright field microscope at 20 X magnification (Olympus, Hamburg, Germany) were used to count cells mainly for transformation. Due to cell motility, 1 mL of algal sample was first treated with 10 µL of tincture of iodine (0.25 g iodine in 100 mL 95% (v/v) ethanol), which immobilised the algal cells.
DCW	The liquid algal samples were diluted into five dilutions. Samples were placed on top of the pre-weighed Whatman fibre glass filter paper (GE healthcare, Little Chalfont, UK) and left in the oven (100 °C) overnight to achieve a constant dry mass. The correlation between OD_{750nm} and DCW is demonstrated in Appendix 3 (A3).

The specific growth rate (µ) was calculated during the exponentially growth phase based on the equation shown below (h^{-1}) (Widdel, 2007):

$$\mu = \frac{lnx_2 - lnx_1}{t_2 - t_1} \qquad \text{[Equation 2]}$$

where x_2 and x_1 are the dry cell weight (g L^{-1}) at time t_2 and t_1 (h), respectively.

2.4 Downstream processing operations

2.4.1 Harvesting

Two different benchtop centrifuges, Eppendorf 5424R or 5810R (Eppendorf, AG, Germany) were used to harvest algal or bacterial cells when volumes were less than 50 mL. Larger cell cultures (> 50 mL) were harvested using a Sorvall Evolution RC Superspeed centrifuge (Thermo Scientific, Paisley, UK). Typical centrifugation conditions were 5,000 rpm, 30 minutes and 4 °C unless otherwise stated.

2.4.2 Cell disruption

The lysis buffer used to disrupt bacterial cultures comprised of: 20 mM HEPES (pH 7.5), 250 mM NaCl, 10 mM EDTA and one protease inhibitor cocktail tablet (cOmplete™, Mini, EDTA-free (Roche Applied Science, Rotkreuz, Switzerland)). The components of the algal lysis buffer are as followed: 1x PBS (137 mM NaCl, 10 mM Phosphate, 2.7 mM KCl, pH 7.4), 10 mM EDTA, 0.01% (w/v) sodium deoxycholate and one protease inhibitor cocktail tablet.

A Soniprep 150 probe sonicator (MSE, Sanyo, Japan) was also used to break open algal and bacterial cell walls for total protein determination. In order to avoid protein degradation by heat, 10 s on / 10 s off mode was employed. The total sonication time was 100 s unless otherwise stated.

For larger samples, a batch-mode, lab-scale homogeniser with a capacity of approximately 5 mL (Constant Systems, Northants, UK) was also used to disrupt cells. The standard operating conditions included two passes at a pressure of 14 ksi (1,000 bar) unless otherwise stated. Yeast cells expressing K1.K1 were resuspended in lysis buffer (20 mM Tris HCl, 100 mM NaCl, 0.1% Triton X-100, pH = 8.0) and disrupted by the homogeniser. The soluble fraction was separated by centrifugation.

2.4.3 Sucrose gradient ultracentrifugation

Crude protein lysates were cleared by ultracentrifugation (38,000 rpm, 1 h, 4 °C) to pellet cellular debris such as thylakoid membranes (Zborowski and Chalmers, 1988), and then concentrated using Vivaspin® 20 columns (GE Healthcare Life Sciences, Pittsburgh, USA). Alternatively, a double sucrose cushion in ultracentrifugation was also employed to remove impurities (Peyret, 2015). 1 mL 75% (w/v) sucrose solution, 4 mL 20% (w/v) sucrose solution and 7.5 mL crude protein lysate were carefully loaded into Ultra-Clear™ 14x89 mm ultracentrifuge tubes (Beckman Coulter, Krefeld, Germany) sequentially. Ultracentrifugation was performed at 39,000 rpm for 2.5 h at 4 °C in a Beckman SW41Ti rotor (Beckman Coulter, Krefeld, Germany).

Two methods were used to prepare the continuous sucrose gradients. For manual loading, 50%, 30% and 10% (w/v) sucrose solutions were prepared and loaded sequentially into Ultra-Clear™ ultracentrifuge tubes. The tubes were kept vertical and left in the fridge overnight to ensure a linear gradient was formed by diffusion. Alternatively, the continuous sucrose gradients were made by gradually mixing a 10% (w/v) sucrose solution and a 50% (w/v) sucrose solution using a SG15 Gradient Maker (GE Healthcare Life Sciences, Pittsburgh, USA).

2.4.4 Size exclusion chromatography

Size exclusion chromatography was carried out using an ÄKTA pure chromatography system (GE Healthcare Life Sciences, Pittsburgh, USA) fitted with a column packed with Sepharose® CL-4B beads (Sigma-Aldrich, Munich, Germany). These beads have a diameter distribution of 40-165 μm. The UNICON software was used to control the purification process as per the manufacturer's instructions. In brief, the system was washed with Milli-Q® water and equilibrated with the lysis buffer (Section 2.4.1) that was used to re-suspend the protein samples. Then, 2 mL of crude protein lysate was injected into the sample loop using a 5 mL disposable syringe. Elution profiles were monitored by the UV absorbance at a wavelength of 280 nm and 14 elution fractions were collected by an automated fraction collector. Subsequently, the elution fractions were analysed by the western blot as described in Section 2.5.5.

2.4.5 Dialysis and concentration

Protein samples were dialyzed against 50 mM HEPES buffer (pH 7.3) in Slide-A-Lyzer™ Dialysis Cassettes (Thermo Scientific, UK) at 4 °C overnight. The membrane sizes and volumes of the dialysis cassettes varied depending on the application.

Vivaspin® filters (Sartorius, Goettingen, Germany) were used to concentrate protein samples as per the manufacturer's instructions. In brief, Milli-Q® water was used to rinse the membranes first. After discarding the water, protein samples were loaded into

the column and centrifuged at a maximum speed of 4,000 g. The membrane sizes and volumes of the concertation filters varied depending on the application.

2.5 Analytical methods

2.5.1 High performance liquid chromatography

The acetate concentration in the TAP medium was measured using a Dionex high performance liquid chromatography (HPLC) system, the UltiMate 3000 HPLC system (Thermo Fisher, UK). The system was fitted with an Aminex HPX-87H ion-exchange column (Bio-Rad Laboratories, Hertfordshire, UK). 10 mL sample was resolved with a mobile phase of 0.1% (w/v) Trifluoroacetic acid (TFA) at a flow rate of 0.6 mL min^{-1}. The sample signal was monitored with a UV-Vis detector (RefractoMax 520 ERC) controlled by the Chromeleon Chromatography Data System (CDS) software (Thermo Scientific, Paisley, UK). Retention time for acetate was 14.8 minutes. A calibration curve between the acetate concentration and the peak height is shown in Figure 2.2.

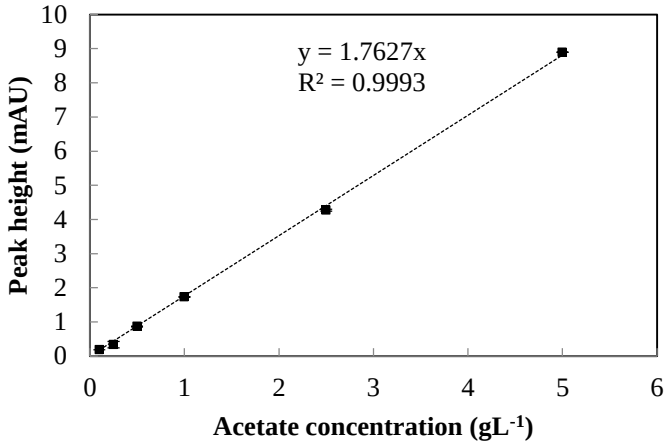

Figure 2.2: Calibration curve between the peak height and acetate concentration from HPLC measurements. Experiments performed as described in Section 2.5.1. Error bars represent the range of the duplicate data points (n=2). Dashed line fitted by linear regression.

2.5.2 Total soluble protein concentration

A microplate method was used to determine the total soluble protein concentration

within *C. reinhardtii*. Algal cells were disrupted either by sonication or homogenization to release the intracellular contents as described in Section 2.4.2. Supernatant was collected after centrifugation (13,000 rpm, 4 °C and 30 mins) and filtered using a syringe filter with a pore size of 0.20 µm. The detergent compatible Bio-Rad protein assay (modified Lowry method) (Bio-Rad Laboratories, Hertfordshire, UK) was used as per the manufacturer's instructions. Briefly, 5µL of protein sample or BSA protein standard was added into the 96 well plate (Sarstedt, Nümbrecht, Germany) followed by the addition of 25 µl Reagent A (with Reagent S) and 200 µl of Reagent B. The plate was gently mixed for 30 seconds and incubated for another 15 minutes. The absorbance (OD_{750nm}) was taken using an Infinite 200 PRO multimode reader (TECAN, Männedorf, Switzerland). The standard curve based on the known concentrations of the standard protein bovine serum albumin (BSA) is shown in Figure 2.3.

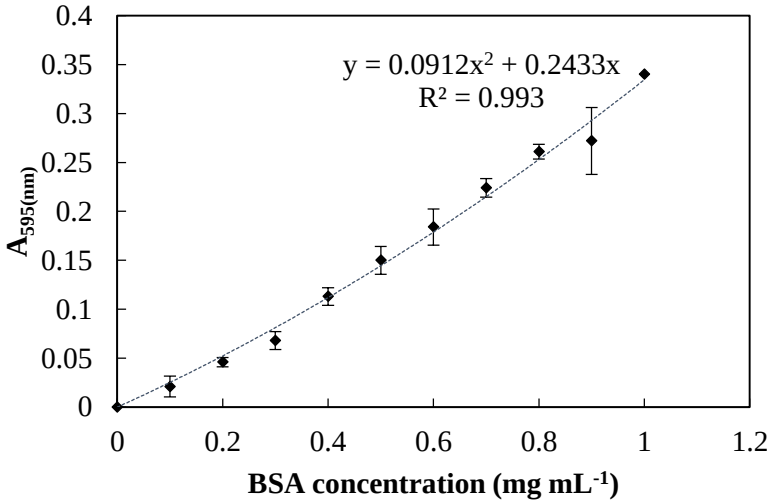

Figure 2.3: The correlation between the BSA concentration and the absorbance at a wavelength of 595 nm. Experiments performed as described in Section 2.5.2. Error bars represent one standard deviation about the mean (n=3). Dashed line fitted by polynomial regression.

2.5.3 Sodium dodecyl sulphate-polyacrylamide gel electrophoresis

SDS-polyacrylamide gel electrophoresis (SDS-PAGE) was used to separate protein samples under denaturing conditions based on their molecular weight. 12% (w/v) pre-cast polyacrylamide gels were run in a Mini-PROTEAN Tetra cell (Bio-Rad Laboratories, Hertfordshire, UK). Dual colour protein loading buffer and reducing

reagent (Lonza, Slough, UK) were added to the protein samples which were standardized either to the same cell density based on OD_{750nm} readings or the same total soluble protein concentrations. The mixture was heated at 99 °C for 10 minutes. Standard running conditions (120 V, 90 mins) in 1X Reservoir buffer were employed unless otherwise stated.

2.5.4 Coomassie® blue staining

A proprietary Coomassie® stain called InstantBlue™ (Expedeon Protein Solutions, Cambridge, UK) was used to stain SDS-PAGE gels as per the manufacturer's instructions. In short, SDS-PAGE gels were washed with Milli-Q® water for five minutes and stained with 10 mL InstantBlue™ solution from 30 minutes to overnight. The staining time varied depending on the particular experiment. Afterwards, gels were rinsed with Milli-Q® water and visualized using the Gel–Doc–it bioimaging system with the Labworks 4.5 software (Bioimaging systems, Cambridge, UK).

2.5.5 Western Blot

Proteins were separated by SDS-PAGE and then transferred onto 0.2 µm nitrocellulose membranes using a semi-dry electro-blotter (Trans-Blot® SD Semi-Dry Transfer Cell, Bio-Rad Laboratories, Hertfordshire, UK) as per the manufacturer's instructions. All transfer materials were soaked in Towbin buffer (Table 2.16) and arranged into the sandwich structure shown in Figure 2.4. Bubbles were rolled out to ensure the conduction of electricity. The electroblotting was run at 12 V for 30 minutes unless otherwise stated.

Table 2.16: Composition of Towbin buffer.

For preparation of 1L Towbin Buffer	Amount	Molar concentration
Tris base	3.0 g	25.0 mM
Glycine	14.4 g	192.0 mM
SDS	1.0 g	3.5 mM
Methanol	200.0 mL	20% (v/v)

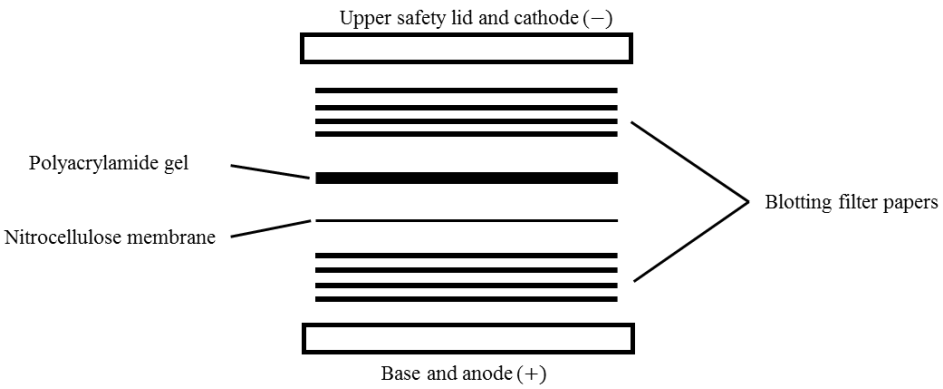

Figure 2.4: Simplified schematic diagram of the semi-dry electro-blotting transfer arrangement.

The membranes were blocked with 0.5% (w/v) skimmed milk in tris-buffered saline-Tween™ 20 (TBS-T) buffer (Table 2.17) at 4 °C overnight to prevent non-specific binding of antibodies to the membranes. After blocking and washing, membranes were probed with different primary antibodies depending on the application as demonstrated in Table 2.18.

Table 2.17: Composition of TBS-T buffer.

For preparation of 1L TBS-T buffer	Amount	Molar concentration
Tris base	2.4 g	20.0 mM
NaCl	8.0 g	137.0 mM
Tween™ 20	1.0 mL	0.1% (v/v)
HCl	Small amount used to adjust buffer to pH 7.6	1.0 M

Table 2.18: Primary antibodies used in this study for western blot analysis.

Primary antibody	Dilution	Species	Supplier (catalogue number)
Polyclonal anti-HA antibody	1: 1,000	Rabbit	Thermo Fisher Scientific (# 71-5500)
Polyclonal anti-HBcAg antibody	1: 8,000	Rabbit	Abcam (ab115992)
Monoclonal anti-HBcAg antibody [10E11]	1: 1,000	Mouse	Thermo Fisher Scientific (# MA1-7608)
Monoclonal anti-HBcAg antibody [14E11]	1: 1,000	Mouse	Thermo Fisher Scientific (# MA1-7610)
Monoclonal anti-Strep® antibody	1: 1,000	Mouse	Sigma-Aldrich (SAB2702216)

After primary antibody incubation, an anti-rabbit or anti-mouse IRDye® secondary antibody (DylightTM 800) was added at 1:20,000 dilution (Li-Cor Biosciences, Cambridge, UK). Then, the membranes were scanned using the Odyssey® Infrared Imaging System (Li-Cor Biosciences, Cambridge, UK). For the Strep-Tactin® detection system, the Strep-Tactin® horseradish peroxidase (HRP) conjugate (IBA Lifesciences, Goettingen, Germany) was used to visualize protein bands.

An Odyssey® Infrared Imaging System with Image Studio™ software (Li-Cor Biosciences, Cambridge, UK) was used for quantitative near-infrared (NIR) fluorescence detection. Rectangles were drawn around each protein band to define the area for quantification. The software automatically subtracts a background from the signal, which is determined as the median of the signal measured in an area of 2 pixels above and below the rectangle. However, the determination of the linear range was necessary before carrying out quantification.

For the electrochemiluminescence (ECL)-based detection method, the membrane was incubated with an anti-rabbit HRP-conjugated secondary antibody (Thermo Fisher Scientific, Paisley, UK) at 1: 10,000 dilution, followed by the SuperSignal® West Pico Chemiluminescence Substrate (Thermo Fisher Scientific, Paisely, UK) for five minutes. Afterwards, the membrane was exposed to a sheet of Hyperfilm ECL (GE Healthcare, Little Chalfont, UK) and the X-ray film was developed by a Xograph automatic film developer (Xograph Healthcare, Gloucestershire, UK) in the dark room. The film development time varied as described in Section 3.2.4.

2.5.6 Negative-stain TEM

Protein samples after buffer-exchange and concentration were spotted onto the carbon-coated copper grids and washed briefly with Milli-Q® water. Then, the grids were stained with 2% (w/v) uranyl acetate for 30-60 seconds and left to dry. The negatively stained samples were examined using a Philips CM120 TEM (Philips, Guilford, UK) and electron micrographs were taken at appropriate magnifications.

2.5.7 Immuno-gold labelling of TEM samples

Around 2 µL protein sample was loaded on to the nickel grid. After incubation for 10 minutes, the grid was washed with three times with TBS buffer (Table 2.19) for 15 minutes in total. Then, the grid was blocked with 10% (w/v) normal goat serum (Thermo Fisher Scientific, Paisley, UK) for 10 minutes. Subsequently, the grid was probed with 1:500 rabbit anti-HBcAg primary antibodies followed by the 1:200 goat anti-rabbit secondary antibodies conjugated with 5 nm gold particles (Abcam, Cambridge, UK). After brief washing in 1×TBS buffer, the grid was observed under the TEM.

Table 2.19: Composition of TBS buffer.

For preparation of 1L TBS-T buffer	Amount	Molar concentration
Tris base	2.4 g	20.0 mM
NaCl	8.0 g	137.0 mM
HCl	Small amount used to adjust buffer to pH 7.6	1.0 M

3 Expression of hepatitis B core antigen in the *C. reinhardtii* chloroplast

3.1 Introduction and aim

As discussed in Section 1.1.1, self-assembled VLPs are attractive and promising vaccine candidates as they are similar to authentic native viruses in terms of structure and antigenicity but are free from infectious viral genetic materials (Grgacic and Anderson, 2006). As a result, a handful of VLP-based vaccines have already been successfully commercialised. Meanwhile, many safe and potent VLP-based vaccine candidates have entered pre-clinical or clinical stages (Roldão *et al.*, 2010). More importantly, some VLPs can serve as particulate carriers which can convey their strong immunogenic properties to linked heterologous antigen epitopes. This can be achieved by either genetic manipulation or chemical conjugation, forming so-called chimeric VLPs (Roose *et al.*, 2013). Such vaccine candidates overcome the problems of heterologous epitopes not possessing optimal immunogenicity or an inability to self-assemble into particulate repetitive forms to elicit strong immune responses (Grgacic and Anderson, 2006; Roldão *et al.*, 2010).

HBcAg is believed to be one of the most promising and well-documented particulate carriers of foreign antigens (Arora *et al.*, 2012; Roose *et al.*, 2013). This is due to the fact that its primary protein sequence can be easily manipulated without damaging its ability to self-assemble into VLPs. Various studies have already demonstrated the ability of HBcAg to accommodate foreign epitopes at either the N-terminus or C-terminus, or into the MIR (Pumpens and Grens, 2001; Filette *et al.*, 2008; Nassal *et al.*, 2008; Arora *et al.*, 2012; Peyret *et al.*, 2015). Schodel *et al.*, (1992) compared these positions for heterologous epitope incorporation and concluded that the MIR is the preferred insertion site in terms of antigen-specific antibody induction. In addition, Arora *et al.*, (2012) have further shown that MIR insertion results in improved immunogenicity and out-performs conventional protein carrier molecules.

Two different symmetries of icosahedral HBcAg VLPs (Figure 1.1) are detectable in the liver of HBV-infected patients (Roose *et al.*, 2013). Not surprisingly, they can also be expressed and assembled outside of their natural contexts in heterologous protein production platforms. These platforms include bacteria, yeast, insect, mammalian and plant expression systems (Burrell *et al.*, 1979; Hirschman *et al.*, 1980; Lanford and Notvall, 1990; Touze *et al.*, 1999; Huang *et al.*, 2006; Freivalds *et al.*, 2011; Peyret *et al.*, 2015). The features of each expression system, together with examples, are described in Section 1.1.4.

The chloroplast of the green alga *C. reinhardtii* has potential as an alternative to conventional protein expression platforms for HBcAg production. Advantages include the absence of viral toxins or human pathogens, cost-effective production and rapid scalability (Stoffels *et al.*, 2017; Dyo and Purton, 2018). Moreover, it is possible to synthesize complex and bioactive protein-based products such as full-length human antibodies, oral vaccine candidates and immunotoxins (Tran *et al.*, 2009, 2013; Demurtas *et al.*, 2013; Specht and Mayfield, 2014). To date, there is only one published work that has exploited *C. reinhardtii* to produce HBcAg-based antigens but this was based on nuclear expression (Soria-Guerra *et al.*, 2013). Not only were the protein levels low (0.02-0.05% (w/w) of TSP), but positional effects of transgene integration were also observed.

The **aim** of the experiments carried out in this chapter was therefore to explore the capability of the *C. reinhardtii* chloroplast as a potential HBcAg production platform. Specific objectives were:

- To express the full-length HBcAg monomer in the *C. reinhardtii* chloroplast;
- To express the truncated HBcAg monomer in the *C. reinhardtii* chloroplast;
- To investigate the stability of the algal-derived HBcAg.

3.2 Expression of the full-length monomer HBc183 in the *C. reinhardtii* chloroplast

3.2.1 *HBc183* gene selection and design

Since no previous work has been carried out to express HBcAg in the *C. reinhardtii* chloroplast, it was sensible to express the unmodified full-length monomer first. Due to the availability of various anti-HBcAg antibodies, epitope tags were not included in the designed protein sequence in order to minimize potential interference with protein expression and capsid formation. With this in mind, the first transgene construct was designed encoding the full-length HBcAg sequence of 183 residues. The amino acid sequence was obtained from the National Centre for Biotechnology Information (NCBI) database (GenBank: AAK62975.1) and reverse-translated into the most likely non-degenerate coding sequence using Bioinformatics software. Then the coding sequence was codon-optimised for expression in the *C. reinhardtii* chloroplast by the CUO software developed in the Purton lab (Table 2.14). Two endonuclease restriction sites SapI and SphI were designed on the 5' and 3'ends of the transgene, respectively. The SapI site was purposely selected as it allows a perfect translational fusion at the ATG of the transgene (Wannathong *et al.*, 2016).

MacVector (MacVector, Inc., USA) was used to perform the simulated digestion and ligation of transgene and pSRSapI to check for the compatibility of sticky ends (Figure 3.1). The next step was to confirm that the codon-optimised gene sequence could be translated back to its original amino acid sequence retrieved from the database. After confirming this using Protein BLAST (NCBI), the optimised transgene was synthesized *de novo* by ATUM (Section 2.2.10) and named *HBc183*. The synthesized *HBc183* gene was inserted into a high copy number plasmid vector (pJ201) carrying a kanamycin resistance gene.

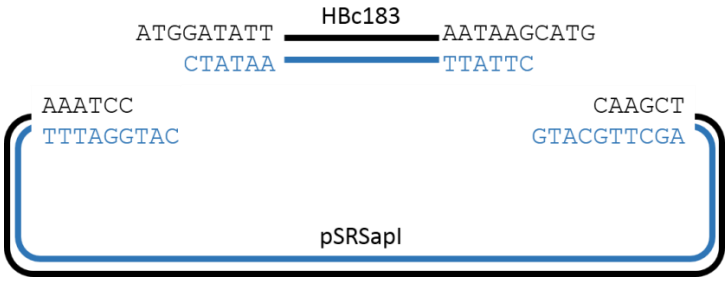

Figure 3.1: Schematic diagram of the sticky-end ligation between the empty algal expression vector pSRSapI and the gene of interest *HBc183*.

3.2.2 Construction of the plasmid pHBc183

Restriction endonuclease digestion of pJ201 and pSRSapI was performed using restriction endonucleases SapI and SphI. In order to test the activities of both enzymes, control reactions with no addition of endonucleases or addition of single enzymes were also carried out. As shown in Figure 3.2, DNA bands of the predicted sizes were seen after double digestion and analysis on an agarose gel.

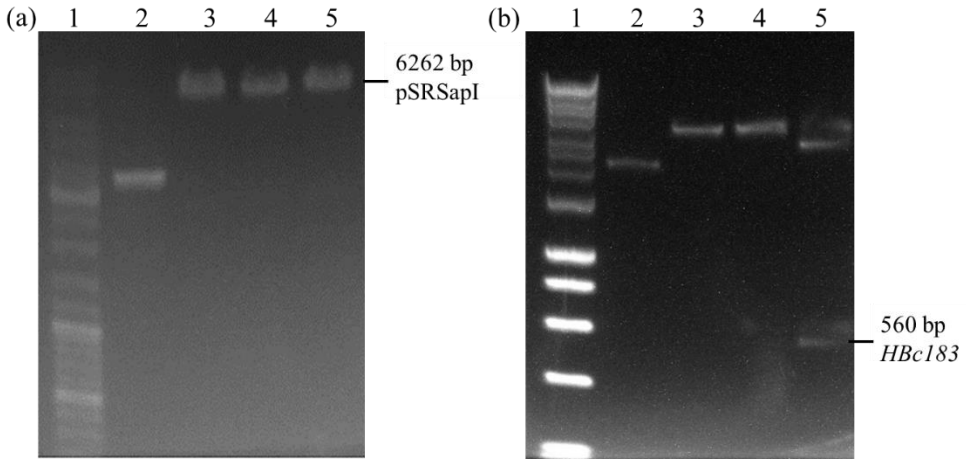

Figure 3.2: Gel electrophoresis to confirm the digestion of (a) pSRSapI and (b) pJ201. Lane 1: GeneRuler DNA Ladder Mix (Thermo Scientific, UK) in (a) and HyperLadder 1kb (Bioline, UK) in (b); Lane 2: no digestion; Lane 3: single digestion with endonuclease SapI; Lane 4: single digestion with endonuclease SphI; Lane 5: double digestion with SapI and SphI. Analysis performed as described in Section 2.2.3 and Section 2.2.5.

After gel extraction (Section 2.2.6), a ligation reaction between the digested plasmid backbone (pSRSapI) and the DNA insert (*HBc183*) was carried out to construct the

plasmid pHBc183 (Figure 3.3). After overnight incubation of *E. coli* transformants at $37°C$, many colonies appeared irrespective of the DNA insert to vector backbone ratios. It was easiest to select single colonies when the ratio between insert to vector was 1:1. Control experiments were also carried out to quantify the level of background caused by un-digested and re-ligated vector backbones (Table 3.1).

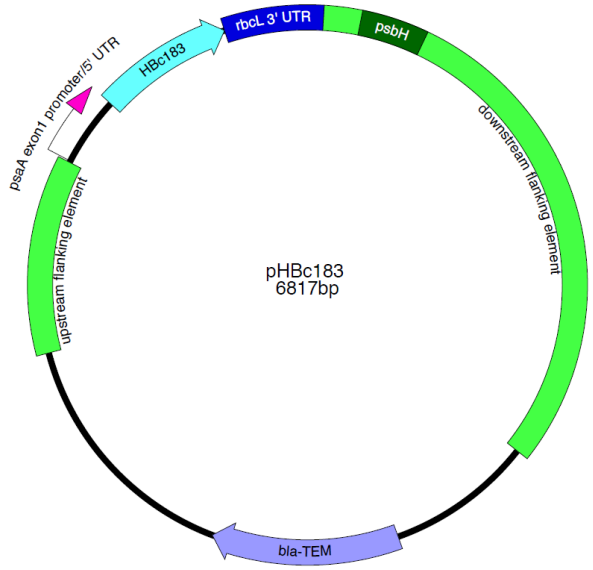

Figure 3.3: Simplified diagram of the algal chloroplast transformation plasmid pHBc183. The *HBc183* gene is placed under the control of the *psaA* promoter/5'UTR and the *rbcL* 3'UTR. Flanking regions indicated upstream and downstream correspond to regions where homologous recombination between the vector and the chloroplast genome occurs.

As shown in Table 3.1 various ligations and transformations were performed for different purposes. The number of colonies in Experiment 4 was almost 10-fold higher than that of Experiment 5. Therefore, re-ligation of vectors was indicated as the main contributor to the background reading. In theory, there is no need to remove the 5' phosphate if sticky end ligation with different restriction sites is carried out (New England BioLabs, UK). However, based on experimental results, dephosphorylation became necessary in order to reduce the background and facilitate colony selection.

Table 3.1: Different ligation conditions and corresponding transformation results. Each ligation mixture was transformed into One Shot® TOP10 chemically competent *E. coli* cells and streaked onto Ampicillin resistant agar plates for transgenic colony selection as described in Section 2.2.8.

Experiment number	Vector (pSRSapI)	Insert (HBc183)	Insert: Vector	T4 DNA ligase	Purpose	Colony number estimation
1	√	√	1:1	√	Quantification of successful ligation products and determination of the most effective vector to insert ratio.	$> 10^5$
2	√	√	3:1	√		$> 10^5$
3	√	√	10:1	√		$> 10^5$
4	√	-	-	√	Quantification of un-digested and re-ligated vectors	~500
5	√	-	-	-	Quantification of un-digested vectors	~50

Therefore, the digested backbone was first treated with AP (Section 2.2.4) before repeating the ligation and transformation procedure. Meanwhile, Experiment 4 was repeated with the dephosphorylated vector to monitor the level of background. As predicted, the number of colonies in Experiment 4 was greatly reduced after dephosphorylation (Figure 3.4).

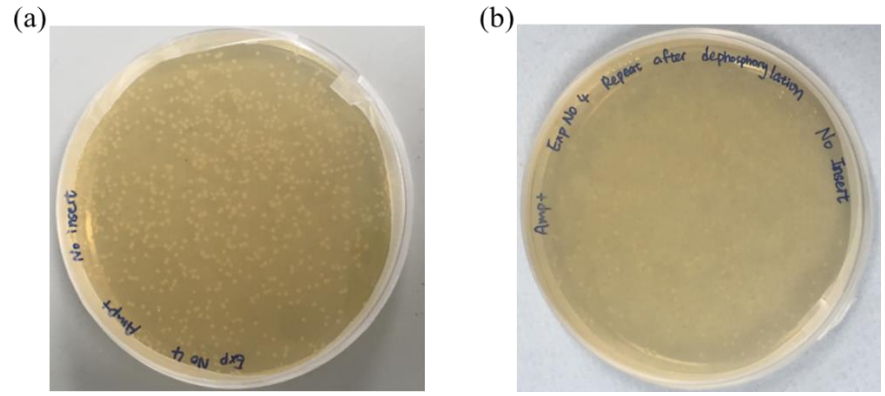

Figure 3.4: Background comparison (a) before dephosphorylation and (b) after dephosphorylation for TOP10 *E. coli* transformation with pHBc183 ligation mix. Experiments performed as described in Section 2.2.8.

After plasmid extraction, DNA samples were sent for sequencing (Section 2.2.10). The forward and reverse primers used were designed within a *psaA* promoter and *rbcL* 3'UTR, respectively. *E. coli* containing the correctly-assembled pHBc183 was preserved as glycerol stocks and a Midiprep of the plasmid was prepared for algal transformation.

3.2.3 Integration of *HBc183* into the chloroplast genome

The chloroplast cloning strategy used throughout this project is illustrated in Figure 3.5. The algal transformation vector pHBc183 described in Section 3.2.2 is designed to introduce the transgene *HBc183* into the chloroplast genome in a neutral site downstream of *psbH* and permit expression under the control of the *psaA* promoter/5'UTR and the *rbcL* 3'UTR. The cell wall-less recipient strain *C. reinhardtii* TN72 carries a mutation in the chloroplast genome where *psbH* gene is replaced by the *aadA* cassette. The absence of the PsbH protein destabilizes the photosystem II complex, leading to the non-photosynthetic phenotype of TN72.

Selection of transformant lines after chloroplast transformation is therefore based on the re-introduction of the wild-type *psbH* gene carried by pHBc183 and the subsequent restoration of prototropy. The use of an endogenous gene like this as the selectable maker eliminates the insertion of a bacterial antibiotic resistance gene into the

chloroplast genome which is beneficial for therapeutic protein production in terms of 'biosafety' (Economou *et al.*, 2014).

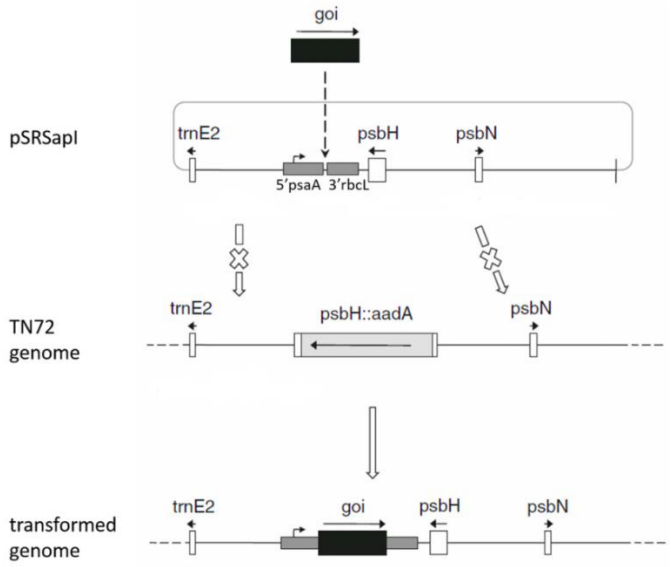

Figure 3.5: Schematic overview of TN72 chloroplast cloning strategy with algal plasmid pSRSapI. Figure modified from Economou *et al.*, (2014).

TN72 *C. reinhardtii* cells were grown to mid-logarithmic phase (approximately 1×10^6 to 2×10^6 cellsmL^{-1}) and transformed using the glass bead agitation method as described in Section 2.2.8. Initially, the transgene *HBc183* is only inserted into several copies of the chloroplast genome. Since the *C. reinhardtii* chloroplast genome has a polyploid nature with around 80 genome copies (Harris, 1989), transformants are usually selected through several rounds of single colony isolation to achieve chloroplast homoplasmy and to obtain stable transformants (Economou *et al.*, 2014). As shown in Figure 3.6, single colonies were first observed after four weeks of incubation and were re-streaked onto selective plates.

Three transgenic lines were isolated and screened by PCR analysis for correct transgene integration and plastome homoplasmy as illustrated in Figure 3.7. For transgene verification, an amplicon of around 950 bp was expected due to the forward and reverse primers designed to the *psaA* promoter and *rbcL* 3' UTR regions, respectively. The *HBc183* gene sequence was further confirmed by sequencing (Section 2.2.10). As for

the homoplasmy check, a band of 850 bp is expected for the TN72 recipient genome with a disruptive *psbH* gene (−). In contrast, TN72 transformant genome copies with an intact *psbH* should generate a product of 1135 bp (+). Successful transformation of TN72 with pHBc183 should therefore give rise to a band of 1135 bp, matching that of the positive control. The absence of any detectable 850 bp band indicates the homoplasmy of chloroplast genomes. These homoplasmic transgenic lines were named TN72_HBc183_T1-T3.

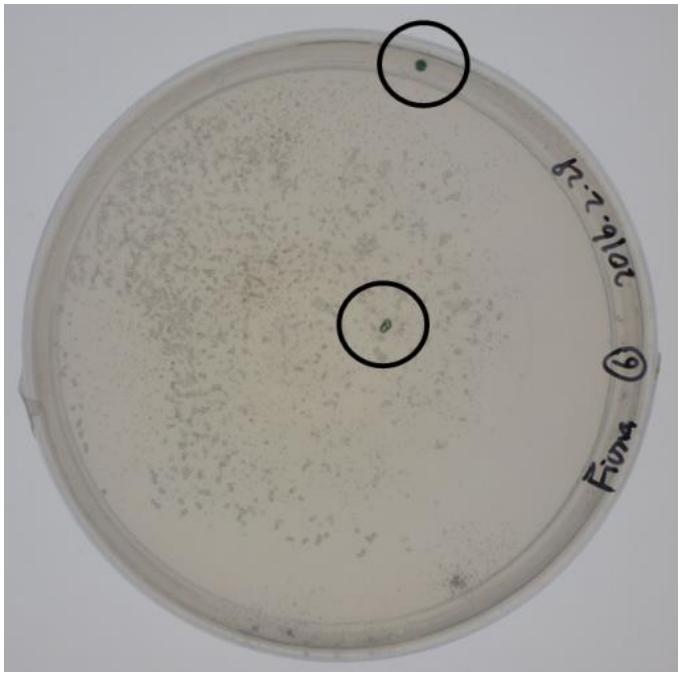

Figure 3.6: First colonies of *C. reinhardtii* transformants appearing on HSM plates four weeks after chloroplast transformation. Experiments performed as described in Section 2.2.8.

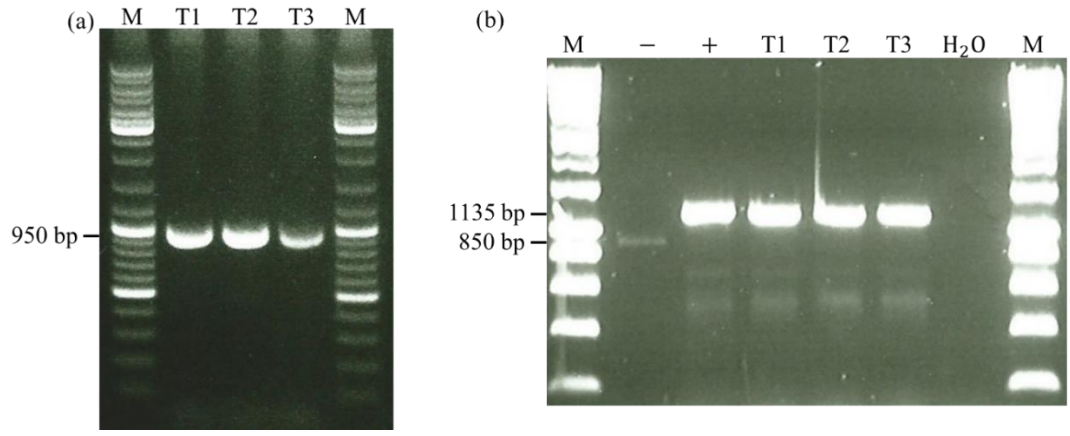

Figure 3.7: Gel electrophoresis of colony PRC products to verify (a) the integration of *HBc183* gene into the chloroplast genome and (b) the homoplasmy of the chloroplast genome in three transgenic lines (T1-T3). M: HyperLadder 1kb (Bioline, UK); −: TN72 was used as the negative control; +: TN72 transformed with the empty pASapI vector (TNE) was the positive control; H_2O served as the negative control for the PCR reactions. Analysis performed as described in Section 2.2.2 and Section 2.2.5.

3.2.4 Expression of *HBc183* in the *C. reinhardtii* chloroplast

ECL-based western blot analysis was carried out to examine the expression of HBc183 in the *C. reinhardtii* chloroplasts. A preliminary analysis with rabbit anti-HBcAg polyclonal antibodies (PA5-16368) (Table 2.16) did not reveal any signal even for the positive control, which was the purified full-length HBcAg monomer (21 kDa) produced in *E. coli* (OBT0909) (BIO-RAD, UK). As a result, the western blot protocol was modified in terms of protein concentration, primary antibody incubation time and X-ray film development time. Only positive controls were loaded in this analysis. As shown in Figure 3.8, strong bands for the *E. coli*-produced positive control were clearly revealed without significant differences under all conditions. Therefore, the conditions with the lowest protein loading concentration (1050 ng), shorter primary antibody incubation time (two hours) and shorter film exposure time (30 s) were selected for subsequent investigations.

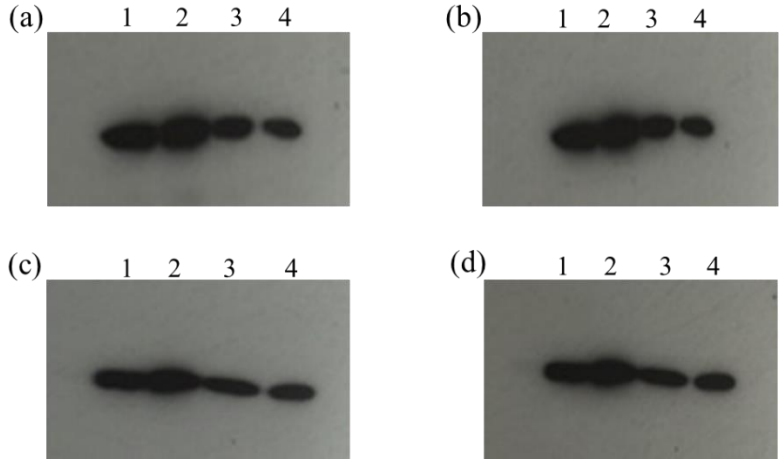

Figure 3.8: Western blot analysis of *E. coli*-produced full-length HBcAg probed with rabbit anti-HBcAg polyclonal antibodies in terms of different primary antibody incubation time, protein concentration and X-ray film development time. (a) 2 hours incubation of primary antibody, 1minute film exposure; (b) 2 hours incubation of primary antibody, 2 minutes film exposure; (c) 4 hours incubation of primary antibody, 30 seconds film exposure; (d) 4 hours incubation of primary antibody, 1 minute film exposure. Reference protein loading amount: 1. 1050 ng; 2. 1400 ng; 3. 1750 ng; 4. 1960 ng. Experiments performed as described in Section 2.5.5.

Based on the above conditions, different dilutions of rabbit anti-HBcAg polyclonal antibodies and two types of blocking buffers were further tested. As demonstrated in Figure 3.9, no bands were revealed for the algal-produced HBc183 (21 kDa) (Lane 2 to 4) except for the positive controls (Lane 1) under all conditions. Moreover, two anti-HBcAg monoclonal antibodies [10E11] and [14E11] (Thermo Scientific, UK), which recognise the regions 1-10 a.a. and 138-145 a.a. on HBcAg, respectively, were also tested with the algal samples. However, the expected band of HBc183 was not detected under any of these conditions. Despite the confirmation of transgene insertion and plastome homoplasmy, it is suggested that the HBc183 expression level was probably below the detection limit of the various anti-HBcAg antibodies.

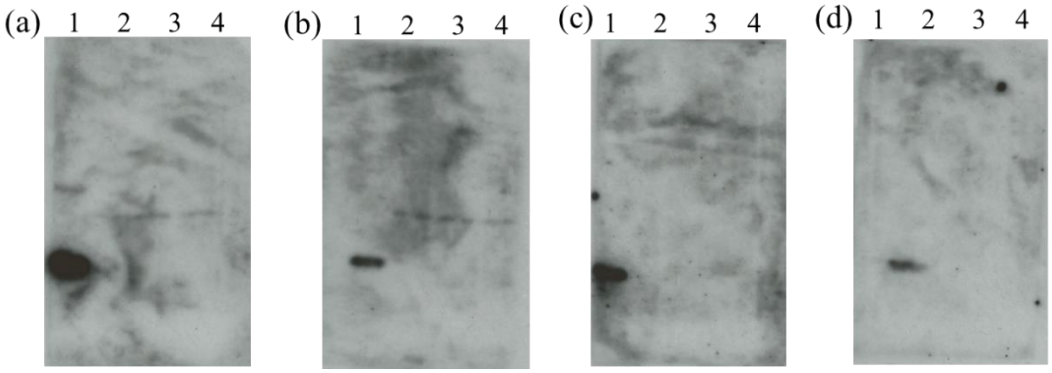

Figure 3.9: Western blot analysis of *E. coli*-based full-length HBcAg (Lane 1) and algal crude extracts (Lane 2-4) probed with rabbit anti-HBcAg polyclonal antibodies in terms of different primary antibody concentrations and different types of blocking solution. (a) 1:2000 dilution primary antibody, 1% (w/v) BSA blocking solution; (b) 1:8000 dilution primary antibody, 1% (w/v) BSA blocking solution; (c) 1:2000 dilution primary antibody, non-protein blocking buffer; (d) 1:8000 dilution primary antibody, non-protein blocking buffer; Reference protein loading amount: 1. 1050 ng. Experiments performed as described in Section 2.5.5.

3.2.5 Summary

The chloroplast expression vector pHBc183 containing the codon-optimised full-length HBcAg transgene *HBc183* has been successfully assembled and introduced into the *C. reinhardtii* TN72 chloroplast genome. Despite the confirmation of transgene insertion and plastome homoplasmy, it was not possible to confirm the expression of *HBc183* by western blot analysis using different anti-HBcAg antibodies under various conditions. The expression level of *HBc183* was probably below the detection limit of the tested anti-HBcAg antibodies, implying the necessity to improve the protein accumulation level and to include a short epitope tag for improved detection. Nevertheless, the molecular biology techniques established in this section served as the essential preparatory work towards the successful expression of HBcAg in the chloroplast of *C. reinhardtii*.

3.3 Expression of the truncated monomer HBc150_Strep in the *C. reinhardtii* chloroplast

Due to the inconclusive Western blot results obtained in Section 3.2.4, two strategies are proposed in Section 3.3.1 and Section 3.3.2 in order to achieve the synthesis of HBcAg in the *C. reinhardtii* chloroplast. First, the manipulation of the primary amino acid sequence of HBcAg was considered to improve heterologous protein expression level. Second, the inclusion of a short affinity tag was explored to facilitate protein detection.

3.3.1 Manipulation of the amino acid sequence of HBcAg to improve protein expression

As discussed in Section 1.1.1, the full-length HBcAg monomer is composed of two domains; the N-terminal assembly domain (1-140 a.a.) and the C-terminal protamine domain (150-183 a.a.). Previous studies have proved that the N-terminal assembly domain is necessary but also sufficient for monomer dimerization and subsequent capsid formation (Böttcher *et al.*, 1997; Wynne *et al.*, 1999). In fact, the truncated version (1-149 a.a.) has been utilized to study capsid dissociation, protein encapsulation and sequence plasticity (Wooi and Siang, 2008; Lu *et al.*, 2015). Moreover, it has been suggested that there is a substantial increase in HBcAg accumulation levels when expressing truncated monomers compared to full-length monomers in bacterial expression systems (Stahl and Murray, 1989; Tan *et al.*, 2003, 2007; Peyret *et al.*, 2015).

However, it is suspected that HBcAg stability, as evidenced by the thermal stability and capsid assembly integrity, is reduced in the absence of the C-terminal protamine domain (Vogel *et al.*, 2005; Sominskaya *et al.*, 2013). This is mainly due to intermolecular disulphide bond formation between C-terminal cysteine residues (183 a.a) (Vogel *et al.*, 2005) and the encapsulation of nucleic acids by the C-terminal protamine domain (Sominskaya *et al.*, 2013). Therefore, the stability of the truncated HBcAg may be partially restored through adding a Cysteine residue at the C-terminus to increase the degree of disulphide cross-linking (Schodel *et al.*, 1992; Vogel *et al.*, 2005).

Furthermore, Apel et al. (2010) have pointed out the significance of the penultimate N-terminal amino acid residue (i.e. coding position +2) on heterologous protein stability in tobacco chloroplasts. The expression of a reporter protein GFP was compared when the penultimate N-terminal amino acid residue was mutated into 20 different amino acids. It was concluded that GFP accumulated to the highest levels in the Glutamic acid, Methionine and Valine transgenic lines. In addition, Valine at the penultimate N-terminal position conferred stability in both *E. coli* and tobacco chloroplasts (Apel *et al.*, 2010). Despite the absence of similar work published for the *C. reinhardtii* chloroplast, both plastids are similar in terms of genome arrangement, transcription and translation machineries (Lisitsky *et al.*, 2001). Since the original penultimate N-terminal amino acid residue of HBcAg is aspartic acid, an additional amino acid residue, Valine (V), was inserted before the aspartic acid. This was hypothesized to increase the stability of heterologous protein accumulation in the microalgal chloroplast (Apel *et al.*, 2010).

3.3.2 Design of short affinity tags to facilitate HBcAg detection

Despite the availability of various anti-HBcAg antibodies, it was still useful to include a well-established short affinity tag to facilitate protein detection. The most widely-used short affinity tags include poly-His-, FLAG-, HA- and Strep II-tags (Terpe, 2003). The choice of the affinity tag mainly depends upon the nature of the target protein, the expression system and the application of the heterologous protein (Terpe, 2003; Wood, 2014).

Despite the prevalent use of poly-His-tag fused with HBcAg, inhibitory effects on protein expression have been observed when using this tag in transgenic microalgal chloroplasts (Demurtas *et al.*, 2013). Among the different affinity tags, Strep-tag®II allows sensitive detection as the interaction between streptavidin and biotin is the strongest non-covalent biological interaction known (Schmidt *et al.*, 2013). It also enables inexpensive purification compared to several other short affinity tags such as FLAG-tag and HA-tag. Twin-Strep-tag® consisting of two Strep-tag®II sequences

(SAWSHPQFEK) in series was used in this study to further increase the chance of signal detection (Schmidt *et al.*, 2013).

The insertion position for such affinity tag depends on the structure of the protein of interest. As mentioned in Section 3.1, HBcAg possesses great structural flexibility in terms of incorporating foreign epitopes into either the N-terminus or C-terminus or into the MIR (Filette *et al.*, 2008; Nassal *et al.*, 2008; Arora *et al.*, 2012; Peyret *et al.*, 2015). Both Schodel et al. (1992) and Arora et al. (2012) have concluded that the MIR is the preferred position for heterologous epitope incorporation with much higher antigen-specific antibody induction. Therefore, the Twin-Strep-tag® was incorporated into the MIR region of the truncated HBcAg monomer.

3.3.3 *HBc150_Strep* gene selection and design

Based on the above considerations, a Twin-Strep-tag® with a linker (SAWSHPQFEKGGGSGGGSGGSAWSHPQFEK) was included and inserted into the major immune-dominant region (82-83 a.a.) of the truncated monomer (1-149 a.a) (GenBank: ABI31779.1). Two unique restriction (NcoI and EcoRI) sites were designed on both sides of the Twin-strep tag to facilitate the cloning of other epitopes into MIR in the future. A Cysteine residue was added at the C-terminus to stabilize the truncated HBc monomer The designed sequence also incorporated an additional penultimate N-terminal amino acid residue, Valine, that was hypothesized to increase the stability of heterologous protein accumulation in the microalgal chloroplasts (Apel *et al.*, 2010). The peptide sequence representing the above design was codon-optimised for expression in the *C. reinhardtii* chloroplast using the CUO software. As explained in Section 3.2.1, SapI and SphI restriction sites were designed on the 5' and 3' ends, respectively, to allow insertion into the algal chloroplast expression vector pSRSapI (Wannathong *et al.*, 2016). The transgene sequence was synthesized *de novo* by ATUM (Section 2.2.10) and named *HBc150_Strep*. The synthesized *HBc150_Strep* gene was inserted into a high copy number plasmid (pJ241) carrying kanamycin resistance.

3.3.4 Construction of the plasmid pHBc150_Strep

All experimental procedures including digestion, dephosphorylation, ligation and sequencing were carried out using protocols established in Section 3.2.1. As shown in Figure 3.10, DNA gel electrophoresis yielded the expected bands following double digestion with SapI and SphI: pSRSapI (6262 bp) and *HBc150_Strep* (582 bp). Figure 3.11 illustrates the simplified diagram of the chloroplast transformation plasmid pSRSapI containing the *HBc150_Strep* transgene, named pHBc150_Strep. After confirmation by DNA sequencing, a Midiprep of pHBc150_Strep was prepared for algal transformation.

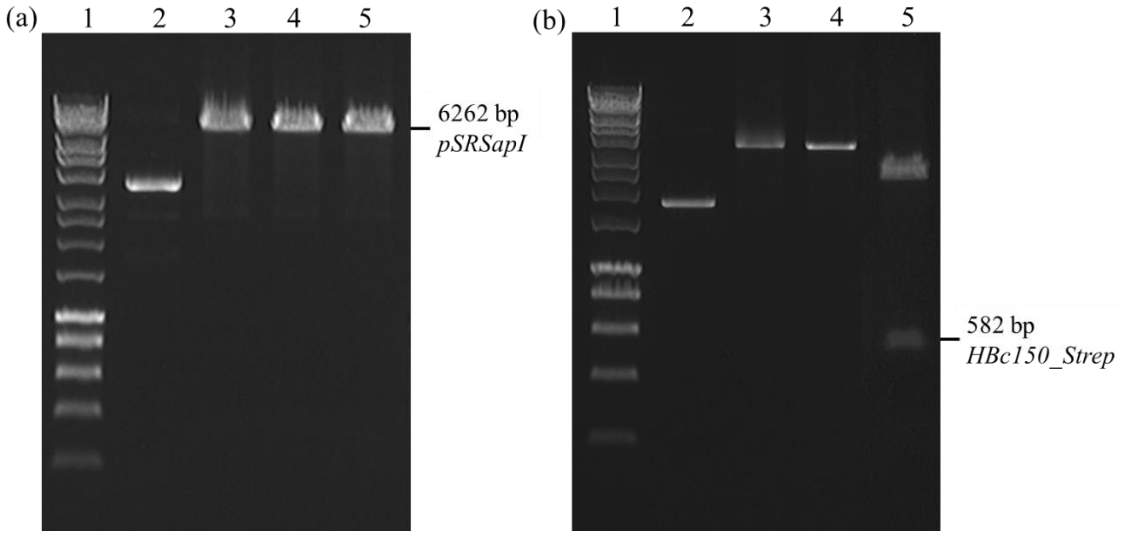

Figure 3.10: Gel electrophoresis to confirm the digestion of pSRSapI (a) and pJ241 (b). Lane 1: GeneRuler DNA Ladder Mix (Thermo Scientific, UK); Lane 2: no digestion; Lane 3: single digestion with endonuclease SapI; Lane 4: single digestion with endonuclease SphI; Lane 5: double digestion with SapI and SphI. Analysis performed as described in Section 2.2.3 and Section 2.2.5.

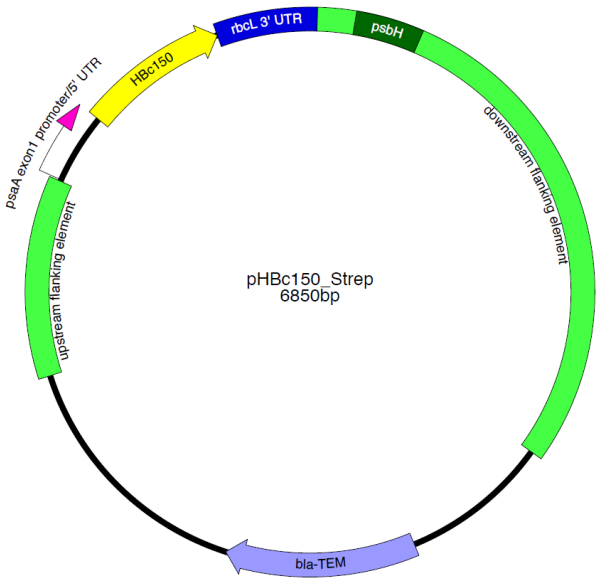

Figure 3.11: Simplified diagram of the chloroplast transformation plasmid pHBc150_Strep. *HBc150_Strep* gene is placed under the control of the *psaA* exon 1 promoter/5'UTR and the *rbcL* 3'UTR. Flanking regions indicated upstream and downstream correspond to regions where homologous recombination between the vector and the chloroplast genome occurs.

3.3.5 Integration of *HBc150_Strep* into the chloroplast genome

The detailed transformation strategy and glass bead method were explained in Section 3.1.1 and Section 2.2.8, respectively. As shown in Figure 3.5, the transgene was introduced in the intergenic region (*trnE2-psbH*) of the chloroplast genome, with transformant selection based on the restoration of the *psbH* gene and hence rescue of prototropy in the non-photosynthetic strain, TN72. HSM plates and light were therefore used as the driving force to recover transformants. After incubation in the light for four weeks, five colonies were isolated and re-streaked onto HSM agar plates several times to achieve plastome homoplasmy.

The insertion of the *HBc150_Strep* gene was confirmed in three transgenic lines (T1-T3) by colony PCR. Primers were designed to the *psaA* promoter and 3' UTR regions such that a PCR product of 1000 bp was expected (Figure 3.12 (a)). The sequence of *HBc150_Strep* was further confirmed by sequencing the PCR product (Source Bioscience, UK). As before, the homoplasmy check was based on the absence of the

850 bp band obtained for the TN72 plastome with a disruptive *psbH* gene (−ve), whereas a transformant plastome with an intact *psbH* should generate a product of 1135 bp (+ve). Successful transformation of TN72 with the plasmid pHBc150_Strep should therefore give rise to an 1135 bp band as seen in Figure 3.12 (b). The absence of any detectable 850 bp bands strongly indicated the homoplasmy of chloroplast genomes. These homoplasmic transgenic lines were named TN72_HBc150_Strep_T1-T3.

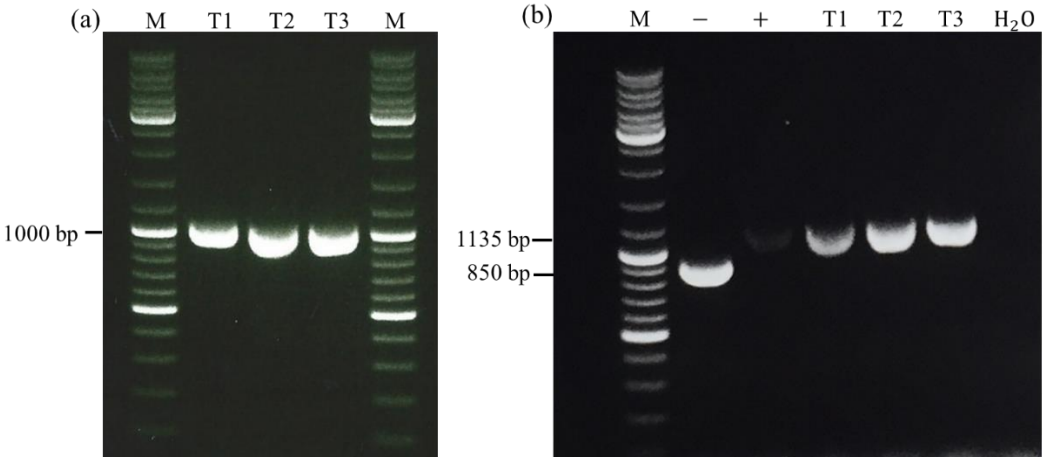

Figure 3.12: Gel electrophoresis of colony PRC products to verify (a) the integration of *HBc150_Strep* gene into the chloroplast genome and (b) the homoplasmy of the chloroplast genome in three transgenic lines (T1-T3). M: HyperLadder 1kb (Bioline, UK); −: TN72 genome was the negative control; +: TNE genome was the positive control; H_2O served as the negative control of PCR reactions. Analysis performed as described in Section 2.2.2 and Section 2.2.5.

3.3.6 Expression of *HBc150_Strep* in the *C. reinhardtii* chloroplast

The size of the truncated HBcAg monomer (1-150 a.a) is approximately 16.7 kDa with a 3 kDa Twin-Strep-tag® (Schmidt *et al.*, 2013). Therefore, the expected size of HBc150_Strep is around 20 kDa. First, western blot analysis was carried using the Strep-Tactin®-HRP conjugate. As demonstrated in Figure 3.13, no clear bands corresponding to the size of HBc150_Strep were detected when using the Strep-Tactin® detection system. However, at least four non-specific bands ranging from 25 kDa to 40 kDa were observed in all samples including the negative control. The noisy background was probably due to the use of direct interaction of proteins with the Strep-Tactin®

system. Therefore, western blot analysis with monoclonal anti-Strep antibodies (Table 2.18) was also carried out to examine *HBc150_Strep* expression and to reduce non-specific bands.

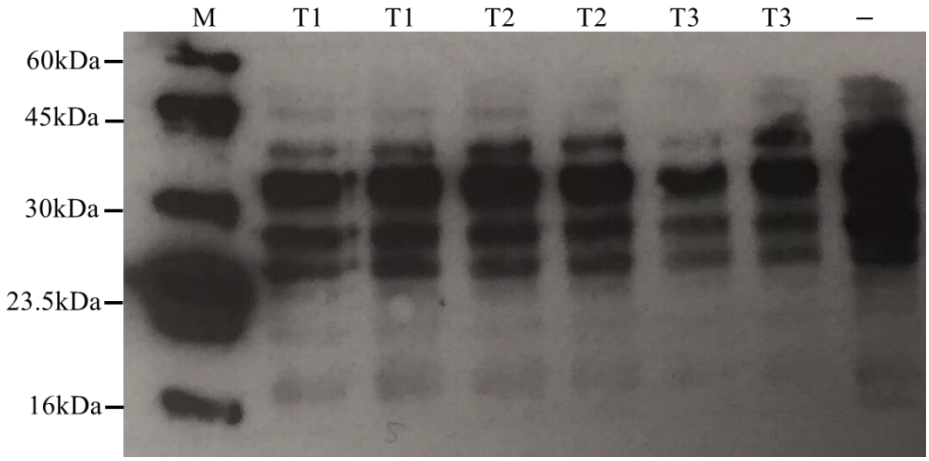

Figure 3.13: Western blot analysis using Strep-Tactin® conjugates in three transgenic lines (T1-T3). –: TNE was the negative control; M: IBA Lifesciences™ Strep-Tag Protein Ladder (16 kDa to 100 kDa) (IBA Lifesciences, Germany). Analysis performed as described in Section 2.5.5.

Figure 3.14 demonstrates the western blot results probed with monoclonal anti-Strep antibodies. Despite the reduction of non-specific bands, it was still not possible to detect a 20 kDa band that would correspond to HBc150_Strep. Only a non-specific protein band (32 kDa) was detected in all samples, which serves as a loading control. As seen in Section 3.2.4, despite the confirmation of transgene insertion and plastome homoplasmy, it is suggested that the HBc150_Strep expression level was probably still below the detection limit of either the Strep-Tactin® conjugates or the monoclonal anti-Strep antibodies.

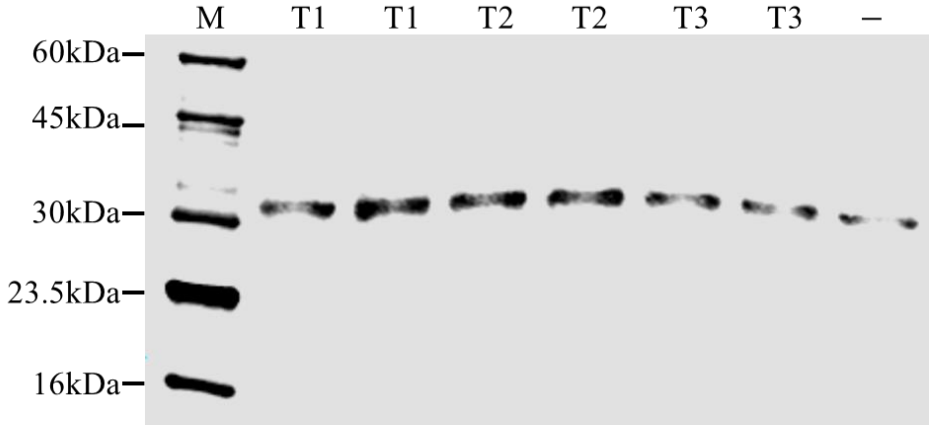

Figure 3.14: Western blot analysis using monoclonal anti-Strep antibodies in three transgenic lines (T1-T3). TNE was the negative control. −: TNE was the negative control; M: IBA Lifesciences™ Strep-Tag Protein Ladder (16 kDa to 100 kDa) (IBA Lifesciences, Germany). Analysis performed as described in Section 2.5.5.

3.3.7 Summary

The transgene *HBc150_Strep* encoding the truncated HBcAg monomer with a Twin-Strep-tag on its MIR has been designed and codon-optimised to match that of the *C. reinhardtii* chloroplast codon usage. The chloroplast expression vector pHBc150_Strep® containing *HBc150_Strep* has been successfully assembled and introduced into the *C. reinhardtii* TN72 chloroplast genome. Despite the confirmation of transgene insertion and plastome homoplasmy in three transgenic lines, it was not possible to confirm the expression of HBc150_Strep by western blot analysis using either the Strep-Tactin® HRP conjugates or the monoclonal anti-Strep antibodies. It is believed that the expression level of HBc150_Strep was below the detection limit of both detection systems. In order to address these issues regarding the expression of HBcAg in the microalgal chloroplasts, a third construct representing the truncated monomer with a HA-tag was investigated in Section 3.4.

3.4 Expression of the truncated monomer HBc150_HA in the *C. reinhardtii* chloroplast

HBcAg possesses great structural flexibility in terms of incorporating foreign epitopes into either N-terminus or C-terminus or into the MIR (Filette *et al.*, 2008; Nassal *et al.*, 2008; Arora *et al.*, 2012; Peyret *et al.*, 2015). Apart from the MIR position, several studies have fused a poly-His-tag onto either the N-terminus or C-terminus of HBcAg to facilitate protein detection and purification when using bacterial expression systems (Tan *et al.*, 2007; Nassal *et al.*, 2008; Wooi and Siang, 2008). It should be noted that Wooi & Siang (2008) have demonstrated that adding a poly-His-tag at the N-terminus of HBcAg does not impede capsid assembly or impair its strong antigenicity. Apart from protein detection, N-terminal poly-His-tag allows native HBcAg purification because its N-terminus tends to protrude out from the capsid surface compared to the buried C-terminus (Vogel *et al.*, 2005; Tan *et al.*, 2007). Therefore, the N-terminus was chosen as another alternative position in which to insert affinity tags in this study.

Despite the prevalent use of poly-His-tag when expressing HBcAg, an inhibitory effect of this tag on *C. reinhardtii* chloroplast expression has been reported in Demurtas et al. (2013). Since the hemagglutinin epitope (HA-tag) derived from the influenza A virus (Schembri *et al.*, 2007) is widely used for fusion protein production in the *C. reinhardtii* chloroplasts in the Purton lab and is similar to that of poly-His-tag in terms of length and function, an N-terminal HA-tag was chosen for this design.

3.4.1 *HBc150_HA* gene selection and design

With the previous findings in mind, the amino acid sequence comprising the truncated HBcAg (1-149 a.a.) (GenBank: ABI31779.1) with the addition of a HA-tag (YPYDVPDYA) and a spacer (GGGGG) at the N-terminus and a Cysteine residue at C-terminus to stabilize the truncated form of HBcAg (Schodel et al. 1992) was designed. It also incorporated an additional penultimate N-terminal amino acid residue, Valine, that was hypothesized to increase the stability of heterologous protein accumulation in the microalgal chloroplasts (Apel *et al.*, 2010). The peptide sequence representing the

above design was codon-optimised for expression in the *C. reinhardtii* chloroplast using the CUO software. As explained in Section 3.1.1, SapI and SphI restriction sites were designed on the 5' and 3' ends, respectively, to allow insertion into the algal chloroplast expression vector pSRSapI (Wannathong *et al.*, 2016). The transgene sequence was synthesized *de novo* by ATUM (Section 2.2.10) and named as *HBc150_HA*. The synthesized *HBc150_HA* gene was inserted into a high copy number plasmid (pJ241) with kanamycin resistance.

3.4.2 Construction of the plasmid pHBc150_HA

All experimental procedures including digestion, dephosphorylation, ligation and sequencing were carried out in the same way as explained in Section 3.2.1. As shown in Figure 3.15, DNA gel electrophoresis results demonstrated correct bands corresponding to pSRSapI (6262 bp) and *HBc150_HA* (506 bp) by double endonuclease digestion (SphI and SapI). Figure 3.16 presents a simplified diagram of the assembled chloroplast transformation plasmid pHBc150_HA containing the correct GOI. After sequence confirmation, a Midiprep of the plasmid pHBc150_HA was prepared for algal transformation.

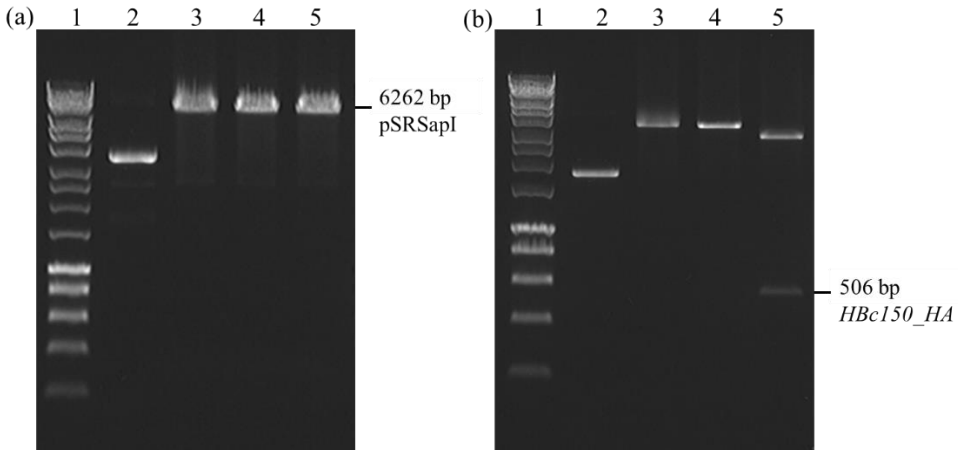

Figure 3.15: Gel electrophoresis to confirm the digestion of pSRSapI (a) and pJ241 (b). Lane 1: GeneRuler DNA Ladder Mix in (a) and HyperLadder 1kb in (b); Lane 2: no digestion; Lane 3: single digestion with endonuclease SapI; Lane 4: single digestion with endonuclease SphI; Lane 5: double digestion with SapI and SphI. Analysis performed as described in Section 2.2.3 and Section 2.2.5.

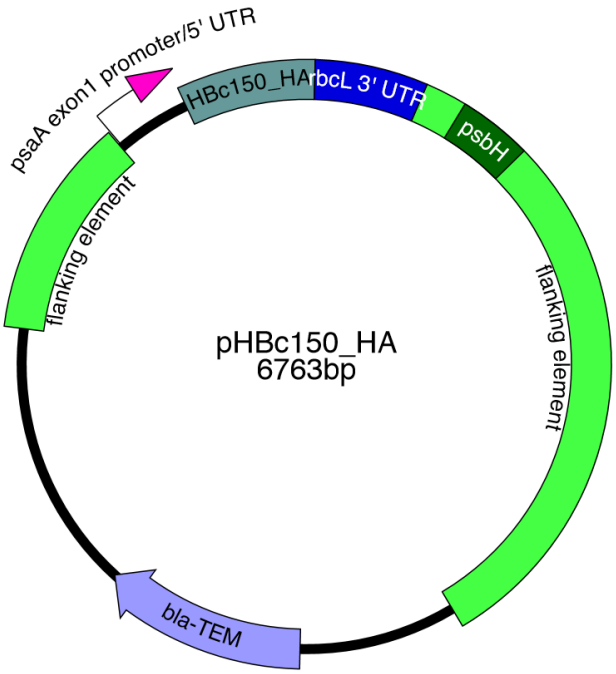

Figure 3.16: Simplified diagram of the chloroplast transformation plasmid pHBc150_HA. *HBc150_HA* gene is placed under the control of the *C. reinhardtii psaA* promoter/5'UTR and the *rbcL* 3'UTR. Flanking regions indicated upstream and downstream correspond to regions where homologous recombination between the vector and the chloroplast genome occurs.

3.4.3 Integration of *HBc150_HA* into the chloroplast genome

The details of the transformation strategy and glass bead transformation method used were exactly as used in Section 2.2.8. After incubation in the light for four weeks, five colonies were isolated and re-streaked onto HSM agar plates to achieve plastome homoplasmy.

The *HBc150_HA* gene was amplified by colony PCR in five transgenic lines (T1-T5). Primers were designed to the *psaA* promoter and 3' UTR regions in which an amplicon of around 900 bp was expected. The integrity of the gene construct was further confirmed by DNA sequencing (Section 2.2.10). As for the homoplasmy check, a band of 850 bp was seen for the TN72 recipient strain. In contrast, transformant lines gave a band of 1135 bp as shown in Figure 3.17. As before, the absence of any detectable 850 bp band strongly indicated the homoplasmy of the transformant plastomes. These

transgenic lines were named TN72_HBc150_HA_T1-T5 and TN72_HBc150_HA_T3 is later referred to as the *psaA* transformant strain in Chapter 4.

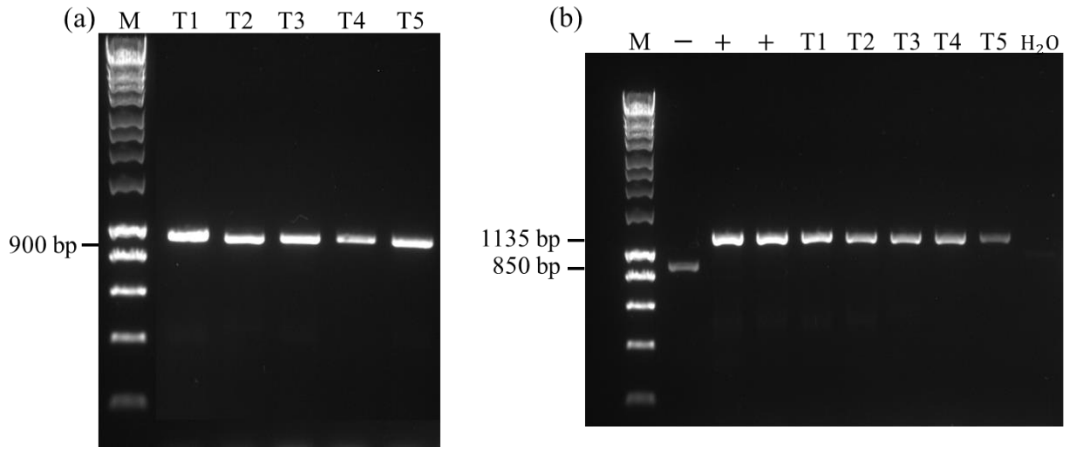

Figure 3.17: Gel electrophoresis of colony PRC products to verify (a) the integration of *HBc150_HA* gene into the chloroplast genome and (b) the homoplasmy of the chloroplast genome in five transgenic lines (T1-T5). M: HyperLadder 1kb (Bioline, UK); H_2O served as the negative control of PCR reactions. Analysis performed as described in Section 2.2.2 and Section 2.2.5.

3.4.4 Expression of *HBc150_HA* in the *C. reinhardtii* chloroplast

The size of the truncated HBcAg monomer is approximately 16.7 kDa with a 1.2 kDa HA-tag attached on its N-terminus (Lu *et al.*, 2015). Therefore, a protein band of approximately 18 kDa would be expected in western blot analysis using anti-HA antibodies. As shown in Figure 3.18, all transformant lines (T1-T5) generated a band at 18 kDa, in agreement with the predicted size for HBc150_HA. In addition, no protein band at 18 kDa was observed for TNE which served as the negative control. Therefore, the western blot results confirmed the expression of the truncated HBcAg monomer in the *C. reinhardtii* chloroplast.

The expression levels of HBc150_HA differed, however, in the five transgenic lines when quantifying the infrared signals on the nitrocellulose membrane. In theory, all transformants should have identical genetic background if chloroplast transformation is preceded by homologous recombination (Surzycki *et al.*, 2009). T3 (the *psaA*

transformant strain) with the highest HBc150_HA expression level was chosen as the representative transgenic line for subsequent studies.

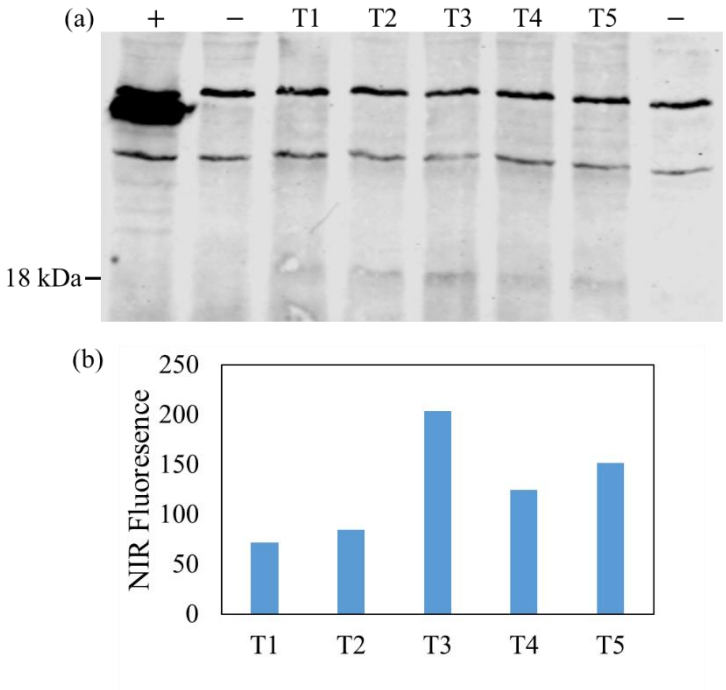

Figure 3.18: Accumulation and quantification of HBc150_HA expression in five transgenic lines (T1-T5). (a) Accumulation of HBc150_HA in five transgenic lines (T1-T5). HA-tagged Pal was the positive control and crude protein extracts from TNE was the negative control. Non-specific bands (25 kDa and 40 kDa) served as a loading control. (b) Relative quantification of HBc150_HA in five transgenic lines by near-infrared (NIR) signal in Odyssey® Infrared Imaging System (Li-Cor Biosciences, UK). Experiments performed as described in Section 2.5.5.

3.4.5 Detection of HBc150_HA by different antibodies

In order to verify the immunoreactivity of the HBc150_HA, rabbit anti-HBcAg polyclonal antibodies were used in comparison to the anti-HA antibodies in western analysis of the algal extracts. The same crude protein samples at different harvest time points were loaded onto an SDS-polyacrylamide gel and transferred to the same membrane. The membrane was divided into two and incubated with anti-HA antibodies and anti-HBcAg antibodies, respectively. Suitable dilutions of both antibodies were examined in Section 3.2.4 and Section 3.4.4, respectively.

As illustrated in Figure 3.19, protein bands corresponding to HBc150_HA (18 kDa) were clearly shown on the left panel probed with anti-HA antibodies (a) but not for the right panel probed with anti-HBcAg antibodies (b). This has demonstrated that anti-HA antibodies were more sensitive in terms of recognizing the HA-tag on the algal-expressed HBc150_HA than that of the anti-HBcAg antibodies. However, the specificity of the anti-HA antibodies was lower as several non-specific bands are seen in the blots as opposed to the anti-HBcAg antibodies. Nonetheless, increasing protein expression level would be a sensible way to increase the chance of detection by anti-HBcAg antibodies and to confirm the immunoreactivity of HBc150_HA.

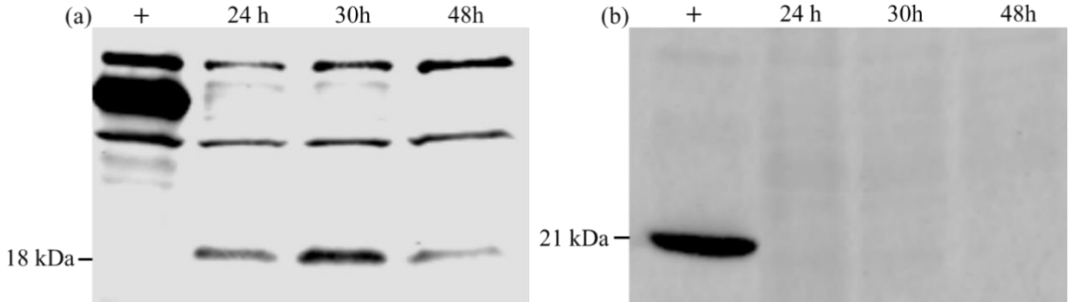

Figure 3.19: Western blot analysis of HBc150_HA by (a) anti-HA polyclonal antibodies and (b) anti-HBc polyclonal antibodies. +: (a) HA-tagged pal (36 kDa) and (b) *E. coli*-produced full-length HBcAg (21 kDa) (BIO-RAD, UK). Analysis performed as described in Section 2.5.5.

3.4.6 Summary

In order to address the problems encountered in Section 3.2.4 and Section 3.3.6, a third transgene construct representing the truncated HBcAg monomer with an N-terminal HA-tag was designed and successfully cloned into the chloroplast expression vector pSRSapI. The resulting plasmid pHBc150_HA was correctly introduced into the *C. reinhardtii* chloroplast genome. Both transgene insertion and plastome homoplasmy were verified by colony PCR and gel electrophoresis. The successful detection of HBc150_HA by rabbit anti-HA polyclonal antibodies in western blot analysis was confirmed in all five transgenic lines with a slight difference in accumulation levels.

Despite the western blot confirmation results probed with anti-HA antibodies, it was still not possible to detect HBc150_HA using anti-HBcAg polyclonal antibodies. This further supports the hypothesis in Section 3.2.4 that the HBc183 expression level was below the detection limit of anti-HBcAg antibodies.

3.5 Investigation of HBc150_HA expression and stability

The net accumulation of recombinant proteins within the chloroplast is a balance between protein synthesis and degradation. Some studies on plants or plant cell cultures have suggested that the environment in chloroplasts is more protective for recombinant proteins than that of the cytosol (Doran, 2006). It is inevitable that these 'foreign' proteins are still subject to proteolytic degradation as various proteolytic enzymes responsible for protein quality control are present in chloroplasts (Adam *et al.*, 2002; Nair and Ramaswamy, 2004; Nishimura *et al.*, 2016). In fact, Birch-Machint et al. (2004) have suggested that rotavirus VP6 protein accumulation was subjected to rapid proteolytic degradation in the transgenic tobacco chloroplasts. In addition, Surzycki et al. (2009) have shown that proteolytic degradation is one of the principal factors affecting vaccine production in microalgal chloroplasts.

Due to the low accumulation level of HBc150_HA observed in Section 3.4.5, it was hypothesized that HBc150_HA was subjected to proteolysis within the *C. reinhardtii* chloroplasts. As a result, a series of protein stability tests was carried out to test this hypothesis and to find potential solutions to solve the issue.

3.5.1 Expression and stability of HBc_150 at different growth stages

In order to compare the accumulation of HBc150_HA at different growth stages and to find the optimum harvesting point, TN72_HBc150_HA_T3 cells were harvested at different time points and analysed by western blots. According to Figure 3.20 (a), HBc150_HA concentration started to decline on the second day of cultivation with a starting OD_{750nm} of 0.3. This was the point when algal cells started to enter the stationary phase of growth as demonstrated in Figure 3.20 (b).

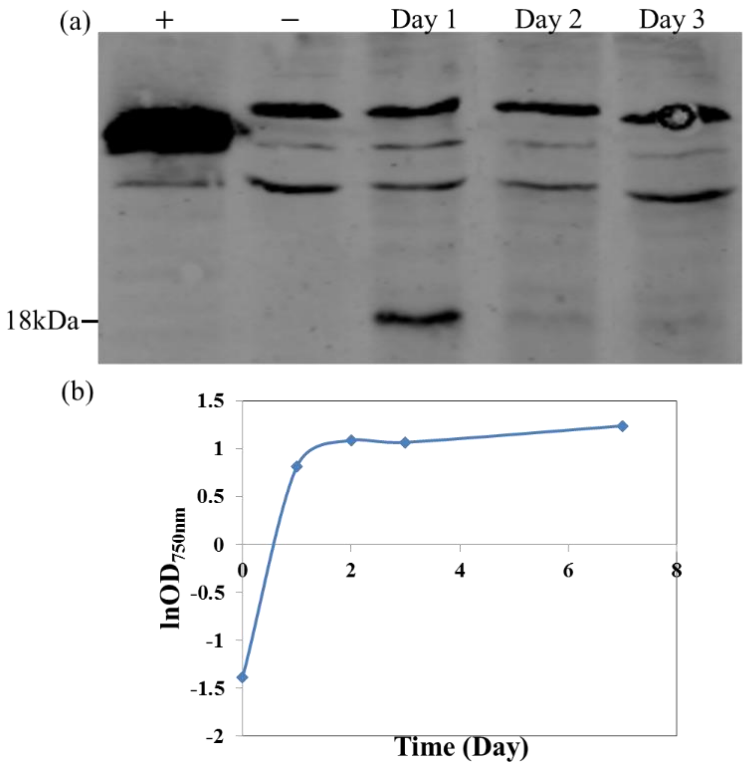

Figure 3.20: Accumulation of HBc150_HA in TN72_HBc150_HA_T3 and the growth kinetics of TN72_HBc150_HA_T3. (a) Accumulation of HBc150_HA in TN72_HBc150_HA_T3 at different time points. +: HA-tagged Pal was the positive control; −: TNE was the negative control. Non-specific bands (25 kDa and 40 kDa) served as a loading control. (b) Growth kinetics of TN72_HBc150_HA_T3 with a starting OD_{750nm} of 0.3. Cultures grown as described in Section 2.3.2 and analysis performed as described in Section 2.3.3 and Section 2.5.5.

To further confirm the time point when protein concentration decrease starts to occur, a cell culture with a lower starting OD_{750nm} of 0.1 was inoculated. Four cell samples prior to late exponential growth phase were harvested and analysed again. As shown in Figure 3.21, the HBc150_HA accumulation level kept increasing in the mid-exponential growth phase and then suddenly dropped at the end of this phase (48 h). HBc150_HA could be subjected to rapid proteolytic degradation triggered at the end of the exponential growth phase when the cells will seek to metabolise additional carbon sources, or alternatively the rate of synthesis could be greatly reduced.

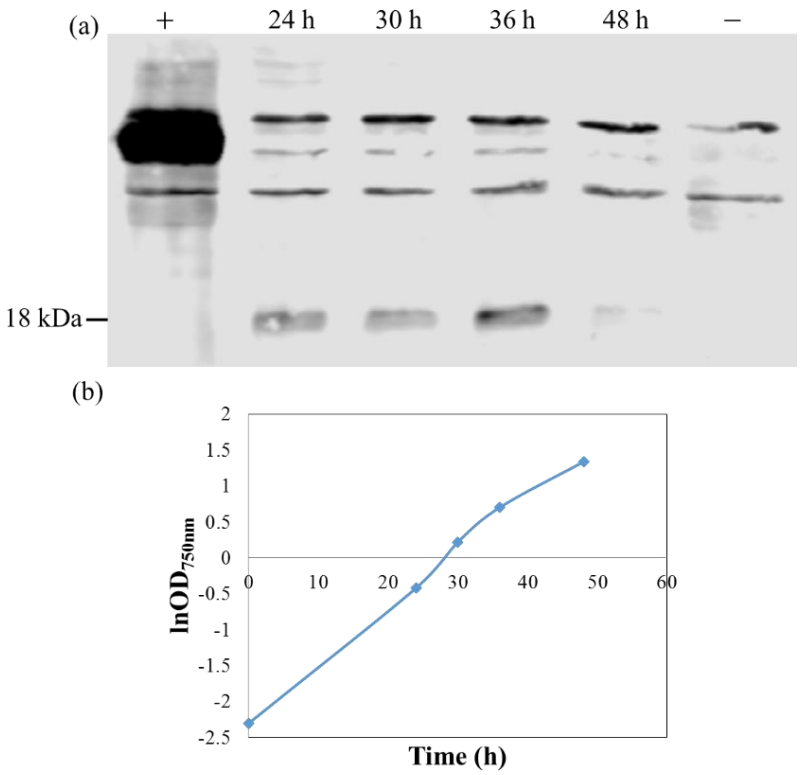

Figure 3.21: Accumulation of HBc150_HA in TN72_HBc150_HA_T3 and the growth kinetics of TN72_HBc150_HA_T3. (a) Accumulation of HBc150_HA in TN72_HBc150_HA_T3 at different time points. +: HA-tagged Pal was the positive control; −: TNE was the negative control. Non-specific bands (25 kDa and 40 kDa) served as a loading control. (b) Growth kinetics of TN72_HBc150_HA_T3 with a starting OD_{750nm} of 0.1. Cultures grown as described in Section 2.3.2 and analysis performed as described in Section 2.3.3 and Section 2.5.5.

3.5.2 Cell treatment with different concentrations of chloramphenicol

From the findings shown in Figure 3.20 and Figure 3.21, it was hypothesized that HBc150_HA was susceptible to proteolytic degradation in the *C. reinhardtii* chloroplast. In order to test this hypothesis, the stability of HBc150_HA was further investigated. Protein stability can be evaluated when a certain amount of the protein is already produced, but any further protein synthesis is fully inhibited. One of the typical antibiotics to inhibit protein synthesis in prokaryotes is chloramphenicol. It prevents protein chain elongation by inhibiting the peptidyl transferase activity on the 23S ribosomal subunit (Hong *et al.*, 2014). Since the algal chloroplast has a prokaryotic origin, which retains a similar transcription and translation machinery to that of

prokaryotes (Howe *et al.*, 2008), chloramphenicol should also be active in microalgal chloroplasts. In fact, several studies have used chloramphenicol to investigate potential proteolytic degradation of recombinant proteins in *C. reinhardtii* chloroplasts (Birch-Machint *et al.*, 2004; Surzycki *et al.*, 2009; Michelet *et al.*, 2011).

Different concentrations of chloramphenicol were first tested in order to find the most effective dose to fully inhibit protein synthesis. Cultures of TN72_HBc150_HA_T3 were grown to the exponential growth phase with OD_{750nm} of 1.3 and split equally into five shake flasks. Four concentrations of chloramphenicol (250 μg mL^{-1}, 371.5 μg mL^{-1}, 625 μg mL^{-1} and 812.5 μg mL^{-1}) and a negative control (pure ethanol) were added into each of the flasks. Subsequently, samples were taken at different time points over a period of 71.5 h and subjected to growth kinetics studies and western blot analyses. The degradation of both HBc150_HA and the endogenous D1 protein was evaluated using anti-HA and anti-D1 antibodies respectively. D1 protein is encoded in the chloroplast genome and forms part of the reaction centre core of photosystem II. Under high light conditions, D1 is rapidly degraded followed by the disassembly of photosystem II (Fischer *et al.*, 2006). In addition, when protein translation is arrested in chloroplasts, D1 proteins usually degrade with a short half-life. Therefore, the degradation of D1 served as a control in this study.

The results presented in Figure 3.22 show that the untreated cells had higher specific growth rate and maximum cell density than that of the chloramphenicol-treated cells. This indicated the inhibition of protein synthesis within chloroplasts and thus cell metabolism by chloramphenicol. However, cells treated with various concentrations of chloramphenicol did not exhibit significant differences as demonstrated by similar slopes during the exponential growth phase.

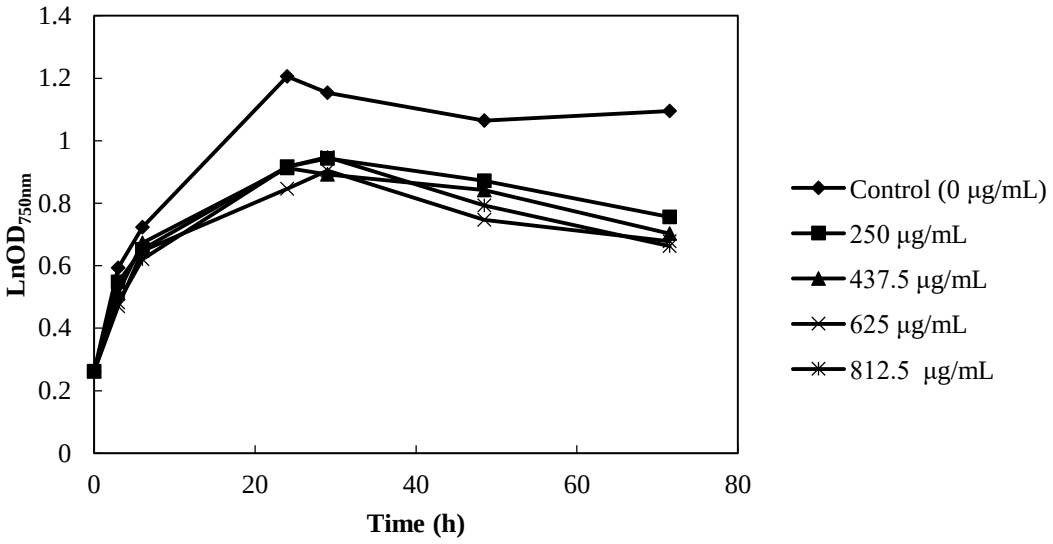

Figure 3.22: Growth kinetics profiles of untreated control and cells treated with different concentrations of chloramphenicol. TN72_HBc150_HA_T3 cells were cultured as described in Section 2.3.2.

As shown in Figure 3.23, lower concentrations of chloramphenicol (250 μg mL^{-1} and 437.5 μg mL^{-1}) did not inhibit the production of D1 proteins completely despite their negative effects on cell growth. On the contrary, when increasing to 625 μg mL^{-1}, D1 protein disappeared after 6 h of treatment, confirming the instability and suggesting that further protein synthesis was blocked. Although D1 degradation pattern remained the same when the concentration was increased to 812.5 μg mL^{-1}, HBc150_HA bands were still visible up to 6 h of treatment at this concentration compared to the complete smear observed at 625 μg mL^{-1}. This was probably due to the relatively low protein expression level of HBc150_HA that resulted in inconclusive results in western blot. Nonetheless, based on the effectiveness of translation inhibition, the results suggested that 625 μg mL^{-1} was a suitable working concentration to carry out the subsequent protein stability tests. As for HBc150_HA, it was seen to be unstable even without the chloramphenicol treatment. Nonetheless, the higher the concentration of chloramphenicol, the quicker HBc150_HA degraded when translation was arrested. Therefore, it could be confirmed that proteolytic degradation was one of the reasons for the low accumulation level of HBc150_HA in the *C. reinhardtii* chloroplast.

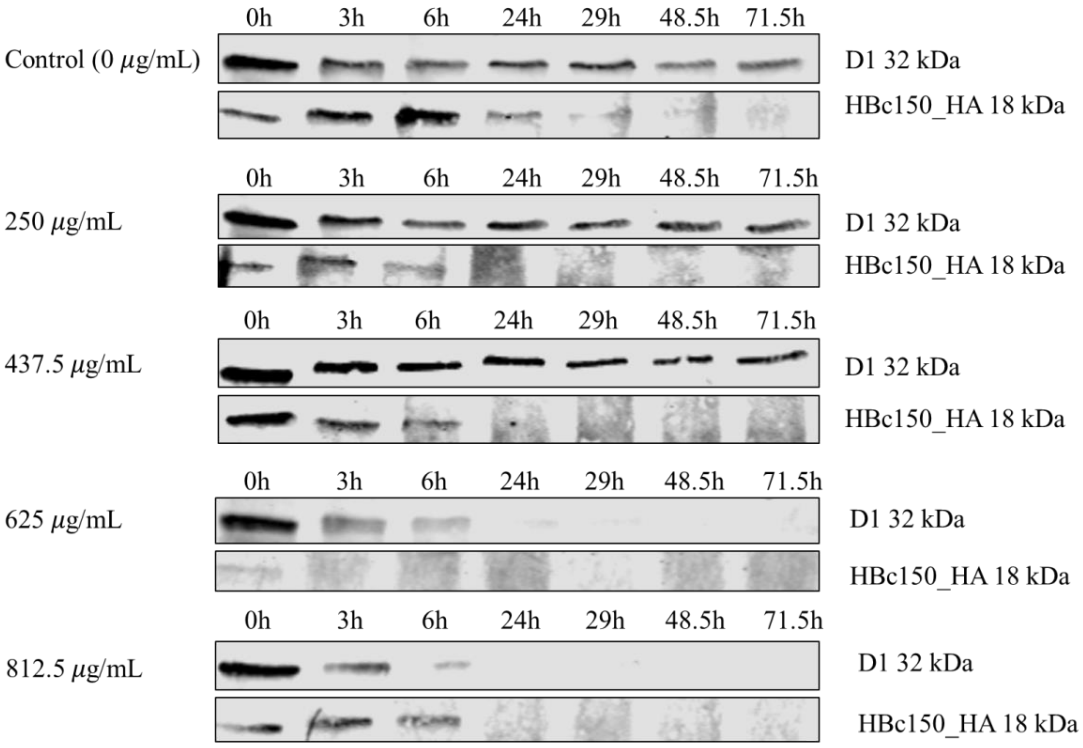

Figure 3.23: Western blot analysis of D1 and HBc150_HA accumulation levels when translation was arrested with the addition of chloramphenicol at four different concentrations (250, 437.5, 625 and 812.5 µg/mL). TN72_HBc150_HA_T3 cells were cultured as described in Section 2.3.2.

3.5.3 Investigation of light-induced proteases and treatment with protease inhibitors

In order to find out if the proteases responsible for HBc150_HA degradation are light-induced or light-sensitive, experiments with the pre-determined working concentration of chloramphenicol (625 µg mL^{-1}) were repeated for cultures performed in the dark. Moreover, protein stability investigation was also carried out with the addition of protease inhibitor cocktail tablets (Section 2.4.2). Protease inhibitors are typically used to inhibit protease activities in the crude protein extracts or purified protein samples. However, Michelet *et al.*, (2011) have shown that protease inhibitors can reduce heterologous protein degradation when adding into liquid cell cultures. Serine protease inhibitors have been supplemented to increase heterologous protein expression level despite the potential cytotoxicity effects on cells (Michelet *et al.*, 2011). Therefore, the

same strategy was adopted in this study to serve as a potential solution for the degradation of HBc150_HA.

As demonstrated in Figure 3.24, mixotrophic cultures grew faster than heterotrophic cultures for the control group in accordance with the literature (Braun Galleani *et al.*, 2015). Under both cultivation modes, protease inhibitors exhibited negative effects on cell growth especially for the heterotrophic cultures. This was probably due to the disruption of normal functions carried out by proteases such as protein biogenesis and proteome maintenance (Nishimura *et al.*, 2017). As previously reported in Section 3.5.2, reduced growth performance was also observed with chloramphenicol-treated cells. The influence was more predominant on mixotrophic cultures than heterotrophic cultures. This echoes the ability of chloramphenicol to inhibit protein synthesis in chloroplasts which are the primary sites for photosynthesis. Since heterotrophic cultures do not rely on photosynthesis to provide energy, the growth rate was not as severely influenced.

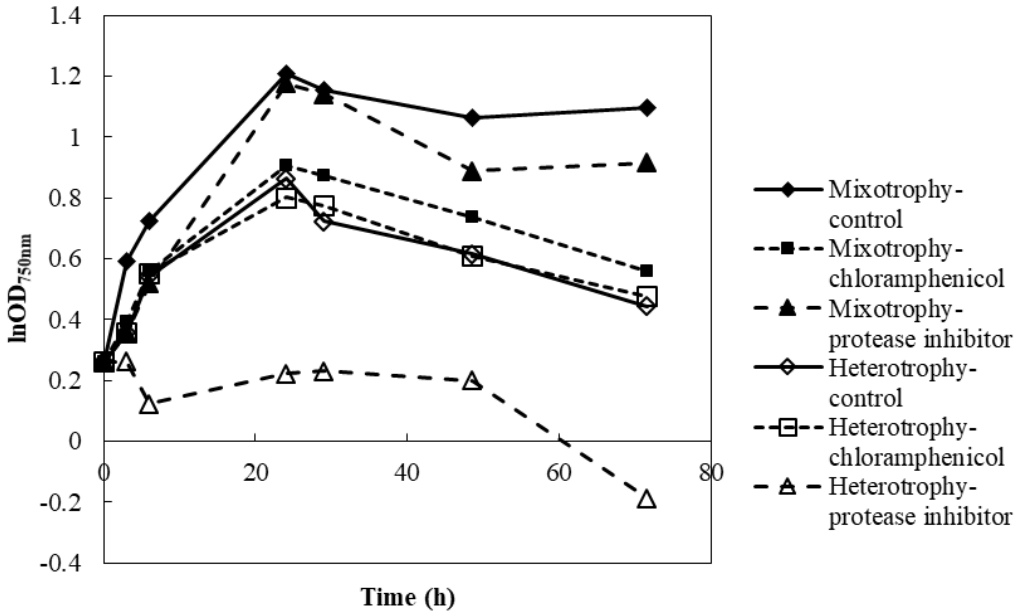

Figure 3.24: Growth kinetics profiles of untreated cells, chloramphenicol-treated and protease inhibitor-treated cells under either mixotrophic or heterotrophic conditions. TN72_HBc150_HA_T3 cells were cultured as described in Section 2.3.2.

The protein accumulation profiles were very similar between the control groups under mixotrophic and heterotrophic conditions (Figure 3.25 (a) and (b)). In both cases, HBc150_HA started to degrade without any treatment 24 h after cells reached the end of the exponential growth phase as demonstrated in Section 3.5.1. In contrast, D1 protein was more stable when cells were treated with chloramphenicol in the dark than in the light. The same phenomenon was observed by (Preiss *et al.*, 2001) in which abnormal D1 protein degradation was delayed in the dark. These results suggest that some of the proteases responsible for D1 degradation are light-activated as their impact was clearly reduced in the dark. However, due to the low expression level of HBc150_HA, it was difficult to determine the presence of light-activated or light-sensitive proteases responsible for its degradation.

When looking at the protein accumulation profiles treated with protease inhibitors, the potential benefits were not observed as reported by Michelet et al. (2011). On the contrary, since normal cell growth was reduced by the protease inhibitor, the protein accumulation was also negatively influenced. Therefore, it was not feasible to use the direct addition of protease inhibitors to liquid cultures to reduce the proteolytic degradation of HBc150_HA.

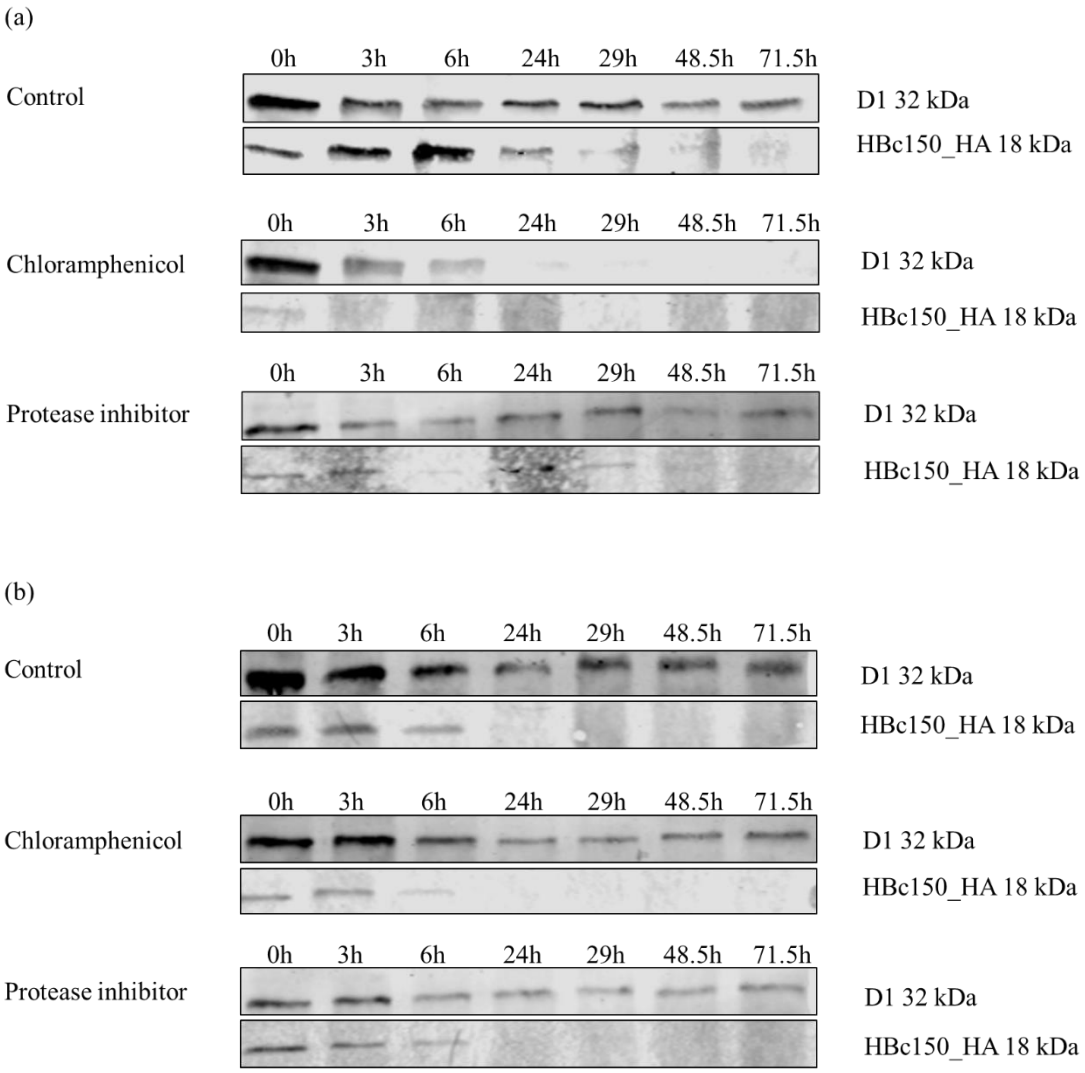

Figure 3.25: Western blot analysis of D1 and HBc150_HA accumulation levels for untreated controls and cells treated with chloramphenicol or protease inhibitor under either (a) mixotrophic or (b) heterotrophic conditions. TN72_HBc150_HA_T3 cells expressing the HBc150_HA in the chloroplast were cultured as described in Section 2.3.2. Analysis performed as described in Section 2.5.5.

3.5.4 Summary

Due to the low HBc150_HA expression level observed in Section 3.4.4, a series of samples were harvested during cell growth and stationary phases and were subjected to western blot analysis probed with anti-HA antibodies. Rapid degradation of HBc150_HA was observed when cells reached the end of the exponential growth phase. These findings are confirmed in Figure 3.20 and Figure 3.21. As a result, protein stability investigation with the supplement of chloramphenicol was carried out to test this hypothesis.

First, cells in the exponential growth phase were treated with different concentrations of chloramphenicol under mixotrophic conditions. Based on the western blot results, the higher the chloramphenicol concentration, the quicker D1 and HBc150_HA degraded in the chloroplasts. These results also revealed that the concentration of chloramphenicol at 625 μgmL^{-1} was the most suitable dose to completely inhibit protein synthesis. In addition, the rate of D1 degradation was reduced under heterotrophic conditions, demonstrating the presence of light-activated proteases. However, due to the low expression level of HBc150_HA, it was difficult to draw a definitive conclusion if proteases responsible for HBc150_HA degradation were light-activated or light-sensitive (Figure 3.25).

In order to reduce the proteolytic degradation, Serine-type protease inhibitors were also added in both mixotrophic and heterotrophic cultures (Section 3.5.3). However, they interfered with the normal metabolism of algal cells with reduced growth rate, biomass production and protein accumulation. As a result, other strategies need to be considered in order to further improve HBcAg expression level in the *C. reinhardtii* chloroplast for the clarification and visualisation of VLPs.

3.6 Overall summary

The aim of this chapter was to explore the capability of the *C. reinhardtii* chloroplast as a potential HBcAg production platform. This has been demonstrated in Figure 3.18

by the successful expression of the truncated HBcAg monomer in the *C. reinhardtii* chloroplasts. Despite various expression systems previously used in the literature to express HBcAg (Roose *et al.*, 2013), this is the first study to demonstrate the capability of *C. reinhardtii* chloroplast to express HBcAg to date. Three transgene constructs explored in this chapter are demonstrated in Figure 3.26.

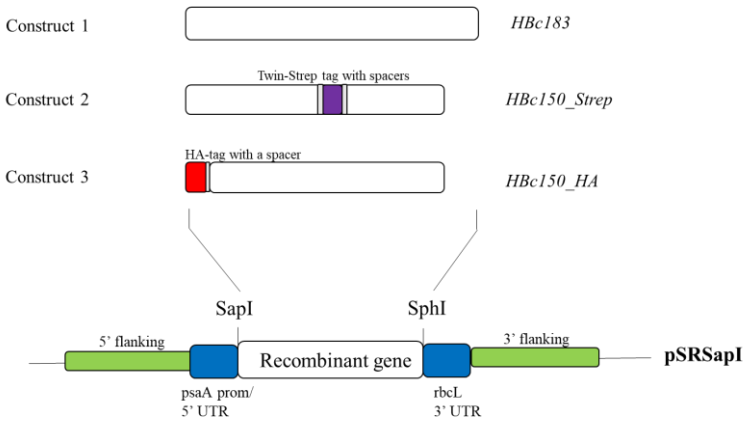

Figure 3.26: Schematic diagram representing the design of three transgene constructs explored in Chapter 3.

The first approach attempted was to express the non-tagged full-length HBcAg monomer (HBc183) in the *C. reinhardtii* chloroplasts (Section 3.2). Although both the transgene insertion and the plastome homoplasmy were confirmed (Figure 3.7), it was not possible to detect HBc183 using anti-HBcAg antibodies in western blot analysis (Figure 3.9). This was probably due to the fact that the HBc183 expression level was too low to be detected by various anti-HBcAg antibodies tested.

Therefore, strategies to improve heterologous protein production and detection were explored in Section 3.3 and Section 3.4. It was suggested that expression of the truncated HBcAg was higher than that of the full-length counterparts (Stahl and Murray, 1989; Tan *et al.*, 2003, 2007; Peyret *et al.*, 2015). In addition, well-established short affinity tags were considered to increase signal detection in western blots. With all the background in mind, transgenes encoding truncated monomers with short affinity tags were designed. The expression of the truncated monomer with an N-terminal HA-tag

(HBc150_HA) was confirmed by western blot analysis using anti-HA primary antibodies (Figure 3.18).

However, the expression of HBc150_HA was still below the detection limit of anti-HBcAg antibodies. It was also found that HBc150_HA tended to degrade when cells reached to the end of exponential growth phase (Figure 3.20 and Figure 3.21). One of the principal reasons for this was due to the proteolytic degradation as evidenced by the protein stability tests using chloramphenicol (Section 3.5). The potential solution was to add protease inhibitors into the liquid cultures to reduce the activities of some proteases as demonstrated by (Michelet *et al.*, 2011). However, protease inhibitors negatively influenced both cell growth and protein accumulation in this study as opposed to the literature.

New strategies to further improve HBcAg expression levels in the *C. reinhardtii* chloroplasts must still be sought. Two strategies to achieve increased expression level are described in Chapter 4.

4 Strategies to improve HBcAg expression in the *C. reinhardtii* chloroplast

4.1 Introduction and aim

High expression of heterologous proteins not only reduces production costs but also alleviates the burden for downstream processing (Ghag *et al.*, 2016). Despite the advantages of using microalgal chloroplast as an alternative protein expression system (Section 1.2.1), the widespread advancement of this approach is hindered by the relatively low protein yields compared to conventional expression systems such as bacteria and yeast. However, it should be noted that a high protein yield of up to 70% (w/w) TSP is achievable in the chloroplasts of transgenic plant (Chebolu and Daniell, 2010). This suggests that there is ample room for improvement in the expression levels seen here for HBcAg production in the *C. reinhardtii* chloroplast. In fact, many of the studies have focused on the understanding of factors that influence protein expression and finding potential solutions to solve these issues in microalgae (Surzycki *et al.*, 2009; Potvin and Zhang, 2010; Michelet *et al.*, 2011).

As discussed in Section 1.2.3, the main factors that affect protein expression in *C. reinhardtii* chloroplasts include, but are not limited to, the codon optimisation of GOI, CREs within promoters and UTRs, and sensitivities of the product to proteolytic degradation. All these factors are confined within the scope of genetic engineering of microalgae. In fact, Tey et al. (2006) have shown that various environmental factors such as pH, temperature and mixing have exerted significant impacts on HBcAg production yield in *E. coli*. Despite the fact that many studies have demonstrated the importance of environmental and culturing conditions on biomass accumulation and lipid production in microalgae (Li *et al.*, 2010; Shen *et al.*, 2010; Cheirsilp and Torpee, 2012; Moon *et al.*, 2013; Zhu *et al.*, 2016), limited work has focused on the bioprocessing optimisation of heterologous protein expression in *C. reinhardtii*. Therefore, the optimisation of the cultivation conditions is another important factor to be considered for protein production in the *C. reinhardtii* chloroplast.

The **aim** of the experiments carried out in this chapter was to explore strategies both from the bioprocessing and genetic engineering aspects in order to further increase the HBc150_HA expression level. Specific objectives were:

- To explore the effects of cultivation modes and operational conditions on growth kinetics and HBc150_HA accumulation of the *C. reinhardtii psaA* transformant strain;
- To create new transformant strains harbouring a stronger 16S rRNA promoter;
- To compare the new transformant strains with the *psaA* transformant strain in terms of HBc150_HA accumulation, degradation and growth kinetics;
- To quantify the yield of HBc150_HA using densitometric analysis and to compare its yield with the yeast-derived HBcAg.

4.2 Study of different cultivation modes and operational conditions in terms of algal growth and HBc150_HA production

Fermentation and cell culture optimisation play an important role to enhance cell growth and improve heterologous protein production. Indeed, various environmental and culture conditions have been explored in order to achieve higher protein yields in conventional expression systems such as bacteria and yeast (Porro *et al.*, 2005; Sivashanmugam *et al.*, 2009; Rosano and Ceccarelli, 2014). However, little work has been done on microalgae. To date, only one published work has examined the impacts of different culturing conditions on heterologous protein production in *C. reinhardtii* chloroplasts (Braun Galleani *et al.*, 2015). Apart from cultivation modes, media composition, light and temperature are also important factors that greatly influence cell growth and recombinant protein production (Zhu *et al.*, 2016). Therefore, it is crucial to optimise these parameters in order to support rapid algal growth and high heterologous protein accumulation.

In this section, the influences of cultivation mode (phototrophy, heterotrophy and mixotrophy) and operational factors (medium composition, light intensity and temperature) are evaluated in terms of growth kinetics and HBc150_HA expression. In

order to compare the growth kinetics under different cultivation modes, the *psaA* transformant strain established in Section 3.4.4 was grown in Algem® photobioreactors with a tight control of light intensity, temperature and rotational mixing speed. The standard conditions used were 120 rpm, 200 μmol $m^{-2}s^{-1}$ (white light) and 25 °C. OD_{740nm} was automatically measured *in situ* every 30 min to monitor the growth whereas OD_{750nm} was measured manually every day to calculate specific growth rates and maximum biomass accumulation. Samples were also harvested to monitor pH changes, acetate consumption and protein expression. Optimum cultivation conditions are suggested at the end of this section.

4.2.1 Cultivation under different modes

As described in Section 1.3.1, *C. reinhardtii* has three main types of metabolism depending on the availability of energy and carbon sources: phototrophic, heterotrophic and mixotrophic modes. Phototrophic cultures convert inorganic CO_2 to sugars using light energy during photosynthesis, whereas heterotrophic cultures use an organic carbon source such as acetate in the TAP medium to support cell growth under dark conditions. In mixotrophic cultivation, both photosynthesis and organic carbon assimilation are carried out by the algal cells.

The *psaA* transformant strain was grown under three different cultivation modes. Both cell growth and HBc150_HA accumulation were monitored during the cultivation. Figure 4.1 demonstrates the effects of different metabolic processes on growth kinetics and acetate consumption. The mixotrophic culture grew with the highest specific growth rate (0.08 h^{-1}) and to the highest biomass concentration (0.71 gL^{-1}) compared to that of the phototrophic (0.02 h^{-1} and 0.07 gL^{-1}) and heterotrophic cultures (0.03 h^{-1} and 0.32 gL^{-1}) as shown in Table 4.1. The results were in accordance with the values reported in the literature (James *et al.*, 2013; Moon *et al.*, 2013; Braun Galleani *et al.*, 2015). This demonstrates that although *C. reinhardtii* can be cultivated heterotrophically, it is not optimal for cell growth without the energy supply from photosynthesis. According to the acetate consumption profile in Figure 4.1, the amount of acetate in the TAP medium was quickly consumed after 72 h cultivation under the

heterotrophic conditions. As a result, the growth of heterotrophic cultures was further limited by the availability of acetate.

As for the phototrophic cultures, they relied only on an inorganic carbon source (CO_2) and light, for growth. In fact, Soletto et al. (2008) have investigated the effects of different concentrations of CO_2 on phototrophic growth. They found that phototrophic growth is limited by the amount of inorganic carbon source supplied. Therefore, cell growth was restricted as the CO_2 concentration (0.039% (v/v)) in the atmosphere is insufficient during phototrophic growth (Zhu *et al.*, 2016).

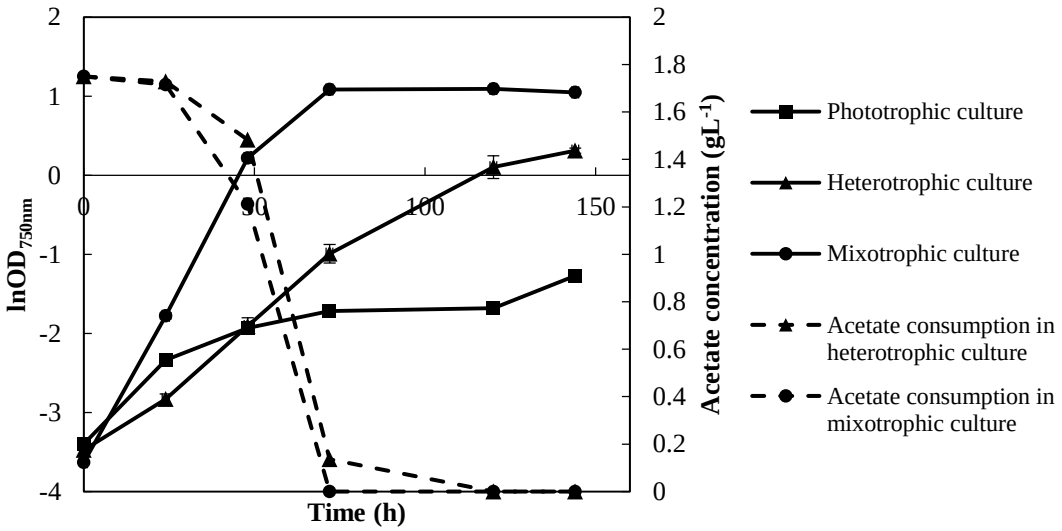

Figure 4.1: Growth kinetics and acetate consumption of the *C. reinhardtii psaA* transformant strain grown under phototrophic, heterotrophic and mixotrophic conditions with a starting OD_{750nm} of 0.03. Error bars represent the range of duplicate points (n=2). Experiments performed as described in Section 2.3.2 and analysis performed as described in Section 2.3.3 and Section 2.5.1.

Table 4.1：Specific growth rate and maximum biomass accumulation obtained for the *C. reinhardtii psaA* transformant strain grown under phototrophic, heterotrophic and mixotrophic conditions. Values calculated from data presented in Figure 4.1.

Cultivation mode	Specific growth rate (h^{-1})	Maximum biomass accumulation (gL^{-1})
Phototrophy	0.02	0.07
Heterotrophy	0.03	0.32
Mixotrophy	0.08	0.71

Mixotrophic cultivation was the most suitable method to grow *C. reinhardtii* with the highest growth rate and best biomass productivity among the three cultivation modes. Some studies have suggested that both phototrophic and heterotrophic metabolic processes function independently during mixotrophic cultivation, meaning the overall growth rate could be the sum of these two individual processes (Marquez-Rocha 2004; Martínez & Orús 1991). Furthermore, the final metabolite of the heterotrophic growth is CO_2 which can be recycled for phototrophic growth (Wan et al. 2011). In fact, the maximum biomass concentration in mixotrophic condition was higher than the sum of those obtained in the other two cultivation modes which was in agreement with the results presented in Cheirsilp and Torpee, (2012). Therefore, mixotrophic cultivation was chosen for the subsequent growth investigation.

Cell growth will also be reflected in the culture pH profiles as demonstrated in Figure 4.2. In general, the media used for microalgae cultivation have limited buffering capacity (Ojo *et al.*, 2014, 2015). The starting pH for both TAP and HSM media was 7.0. In mixotrophic cultivation, there was a rapid increase in the pH from 7.0 to approximately 8.5 when the cells were in the exponential growth phase. The increase in pH was due to the photosynthetic consumption of dissolved CO_2 and the utilization of acetate (Huang *et al.*, 2017). Then, the pH began to plateau when acetate was completely used up during the stationary phase. Similarly, there was a steady increase in pH from 7.0 to around 8.4 in heterotrophic cultures as the consumption of acetate was slightly slower compared to that of the mixotrophic cultures. In contrast, the pH remained unchanged under phototrophic conditions as the growth rate was relatively slow with minimal utilisation of the dissolved CO_2.

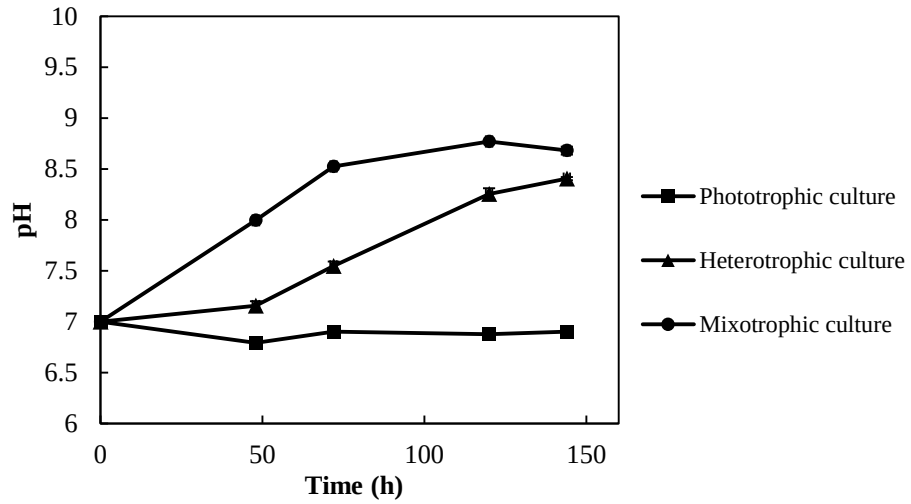

Figure 4.2: pH profile of the *C. reinhardtii psaA* transformant strain grown under phototrophic, heterotrophic and mixotrophic conditions. Error bars represent the range of duplicate points (n=2). Experiments performed as described in Section 2.3.2.

In addition to cell growth, HBc150_HA accumulation under different cultivation modes was also examined. The algal samples were harvested at different time points and subjected to western blot analysis using anti-HA antibodies. As shown in Figure 4.3, the expression level of HBc150_HA was highest under mixotrophic conditions. However, rapid degradation was also observed after 48 h of cultivation in all modes as discussed in Section 3.5.1. Both phototrophic and heterotrophic cultures produced a minimal amount of HBc150_HA at the time points sampled. It has been suggested that heterotrophic cultivation supports higher protein accumulation compared to the mixotrophic and phototrophic conditions mainly due to the inactivation of certain light-induced proteases present in the chloroplast (Braun Galleani *et al.*, 2015). However, such effects were not observed for HBc150_HA in this study. It is believed that the inactivation of certain light-induced proteases present in the chloroplast is protein-specific.

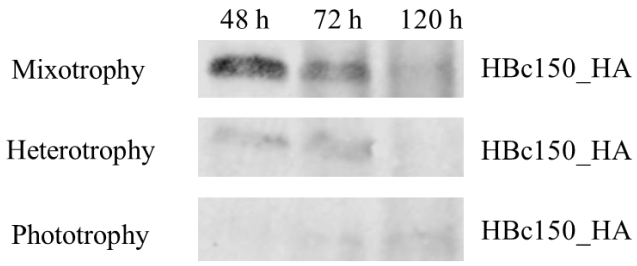

Figure 4.3: Western blot analysis of the HBc150_HA expressed in the *C. reinhardtii psaA* transformant strain under mixotrophic, heterotrophic and phototrophic conditions at different time points. Cells cultured as described in Figure 4.1 and analysis performed as described in Section 2.5.5.

4.2.2 Cultivation at different initial acetate concentrations

Under mixotrophic conditions, the organic carbon source plays an important role in algal growth and protein accumulation. In fact, Moon et al. (2013) have demonstrated that the lipid accumulation profile and growth kinetics of *C. reinhardtii* are greatly influenced by the initial concentration of acetate under mixotrophic conditions. They concluded that the optimum biomass accumulation (2.15 gL^{-1}) and lipid yield (16.4% (w/w) of biomass) were achieved when 10 gL^{-1} acetate was supplied in mixotrophic cell cultures. The results in Figure 4.4 show that the acetate concentration in the standard TAP medium was approximately 1.7 gL^{-1} measured by HPLC. It was completely consumed within 72 h of cultivation and the cell growth was thought to be limited afterwards. As a result, higher initial acetate concentrations (10 gL^{-1} and 20 gL^{-1}) were prepared by the addition of sodium acetate into the standard TAP medium.

As shown in Figure 4.4 and Table 4.2, increasing the initial acetate concentration to 10 gL^{-1} did not improve the specific growth rate but it did double the maximum cell density (1.43 gL^{-1}) compared to the standard TAP medium (0.71 gL^{-1}). This was explained by the acetate consumption profile in which the amount of acetate was sustained for more than 120 h with a higher initial acetate concentration (10 gL^{-1}) as opposed to only 72 h in the standard TAP medium. However, severe inhibitory effects on cell growth (specific growth rate: 0.01 h^{-1}) were observed when the acetate concentration was further increased to 20 gL^{-1}. It was suggested that *C. reinhardtii* growth inhibition was

mainly due to the high salt concentration rather than the high acetate concentration in the medium (Chen and Johns, 1996). In addition, the growth profiles were correlated with the pH changes (Figure 4.5). In general, the higher the acetate consumption rate, the higher the pH increase. pH values began to plateau around 8.7 and 9.4 when cells reached to the stationary phase in the standard TAP medium and the medium with 10 gL^{-1} initial acetate concentration, respectively.

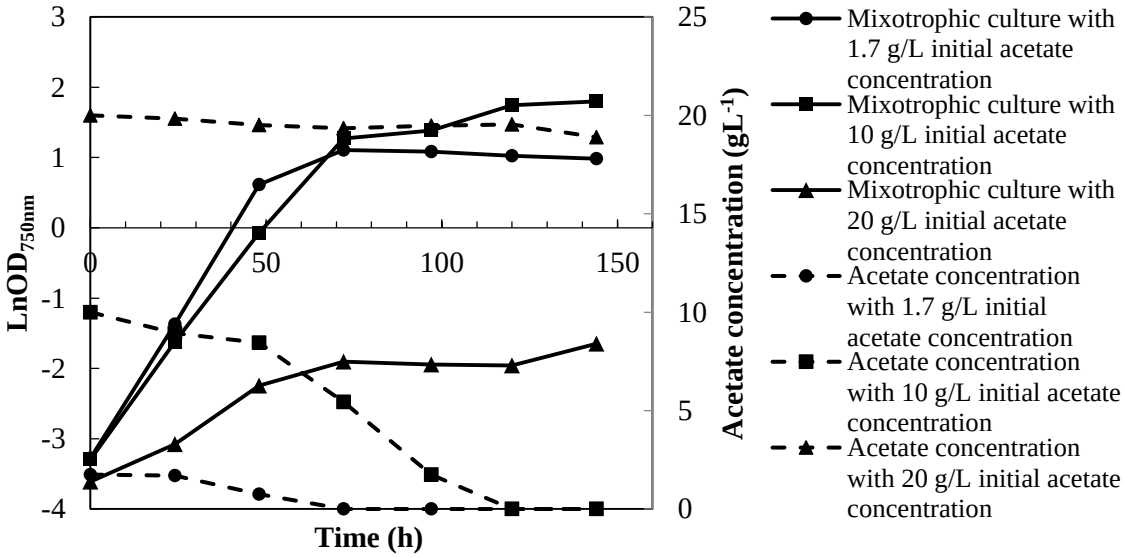

Figure 4.4: Growth kinetics and acetate consumption of the *C. reinhardtii psaA* transformant strain grown under mixotrophic conditions with different initial acetate concentrations with a starting OD_{750nm} of 0.03. Error bars represent the range of duplicate points (n=2). Experiments performed as described in Section 2.3.2 and analysis performed as described in Section 2.3.3 and Section 2.5.1.

Table 4.2: Specific growth rate and maximum biomass accumulation obtained for the *C. reinhardtii psaA* transformant strain grown under mixotrophic conditions with three different initial acetate concentrations. Values calculated from data presented in Figure 4.4.

Initial acetate concentration (gL^{-1}) under mixotrophic conditions	Specific growth rate (h^{-1})	Maximum biomass accumulation (gL^{-1})
1.7	0.08	0.71
10	0.06	1.43
20	0.01	0.05

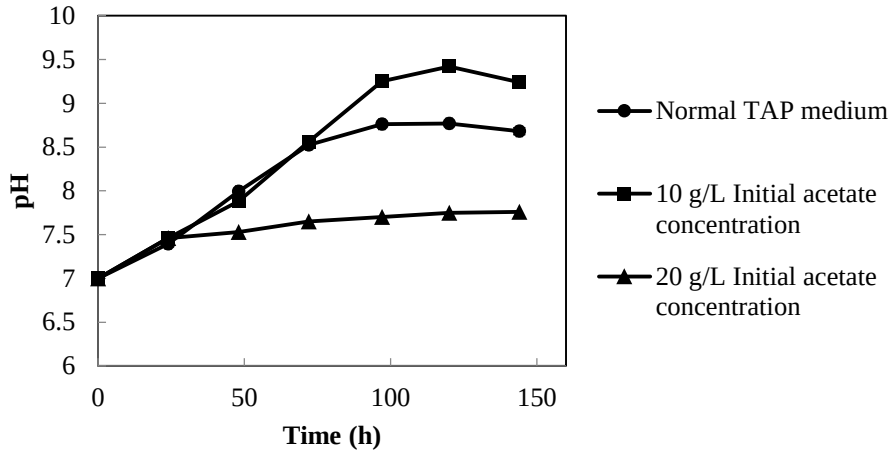

Figure 4.5: pH profile of the *C. reinhardtii psaA* transformant strain grown under mixotrophic conditions with different initial acetate concentrations. Error bars represent the range of duplicate points (n=2). Experiments performed as described in Section 2.3.2.

It is concluded that increasing the initial acetate concentration to 10 gL^{-1} could further support cell growth even at the stationary phase with no inhibitory effects on specific growth rate. This is in accordance with the literature in which mixotrophic cultivation with 10 gL^{-1} acetate supported the highest biomass accumulation and lipid production in *C. reinhardtii* (Moon *et al.*, 2013). Moreover, HBc150_HA accumulation with three different starting acetate concentrations was assessed by western blots. However, protein bands were very faint due to the low expression obtained and are not presented here.

4.2.3 Cultivation at different light intensities

Light intensity is one of the key physical parameters that has been extensively investigated to improve microalgal growth and lipid production (Cheirsilp and Torpee, 2012; Zhu *et al.*, 2016; Severes *et al.*, 2017). There is, however, a range of light intensity that is suitable for microalgal growth and protein production. If the light intensity is too low, for example, below the compensation point, then cell growth is severely limited, as is the protein yield (Zhu et al. 2016). After the compensation point, the specific growth rate is generally proportional to the light intensity for photosynthetic cultures. However, there is a maximum threshold for the light supply as light saturation occurs in *C. reinhardtii* when the intensity exceeds 400 $\mu molm^{-2}s^{-1}$ (Janssen *et al.*, 2000). In

this study, the growth kinetics of the *psaA* transformant strain were evaluated under the mixotrophic conditions with low (50 $\mu molm^{-2}s^{-1}$), standard (200 $\mu molm^{-2}s^{-1}$) or high (400 $\mu molm^{-2}s^{-1}$) white light intensities.

The results shown in Figure 4.6 and Table 4.3 revealed very similar maximum biomass accumulation under three different light intensities with the highest value in the low light condition (0.71 gL^{-1}). However, it was interesting to see that the higher the light intensity, the lower the specific growth rate and the lower the acetate consumption rate. This was probably associated with photoinhibition occurring under high light conditions (Janssen *et al.*, 2000). When the rate of photosynthesis becomes saturated at a light intensity of 400 $\mu molm^{-2}s^{-1}$, the excess light absorbed by *C. reinhardtii* will cause photo-oxidative damage to the photosynthetic reaction centres (Erickson *et al.*, 2015). This will in turn reduce the rate of photosynthesis and the specific growth rate. Furthermore, the pH profiles shown in Figure 4.7 also supported the trends observed in growth kinetics.

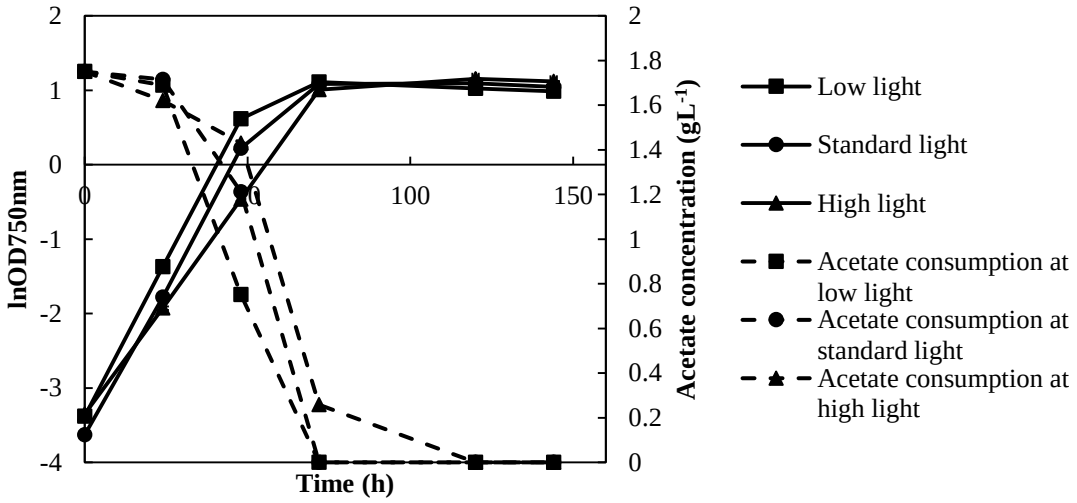

Figure 4.6: Growth kinetics and acetate consumption of the *C. reinhardtii psaA* transformant strain grown under mixotrophic conditions at different light intensities with a starting OD_{750nm} of 0.03. Error bars represent Error bars represent the range of duplicate points (n=2). Experiments performed as described in Section 2.3.2 and analysis performed as described in Section 2.3.3 and Section 2.5.1.

Table 4.3: Specific growth rate and maximum biomass accumulation obtained for the *C. reinhardtii psaA* transformant strain grown at three different light intensities under mixotrophic conditions. Values calculated from data presented in Figure 4.6.

Light intensity ($\mu molm^{-2}s^{-1}$) under mixotrophic conditions	Specific growth rate (h^{-1})	Maximum biomass accumulation (gL^{-1})
50	0.08	0.69
200	0.08	0.71
400	0.06	0.69

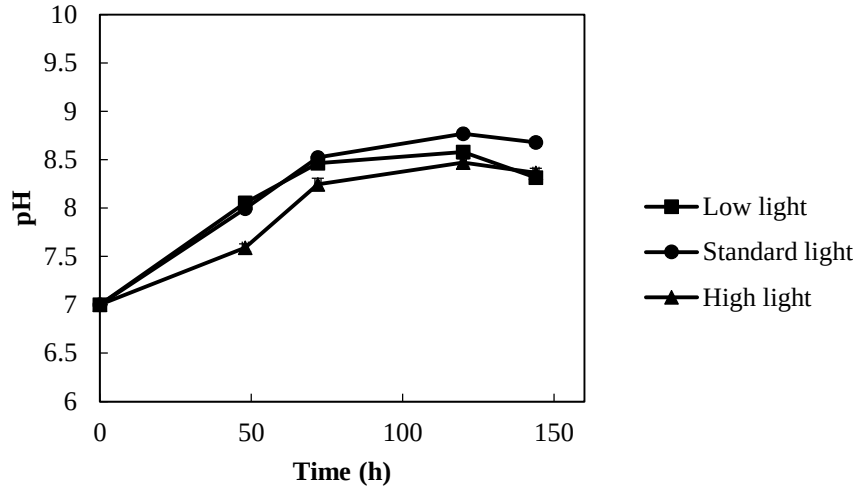

Figure 4.7: pH profile of the *C. reinhardtii psaA* transformant strain grown under mixotrophic conditions with different light intensities. Error bars represent the range of duplicate points (n=2). Experiments performed as described in Section 2.3.2.

In terms of protein production, HBc150_HA accumulation under the three different light conditions was assessed by western blots. However, the same problem was encountered again as mentioned in Section 4.2.3. The protein bands were very faint due to the low level of HBc150_HA and are not presented here.

4.2.4 Cultivation at different temperatures

Temperature is another important cultivation parameter since it affects metabolic rates such as the photosynthetic rate and the specific growth rate in microalgae. It is suggested that the specific growth rate doubles for every 10 °C increase in temperature (Doran, 1995, p. 285). Moreover, hepatitis B viruses infect humans and nonhuman mammals so the temperature around 37 °C is predicted to be suitable for survival and

propagation of the virus (Bonvicino *et al.*, 2014). However, Harris (1989) has shown that the maximum photosynthetic rate and maximum carbon concentrating mechanism (CCM) activity in *C. reinhardtii* were detected at 15 °C and 20 °C, respectively. Therefore, cultivation at high (37 °C), standard (25 °C) and low temperatures (18 °C) was investigated in terms of cell growth and Hbc150_HA accumulation.

As shown in Figure 4.8 and Table 4.4, very similar specific growth rates were observed under standard and high temperatures. Cells grown at standard temperature showed a steep exponential growth phase. Despite a very similar specific growth rate when cells were grown at the higher temperature, there was a gradual decline during the stationary phase. This was in agreement with the declining growth profiles of *C. reinhardtii* at 37 °C or 38 °C reported in the literature (James *et al.*, 2013; Braun Galleani *et al.*, 2015). The phenomenon was probably associated with the heat shock response after prolonged cultivation at high temperatures. Although *C. reinhardtii* cells can tolerate a maximum temperature of 43.5 °C, they usually start to produce heat shock proteins and reduce the production of biomass-related proteins when the temperature exceeds 37 °C (Schroda *et al.*, 2015).

In contrast, there was a 2.5-fold reduction in cell growth at 18 °C with a specific growth rate of only 0.03 h^{-1}. It also took the cells much longer to reach the stationary phase at the lower temperature due to the reduced metabolic rate. Overall, the results were also in accordance with the values reported in the literature (James *et al.*, 2013; Braun Galleani *et al.*, 2015).

The growth kinetics at different temperatures were also reflected by the rate of acetate consumption (Figure 4.8) and pH changes (Figure 4.9). Acetate was consumed quickly and used up completely after 72 h for cultivation under standard and high temperature conditions. In contrast, the acetate concentration only dropped by a third at the lower temperature as cells had a slower growth rate. As for the pH profile, the higher the acetate consumption rate, the higher the pH increase. Therefore, pH values steadily increased from 7.0 to 8.5 and began to plateau around 8.7 and 8.5 when cells reached to the stationary phase at the standard temperature and high temperature, respectively.

In contrast, the pH value gradually increased from 7.0 to 8.0 during the whole course of growth under low temperature conditions.

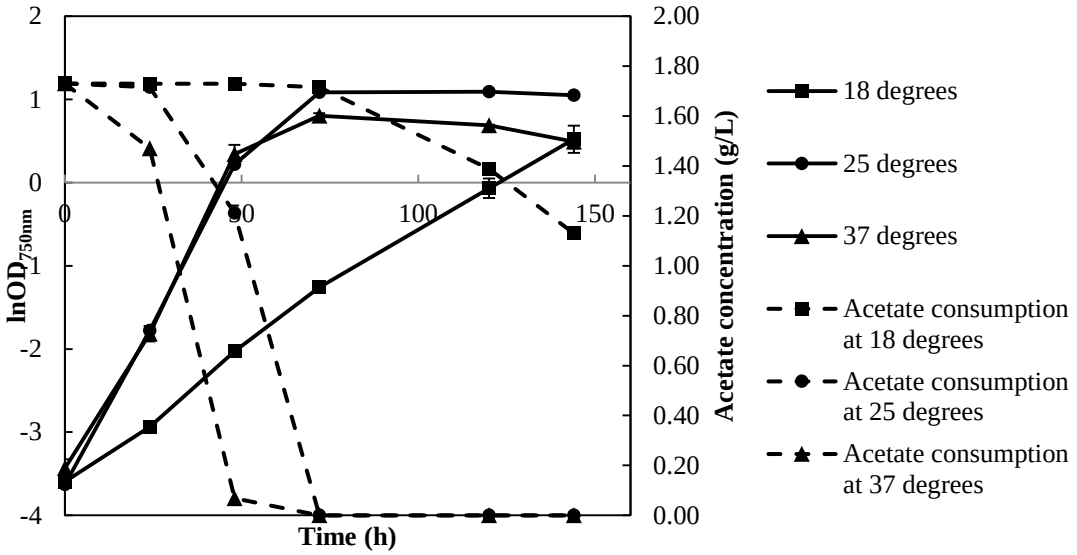

Figure 4.8: Growth kinetics and acetate consumption of the *C. reinhardtii psaA* transformant strain grown under mixotrophic conditions at different temperatures with a starting OD_{750nm} of 0.03. Error bars represent range of the duplicate points (n=2). Experiments performed as described in Section 2.3.2 and analysis performed as described in Section 2.3.3 and Section 2.5.1.

Table 4.4: Specific growth rate and maximum biomass accumulation obtained for the *C. reinhardtii psaA* transformant strain grown at three different temperatures under mixotrophic conditions. Values calculated from data presented in Figure 4.8.

Temperature (°C) under mixotrophic conditions	Specific growth rate (h^{-1})	Maximum biomass accumulation (gL^{-1})
18	0.03	0.41
25	0.08	0.71
37	0.08	0.53

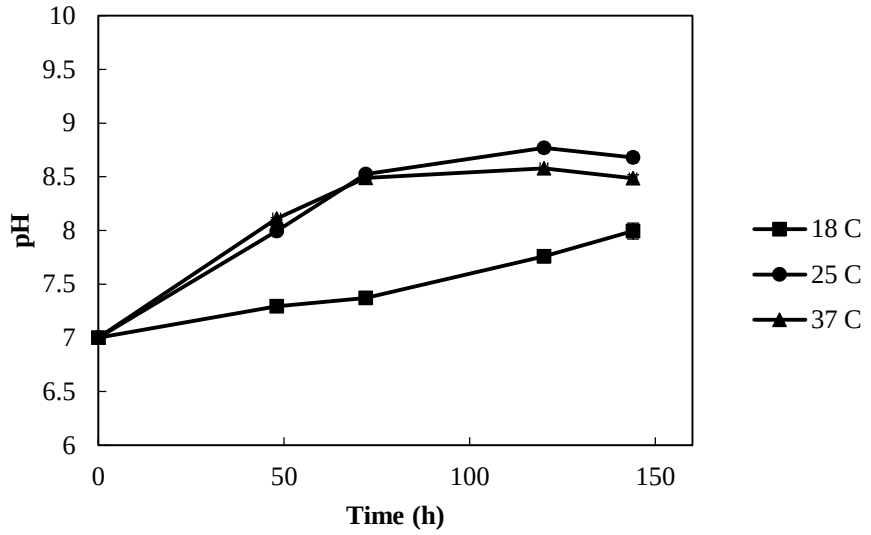

Figure 4.9: pH profiles of the *psaA* transformant strain grown under mixotrophic conditions at different temperatures. Error bars represent the range of duplicate points (n=2). Experiments performed as described in Section 2.3.2.

The effects of different temperatures on HBc150_HA expression were examined. Samples were harvested at different time points and subjected to western blot analysis with anti-HA antibodies. As shown in Figure 4.10, the accumulation level of HBc150_HA increased from 24 h to 72 h at 18 °C whereas it degraded over time at the other two temperatures. During this time period, cells were at early exponential growth phase at 18 °C whereas they reached the stationary phase at higher temperatures. Based on Figure 4.8, although the OD_{750nm} after 48 h cultivation at 18 °C was lower than that of the readings after 24 h cultivation at 25 °C and 37 °C, HBc150_HA expression seemed to accumulate more with a stronger band in the former condition. This may suggest the potential benefits of lowering the temperature in HBcAg expression in algae. However, due to the limited data available and long cultivation time at lower temperature, this temperature was not further changed in subsequent studies.

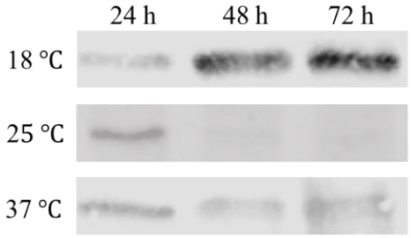

Figure 4.10: Western blot analysis of HBc150_HA accumulation in *C. reinhardtii* at different temperatures under mixotrophic conditions. Cells cultured as described in Figure 4.8 and analysis performed as described in Section 2.5.5.

4.2.5 Summary

In this section, the effects of different bioprocess conditions on *C. reinhardtii* growth and protein accumulation were explored for the *psaA* transformant strain. Based on the results obtained in Section 4.2.1, mixotrophic cultivation was the preferred method to grow *C. reinhardtii* with the highest specific growth rate and biomass concentration among the three cultivation modes. Moreover, different initial acetate concentrations (Section 4.2.2), light intensities (Section 4.2.3) and temperatures (Section 4.2.4) were further evaluated in mixotrophic cell cultures.

First, increasing the initial acetate concentration from 1.7 gL^{-1} to 10 gL^{-1} did not influence specific growth rate but supported a much higher biomass accumulation during the stationary phase (Figure 4.4). This was mainly due to the availability of acetate at a later growth phase. However, there was a severe growth inhibition when the salt concentration exceeded the maximum threshold of *C. reinhardtii*. Second, varying light intensities from 50 to 400 $\mu molm^{-2}s^{-1}$ hardly influenced the growth rates or the biomass production of *C. reinhardtii* (Figure 4.6). In general, the higher the light intensity, the slower the growth rate and acetate consumption. It is possible that the light intensity is not as crucial as organic carbon source for cell growth and biomass accumulation under mixotrophic conditions as long as the amount of light supplied exceeds the compensation point of *C. reinhardtii*. On the contrary, temperature played a crucial role in cell growth and biomass production. The higher the temperature, the higher the specific growth rate. However, heat shock responses reduced the biomass concentration at high temperatures such as 37 °C used in Section 4.2.4.

Overall, the improved cultivation conditions were 120 rpm, 25 ºC and 200 $\mu molm^{-2}s^{-1}$ white light in standard TAP medium under mixotrophic conditions. Due to the low HBc150_HA level in all experiments, it was difficult to analyse the shift of heterologous protein accumulation under different culture conditions in the *psaA* transformant strain.

Nevertheless, the growth study presented in this section deepened the understanding of *C. reinhardtii* growth requirements and facilitated the identification of suitable cultivation method for future work.

4.3 Expression of the truncated monomer HBc150_HA in the *C. reinhardtii* chloroplast under the control of the 16S rRNA promoter

The net accumulation of a heterologous protein is a balance between protein production and protein degradation. Protein degradation has been observed in algal chloroplasts but the addition of protease inhibitors into liquid cell cultures directly did not mitigate this complicated phenomenon (Section 3.5.3). It is known that chloroplast gene expression is controlled at the post-transcriptional level in which several CREs within 5' UTRs are found to be essential for mRNA stability and translation efficiency (Eberhard *et al.*, 2002; Zou *et al.*, 2003; Barnes *et al.*, 2005). However, the control of transcription rate by another group of CREs called promoters is also crucial for chloroplast protein accumulation (Michelet *et al.*, 2011; Rasala *et al.*, 2011).

To date, one of the most robust promoters supporting heterologous protein expression in plant chloroplasts is the 16S rRNA promoter. For example, a foreign gene encoding the membrane protein, plastid terminal oxidase, was successfully expressed in the tobacco chloroplast under the control of the chimeric 16S rRNA promoter/5'UTR of gene 10 from phage T7 regulatory elements (Ahmad *et al.*, 2012). In addition, the same chimeric elements were used to drive the over-expression of a gene for a highly stable phage lytic protein, yielding up to 70% (w/w) TSP in the tobacco chloroplasts (Oey *et al.*, 2009).

Furthermore, the 16S rRNA is among the most actively transcribed RNAs in the *C. reinhardtii* chloroplasts (Blowers *et al.*, 1990). Rasala et al. (2011) fused the 16S promoter with the 5'UTR of either *psbA* or *atpA* to drive heterologous protein expression in the *C. reinhardtii* chloroplasts. The fusion of 16S promoter/*atpA* 5'UTR significantly boosted mRNA levels and heterologous protein expression, but little

improvement was observed for the combination of 16S promoter/*psbA* 5'UTR over the *psbA* promoter (Rasala *et al.*, 2011). It was speculated that there was a limiting supply of nuclear-coded *psaA*-specific translation factors in this case. Therefore, a further increase in mRNA levels driven by the 16S promoter did not contribute to the rate of protein translation.

The *psaA* and *psbA* genes encode the PsaA and D1 proteins in photosystem II and photosystem I, respectively. Both of these proteins are highly expressed in the *C. reinhardtii* chloroplasts as they are critical for photosynthesis (Michelet *et al.*, 2011). Although *psaA* and *psbA* 5'UTRs are believed to be similar in strength, the combination of the *C. reinhardtii* 16S rRNA promoter/*psaA* 5'UTR regulatory element was examined here in terms of HBc150_HA expression levels.

4.3.1 Construction of plasmid p16SHA using Gibson assembly

The strategy to construct the new plasmid p16SHA was to replace the original *psaA* promoter region in the existing chloroplast expression vector pHBc150_HA (constructed in Section 3.4.3) by the endogenous *C. reinhardtii* 16S rRNA promoter.

As shown in Figure 4.11, the Gibson assembly strategy used in this study was to combine three fragments (16S rRNA promoter, Backbone 1 and Backbone 2) with complementary overhangs (a', b, c', d and e') during the isothermal single-step reaction. The sequence of the endogenous 16S rRNA promoter region (219 bp) (Appendix 5 (A5)) was amplified from the *C. reinhardtii* TN72 genome by colony PCR. Meanwhile, the pHBc150_HA backbone was amplified with a split within the *bla* (Amp^R) gene to give two shorter PCR fragments (Backbone 1 and Backbone 2). Following Gibson assembly of the three parts, only colonies transformed with correctly-assembled p16SHA could grow on the LB (Amp^R) agar plates.

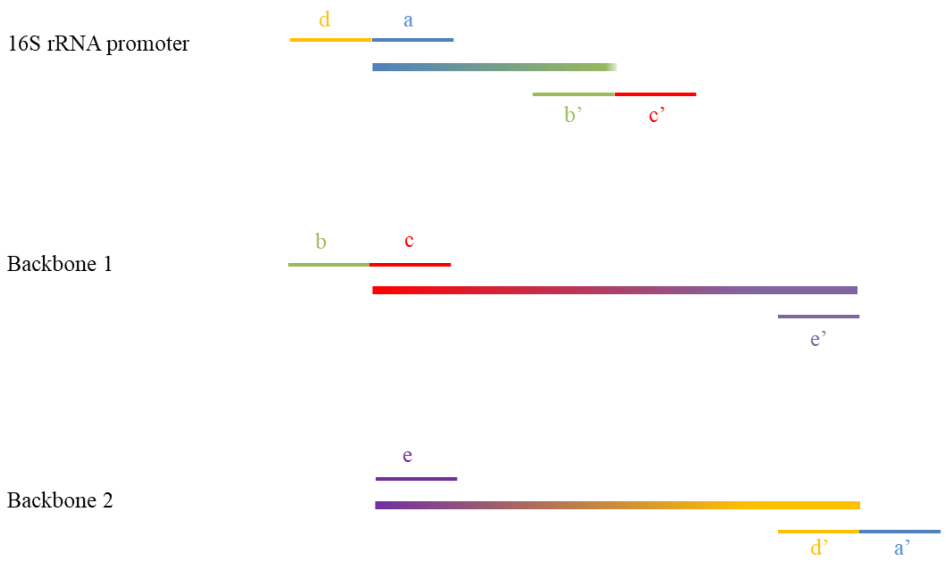

Figure 4.11: Schematic representation of the Gibson assembly strategy to replace the *psaA* promoter region by the 16S rRNA promoter region. The sequences of primers used (a-e and a'-e') are shown in Appendix 5 (A5).

As shown in Figure 4.12 (a), the 16S rRNA promoter was first amplified by the primer set a and b' with a predicted band size of 219 bp. Then, the resulting PCR fragment was further amplified to include 40 bp overhangs (d and c') designed for seamless annealing during Gibson assembly (Figure 4.12 (b)).

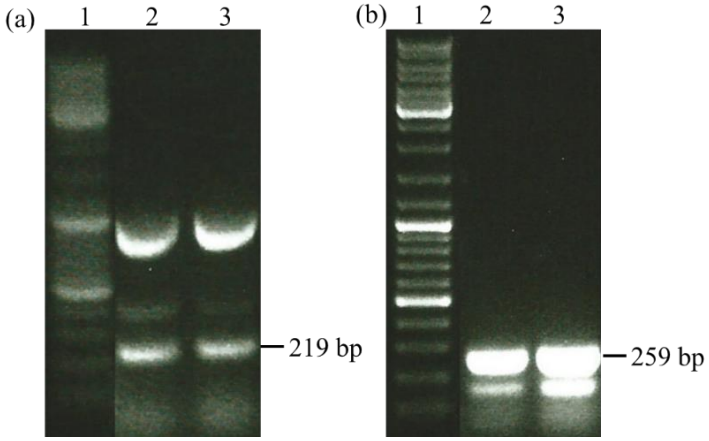

Figure 4.12: Gel electrophoresis results of (a) PCR amplification of 16S rRNA promoter region from TN72 genomic DNA. (b) PCR amplification of 16S rRNA promoter with overhangs designed for Gibson assembly. Lane 1: GeneRuler™ DNA Ladder Mix (Thermo Fisher Scientific, UK); Lane 2-3: duplicate PCR reactions. Analysis performed as described in Section 2.2.2 and Section 2.2.5.

Both Backbone 1 and Backbone 2 were amplified using the pHBc150_HA as the template with primers indicated in Figure 4.11. The amplified PCR fragments were monitored by gel electrophoresis. Amplification of Backbone 1 was not successful in the first attempt as the expected bands (4116 bp) did not appear in Lane 2 and 3 in Figure 4.13 (a). Annealing temperature is probably the most important factor when optimizing the specificity of a PCR reaction (Lorenz, 2012). Therefore, gradient PCR with a range of temperatures (59 °C ± 5 °C) was tested to find the optimum annealing temperature during amplification (Figure 4.13 (b)). It was suggested that annealing temperatures above 58.5 °C were suitable to amplify Backbone 1 in the PCR reaction.

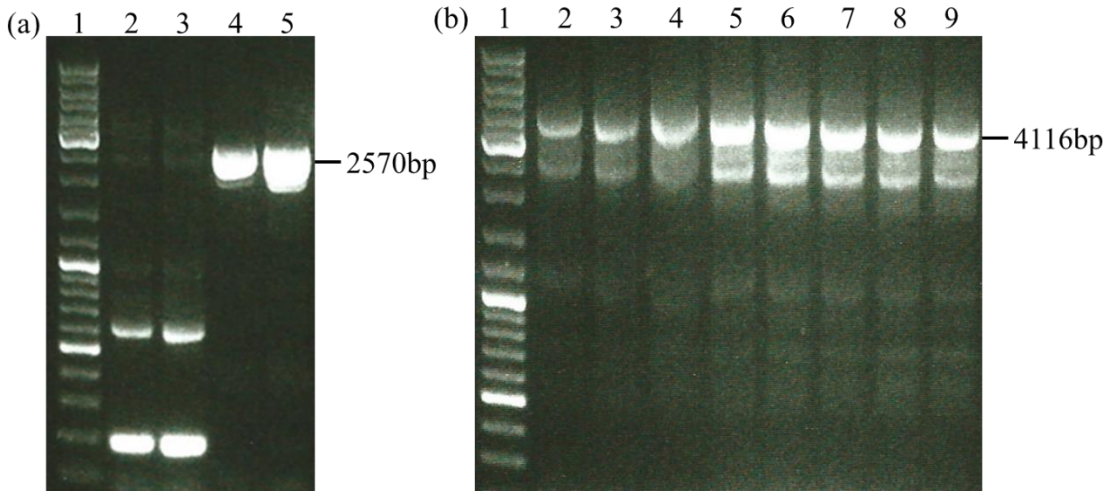

Figure 4.13: Gel electrophoresis results of (a) PCR amplification of pHBc150_HA Backbone 1 and Backbone 2 with a split within the *AmpR* gene. Lane 1: GeneRuler™ DNA Ladder Mix (Thermo Fisher Scientific, UK); Lane 2-3: amplification of Backbone 1 with an expected band size of 4116 bp; Lane 4-5: amplification of Backbone 2 with an expected band size of 2570 bp. (b) Gradient PCR to optimise annealing temperature to amplify this fragment. Lane 1: GeneRuler™ DNA Ladder Mix (Thermo Fisher Scientific, UK); Lane 2-9: amplification of Backbone 1 with an expected band size of 4116 bp. The annealing temperature in Lane 2: 55.5 °C; Lane 3: 56.5 °C; Lane 4: 57.5 °C; Lane 5: 58.5 °C; Lane 6:59.5 °C; Lane 7:60.5 °C; Lane 8:61.5 °C; Lane 9:62.5 °C. Analysis performed as described in Section 2.2.2 and 2.2.5.

All amplified DNA fragments were extracted and purified for Gibson assembly. The detailed components of Gibson assembly were explained in Section 2.2.11. In brief, the reaction mixtures with three fragments (2.35 ng 16S rRNA promoter, 37.4 ng Backbone 1 and 23.3 ng Backbone 2) were incubated in a thermocycler at 50 °C for one hour.

Then, the mixtures were used to transform *E. coli* TOP10 cells as described in Section 2.2.8. Two colonies were isolated on LB ampicillin agar plates after overnight incubation at 37 °C. DNA sequencing results confirmed that the 16S rRNA promoter was precisely inserted into the correct position to replace the *psaA* promoter region. The *HBc150_HA* gene was also sequenced to make sure that no errors were introduced during PCR amplification. The correctly assembled plasmid p16SHA was used for subsequent algal transformation.

4.3.2 Integration of *HBc150_HA* into the chloroplast genome under 16S promoter

The details of the transformation strategy and glass bead transformation method used were as described in Section 2.2.8. After a four-week incubation in the light, six colonies were isolated and re-streaked onto HSM agar plates several times to achieve plastome homoplasmy.

Transgene (*HBc150_HA*) insertion was confirmed as described in Section 3.2.3. The integrity of the gene construct was further confirmed by DNA sequencing. As for the homoplasmy check, a band of 850 bp was seen for the TN72 recipient strain. In contrast, transformant lines gave a band of 1135 bp as shown in Figure 4.14. As before, the absence of any detectable 850 bp band strongly indicated the homoplasmy of the transformant plastomes. These homoplasmic transgenic lines were named TN72_16S_HBc150_HA_T1-T6.

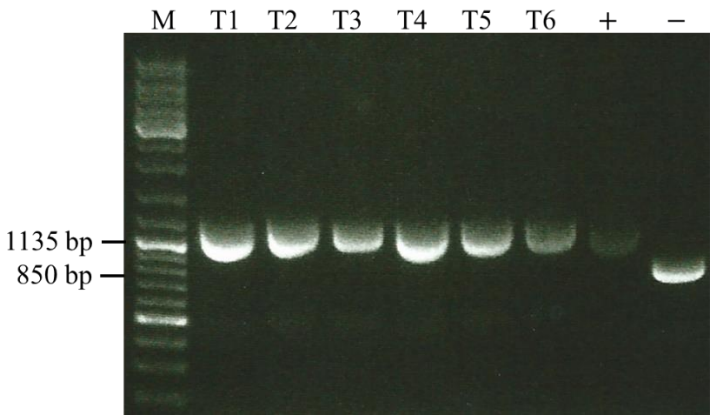

Figure 4.14: Gel electrophoresis of colony PRC products to verify the homoplasmy of the chloroplast genome in six transgenic lines (T1-T6). M: GeneRuler^{TM} DNA Ladder Mix (Thermo Fisher Scientific, UK); −: TN72 genome was the negative control; +: TNE genome was the positive control; H_2O served as the negative control of PCR reactions. Analysis performed as described in Section 2.2.2 and Section 2.2.5.

4.3.3 Expression of HBc150_HA in the 16S fusion transformant strain

According to Section 3.4.4, a protein band at 18 kDa was expected for HBc150_HA in western blot analysis. As shown in Figure 4.15 (a), all transgenic lines (T1-T6) generated a band at 18 kDa, confirming the expression of the truncated HBcAg monomers in the *C. reinhardtii* chloroplasts driven by the 16S rRNA/*psaA* 5'UTR regulatory element. Although different transgenic lines seemed to express HBc150_HA at different levels based on the densitometric analysis, the differences could actually be attributed by limited data available and experimental errors introduced during western blot. In theory, all transgenic lines should be genetically identical after homologous recombination. Therefore, TN72_16S_HBc150_HA_T5 with the highest HBc150_HA expression level (Figure 4.15 (b)) in this blot was chosen as the representative transgenic line and was named as the 16S fusion transformant strain for subsequent studies.

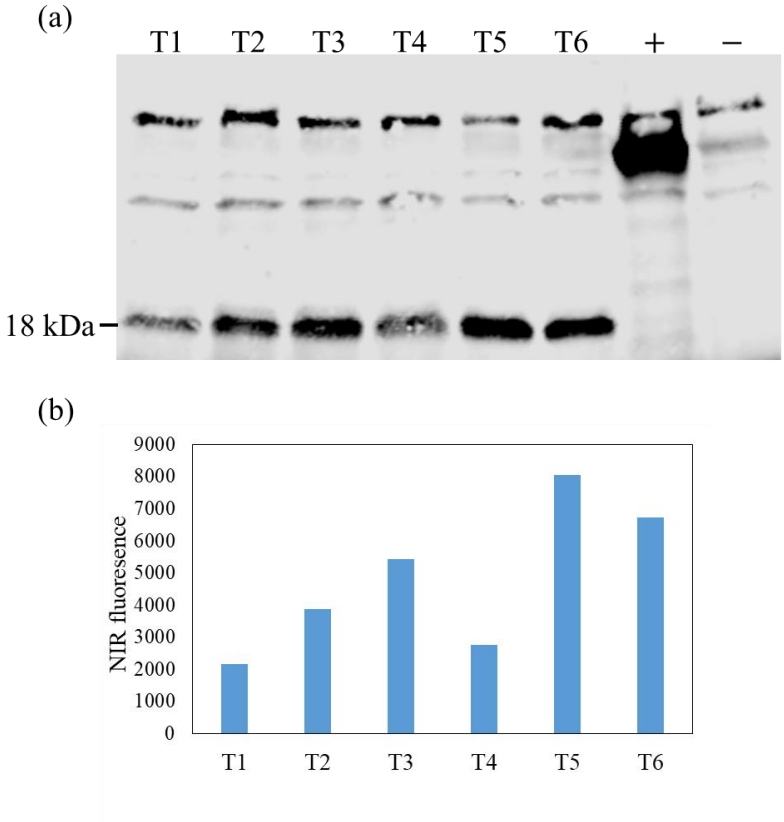

Figure 4.15: Accumulation and relative quantification of HBc150_HA in six transgenic lines (T1-T6). (a) Accumulation of HBc150_HA in six transgenic lines (T1-T6). +: HA-tagged Pal was the positive control; −: TN72-empty was the negative control. Non-specific bands (25 kDa and 40 kDa) served as a loading control. (b) Relative quantification of HBc150_HA in six transgenic lines (T1-T6) in Odyssey® Infrared Imaging System (Li-Cor Biosciences, UK). Cultivation conditions were 120 rpm, 25 ºC and 200 µmol $m^{-2}s^{-1}$ white light in standard TAP medium under mixotrophic conditions. The cells were harvested after 48 h of cultivation. Analysis performed as described in Section 2.5.5.

In order to determine the immunoreactivity of the algal-based HBc150_HA, crude protein lysates of the 16S fusion transformant strain harvested at different time points were tested. Two anti-HBcAg antibodies were used in this study. One was the mouse anti-HBcAg monoclonal antibody [10E11] (ab8639) that recognises the first 10 amino acid residues of HBcAg, and the other was the rabbit anti-HBcAg polyclonal antibody (ab115992) that recognise multiple epitopes on the HBcAg polypeptide (Table 2.18). The *P. pastoris*-produced hetero-tandem HBcAg dimer (K1.K1) was used as the positive control in which a protein band around 39 kDa should be expected (Peyret *et al.*, 2015).

The results presented in Figure 4.16 show that strong signals from HBc150_HA were revealed at all harvest time points despite a declining trend from 72 h to 144 h when probed with the polyclonal anti-HBcAg antibodies. In contrast, HBc150_HA could only be detected in the 72 h-sample when the monoclonal antibody [10E11] was used. In general, polyclonal antibodies have high sensitivity as they usually bind multiple epitopes on the same antigen to amplify the detection signal (Saper, 2009). However, this can also result in non-specific binding, leading to low specificity. On the contrary, monoclonal antibodies usually recognise one main epitope on the antigen that is highly specific, but with a low sensitivity (Saper, 2009). Moreover, the primary peptide sequence of the HBc150_HA was modified by inserting an additional amino acid residue, Valine, in the penultimate N-terminal position as explained in Section 3.3.1. This could potentially influence the antibody-antigen interaction since [10E11] recognises the first 10 amino acids of HBcAg, leading to a reduced sensitivity.

However, the opposite results were observed for the *P. pastoris*-produced K1.K1 in which monoclonal antibodies were more sensitive in terms of picking up the signal. Indeed, different antibodies usually have distinct sensitivities and specificities towards the same antigen (Saper, 2009). Nevertheless, HBc150_HA was successfully recognised by both anti-HBcAg antibodies. This analysis indicates that the algal-expressed HBc150_HA was correctly translated in the chloroplasts and retained its antigenic immunoreactivity (Huang *et al.*, 2006).

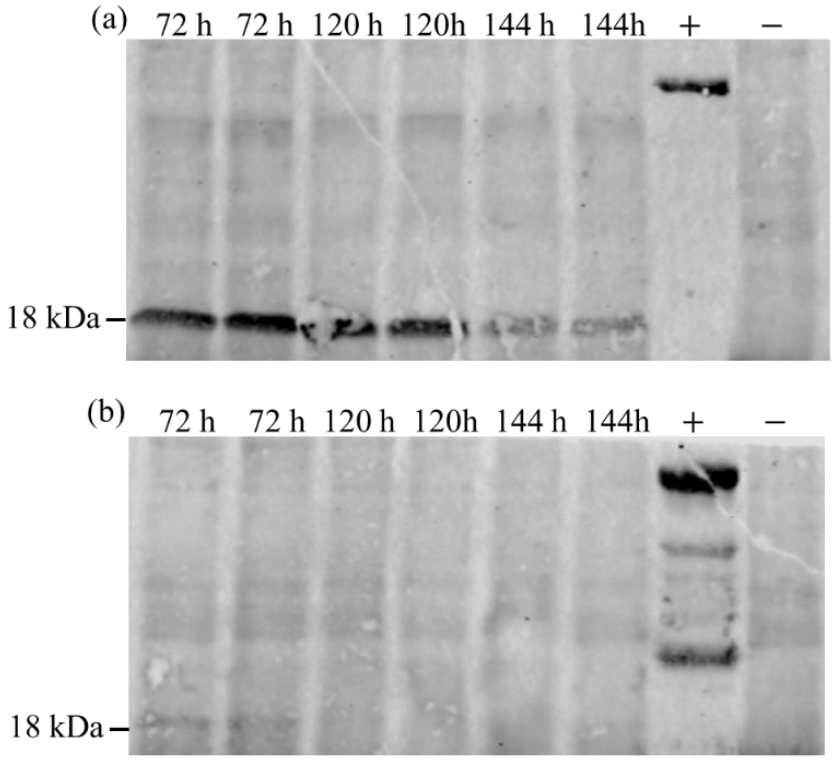

Figure 4.16: Detection of HBc150_HA under the control of 16S rRNA promoter by (a) rabbit anti-HBcAg polyclonal antibodies and (b) mouse anti-HBcAg monoclonal antibodies [10E11] in Western blot analyses. +: K1.K1 was the positive control; −: TN72-empty was the negative control. Cultivation conditions were 120 rpm, 25 ºC and 200 µmol $m^{-2}s^{-1}$ white light in standard TAP medium under mixotrophic conditions. Analysis performed as described in Section 2.5.5.

4.3.4 Summary

The new algal expression vector p16SHA harbouring the chimeric 16S rRNA promoter/*psaA* 5'UTR regulatory element has been successfully constructed by Gibson assembly. Despite low efficiency after *E. coli* transformation, plasmids isolated from two colonies both had the correct sequences (Section 4.3.1). It was then successfully introduced into the *C. reinhardtii* chloroplast genome (Section 4.3.2). After confirmation of HBc150_HA production in six transgenic lines, the 16S fusion transformant strain with the highest expression level was chosen for subsequent studies in western blot analyses probed with anti-HBcAg antibodies (Figure 4.15). This was the first time that the algal-produced HBc150_HA could be recognised by polyclonal anti-HBcAg antibodies, and to a lesser extent, by monoclonal anti-HBcAg antibodies.

Overall, these results not only confirmed the expression of HBc150_HA in the *C. reinhardtii* chloroplasts but also demonstrated its immunoreactivity under denaturing conditions.

In Section 3.4.4, the expression of HBc150_HA in the *psaA* transformant strain has already been confirmed by anti-HA antibodies in western blot analysis. As a result, it was possible to investigate the effects of different promoters on HBc150_HA expression in the *C. reinhardtii* chloroplasts. Further analysis of the HBc150_HA in these transgenic lines is presented in the next section.

4.4 Further analysis of HBc150_HA expressed in the 16S fusion transformant strain

In this section, the effects of promoter strength on heterologous protein expression were investigated by comparing HBc150_HA production in both the *psaA* and 16S fusion transformant strains. Further comparisons between growth kinetics and protein degradation were also made between these transgenic lines. In addition, HBc150_HA produced in the 16S fusion transformant strain was quantified based on densitometric analysis and compared to that of the *P. pastoris*-produced K1.K1.

4.4.1 Comparison of HBc150_HA expression using the *psaA* and 16S rRNA promoters

The expression of HBc150_HA is compared here in the *psaA* transformant strain and the 16S fusion transformant strain. Crude protein samples from both strains were transferred onto the same nitrocellulose membrane and probed with anti-HA antibodies. As shown in Figure 4.17 (a) and (c), there was approximately a 26-fold increase in HBc150_HA accumulation level in the 16S fusion transformant strain based on the densitometric analysis of protein bands in the western blot analysis. In addition, the same protein samples were probed with polyclonal anti-HBcAg antibodies. The results in Figure 4.17 (b) showed that the HBc150_HA produced in the 16S fusion

transformant strain was successfully recognised by anti-HBcAg antibodies whereas no signal was revealed in the protein sample of the *psaA* transformant strain.

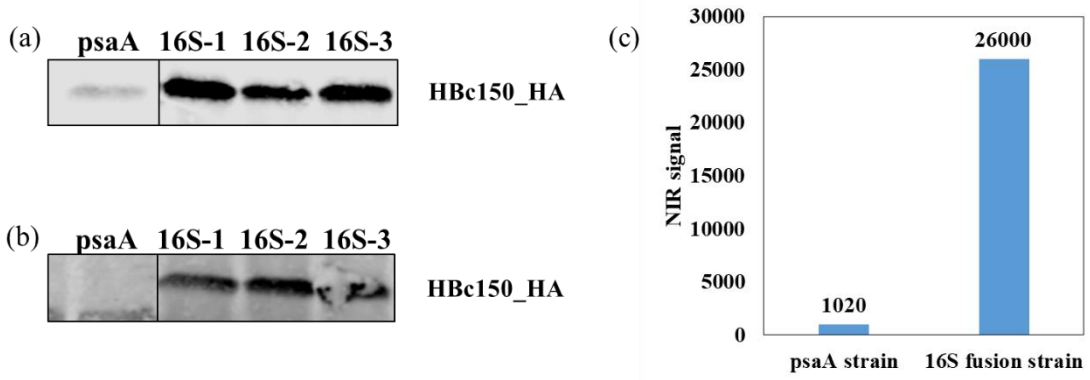

Figure 4.17: Accumulation and relative quantification of HBc150_HA in *psaA* and 16S fusion transformant lines. Western blot analysis of whole cell extracts probed with (a) anti-HA antibodies and (b) anti-HBcAg antibodies to compare HBc150_HA expression levels in *psaA* (left) and 16S fusion transformant (right) strains. (c) Relative average quantification of HBc150_HA in the *psaA* transformant strain and the 16S fusion transformant strain shown in (a) in Odyssey® Infrared Imaging System (Li-Cor Biosciences, UK). Cultivation conditions were 120 rpm, 25 ºC and 200 µmol $m^{-2}s^{-1}$ white light in standard TAP medium under mixotrophic conditions. Analysis performed as described in Section 2.5.5.

The improvement in protein expression is believed to be due to the increase in transcription rates and steady-state mRNA levels under the control of a stronger promoter. This has confirmed the benefits of using the strong 16S rRNA promoter with the *psaA* 5'UTR to support heterologous protein expression in the *C. reinhardtii* chloroplasts. This contrasts with the results obtained in a previous study (Rasala et al. 2011), in which the heterologous protein expression level was not improved when combining the 16S promoter with the *psbA* 5'UTR which has a similar strength to the *psaA* 5'UTR. Therefore, it is hypothesized that the supply of nuclear-encoded *psaA*-mRNA translational factors is not limited in this case. Overall, the results obtained in this section have shed light on the rational design of combining strong promoters with strong 5'UTRs to control heterologous protein expression in the *C. reinhardtii* chloroplast.

Furthermore, when comparing the immunoblot results, it was suggested that polyclonal anti-HA antibodies had a higher sensitivity towards HBc150_HA than that of the

polyclonal anti-HBcAg antibodies. The specificity of the anti-HA antibodies was slightly lower as they revealed non-specific bands in the blots. Nonetheless, these results demonstrated the benefits of using well-established affinity tags to facilitate heterologous protein detection.

4.4.2 Growth kinetics and HBc150_HA degradation in the 16S fusion transformant strain

Sometimes, the production of recombinant proteins can severely burden cell metabolism, leading to series of cellular stress responses (Carneiro *et al.*, 2013). One of the main stress responses is usually characterised by the decrease of overall cell fitness with a reduced biomass production. This is usually caused by a shift of host metabolism in which less biomass precursors and biomass-related proteins are produced due to the unequal competition for the translation apparatus during high-level heterologous protein production (Carneiro *et al.*, 2013). Since both product quality and yield are critical when choosing suitable production hosts, it is important to investigate the effects of protein accumulation on algal growth (Porro *et al.*, 2005).

It was interesting to see whether a 26-fold higher protein expression would burden the cell metabolism and growth. Based on the results of the growth kinetics investigation in Section 4.2, the improved condition to grow *C. reinhardtii* was 120 rpm, 200 $\mu molm^{-2}s^{-1}$ (white light) and 25 °C under mixotrophic conditions. As a result, both the 16S fusion transformant strain and the *psaA* transformant strain were grown under the pre-determined conditions in the well-controlled Algem® photobioreactor (Section 2.3.2). OD_{740nm} was automatically measured *in situ* every half an hour to monitor the growth profiles whereas OD_{750nm} was measured manually every day to calculate specific growth rates.

As shown in Figure 4.18 and Table 4.5, the *psaA* transformant strain had a higher specific growth rate (0.08 h^{-1}) and maximum biomass concentration (0.71 gL^{-1}) than that of the 16S fusion transformant strain (0.07 h^{-1} and 0.53 gL^{-1}). This demonstrated that the increase in HBc150_HA accumulation by 26-fold exerted minor negative

effects on cell growth and biomass accumulation. However, it should be noted that the protein expression in the 16S fusion transformant strain is not comparable to the greater over-expression of heterologous proteins that cause severe growth inhibition in *E. coli* or tobacco chloroplasts (Oey *et al.*, 2009; Rosano and Ceccarelli, 2014).

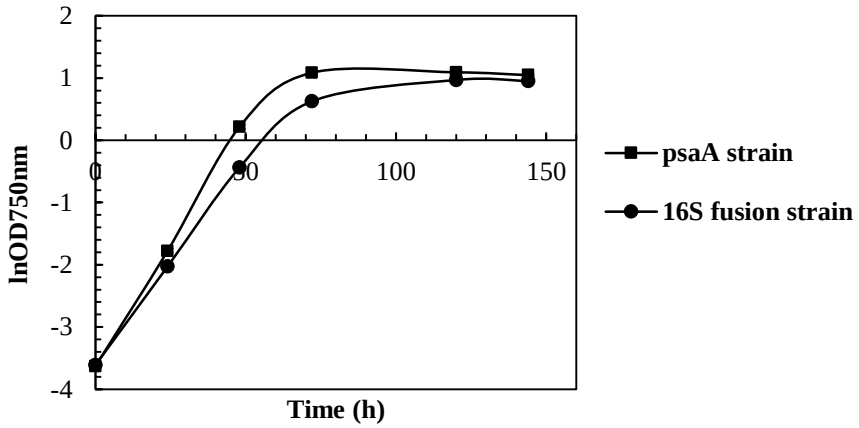

Figure 4.18: Growth kinetics of the transgenic line expressing HBc150_HA (T5) and the control strain (TNE). Cell cultures were grown under mixotrophic conditions (120 rpm, 25 ºC and 200 µmolm^{-2}s^{-1} white light) in TAP medium in the Algem® photobioreactor. Starting OD_{740nm} was 0.20. Error bars represent the range of duplicate points (n=2). Experiments performed as described in Section 2.3.2 and Section 2.3.3.

Table 4.5: Specific growth rate and maximum biomass accumulation of the *psaA* transformant strain and the 16S fusion transformant strain grown in standard mixotrophic conditions. Values calculated from data presented in Figure 4.18.

Transgenic strain	Specific growth rate (h^{-1})	Maximum biomass accumulation (gL^{-1})
16S fusion strain	0.07	0.53
psaA strain	0.08	0.71

In Section 3.5.1, it was shown that HBc150_HA produced in the *psaA* transformant strain degraded quickly after 48 h of growth and diminished in the stationary growth phase. In order to compare the accumulation of HBc150_HA at different growth stages in the 16S fusion transformant strain, cells were harvested at different time points and analysed by western blots probed with anti-HA antibodies. As shown in Figure 4.19 (a), the accumulation of HBc150_HA in the 16S fusion transformant strain was very robust with a strong protein band detectable in the 120 h sample. However, there was still some degradation in the 144 h sample. It has been suggested that the net protein production

is the balance between protein production and protein degradation (Potvin and Zhang, 2010). In this case, HBc150_HA accumulation driven by the stronger 16S rRNA promoter has compensated for the loss of proteins due to proteolytic degradation. But the compensation effects start to wane after 120 h of cultivation as demonstrated in Figure 4.19.

Overall, despite the slight reduction of specific growth rate and maximum biomass accumulation of the 16S fusion transformant strain, the chimeric 16S rRNA promoter/*psaA* 5'UTR regulatory element supported robust HBc150_HA accumulation in the *C. reinhardtii* chloroplasts.

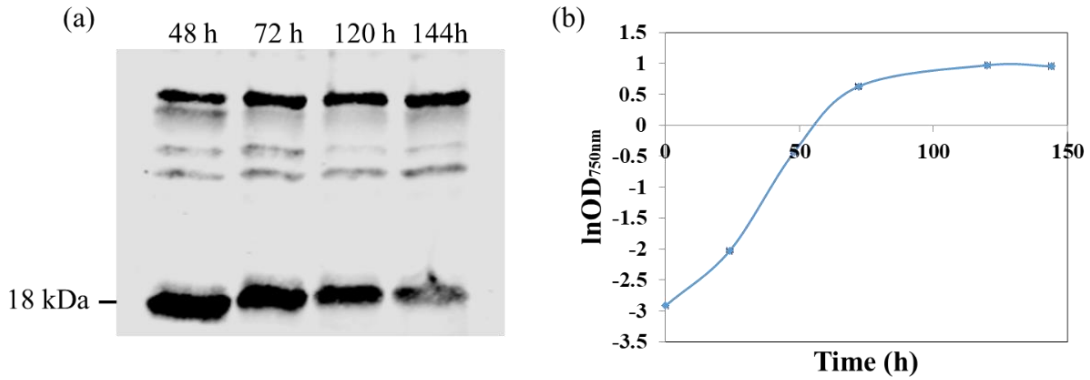

Figure 4.19: Accumulation of HBc150_HA in the 16S fusion transformant strain and the growth kinetics of the 16S fusion transformant strain. (a) Accumulation of HBc150_HA in the 16S fusion transformant strain at different time points. Non-specific bands (25 kDa and 40 kDa) served as a loading control. (b) Growth kinetics of the 16S fusion transformant strain with a starting OD_{750nm} of 0.03. Error bars represent the range of duplicate points (n=2). Experiments performed as described in Section 2.3.2 and analysis performed as described in Section 2.3.3 and 2.5.5.

4.4.3 Quantification of HBc150_HA in the 16S fusion transformant strain and comparison to the yield of K1.K1 in *P. pastoris*

In order to examine the potential of the *C. reinhardtii* chloroplast as an alternative expression platform for HBcAg to other established platforms, it was imperative to determine the yields of HBc150_HA produced in the 16S fusion transformant strain. In this study, protein quantification was based on densitometric analysis of the western

blots. This method has been proved to be an efficient and reliable way to quantify proteins (Wang *et al.*, 2007; Thomson *et al.*, 2011; Zedler *et al.*, 2014).

The detailed quantification protocol is described in Section 2.5.5. In brief, nitrocellulose membranes were probed with polyclonal anti-HBcAg primary antibodies followed by the anti-rabbit IRDye® secondary antibodies. Since the secondary antibodies were linked with the NIR fluorescent dyes, the NIR fluorescent signals could be detected using the Odyssey® Infrared Imaging System. The integrated imaging and analysis software Image Studio™ then recorded the total fluorescent signals. Background subtraction in an area of 2 pixels above and under the signal was selected to give more accurate results.

In order to establish the standard curve between the NIR fluorescent signals and protein concentration, a purified *E. coli*-based HBcAg with known concentrations was used (Bio-Rad, Watford, UK). According to Figure 4.20 (a) and (c), there was a linear correlation between the NIR fluorescent signals and the standard protein concentrations (250-1000 ng), with an R^2 value of 0.992 for the experimental data.

Based on the results obtained in Section 4.2, the 16S fusion transformant strain was grown under standard mixotrophic conditions (120 rpm, 200 µmol $m^{-2}s^{-1}$ and 25 °C). Once the cell cultures reached an OD_{750nm} of 1, a 10 mL sample was harvested to prepare the whole cell extract for western blot analysis. Different dilutions of samples were loaded to find the linear range of detection in the imaging system. It was found that dilutions of 0.25-1X were proportional to the NIR fluorescent signals detected (Figure 4.20 (b) and (d)), with an R^2 value of 0.998 for the experimental data. Based on the correlation (y=10.93x-2466) obtained between the NIR signal and the standard protein concentration, it was estimated that the yield of HBc150_HA was 4.9 mg per gram of dry cell weight. The detailed calculations are presented in Appendix 6 (A6).

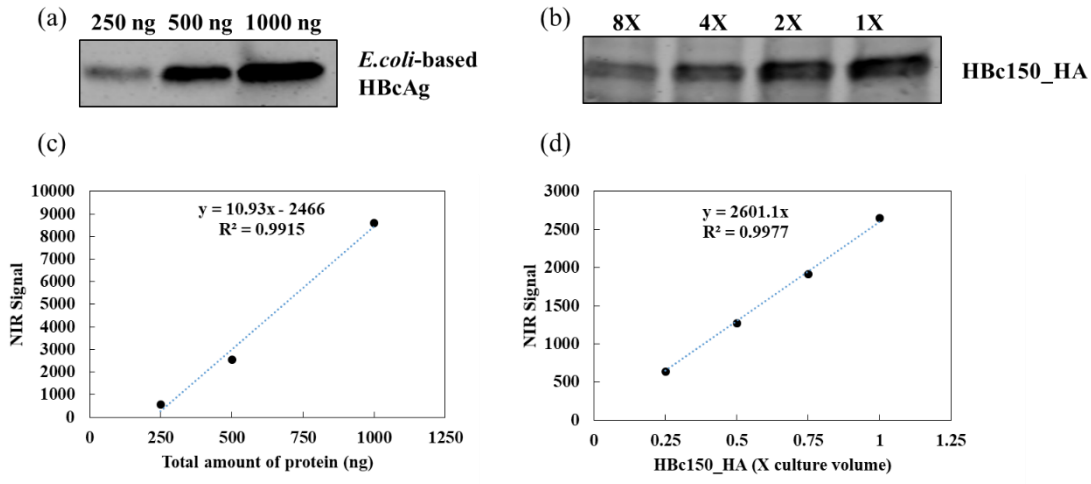

Figure 4.20: Densitometric analysis for HBc150_HA quantification in the 16S fusion transformant strain. (a): Western blot analysis of the purified *E. coli*-produced HBcAg at different protein amounts (250-1000 ng). (b): Western blot analysis of algal extracts with HBc150_HA in 16S fusion transformant strain with different protein loading volumes (0.25-1X). Membranes were probed with polyclonal anti-HBcAg primary antibodies and secondary antibodies linked to NIR fluorescent dyes. (c): Plot of total NIR fluorescent signal of the bands in (a) against standard protein amounts. (d): Plot of total NIR fluorescent signal of the bands in (b) against different protein loading volumes. Linear relationships were found in both (c) and (d) and used the slopes of the lines to calculate HBc150_HA expression level in the 16S fusion transformant strain. Analysis performed as described in Section 2.5.5.

In addition, another 10 mL crude protein extracts were also harvested and clarified by centrifugation (13,000 g, 15 min, 4 °C). The TSP concentration was determined using the Bradford assay (Bio-Rad, Watford, UK). The standard curve was established using known concentrations of BSA (Figure 2.3). It was estimated that the TSP of the crude extract was approximately 1 mg mL^{-1}. Based on the above calculations, HBc150_HA produced in the 16S fusion transformant strain represents approximately 2.34% (w/w) TSP. This result was in accordance to the protein yields reported in the literature for *C. reinhardtii* chloroplasts as demonstrated in Table 4.6. The detailed calculations are presented in Appendix 6 (A6). In fact, the yield of HBc150_HA obtained in this study is estimated to be sufficient for commercial production (Rasala *et al.*, 2010).

Table 4.6: Heterologous protein yields reported for expression in the *C. reinhardtii* chloroplasts.

Heterologous protein	Yield (% (w/w) TSP)	Reference
Fusion protein comprising FMDV VP1 protein and the cholera toxin B subunit (CtxB)	3-4	Sun *et al.*, 2003
Mammary-associated serum amyloid (M-SAA)	5	Manuell *et al.*, 2007
Human vascular endothelial growth factor (VEGF) isoform 121	2	Rasala *et al.*, 2010
D2 fibronectin-binding domain of *Staphylococcus aureus* fused with the cholera toxin B subunit (CTB)	0.7	Dreesen *et al.*, 2010
Plasmodium falciparum surface protein (Pfs25) fused to the CtxB	0.09	Gregory *et al.*, 2013
Human Papillomavirus 16 E7	0.12	Demurtas *et al.*, 2013
Variable domain of camelid heavy chain-only antibodies	1.4-4.6	Barrera *et al.*, 2014
Endolysins identified from *Streptococcus pneumoniae*-infecting phages: Cpl-1, a lysozyme hydrolysing the polysaccharide chains in the bacterial cell wall; Pal, an amidase cleaving the linker peptides in the peptidoglycan network	0.9-1.2	Stoffels *et al*., 2017
Truncated HBcAg monomer (HBc150_HA)	**2.34**	**This study**

In order to compare HBcAg yields in different expression systems, the same quantification strategy was used to examine the yield of K1.K1 produced in *P. pastoris*. The same *E. coli*-derived HBcAg standard was used to establish the standard curve between the NIR fluorescent signals and the protein concentrations. As shown in Figure 4.21 (a) and (c), there was a linear correlation between the NIR fluorescent signals and the standard protein concentrations (250-1000 ng), with an R^2 value of 0.999 for the experimental data. In addition, Figure 4.21 (b) and (d) shows that different dilutions (4.5-18X) of crude extracts were within the linear detection range of the Odyssey®

Infra-red signal system. Based on the assumptions that the wet weight of *P. pastoris* was 30 mg mL^{-1} and 1g wet weight was estimated to be equivalent to 0.3 g dry weight (Glazyrina *et al.*, 2010), the yield of K1.K1 was estimated to be 1.3 mg per gram of dry cell weight.

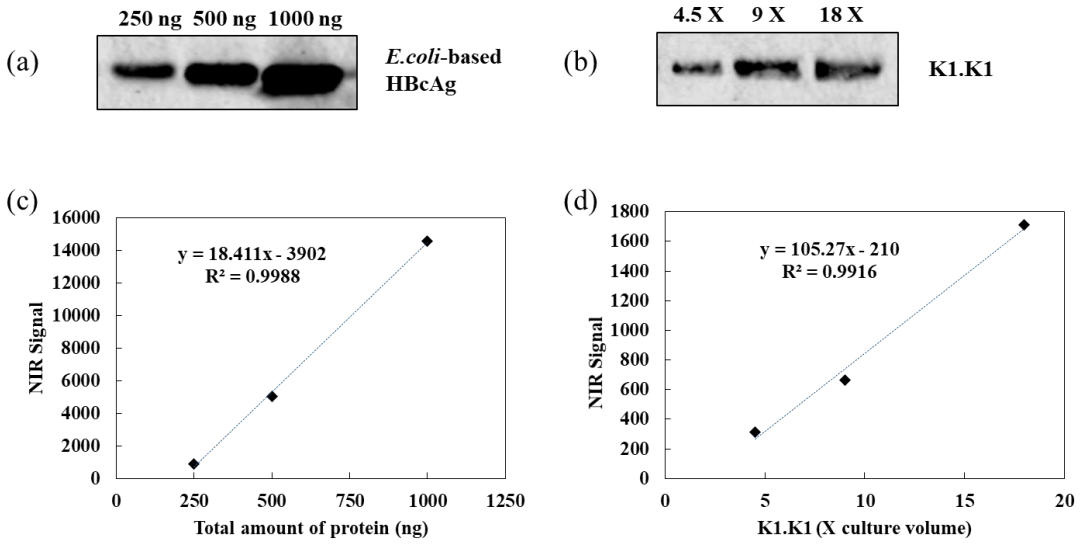

Figure 4.21: Densitometric analysis for K1.K1 in *P. pastoris*. (a): Western blot analysis of the purified *E. coli*-produced HBcAg at different protein amounts (250-1000 ng). (b): Western blot analysis of crude protein extracts of K1.K1 with different protein loading volumes (4.5-18X). Membranes were probed with polyclonal anti-HBcAg primary antibodies and secondary antibodies linked to NIR fluorescent dyes. (c): Plot of total NIR fluorescent signal of the bands in (a) against standard protein amounts. (d): Plot of total NIR fluorescent signal of the bands in (b) against different protein loading volumes. Linear relationships were found in both (c) and (d) and used the slopes of the lines to calculate the expression level of K1.K1. Analysis performed as described in Section 2.5.5.

It was interesting to observe that the production yield of HBc150_HA produced in the algal chloroplast was almost four-fold higher than that of the K1.K1 produced in the *P. pastoris*. However, it should be noted that K1.K1 was a hetero-tandem HBcAg dimer whereas HBc150_HA was a truncated monomer. Indeed, antibodies will have different affinities towards the same antigen even due to the slight sequence change (Saper, 2009). Moreover, Li et al. (2007) have shown that the yield of the *P. pastoris*-based HBcAg monomer was 64 mgL^{-1} which was estimated to be 7.1 mg per gram of dry cell weight. This was also five-fold higher than the yield of K1.K1, suggesting that K1.K1 was difficult to be expressed in yeast. In addition, the biomass accumulation of *P. pastoris*

was usually more than that of *C. reinhardtii*. Nevertheless, the production of HBc150_HA in the 16S fusion transformant strain lays a solid foundation for the successful assembly and detection of HBcAg VLPs.

4.4.4 Summary

The HBc150_HA expression level was increased by 26-fold by replacing the original *psaA* promoter (Figure 4.17) with a stronger 16S rRNA promoter (Section 4.4.1). This was mainly due to the increase in transcription rate and steady-state mRNA levels driven by the stronger promoter. In addition, there seemed to be no supply limit of the nuclear-coded *psaA*-specific factors as opposed to the results demonstrated in the literature (Rasala *et al.*, 2011).

Growth kinetics for both the *psaA* and the 16S fusion transformant strains were performed in the well-controlled Algem® photobioreactor under standard mixotrophic conditions (Section 4.4.2). Based on the growth kinetics profiles, it was concluded that high HBc150_HA expression levels in the 16S fusion transformant strain exerted only minor metabolic burdens on *C. reinhardtii* growth and biomass accumulation (Figure 4.18). Therefore, the *C. reinhardtii* chloroplast is regarded as a feasible platform to produce HBcAg in the future.

Based on the densitometric analysis, HBc150_HA in the 16S fusion transformant strain accumulated to approximately 2.34% (w/w) TSP and 4.9 mg per g of dry cell weight. The yield of the *P. pastoris*-produced K1.K1 was estimated to be 1.3 mg per gram of dry cell weight using the same quantification strategy. It was interesting to see that there was a four-fold higher level of protein in the microalgal chloroplast. It is also suggested that protein yield above 2% (w/w) TSP in microalgae is sufficient for commercial production as evaluated in Rasala et al. (2010). Since the production yield of HBc150_HA is 2.34% (w/w) TSP in the 16S fusion transformant strain, it is a promising alternative protein expression host for commercial HBcAg production.

4.5 Overall summary

In this chapter, two strategies to improve HBc150_HA expression in the *C. reinhardtii* chloroplast were explored. From the bioprocessing aspect, the effects of cultivation mode, acetate concentration, light intensity and temperature on cell growth and protein expression were examined (Section 4.2). It was noted that the changes of acetate consumption and pH values were in line with changes in the measured growth kinetics. After comparing the growth parameters (specific growth rate and maximum biomass concentration, Table 4.1-Table 4.5), it was concluded that standard mixotrophic conditions are the most suitable way to cultivate transgenic *C. reinhardtii*. Moreover, it was difficult to identify the most suitable cultivation condition for HBc150_HA expression due to the limited amount of proteins expressed in the *psaA* transformant strain.

In Section 4.3, low protein expression was addressed from the genetic engineering perspective. Since the promoter plays a critical role in terms of transcription initiation and mRNA accumulation, a well-known strong endogenous promoter, the 16S rRNA promoter, was incorporated into the existing algal vector pHBc150_HA to form the new vector p16SHA. The 16S fusion transformant strain T5 with the highest HBc150_HA expression in this experiment was selected among six transgenic lines (Figure 4.15). There was a 26-fold increase in HBc150_HA accumulation driven by the stronger 16S promoter as evidenced in Section 4.4.1. It was suggested that the rate of transcription or the steady-state mRNA level were further improved when a stronger promoter was in use (Rasala *et al.*, 2011). In addition, HBc150_HA expressed in the 16S fusion transformant strain was detected by both polyclonal and monoclonal anti-HBcAg antibodies (Figure 4.16), confirming its immunoreactivity under denaturing conditions (Soria-Guerra *et al.*, 2013).

Apart from heterologous protein expression, protein degradation and growth kinetics were also compared between the 16S fusion transformant and the *psaA* transformant strain. The results in Section 4.4.2 demonstrated that there was a slight reduction in growth rate and biomass concentration in the former strain (Figure 4.18). This was

probably due to the increase in HBc150_HA expression, leading to a competition of translation factors between heterologous proteins and the biomass-related proteins. In addition, HBc150_HA in the 16S fusion transformant strain was much more stable even during the stationary growth phase. This was probably due to the rate of protein accumulation outperforming the rate of degradation.

The production yields of HBc150_HA in the 16S fusion transformant strain and the HBcAg dimer K1.K1 produced from *P. pastoris* were quantified using densitometric methods of western blots probed with polyclonal anti-HBcAg antibodies. It was interesting to see that the yield of HBc150_HA was almost four-fold higher than K1.K1 on the basis of dry cell weight (Figure 4.20 and Figure 4.21). In addition, the protein yield obtained in the *C. reinhardtii* chloroplast was consistent with the values reported in the literature (Table 4.6).

Overall, the yield of HBc150_HA was significantly increased by using a stronger chimeric regulatory element such as the combination of the 16S rRNA promoter and the *psaA* 5'UTR in this study. These data also shed light on the new design of promoter/5'UTR regulatory elements towards high level recombinant protein production in microalgal chloroplasts. The final step in this work is verification of HBcAg VLP formation in the *C. reinhardtii* chloroplast i.e. self-assembly of the HBcAg monomers into structural VLPs. This is examined in Chapter 5.

5 Partial purification of HBc150_HA and verification of algae-based VLP

5.1 Introduction and aim

Good expression of the HBc150_HA protein was demonstrated in Section 4.4 with an estimated yield of 2.34% (w/w) of TSP or equivalently 4.9 mg per g $_{DCW}$. In fact, the protein yield obtained in this study has met the suggested requirement for commercial protein production in microalgae (Rasala *et al.*, 2010). To date, commercially relevant products derived from the *C. reinhardtii* chloroplasts include, amongst others, full-length human antibodies, oral vaccine candidates and immunotoxins (Tran *et al.*, 2009, 2013; Demurtas *et al.*, 2013; Specht and Mayfield, 2014; Dyo and Purton, 2018). This suggests that it might also be possible to correctly assemble more complex VLP structures in the *C. reinhardtii* chloroplast as an alternative to conventional protein production platforms.

Currently, there is only one published work that has exploited *C. reinhardtii* to produce HBcAg-based antigens but this was based on nuclear expression (Soria-Guerra et al. 2013). Not only were low protein expression levels (0.02-0.05% (w/w) of TSP) obtained, but the site positional effect of transgene integration in the nuclear genome was also observed to affect expression levels. Additionally, the authors did not demonstrate the formation of VLPs from the expressed HBcAg protein. Another study used the diatom *Phaeodactylum tricornutum* to express the hepatitis B surface antigen; this also did not visually demonstrate the formation of VLPs (Hempel *et al.*, 2011).

Therefore, the **aim** of the experiments carried out in this chapter was to explore the HBcAg VLP formation in the *C. reinhardtii* chloroplasts for the first time. Specific objectives were:

- To generate both positive and negative controls for TEM analysis. The positive control involved the use of *E. coli*-expressed ΔHBc150_HA which had the identical protein sequence to the algal-based HBc150_HA. In addition, two

algal transgenic lines (TNE and TN72_SR_pal-HA) without HBcAg expression were used as the negative controls;

- To identify suitable VLP clarification methods using the bacterial protein lysates and to establish a standard clarification protocol of the algal-based VLPs for TEM observations;
- To confirm VLP formation in the HBc150_HA-expressing 16S fusion transformant strain by TEM. An immunogold labelling technique was also employed to further verify the presence and immunoreactivity of algal-based HBcAg VLPs.

5.2 Expression of HBc150_HA and assembly of VLPs in *E. coli*

In order to verify HBcAg VLP formation in the *C. reinhardtii* chloroplast, it was necessary to generate positive controls for TEM analysis. As a result, a transgene sequence encoding the truncated HA-tagged HBcAg monomer (HBc150_HA) was codon-optimised and expressed in *E. coli* BL21 (DE3) as described in Section 2.3.1. Two conventional VLP clarification methods, namely sucrose gradient ultracentrifugation (Section 2.4.3) and gel filtration (Section 2.4.4), were examined and compared in terms of isolation ability and sample purity in TEM analysis. The experimental conditions established in this section facilitated the subsequent algal-based VLP clarification and identification. More importantly, this study also served as the positive control to examine if the inclusion of an HA-tag and primary sequence manipulation would influence capsid assembly.

5.2.1 Expression of the ΔHBc150_HA in *E. coli* BL21 (DE3)

The transgene sequence encoding the truncated HA-tagged HBcAg monomer (HBc150_HA) (Section 3.4.1) was codon-optimised to the codon usage preference of *E. coli*. It was then synthesized *de novo* by ATUM (Section 2.2.10) and cloned into a bacterial plasmid (pD454-SR) such that the gene was downstream of an IPTG-inducible T7 promoter as illustrated in Figure 5.1. The core protein encoded by this *E. coli* gene

construct was named ΔHBc150_HA (the full codon-optimised sequence is given in Appendix 4 (A4)) to differentiate it from the algal-expressed HBc150_HA.

E. coli BL21 (DE3) cells were transformed with pD454-SR as described in Section 2.2.8. Three colonies were selected and propagated in LB medium for plasmid isolation and protein expression. The insertion of the transgene was confirmed by sequencing the isolated plasmids with the universal forward T7 primer (Section 2.2.10). Glycerol stocks were made after sequence confirmation. These transgenic lines were named BL21_HBc150_HA_T1-T3.

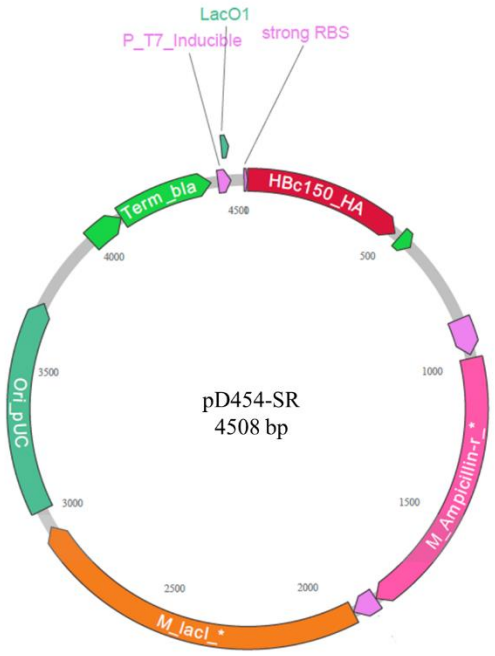

Figure 5.1: The simplified diagram of the bacterial plasmid pD454-SR synthesized by ATUM (Section 2.2.10). The *HBc150_HA* gene was placed under the control of the IPTG-inducible T7 promoter with a strong ribosome binding site (RBS).

The detailed protein induction protocol is described in Section 2.3.1. In brief, glycerol stocks of three transgenic lines were inoculated into LB medium to grow for five hours. Subsequently, they were inoculated into three shake flasks containing LB medium and grown at 37 °C for three hours. 1 mM IPTG was added to the cell cultures when they reached to the exponential growth phase (OD_{600nm} at 0.6-0.8). It has been suggested that

reducing the temperature during the protein production phase can avoid the aggregation of the protein *in vivo* (Groot and Ventura, 2006). Therefore, the cultivation temperature after IPTG induction was lowered from 37 °C to 18 °C.

E. coli cells were harvested 16-18 h after induction and re-suspended in the bacterial lysis buffer. The cells were completely broken by the homogeniser as described in Section 2.4.2. In order to check the expression and solubility of ΔHBc150_HA in *E. coli*, both the supernatant and the cell pellet were analysed by SDS-PAGE. Figure 5.2 demonstrates that there was a high expression of ΔHBc150_HA that was mainly recovered in a soluble form in the supernatant. As a result, the supernatant was subjected to subsequent partial purification and TEM analysis.

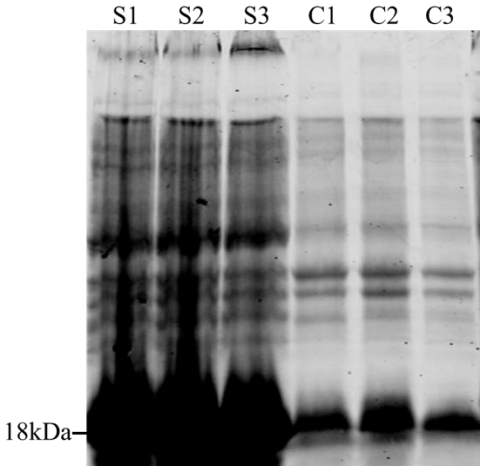

Figure 5.2: Coomassie® blue stained SDS-PAGE gel showing the over-expression of ΔHBc150_HA in *E. coli* BL21 (DE3). S1-S3: supernatant in transgenic lines BL21_HBc150_HA_T1-T3; C1-C3: cell pellet in transgenic lines BL21_HBc150_HA_T1-T3. Experiments performed as described in Section 2.5.3 and Section 2.5.4.

5.2.2 Sucrose gradient ultracentrifugation of the *E. coli*-produced ΔHBc150_HA

Continuous sucrose gradient ultracentrifugation is one of the most commonly used separation methods for VLPs (Section 1.4.1). One of the main factors influencing the successful separation of VLPs from other contaminants is the quality of the continuous sucrose gradient. Two common gradient preparation methods were compared in order

to determine the best technique for subsequent investigations. The gradient was prepared by either manual loading or by using a gradient maker. Bromophenol blue was added as a colour indicator to examine the linearity of the sucrose gradient. The amount of blue dye added was proportional to the sucrose gradient concentration ranging from 10% to 50% (w/v). Once the gradients were formed, 24 aliquots from the top to the bottom of the ultracentrifuge tube were taken. The concentration of the blue dye was analysed by spectrophotometry at a wavelength of 598 nm.

As shown in Figure 5.3 (a), the blue dye concentration reflecting the target sucrose concentration was not linear in the manually loaded gradient especially in fractions 1-12 and 19-20. In contrast, there was a strong linear relationship (R^2=0.993) between the blue dye concentration and the fractions prepared using the gradient maker (Figure 5.3 (b)). Therefore, all of the continuous sucrose gradients in this study were prepared using the gradient maker.

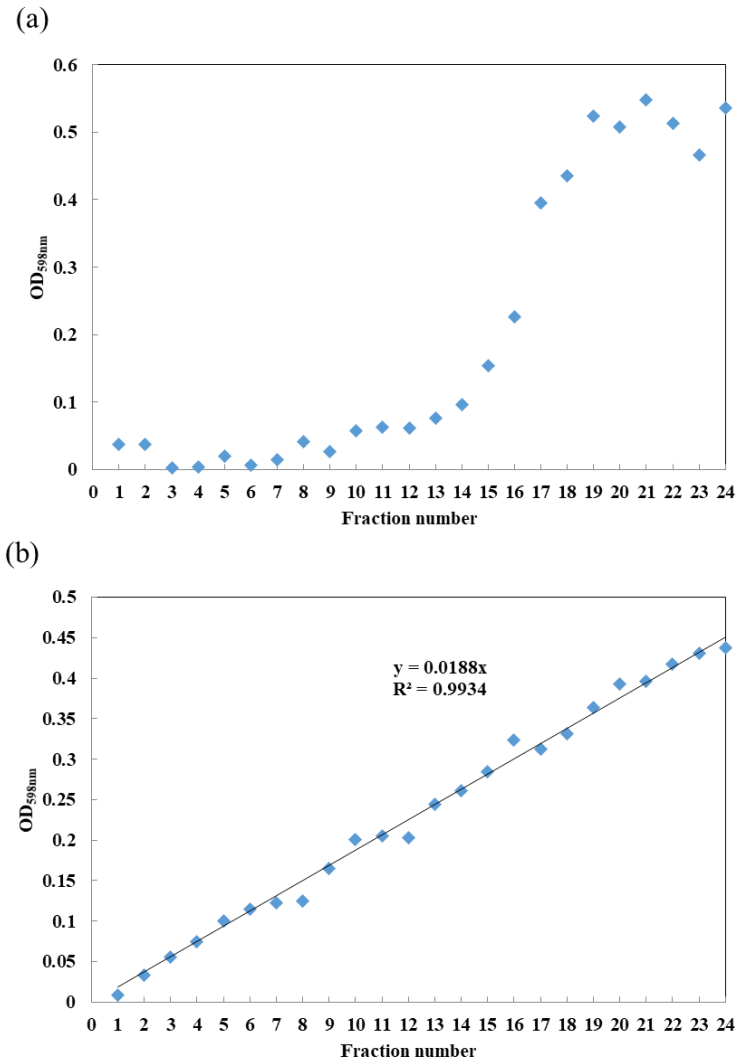

Figure 5.3: Correlation between the concentration of blue dye reflected by OD_{598nm} readings and the gradient fractions formed by (a) manual loading and (b) using a SG15 Gradient Maker. Experiments performed as described in Section 2.4.3. Solid line fitted by linear regression.

Since the expression of ΔHBc150_HA in *E. coli* was confirmed, the supernatant obtained in a BL21_HBc150_HA_T1 culture (Section 5.2.1) was subjected to ultracentrifugation using a 10-50% (w/v) continuous sucrose gradient. From the top to bottom, 18 fractions were sampled and labelled as 1 to 18 sequentially. Figure 5.4 shows the SDS-PAGE analysis of the 18 gradient fractions following Coomassie® blue staining. Protein bands with the correct molecular weight of ΔHBc150_HA (18 kDa) were mainly detected in fractions 7 to 12, corresponding to 25-35% (w/v) sucrose concentration. This was in accordance with the migration pattern (25-32% (w/v)

sucrose) reported for VLPs formed by the truncated HBcAg monomers in *E. coli* (Wooi and Siang, 2008). In addition, there were faint bands in fractions 1 and 2, indicating the presence of lower molecular-weight-forms such as monomers and dimers. The bands detected in fractions 16 and 18 were most likely to be larger aggregates of core protein material. Hence, fractions 7 to 12 were pooled, dialyzed against 50 mM HEPES buffer (pH 7.5) and subjected to TEM analysis as described in Section 5.2.4.

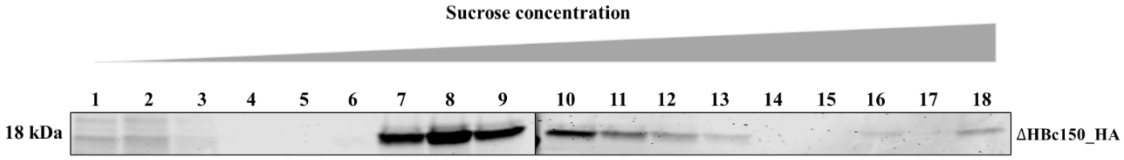

Figure 5.4: Coomassie® blue stained SDS-PAGE gel showing 18 gradient samples of BL21_HBc150_HA_T1 after continuous 10-50% (w/v) sucrose gradient ultracentrifugation. Experiments performed as described in Section 2.5.3 and Section 2.5.4.

5.2.3 Gel filtration of the *E. coli*-based ΔHBc150_HA

Gel filtration is another frequently used technique for VLP separation (Li et al. 2007; Sominskaya et al. 2013). The detailed protocol for the gel filtration process used here is explained in Section 2.4.4. In brief, 2 mL crude protein lysate of BL21_HBc150_HA_T1 containing ΔHBc150_HA was run through a Sepharose® CL-4B column in an ÄKTA pure chromatography system. Elution profiles were monitored by UV absorbance at a wavelength of 280 nm.

During the process, 14 elution fractions (3-16) were collected automatically as shown in Figure 5.5. Fraction 2 was not collected due to the absence of protein. As shown in Figure 5.5, separation of the bacterial protein lysate of BL21_HBc150_HA_T1 resulted in two major peaks in the chromatogram, representing large and small molecules, respectively. However, due to sample overload, the two major peaks were merged together between fractions 7-12. Nonetheless, based on the characteristics of the Sepharose® CL-4B column, HBcAg VLPs were predicted to be eluted in fractions 5 to 8. Therefore, these fractions were pooled and subjected to TEM analysis as presented in Section 5.2.4. It should be noted that dialysis was not carried out in this study as the

elution buffer used in gel filtration was compatible with the negative staining procedure for TEM analysis.

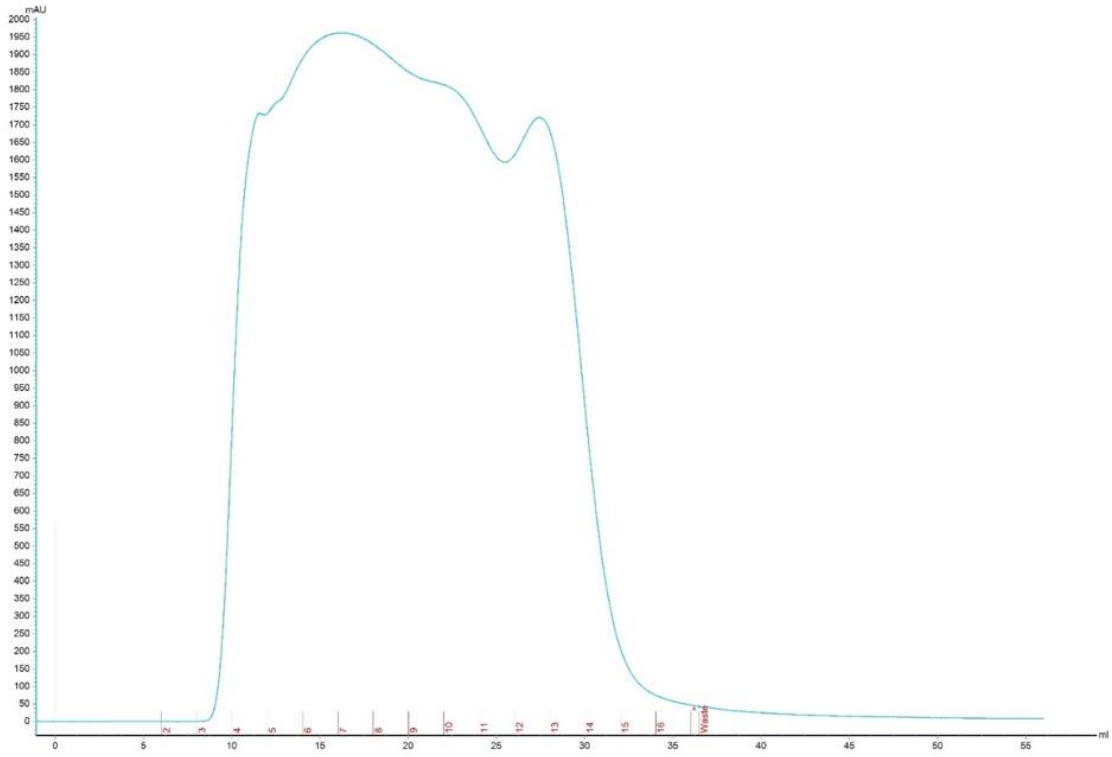

Figure 5.5: Chromatogram of the UV absorbance at 280 nm for 14 elution fractions of the crude protein lysate of BL21_HBc150_HA_T1. Fraction numbers are labelled in red. Experiments performed as described in Section 2.4.4.

5.2.4 TEM analysis

The clarified bacterial protein samples obtained by sucrose gradient ultracentrifugation (Section 5.2.2) and gel filtration (Section 5.2.3) were negatively stained with 2% (w/v) uranyl acetate and visualized under TEM.

The micrographs in Figure 5.6 show the presence of isometric particles with a diameter of 25-30 nm for both sample preparation methods. Their morphologies with small spikes on the particle surfaces were also typical for HBcAg particles produced in *E. coli* as reported in the literature (Holmes *et al.*, 2015; Peyret *et al.*, 2015). As a result, both clarification techniques were considered sufficient to isolate VLPs from the crude

bacterial lysate. It was interesting to observe that there were fewer impurities when the protein samples were processed by gel filtration. These results demonstrated that the both the addition of an N-terminal HA-tag and the insertion of additional amino acids into the penultimate N-terminal and C-terminal positions of the truncated HBcAg monomer (Section 3.4.1) did not influence correct assembly of the capsid.

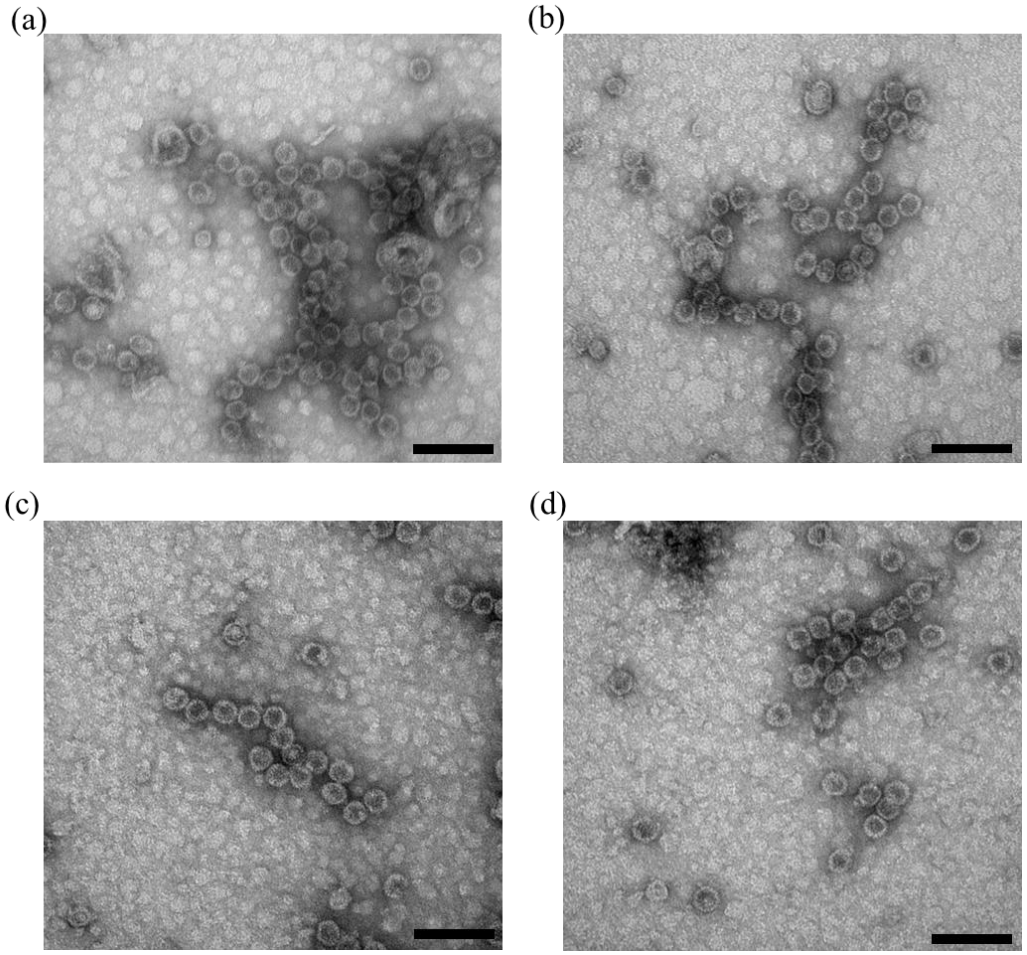

Figure 5.6: Example electron micrographs of ΔHBc150_HA particles produced in protein lysate of BL21_HBc150_HA_T1 and clarified by either (a)-(b) sucrose gradient ultracentrifugation (fractions in 7 – 12 in Figure 5.4) or (c)-(d) gel filtration (fractions 5 - 8 in Figure 5.5). Size bars, 100 nm. Magnification, 180 k. TEM performed as described in Section 2.5.6.

5.2.5 Summary

In this section, a positive control for the algae-based HBc150_HA, ΔHBc150_HA, was successfully produced in *E. coli*. Its accumulation was confirmed by SDS-PAGE analysis (Figure 5.2) followed by Coomassie® blue staining and gave the predicted molecular weight of 18 kDa.

After clarification by either continuous sucrose gradient ultracentrifugation or gel filtration, the formation of HBcAg VLPs in *E. coli* was confirmed by TEM analysis (Figure 5.6). These capsids were in the correct size range (25-30 nm) and showed typical morphologies of VLPs formed by the core protein. This showed that the inclusion of an HA-tag and slight manipulations of the core protein sequence did not impede its ability to form VLPs. Moreover, the techniques and conditions established in this section served as useful techniques for the preparation and visualisation of the algal-based VLPs.

5.3 Partial purification of the microalgal cell cultures

In order to facilitate the isolation and visualisation of the algal-based VLPs, it was imperative to establish an efficient and robust clarification process for the algal material. In Section 5.2, the combination of low-speed centrifugation with either sucrose gradient ultracentrifugation or gel filtration was sufficient to clarify bacterial cultures for VLP visualisation. However, after algal cell disruption, thylakoid membrane fragments containing proteins, lipids and chlorophylls are known to remain in the supernatant after low-speed centrifugation (Stoffels, 2015). Based on previous experience, these host impurities tended to clog the 0.22 µm syringe filters and interfere with the performance of subsequent purification operations. Therefore, three methods to remove these impurities were examined.

The proposed protocol for the preparation of algal material for TEM analysis is shown in Figure 5.7. Three methods, namely heat treatment, double sucrose cushion and ultracentrifugation, were assessed and compared in order to remove the thylakoid

membrane fragments present in the algal samples. The most suitable method was selected and incorporated into the standard VLP clarification protocol. Moreover, two transgenic *C. reinhardtii* lines without HBcAg expression were partially purified based on the proposed protocol, serving as negative controls in the TEM analysis.

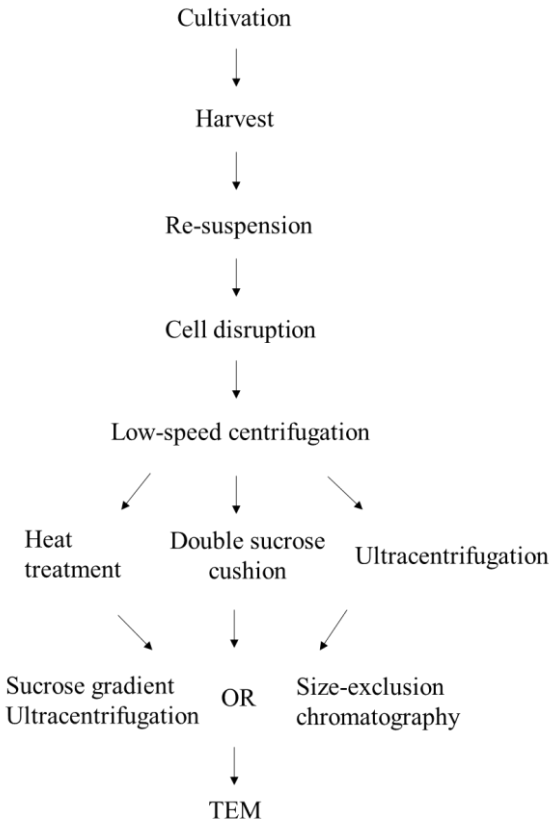

Figure 5.7: Schematic diagram of the primary clarification protocols evaluated for the isolation and visualisation of VLPs from the protein material in the *C. reinhardtii* chloroplasts.

5.3.1 Heat treatment

Heat precipitation is a simple and effective technique to purify thermostable proteins in which most host heat-labile proteins and proteases are denatured during the treatment (Ng *et al.*, 2006). Studies have shown that HBcAg VLPs possess good thermal stability in which their antigenicity is still detectable after heat-treatment at 80 °C and can only be denatured at 85 °C (Dyson and Murray, 1995; Ng *et al.*, 2006). Their good thermal stability is mainly due to the formation of disulphide bonds between cysteine residues

of two monomers within the capsid structure. In fact, both Rolland et al. (2001) and Freivalds et al. (2011) have shown that heat treatment at 65 ℃ for 1 h is a suitable condition to isolate HBcAg from host contaminants in bacterial and yeast expression systems.

In this study the 16S fusion transformant strain (Section 4.3.3) was initially grown mixotrophically as described in Section 4.2.5. After harvesting by centrifugation and cell disruption using a homogeniser, the whole cell homogenate was initially clarified by low-speed centrifugation. Then, the supernatant was incubated in a heat block at 65 ℃ for 1 h. After centrifugation at 13,000 rpm for 25 minutes, both supernatant and precipitate were collected and subjected to western blot analysis probed with anti-HA antibodies. HBc150_HA was only detectable in the supernatant prior to heat treatment (data no shown). Unfortunately, no protein bands were observed for the heat-treated samples, including both the supernatant and the precipitation. The results demonstrated that the heat treatment method was not suitable for the isolation of HBc150_HA from the *C. reinhardtii* contaminants.

5.3.2 Double sucrose cushion

As mentioned in the previous section, heat treatment seemed to denature the HBc150_HA from the 16S fusion transformant strain. Another gentler method to remove the algal-related impurities was to load protein samples onto a double sucrose cushion during ultracentrifugation. The assumption here is that the correctly-assembled VLPs with particulate nature will migrate through the first sucrose cushion layer with a lower density but will sediment on the second layer with a higher density. Peyret (2015) has previously combined the double sucrose cushion method with continuous sucrose gradient ultracentrifugation to successfully isolate plant-expressed HBcAg VLPs with high recovery yield.

The detailed protocol of setting up the double sucrose cushion is explained in Section 2.4.4. In brief, 1 mL 75% (w/v) sucrose solution, 4 mL 20% (w/v) sucrose solution and 7.5 mL crude protein lysate of the 16S fusion transformant strain were sequentially

loaded into the ultracentrifuge tube without causing disturbance of each layer. The samples were then run in a Beckman SW41Ti ultracentrifuge rotor at 39,000 rpm for 2.5 h at 4 °C. Once the gradient was formed 12 fractions, as illustrated in Figure 5.8, were taken from the top to the bottom of the tube and subjected to western blot analysis probed with anti-HA antibodies.

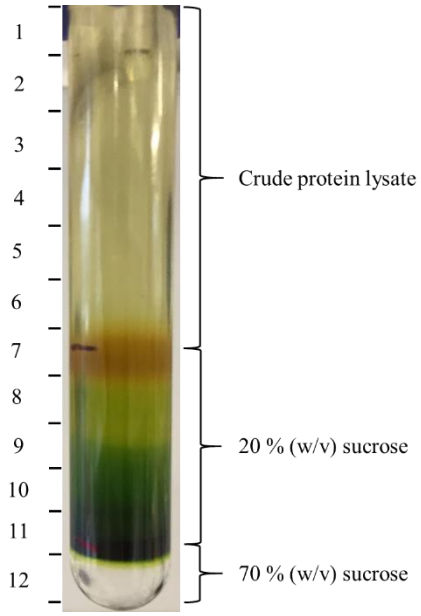

Figure 5.8: White light photograph of a 14 × 89 mm ultracentrifuge tube after double sucrose cushion ultracentrifugation. Gradient fraction numbers are labelled from 1 to 12 on the left. The positions of crude protein lysate, 20% (w/v) and 70% (w/v) sucrose solutions were labelled on the right. Experiments performed as described in Section 2.4.4.

The western blot results shown in Figure 5.9 revealed protein bands for HBc150_HA at 18 kDa in all of the fractions collected. As expected, the majority of HBc150_HA accumulated at the interface of the 20% (w/v) and 70% (w/v) sucrose cushions (fractions 10-11). In addition, there was no protein detected in fraction 12, meaning 70% (w/v) sucrose was dense enough to serve as a protective cushion at the bottom of the ultracentrifuge tube. This was in line with the migration pattern of particulate HBcAg VLPs, in which they were shown to settle at sucrose concentrations between 25-35% (w/v) (Wooi and Siang, 2008). It was interesting to note, however, that there was significant protein loss into all of the upper fractions (1-9). This might suggest the

presence of HBc150_HA monomers or dimers in the solution or the incomplete assembly of capsids.

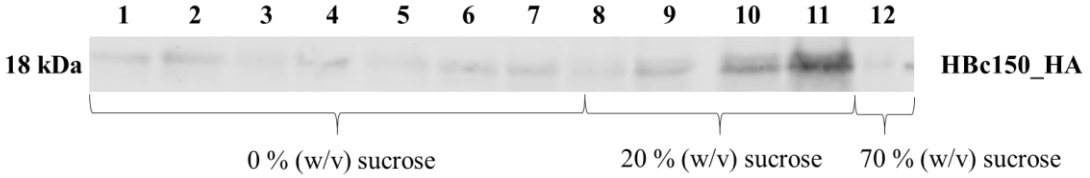

Figure 5.9: Western blot analysis of HBc150_HA in 12 fraction samples after double sucrose cushion ultracentrifugation of protein samples prepared in the 16S fusion transformant strain. The positions of 0% (w/v), 20% (w/v) and 70% (w/v) sucrose solutions are labelled under the immunoblot. Samples taken from ultracentrifuge tube shown in Figure 5.8. Analysis performed as described in Section 2.5.5.

Protein samples in fractions 10-11 were pooled, dialyzed against 50 mM HEPES buffer to remove sucrose and loaded onto a 10-50% (w/v) continuous sucrose gradient for further VLP separation from host contaminants. As shown in Figure 5.10, very faint protein bands in fractions 6-8 were detected in the western blot. This again has confirmed the particulate nature of the HBc150_HA expressed in the 16S fusion transformant strain. However, there was a slight shift towards the lower concentration of sucrose (23-28% (w/v)) compared to the 25-32% (w/v) in the bacterial material (Section 5.2.2). Fractions 6 to 8 were pooled and dialyzed against 50 mM HEPES buffer before TEM observations. Unfortunately, it was not possible to detect any VLP structures in the electron micrographs owing to the very low HBc150_HA concentration.

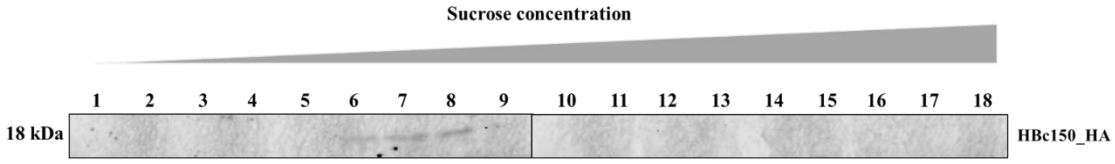

Figure 5.10: Western blot analysis of HBc150_HA in 18 fraction samples of the 16S fusion transformant strain after continuous sucrose gradient ultracentrifugation of protein samples taken in fractions 10 and 11 in Figure 5.9. Analysis performed as described in Section 2.5.5.

5.3.3 Ultracentrifugation

Ultracentrifugation is another efficient method of removing the thylakoid membranes. Unlike the double sucrose cushion, it does not involve the use of any cushion, which can be potentially harsh to particulate structures such as VLPs during pelleting (Peyret, 2015). Ultracentrifugation refers to the very high speed employed during differential centrifugation. In general, low-speed centrifugation is carried out to remove unbroken whole cells, cell debris and large insoluble fragments whereas high-speed centrifugation is used to pellet smaller impurities such as membrane-bound chlorophyll-protein complexes in algal samples (Stoffels, 2015). However, there is a tendency for loss of products such as VLPs with a known particulate nature.

In order to assess protein loss during ultracentrifugation, cell cultures of the 16S fusion transformant strain grown to the exponential growth phase in mixotrophic cultures were harvested. After cell disruption, the whole cell homogenate was first subjected to low-speed centrifugation (5,000 rpm), and then the resulting supernatant was subjected to a second round of high-speed centrifugation (ultracentrifugation, 38,000 rpm) to remove the thylakoid membranes. The resulting supernatant and precipitate were collected and subjected to western blot analysis to monitor potential HBc150_HA loss during clarification.

As shown in Figure 5.11, approximately a quarter of the HBc150_HA material was lost in the sediment after ultracentrifugation. This was likely due to the particulate nature of HBc150_HA as demonstrated in Figure 5.10 and Figure 5.11. In addition, trapping of the HBc150_HA by the membrane vesicles could be another reason as there are reports of soluble protein loss after ultracentrifugation (Stoffels, 2015). However, compared to the double sucrose cushion, the concentration of HBc150_HA was sufficient to carry out subsequent studies.

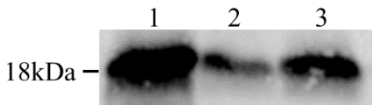

Figure 5.11: Western blot analysis of HBc150_HA in protein samples that were collected in (1) low-speed centrifugation supernatant, (2) ultracentrifugation sediment and (3) ultracentrifugation supernatant. Analysis performed as described in Section 2.5.5.

5.3.4 Proposed algal-based VLP clarification protocol

Unlike the successfully removal of host contaminants by heat treatment in bacterial and yeast cultures, HBc150_HA expressed in the *C. reinhardtii* chloroplasts was probably denatured during the heat treatment. As for the double sucrose cushion method, there was considerable product loss mainly due to the successive dialysis and concentration steps involved. This also complicated the whole procedure and prolonged the total clarification time. In contrast, direct ultracentrifugation was quick to apply and was found to be a suitable method to remove thylakoid membranes with an acceptable product loss at this stage. Hence, ultracentrifugation was incorporated in the final clarification protocol after low-speed centrifugation. The proposed clarification process to prepare HBcAg VLPs from the *C. reinhardtii* chloroplasts is illustrated in Figure 5.12.

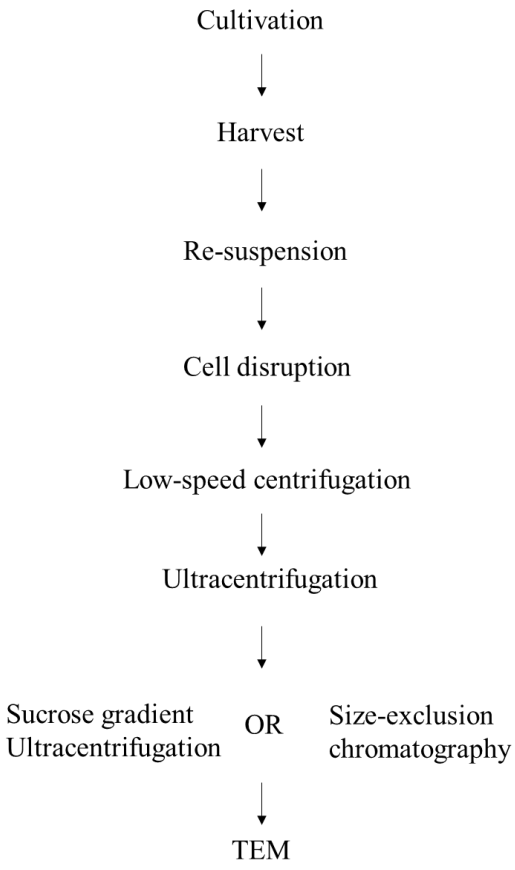

Figure 5.12: Schematic diagram of the final clarification protocol used for the isolation and visualisation of VLPs from the clarified protein materials in the *C. reinhardtii* chloroplasts.

5.3.5 Generation of negative controls for TEM analysis

In Section 5.2, *E. coli*-based HBc150_HA were successfully expressed and visualized by TEM. This served as a positive control to demonstrate the morphologies of VLPs formed by the same core protein monomer. Meanwhile, it was crucial to generate negative controls to further understand the background of algal material in the TEM analysis. Hence, two additional transgenic *C. reinhardtii* lines without HBcAg expression were grown and their crude protein lysates were clarified according to the proposed flowsheet (Figure 5.12). Then, partially purified protein lysates were subjected to TEM analysis to monitor the background of algal material.

The first transgenic line was TNE in which TN72 was transformed with the empty pSRSapI vector (Table 2.1). Despite the fact that there was no heterologous protein accumulation in TNE, the gradient fractions were collected and analysed by Western blot using anti-HA antibodies. The results in Figure 5.13 demonstrated the presence of non-specific bands at approximately 38 kDa and 48 kDa in fractions 2-3 in algal-based materials. These probably corresponded to the remaining thylakoid membrane fragment.

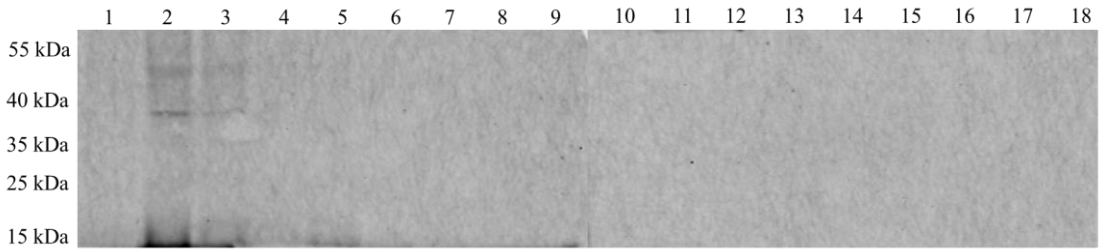

Figure 5.13: Western blot analysis of 18 fraction samples after continuous sucrose gradient ultracentrifugation of protein samples prepared in TNE. Protein markers are labelled on the left. Analysis performed as described in Section 2.5.5.

Since HBcAg VLPs usually migrate and settle at 25-30% (w/v) sucrose concentration, fractions 8-11 were collected and subjected for TEM analysis. As shown in Figure 5.14, morphologies of the impurities in the algal host were clearly demonstrated. The irregular vascular structures with a size around 100 nm in (a) were probably the debris of thylakoid membranes. In addition, smaller structures (5-10 nm) found in (b) were most likely to be the lipid bodies in algae. In general, they showed entirely different characteristics to that of the isometric HBcAg VLPs shown in Figure 5.6.

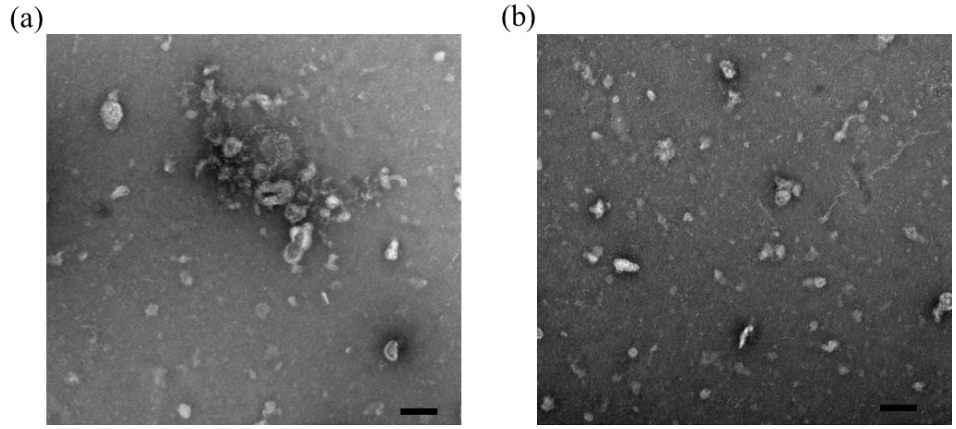

Figure 5.14: Example electron micrographs of particulate material present in TN72_SR_pal-HA clarified by continuous sucrose gradient ultracentrifugation (fractions 8-11 in Figure 5.13) (a)-(b). Size bars, 100 nm. Magnification, 93 k. TEM performed as described in Section 2.5.6.

Meanwhile, a second transgenic line TN72_SR_pal-HA expressing an endolysin was grown and processed based on the same protocol illustrated in Figure 5.12. Instead of using ultracentrifugation on sucrose, gel filtration was carried out. As demonstrated in Section 5.2.3, *E. coli*-expressed ΔHBcAg VLPs were detected in the eluates in fractions 5-8 based on the particle size distribution packed inside of the Sepharose® CL-4B column. Therefore, these fractions were pooled and subjected to TEM analysis.

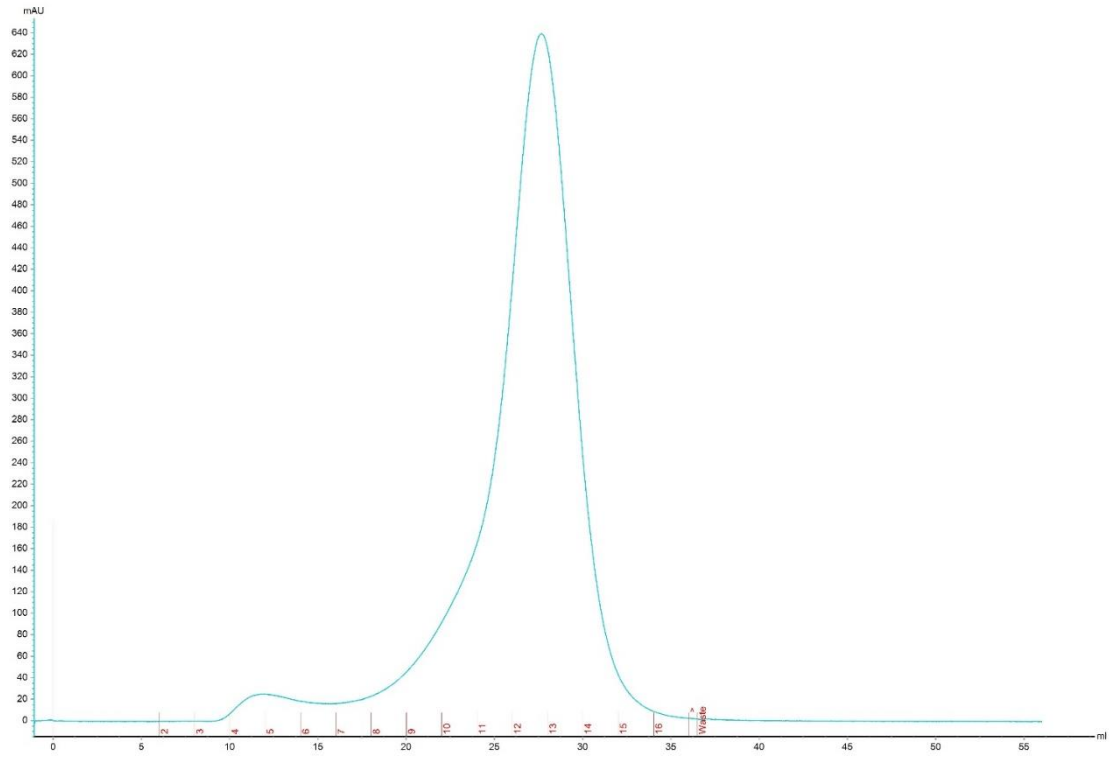

Figure 5.15: Chromatogram of the UV absorbance at 280 nm for 14 elution fractions for the clarified protein lysate of TN72_SR_pal-HA. Fraction numbers were labelled in red. Experiments performed as described in Section 2.4.4.

The micrographs in Figure 5.16 clearly demonstrated the morphologies of the algal-based material. This was very similar to that obtained in Figure 5.14 (a), whereby irregular vascular structures with a size around 100 nm were observed. It could be confirmed that they showed distinctly different characteristics to that of the isometric HBcAg VLPs seen in Figure 5.6. As a result, the HBcAg VLPs expressed in the *C. reinhardtii* chloroplasts should be easily identified from the background.

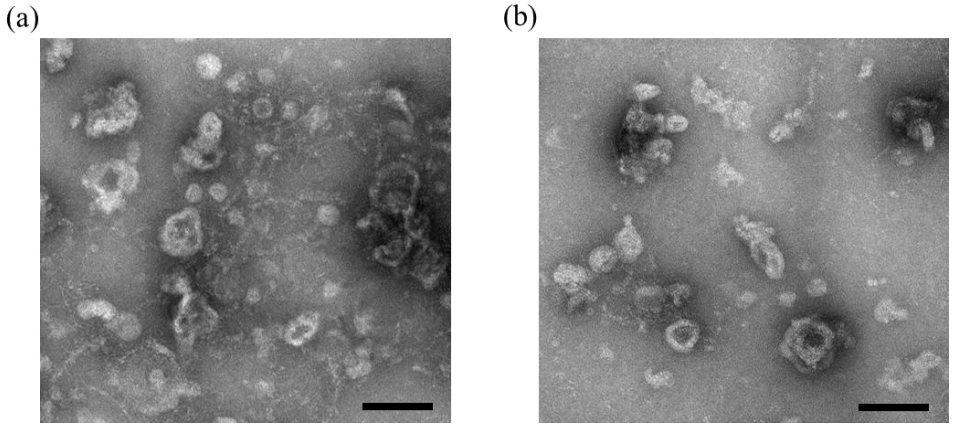

Figure 5.16: Example electron micrographs of particulate material present in TN72_SR_pal-HA by gel filtration (fractions 5-8 in Figure 5.15) (a)-(b). Size bars, 100 nm. Magnification, 180 k. TEM performed as described in Section 2.5.6.

5.3.6 Summary

Unlike bacterial cultures (Section 5.2), an additional purification step after low-speed centrifugation was necessary to remove thylakoid membranes containing proteins, lipids and chlorophylls in microalgae. Therefore, heat treatment, double sucrose cushion and ultracentrifugation were examined and compared. Ultracentrifugation was the most suitable method in terms of shorter preparation time, lower complexity and less product loss. Thus, this step was incorporated into the standardized VLP clarification protocol (Figure 5.12).

Two transgenic *C. reinhardtii* lines TNE and TN72_SR_pal-HA without HBcAg expression were clarified based on the proposed protocol. The resulting clarified protein lysates were used for electron microscopic observations. The TEM results have confirmed the presence of thylakoid membranes that could be easily distinguishable from that of VLP structures. This served as a negative control for the analysis of algal-based VLPs.

5.4 Assembly of HBc150_HA VLPs in the *C. reinhardtii* chloroplast

With the establishment of the standard clarification protocol and the generation of both positive and negative controls for TEM analysis, the potential formation of VLPs in the

C. reinhardtii chloroplasts was examined. Ultracentrifugation-processed protein samples of the 16S fusion transformant strain, cultured mixotrophically, were clarified by either sucrose gradient ultracentrifugation or gel filtration. The resultant clarified protein samples were visualized by TEM. Moreover, immunogold labelling was performed in order to further confirm the presence and immunoreactivity of the algal-based HBc150_HA VLPs.

5.4.1 Sucrose gradient ultracentrifugation of HBc150_HA expressed in the *psaA* transformant strain and the 16S fusion transformant strain

It has been suggested that capsid assembly is a highly cooperative but concentration-dependent process (Wingfield *et al.*, 1995). In order to test this hypothesis, HBc150_HA expressed from both the *psaA* transformant strain (that expresses HBc150_HA at low levels, Figure 3.18) and the 16S fusion transformant strain (that expresses HBc150_HA at higher levels, Figure 4.15) was analysed in terms of its particulate nature through the sucrose gradient ultracentrifugation step. Cultures of both strains were broken by the homogeniser and clarified by ultracentrifugation as presented in Figure 5.12. The resulting supernatant was then loaded on to a 10-50% (w/v) continuous sucrose gradient. From the top to the bottom, 18 fractions were sampled and then assayed in western blot analysis probed with anti-HA primary antibodies.

As shown in Figure 5.17 (a), the majority of the HBc150_HA expressed in the *psaA* transformant strain was detected at the top of the gradient (10-17% (w/v) of sucrose concentration), indicating the presence of monomers or dimers. In contrast, HBc150_HA produced in the 16S fusion transformant strain was mainly observed in fractions 8-11, and to a lesser extent, in fractions 1-3. The fact that most proteins were detected in 23-28% (w/v) sucrose demonstrated the particulate nature of the HBc150_HA expressed in the 16S fusion transformant strain. Therefore, cultures of the 16S fusion transformant strain were used for subsequent studies. Fractions 8-11 in Figure 5.17 (b) were pooled and dialyzed against 50 mM HEPES buffer overnight to remove sucrose. Then, the dialyzed protein sample was concentrated and negatively stained for TEM analysis.

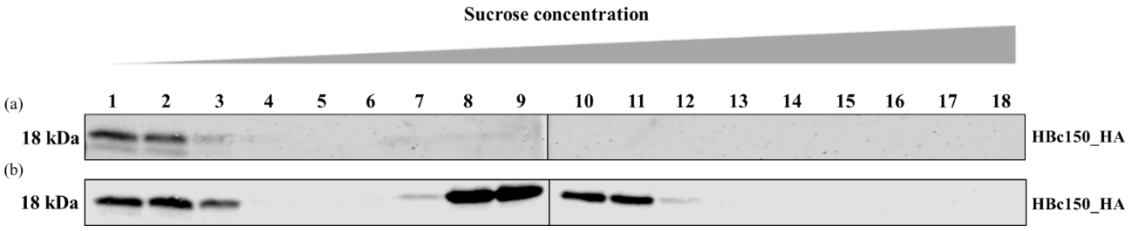

Figure 5.17: Western blot analysis of HBc150_HA in 18 fraction samples after continuous sucrose gradient ultracentrifugation of protein samples prepared in the *psaA* transformant strain (a) and the 16S fusion transformant strain (b). Analysis performed as described in Section 2.5.5.

This study further proved the importance of monomer concentration for VLP formation when compared to the data obtained with HBc150_HA accumulated in the *psaA* transformant and the 16S fusion transformant strains. Alexander et al. (2013) have suggested that the capsid assembly from truncated HBcAg monomers follows a three-state folding mechanism. First, dimerization takes place where two truncated monomers associate to form partially structured, dimeric and α-helical intermediates. These intermediates can then form multiple native conformers in which only some of them can form capsids. Therefore, it was suspected that the concentration of HBc150_HA in the *psaA* transformant strain was below the threshold concentration either for the initial formation of dimeric intermediates or the subsequent capsid-assembly-competent conformers.

5.4.2 Gel filtration of HBc150_HA expressed in the 16S fusion transformant strain

Apart from ultracentrifugation on sucrose, gel filtration is another commonly used technique to purify VLPs based on their sizes. In Section 5.2.3, the *E. coli*-expressed HBc150_HA had been successfully detected in fractions 5-8 using a Sepharose® CL-4B column. The same protocol was applied to the clarified protein lysate of the 16S fusion transformant strain. Elution profiles were monitored by UV absorbance at a wavelength of 280 nm.

During the filtration, 14 elution fractions (3-16) were collected as shown in Figure 5.18. Separation of the algal protein lysate resulted in two distinct peaks in the chromatogram,

separating the high-molecular-mass components (first peak) from the low-molecular-mass ones (second peak). All of the fractions were assayed by western blot probed with anti-HA antibodies (Figure 5.19). HBc150_HA was found in fractions 3 to 12, proving the presence of monomers as well as the high-molecular-mass multimers formed by core proteins. Based on the characteristics of the Sepharose® CL-4B column, bacterial ΔHBc150-HA VLPs were eluted in fractions 5-8. Therefore, these fractions were pooled and subjected to TEM analysis. It should be noted that dialysis was not carried out in this study as the elution buffer in gel filtration was compatible with the negative staining procedure for TEM analysis.

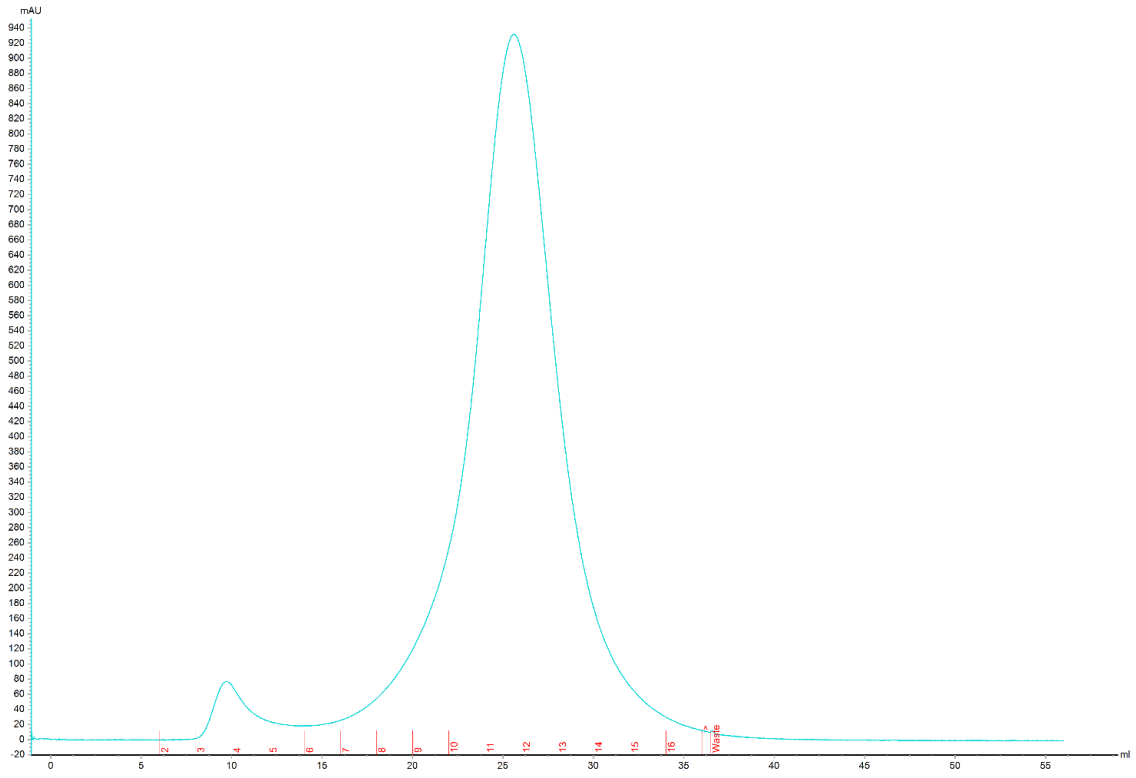

Figure 5.18: Chromatogram of the UV absorbance at 280 nm for 14 elution fractions for the clarified protein lysate of the 16S fusion transformant strain. Fraction numbers were labelled in red. Experiments performed as described in Section 2.4.4.

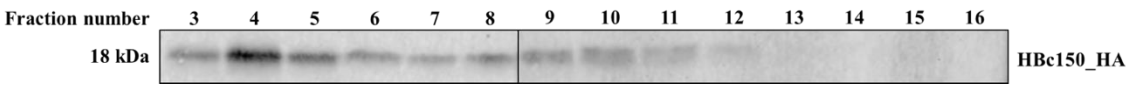

Figure 5.19: Western blot analysis of HBc150_HA in 14 fraction samples after gel filtration (Figure 5.18) prepared in the 16S fusion transformant strain. Analysis performed as described in Section 2.5.5.

5.4.3 TEM analysis

Clarified algal protein samples of the 16S fusion transformant strain prepared by sucrose gradient ultracentrifugation (Section 5.4.1) and gel filtration (Section 5.4.2) were negatively stained with 2% (w/v) uranyl acetate and visualized by TEM.

Despite low abundance, isometric particles of 25-30 nm diameter with a morphology typical for HBcAg VLPs were seen in algal samples prepared by either ultracentrifugation (Figure 5.20 (a) and (b)) or gel filtration (Figure 5.20 (c) and (d)). Hence, both clarification techniques in conjunction with ultracentrifugation were sufficient to isolate VLPs from the crude algal lysate. However, it was interesting to observe that there were fewer impurities when the algal materials were processed by gel filtration, similar to what was observed for the bacterial samples (Section 5.2.4). Moreover, the micrographs of the negative controls (Figure 5.14 and Figure 5.16) demonstrated that there were no such isometric morphologies present in the algal samples without HBcAg accumulation.

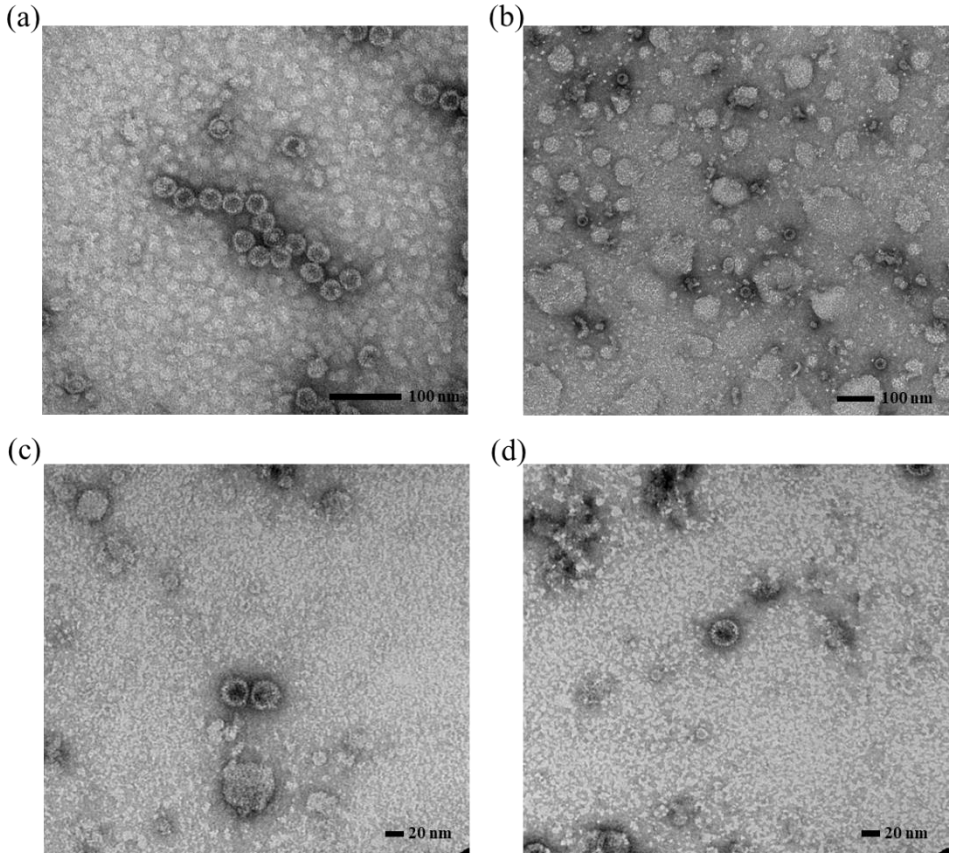

Figure 5.20: Example electron micrographs of HBc150_HA particles produced in the 16S fusion transformant line clarified by either (a)-(b) sucrose gradient ultracentrifugation (fraction 8-11 in Figure 5.17 (b)) or (c)-(d) gel filtration (fraction 5-8 in Figure 5.19). Size bars, 20 nm. Magnification, 245 k. TEM performed as described in Section 2.5.6.

Direct comparisons were made between bacterial and algal expression systems in Figure 5.21, in which isometric particles of 25-30 nm diameter with a morphology typical for HBcAg VLPs in algal samples (Figure 5.21 (b)-(d)) were similar to that produced in *E. coli* (Figure 5.21 (a)). Despite the fact that there were more impurities in the ultracentrifugation-processed sample, it was possible to capture more HBc150_HA VLPs in a single micrograph as demonstrated in Figure 5.21 (b). However, due to the low number, it was difficult to determine the structural details of these capsids. Nonetheless, this was the first study to successfully demonstrate the formation of HBcAg VLPs in the *C. reinhardtii* chloroplast.

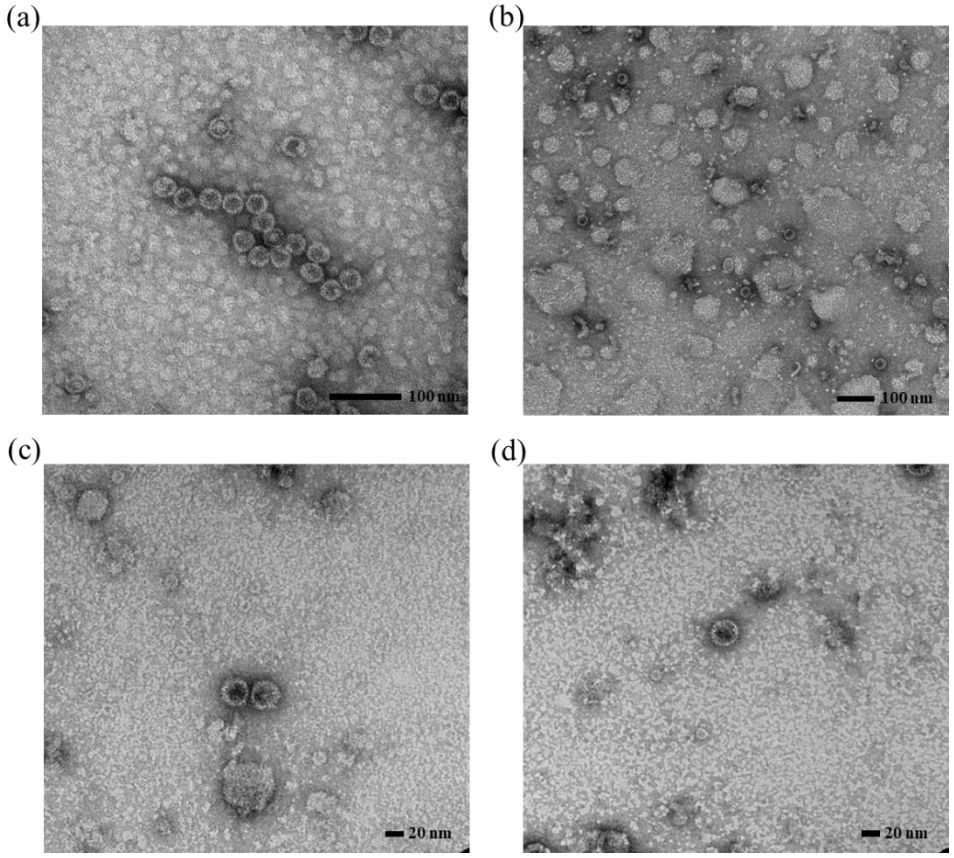

Figure 5.21: Assembly of HBc150_HA VLPs expressed in *E. coli* and *C. reinhardtii* 16S fusion transformant strain. (a). Example electron micrographs of HBc150_HA particles produced in protein lysate of *E. coli* clarified by sucrose gradient ultracentrifugation. Size bar, 100 nm. (b). Example electron micrographs of HBc150_HA particles produced in the 16S fusion transformant strain clarified by sucrose gradient ultracentrifugation. Size bar: 100 nm. (c)-(d). Example electron micrographs of HBc150_HA particles produced in the 16S fusion transformant strain clarified by sucrose gradient ultracentrifugation. Size bar: 20 nm. TEM performed as described in Section 2.5.6.

5.4.4 Immuno-gold labelling of HBc150_HA VLPs expressed in the 16S fusion transformant strain

Immunogold labelling is a powerful staining technique that enables the localisation of antigens within an electron microscope sample (Section 1.4.2). In order to further confirm the formation of algal-based HBcAg VLPs, the immunogold labelling technique was applied to the TEM in this work. The rabbit polyclonal anti-HBcAg primary antibody and an anti-rabbit secondary antibody with 5 nm gold particles were used. In order to determine the labelling capacity of the secondary antibody, a negative control without primary antibody binding was also carried out.

The results of the negative control are shown in Figure 5.22 (a) and (b) in which gold particles (‘dark spots’) were scattered evenly in the electron micrographs. This was expected as the primary antibody incubation step was omitted. With the absence of primary antibodies, gold-labelled secondary antibodies were not able to aggregate and were dispersed evenly throughout the sample.

(a)

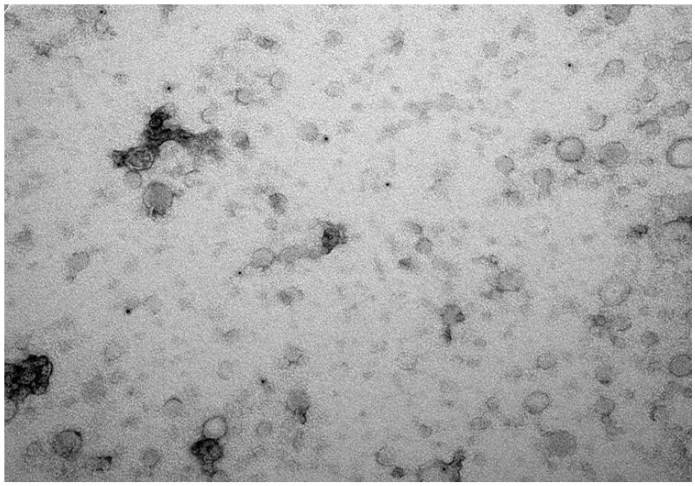

(b)

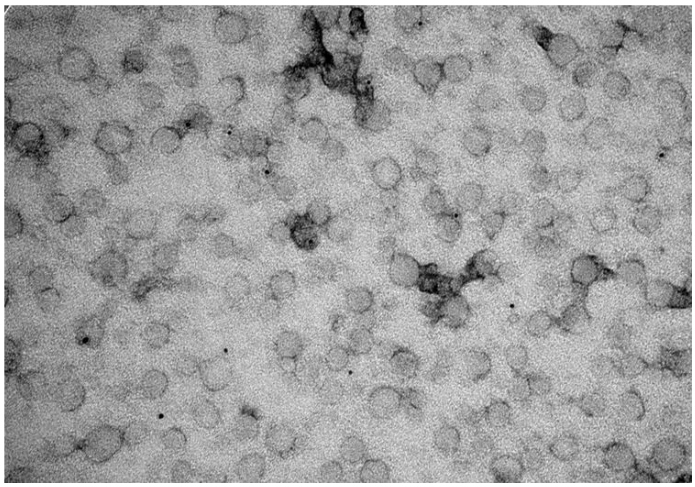

Figure 5.22: Example electron micrographs of the immunogold labelled protein samples of the 16S fusion transformant strain clarified by sucrose gradient ultracentrifugation (fraction 8-11 in Figure 5.17 (b)) without primary antibody incubation to serve as the negative control (a)-(b). Size bars, 20 nm. Magnification, 245 k. Analysis performed as described in Section 2.5.6 and Section 2.5.7.

In contrast, Figure 5.23 demonstrates the aggregation of gold particles around the structures that were concluded to be the HBcAg VLPs observed in Figure 5.20 and Figure 5.21. This finding is also in accordance with the immunogold labelling results reported in (Millán *et al.*, 2008), whereby particles with a size of around 30 nm were observed with electron-dense rings enclosing a lighter central region. However, it was not possible to further visualize the surface characteristics of these particles due to the attachment of gold particles. Such aggregation was never observed in the samples prepared without primary antibody incubation (Figure 5.22). In addition, previous western blot results have shown that the use of anti-HBcAg primary antibodies hardly resulted in any non-specific bands, unlike the anti-HA antibodies. Therefore, the possibility of non-specific binding was low during the immunogold labelling.

(a)

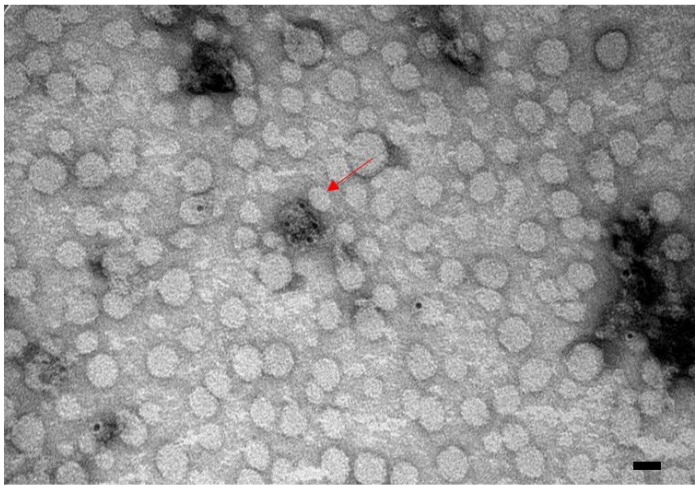

(b)

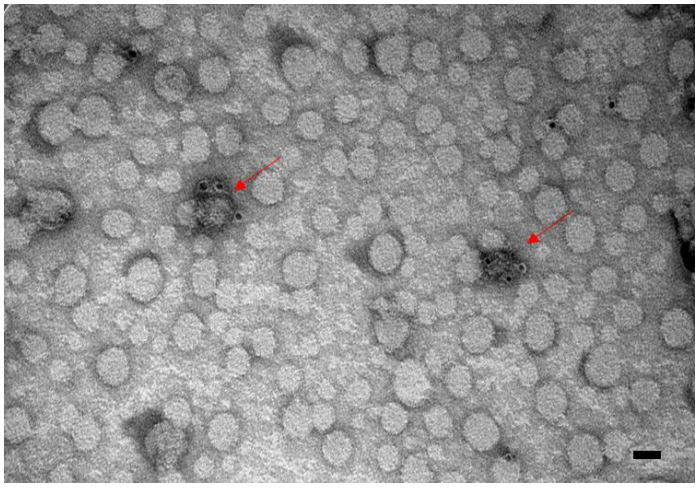

Figure 5.23: Example electron micrographs of the immunogold labelled protein samples of the 16S fusion transformant strain clarified by sucrose gradient ultracentrifugation (fraction 8-11 in Figure 5.17 (b)) with both primary and secondary antibody incubation (a)-(b). Size bars, 20 nm. Magnification, 245 k. Red arrows show the positions of HBc150_HA VLPs. Analysis performed as described in Section 2.5.6 and Section 2.5.7.

5.4.5 Summary

By comparing the migration pattern of the HBc150_HA expressed in the *psaA* transformant strain and the 16S fusion transformant strain in the sucrose gradients, it was concluded that the particulate nature (VLP formation) was concentration-dependent. If the concentration was below the level needed for initial formation of dimeric intermediates or the subsequent capsid-assembly-competent conformers, such as the HBc150_HA expressed in the *psaA* transformant strain, the protein was unable to form VLPs. As a result, the clarified protein samples in the 16S fusion transformant strain were used for subsequent VLP verification studies.

TEM results shown in Section 5.4.3 confirm the formation of HBc150_HA VLPs in the *C. reinhardtii* chloroplast (Figure 5.20 and Figure 5.21). In addition, immunogold labelling was employed to further confirm the presence of VLPs (Figure 5.23). To date, this was the first study to show that HBcAg VLPs can be synthesized and correctly assembled in microalgal chloroplasts.

5.5 Overall Summary

In Section 5.2, ΔHBc150_HA, having the same protein sequence as the algal-based HBc150_HA, was successfully expressed in *E. coli* BL21(DE3) cells and served as the positive control in TEM analysis. Morphologies typical for HBcAg VLPs were observed in the bacterial protein lysates (Figure 5.6). The positive results demonstrated the design of an N-terminal HA-tag and the manipulation of the core protein sequence did not influence the process of capsid assembly. Moreover, both sucrose gradient ultracentrifugation (Figure 5.6 (a)) and gel filtration (Figure 5.6 (b)) produced satisfactory results for clarifying bacterial lysates for VLP visualisation, in which the latter had relatively few impurities.

In Section 5.3, the purification steps were modified to mainly target the removal of the algal-based thylakoid membranes containing proteins, lipids and chlorophylls. Three methods (heat treatment, double sucrose cushion ultracentrifugation and direct ultracentrifugation) were assessed and compared using the protein samples prepared in the 16S fusion transformant strain. Ultracentrifugation was the most suitable method in spite of some product loss. Hence, a standard clarification protocol for the isolation and visualisation of VLPs from the microalgal materials was proposed in Figure 5.12. Subsequently, the clarification protocol was applied to two transgenic lines (TNE and TN72_SR_pal-HA) without HBcAg accumulation in order to obtain clarified algal protein samples for electron microscopy observations as negative controls. The large vascular (100 nm) and small round structures (5-10 nm) obtained in these algal samples (Figure 5.14 and Figure 5.16) were easily differentiated from the typical morphologies of HBcAg VLPs.

Finally, the formation of VLPs by HBc150_HA expressed in the 16S fusion transformant strain was confirmed by TEM analysis in Figure 5.20 and Figure 5.21. Isometric particles with a size range of 25-30 nm and surface spikes were observed. Due to limited numbers available, it was difficult to determine the detailed structural characteristics of these particles. Moreover, the immunogold labelling technique was applied to further support the evidence of capsid assembly in the HBc150_HA-expressing protein samples (Figure 5.23).

Overall, the results presented in this chapter clearly demonstrated the capacity of the *C. reinhardtii* chloroplasts to synthesize and assemble complex protein structures such as HBcAg VLPs. Currently, no other published studies have demonstrated the formation of HBcAg VLPs in microalgal chloroplasts. The work highlights the unexplored potential of this novel protein expression platform for producing complex protein structures, such as VLPs. Moreover, it also supports the use of eukaryotic algae as a versatile platform for the rapid and cost-effective production of recombinant therapeutic proteins.

6 General discussion and future work

6.1 Summary of findings

6.1.1 Expression of the truncated HBcAg monomer in the *C. reinhardtii* chloroplasts

The research presented in Chapter 3 describes the successful expression of the truncated HBcAg monomer in the *C. reinhardtii* chloroplast (Figure 3.18). For the past decades, efforts have been put into producing HBcAg in various prokaryotic and eukaryotic expression systems. In particular, HBcAg has been produced with relatively high yield (7.14% (w/w) TSP by Huang *et al.*, (2006)) and assembled correctly in plant chloroplasts (Huang *et al.*, 2006; Peyret *et al.*, 2015). However, this is the first study to demonstrate the feasibility of expressing the truncated HBcAg monomer in an algal chloroplast. This served as the basis for the HBcAg VLP assembly investigation in subsequent studies.

In Section 3.2, the first attempt was to express the non-tagged full-length HBcAg monomer (HBc183) in the *C. reinhardtii* chloroplast. Although both the transgene insertion and the plastome homoplasmy were confirmed, it was not possible to detect HBc183 in western blot analysis (Figure 3.8). Therefore, strategies to improve heterologous protein production and detection were explored in Sections 3.3-3.4. It was suggested that the truncated HBcAg accumulates at higher levels than that of the full-length counterparts in bacterial expression systems (Stahl and Murray, 1989; Tan *et al.*, 2003; Sominskaya *et al.*, 2013; Peyret *et al.*, 2015). Moreover, the inclusion of well-established short affinity tags was also helpful in terms of protein detection (Brizzard, 2008). Bearing this background literature in mind and with suitable molecular biology techniques established in Section 3.2, the codon-optimised transgene coding for the truncated monomer with an N-terminal HA-tag (HBc150_HA) was designed (Figure 3.16). The expression of HBc150_HA in the *psaA* transformant strain was confirmed by western blot analysis using anti-HA antibodies (Figure 3.18).

However, the expression of HBc150_HA was still below the detection limit of anti-HBcAg antibodies (Figure 3.19). Protein stability tests revealed proteolytic degradation of HBc150_HA at the late exponential growth phase (Figure 3.20 and Figure 3.21). The solution was to add protease inhibitors into the liquid cultures to reduce the proteolytic activities of certain proteases as demonstrated by Michelet et al. (2011). However, results presented in Figure 3.24 and Figure 3.25 revealed a negative impact of protease inhibitor addition on cell growth and protein accumulation. This led to the continued exploration of new strategies to improve HBc150_HA expression level in the *C. reinhardtii* chloroplast in Chapter 4.

6.1.2 Strategies to improve heterologous protein accumulation in the *C. reinhardtii* chloroplast

In Chapter 4, strategies from both the bioprocessing (Section 4.2) and genetic engineering (Section 4.3) aspects were addressed in order to boost HBc150_HA expression in the chloroplast. Despite the importance of cultivation modes and operational conditions on cell growth, it was difficult to identify the most suitable cultivation condition for HBc150_HA expression due to the low protein production observed in the *psaA* transformant strain (Figure 4.3 and Figure 4.10). However, the improved growth conditions established in Section 4.2.5 was useful for subsequent algal biomass preparation. Since the CREs within promoters play a critical role in transcription initiation and mRNA accumulation, a new transgenic line harbouring the chimeric 16S rRNA promoter/*psaA* 5' UTR regulatory element was created in Section 4.3.2. As a result, the yield of HBc150_HA was dramatically increased by approximately 26-fold (Figure 4.17) through this use of a stronger promoter that drives higher transcription rates or supports higher steady-state mRNA-levels (Rasala *et al.*, 2011). These data shed light on the design of novel combinations of chimeric promoter/5'UTR regulatory elements towards high level recombinant protein production in microalgal chloroplasts.

More importantly, HBc150_HA expressed in the 16S fusion transgenic strain was detected by both polyclonal and monoclonal anti-HBcAg antibodies (Figure 4.16), confirming immunoreactivity of the recombinant protein under denaturing conditions

(Soria-Guerra et al. 2013). Additionally, the HB150_HA accumulated in the 16S fusion transgenic strain was more stable with relatively less degradation during the stationary growth phase compared to the *psaA* transformant strain (Figure 4.18 and Figure 4.19). This was probably due to the fact that the rate of protein accumulation outperformed the rate of degradation. Furthermore, it was interesting to observe that the yield of HBc150_HA (4.9 mg) was almost four-fold higher than the yeast-derived HBcAg (1.3 mg) on the basis of dry cell weight in densitometric analysis (Figure 4.20 and Figure 4.21). Equivalently, it was estimated to accumulate to 2.34% (w/w) of TSP in the *C. reinhardtii* chloroplast (Section 4.4.3). The yield obtained in this study was hypothesized to be sufficient for commercial production (Rasala *et al.*, 2010). Overall, the results presented in Chapter 4 not only facilitated the quantification of HBc150_HA but also laid a foundation for the verification of HBcAg VLP formation in the *C. reinhardtii* chloroplast in Chapter 5.

6.1.3 Formation of HBcAg VLPs in the *C. reinhardtii* chloroplast

Following the establishment of the 16S fusion transformant strain with relatively reasonable HBc150_HA expression level (2.34% (w/w) of TSP), the formation of VLPs in the *C. reinhardtii* chloroplasts was investigated in Chapter 6. No published works have previously demonstrated the correct assembly of HBcAg VLPs in microalgal chloroplasts. In order to facilitate the verification of algal-based VLPs, both positive (Section 5.2) and negative (Section 5.3) controls for TEM analysis were established.

ΔHBc150_HA, having the same protein sequence as the algal-based HBc150_HA, was successfully expressed in *E. coli* BL21 (DE3) cells (Figure 5.2) and morphologies typical for HBcAg VLPs were observed in TEM analysis (Figure 5.6). These results confirm that the design of an N-terminal HA-tag and the manipulation of the core protein sequence did not influence the process of capsid assembly. Moreover, both sucrose gradient ultracentrifugation and gel filtration produced satisfactory results for clarifying bacterial lysates for electron microscopic observations, in which the latter method demonstrated fewer impurities (Figure 5.6). In Section 5.3, the purification steps were modified and an additional ultracentrifugation step was incorporated into the

standard clarification protocol for isolation and visualisation of VLPs from the microalgal material (Figure 5.12). Subsequently, the clarification protocol was applied to two *C. reinhardtii* transgenic lines (TNE and TN72_SR_pal-HA) without HBcAg accumulation in order to obtain clarified algal protein samples as negative controls for TEM analysis (Section 5.3.5). The large vesicular (100 nm) and small round structures (5-10 nm) obtained in these algal samples (Figure 5.14 and Figure 5.16) were easily differentiated from the typical morphologies of HBcAg VLPs.

Finally, the formation of VLPs by HBc150_HA expressed in the 16S fusion transformant strain was confirmed by TEM analysis in Section 5.4. Isometric particles with a size range of 25-30 nm and characteristic surface spikes were observed (Figure 5.20 and Figure 5.21). Due to the limited number of particles available, it was difficult to determine the detailed structural characteristics of these VLPs. Immunogold labelling technique was applied to further support the evidence of capsid assembly in the HBc150_HA-expressing protein samples as demonstrated in Figure 5.22 and Figure 5.23. Overall, the results presented in this chapter show that the original aim of this work was achieved i.e. the capability of the *C. reinhardtii* chloroplast to synthesize and assemble complex protein structures such as HBcAg VLPs.

Although the yield of HBc150-VLP produced in *C. reinhardtii* was much lower than that of *E. coli* in this work, it should be noted that *E. coli* is a well-established protein expression system with numerous molecular tools and protocols at hand for the high-level protein production. However, despite *C. reinhardtii* being the most widely researched microalga for heterologous protein production, more resources and research are still needed in order to fully optimise microalgae as a protein factory. Since *C. reinhardtii* is a GRAS organism that does not produce any endotoxins and infectious agents, it should not raise any health risk or environmental contamination concerns as opposed to bacterial cultures. In addition, phototrophic microalgae can convert energy obtained from natural sunlight and carbon dioxide to heterologous proteins with therapeutic potential, contributing to the global sustainable development. Therefore, the potential of *C. reinhardtii* as a valuable VLP production platform in the future should not be neglected. This work serves as an initial “prove-of-concept” study and further

supports the continued exploration of eukaryotic microalgae as a system for the rapid and cost-effective production of VLP-based vaccine candidates for therapeutic purposes.

6.2 Future work

6.2.1 Short-term experiments

Due to the time constraints, there are further experiments that needed to be carried out in order to fully understand the immunogenic properties and structural characteristics of the algal-derived HBcAg VLPs produced in this study.

First, the antigenicity of the algal chloroplast-derived HBc150_HA could be examined by ELISA (Huang *et al.*, 2006). Despite the positive results obtained in the immunogold labelling (Section 5.4.4), it is still beneficial to carry out ELISA using monoclonal primary antibodies that can recognise HBc150_HA under native conditions. Meanwhile, ELISA could also be used to quantify the yield of HBc150_HA. Hence, the quantification results could be compared to that of the densitometric analysis demonstrated in Section 4.4.3 in order to have a thorough understanding of recombinant protein accumulation in microalgal chloroplasts. In addition, it would be interesting to see if the new 16S rRNA promoter supports the expression of non-tagged full-length or truncated HBcAg monomers. This could facilitate the understanding of protein yields obtained and VLP morphology formed by different transgenic constructs.

Second, the yield of HBc150_HA could be further improved thorough experimenting with different cultivation conditions. Although the western blot results obtained in Section 4.2.4 were not conclusive, lowering cultivation temperature could potentially play a crucial role in HBcAg production in microalgal chloroplasts. Therefore, it would be sensible to repeat such work using the 16S fusion transformant strain under low temperature (18 ℃) and to observe any improvement in protein accumulation. Another potential method is to use a fed-batch fermentation regime (Cheirsilp and Torpee, 2012). As demonstrated in Section 4.2.2, the organic carbon source in TAP medium, acetate, was quickly used up when cells reached the early stationary phase. Feeding acetate

before the stationary phase could potentially extend the exponential growth phase and provide sufficient organic nutrients for sustained HBc150_HA accumulation (Cheirsilp and Torpee, 2012). Once the desirable yield is achieved, additional purification steps such as ion-exchange and affinity chromatography could be selected, optimised and incorporated into the existing VLP clarification protocol to further isolate HBc150_HA from algal impurities. Once a purified and concentrated HBc150_HA sample is obtained, a more powerful visualisation technique cryo-EM could be applied to determine the detailed 3D structure of the algal chloroplast-derived HBcAg VLPs using single particle analysis. The information obtained on the structural characteristics such as symmetry and integrity could be compared to that of existing HBcAg VLP structures resulting from conventional expression systems.

Since the main application of the algal-based HBcAg VLP is to carry and present heterologous epitopes, it is crucial to understand immunological properties of these particles. This will inevitably involve the systemic immunization of animals using the purified HBcAg protein samples. As a result, the non-tagged HBcAg will be preferred to the HBc150_HA expressed in the 16S fusion transformant strain, further demonstrating the necessity to express non-tagged full-length and truncated HBcAg in the microalgal chloroplasts. Subsequently, standard western blot and ELISA analyses could be carried out to detect specific serum antibody response against HBcAg in blood samples. Hence, the immunogenicity of algal-derived HBcAg VLPs could also be compared to that of the core proteins expressed in other expression systems. This will further evaluate the capability of microalgal chloroplasts to produce complex and functional therapeutic proteins.

6.2.2 Long-term prospects

HBcAg VLP is an excellent particulate carrier for the presentation of foreign epitopes (Roose *et al.*, 2013). Insertion of suitable epitopes in the MIR is usually preferred as it is the most exposed region on the VLP surface and the most optimal locus for antigen-presentation cell (APC) recognition (Grgacic and Anderson, 2006). Since *C. reinhardtii* is a GRAS organism (Murbach *et al.*, 2018), the concept of a bio-encapsulated oral

vaccine derived from the dried algal biomass has attracted much attention in recent years (Dyo and Purton, 2018). One of the most significant advantages of an oral vaccine is the ability to elicit not only mucosal but also systemic immune responses (Huang *et al.*, 2006; Specht and Mayfield, 2014). In addition, the number of costly purification steps will be dramatically reduced, making the production of oral vaccines more cost-effective (Gregory *et al.*, 2013). Algae-based oral vaccines are usually heat-stable with a long shelf-life that reduces the need for cold storage (Dreesen *et al.*, 2010). Last, but not least, higher patient compliance is usually expected for oral vaccines compared to parenteral administration (Aziz *et al.*, 2007).

The research conducted in this study has confirmed the feasibility of using the microalgal chloroplast as VLP production platform. However, protein yields need to be further improved in order to match to that of conventional expression systems such as *E. coli* and yeast. Apart from yield, finding heterologous epitopes suitable for oral immunization would be the best approach to exploit the distinct advantages of microalgae as a commercial vaccine production platform. This will involve the selection of suitable epitopes against various human pathogens that can cause enteric, respiratory or sexually transmitted diseases. For example, potential candidates may include the FMDV structural VP1 protein, *P. falciparum* surface proteins (Pfs25 and Pfs28) and HPV type 16 E7 protein (Specht and Mayfield, 2014). Subsequently, these chimeric HBcAg VLP-based vaccine candidates can be expressed in *C. reinhardtii* chloroplasts. Once desirable physio-chemical and structural results are obtained, both mucosal and systemic immunization of animals can be performed with the lyophilized algal biomass to analyse specific antibody responses. In addition, mucosal adjuvants such as cholera toxin B subunit can be fed together (Kong *et al.*, 2001), or produced in the same chloroplast as a recombinant protein fused to the VLPs, to boost the immune response (Dyo and Purton, 2018).

These results would then indicate the potential capability of microalgal chloroplast-derived HBcAg VLPs as a particulate carrier for the immunogenic presentation and oral delivery of foreign epitopes. With the continued exploration in this field, the microalgal

chloroplast may become a prime VLP-based vaccine expression platform for the cost-effective development and manufacturing of oral vaccines in the future.

References

Adam, Z., Clarke, A. K. and Clarke, A. K. (2002) Cutting edge of chloroplast proteolysis. *Trends in Plant Science*, 7, 451–456.

Ahmad, A. L., Yasin, N. H. M., Derek, C. J. C. and Lim, J. K. (2014) Comparison of harvesting methods for microalgae *Chlorella sp.* and its potential use as a biodiesel feedstock. *Environmental Technology*, 35, 2244–2253.

Ahmad, N., Michoux, F. and Nixon, P. J. (2012) Investigating the production of foreign membrane proteins in tobacco chloroplasts: Expression of an algal plastid terminal oxidase. *PLoS ONE*, 7, e41722.

Alexander, C. G., Jürgens, M. C., Shepherd, D. A., Freund, S. M. V, Ashcroft, A. E. and Ferguson, N. (2013) Thermodynamic origins of protein folding, allostery, and capsid formation in the human hepatitis B virus core protein. *Proceedings of the National Academy of Sciences of the United States of America*, 110, 2782–91.

Apel, W., Schulze, W. X. and Bock, R. (2010) Identification of protein stability determinants in chloroplasts. *Plant Journal*, 63, 636–650.

Arora, U., Tyagi, P., Swaminathan, S. and Khanna, N. (2012) Chimeric hepatitis B core antigen virus-like particles displaying the envelope domain III of dengue virus type 2. *Journal of Nanobiotechnology*, 10, 1–6.

Aslan, S. and Kapdan, I. K. (2006) Batch kinetics of nitrogen and phosphorus removal from synthetic wastewater by algae. *Ecological Engineering*, 28, 64–70.

Aziz, M. A., Midha, S., Waheed, S. M. and Bhatnagar, R. (2007) Oral vaccines: new needs, new possibilities. *BioEssays: News and Reviews in Molecular, Cellular and Developmental Biology*, 29, 591–604.

Bai, X. C., McMullan, G. and Scheres, S. H. W. (2015) How cryo-EM is revolutionizing structural biology. *Trends in Biochemical Sciences*, 40, 49–57.

Barnes, D., Franklin, S., Schultz, J., Henry, R., Brown, E., Coragliotti, A. and Mayfield, S. P. (2005) Contribution of 5'- and 3'-untranslated regions of plastid mRNAs to the expression of *Chlamydomonas reinhardtii* chloroplast genes. *Molecular Genetics and Genomics*, 274, 625–36.

Barrera, D. J. *et al.* (2014) Algal chloroplast produced camelid V_HH antitoxins are capable of neutralizing botulinum neurotoxin. *Plant Botechnology Journal*, 13, 117–124.

Belnap, D. M., Watts, N. R., Conway, J. F., Cheng, N., Stahl, S. J., Wingfield, P. T. and Steven, a C. (2003) Diversity of core antigen epitopes of hepatitis B virus. *Proceedings of the National Academy of Sciences of the United States of America*, 100, 10884–10889.

Birch-Machint, I., Newell, C. A., Hibberd, J. M. and Gray, J. C. (2004) Accumulation of rotavirus VP6 protein in chloroplasts of transplastomic tobacco is limited by protein stability. *Plant Biotechnology Journal*, 2, 261–270.

Bitog, J. P. *et al.* (2011) Application of computational fluid dynamics for modeling and designing photobioreactors for microalgae production: A review. *Computers and Electronics in Agriculture*, 76, 131–147.

Blowers, A., Ellmore, G., Klein, U. and Bogorad, L. (1990) Transcriptional analysis of endogenous and foreign genes in chloroplast transformants of *Chlamydomonas*. *The Plant Cell*, 2, 1059–1070.

Blowers, A. D., Bogorad, L., Shark, K. B. and Sanford, J. C. (1989) Studies on *Chlamydomonas* chloroplast transformation : foreign DNA can be stably maintained in the chromosome. *The Plant Cell*, 1, 123–132.

Bonvicino, C. R., Moreira, M. A. and Soares, M. A. (2014) Hepatitis B virus lineages in mammalian hosts: Potential for bidirectional cross-species transmission. *World Journal of Gastroenterology*, 20, 7665–7674.

Böttcher, B., Wynne, S. A. and Crowther, R. A. (1997) Determination of the fold of the core protein of hepatitis B virus by electron cryomicroscopy. *Nature*, 386, 88–91.

Boynton, J. E. *et al.* (1988) Chloroplast transformation in *Chlamydomonas* with high velocity microprojectiles. *American Association for the Advancement of Science*, 240, 1534–1538.

Braun Galleani, S., Baganz, F., Purton, S., Braun-Galleani, S., Baganz, F. and Purton, S. (2015) Improving recombinant protein production in the *Chlamydomonas reinhardtii* chloroplast using vivid Verde Fluorescent Protein as a reporter. *Biotechnology Journal*, 10, 1289–1297.

Brennan, L. and Owende, P. (2010) Biofuels from microalgae-A review of technologies for production, processing, and extractions of biofuels and co-products. *Renewable and Sustainable Energy Reviews*, 14, 557–577.

Brizzard, B. (2008) Epitope tagging. *BioTechniques*, 44, 693–695.

Brown, L. E., Sprecher, S. L. and Keller, L. R. (1991) Introduction of exogenous DNA into *Chlamydomonas reinhardtii* by electroporation. *Molecular and Cellular Biology*, 11, 2328–2332.

Burrell, C. J., Mackay, P., Greenaway, P. J., Hofschneider, P. H. and Murray, K. (1979) Expression in *Escherichia coli* of hepatitis B virus DNA sequences cloned in plasmid pBR322. *Nature*, 279, 43–47.

Carneiro, S., Ferreira, E. C. and Rocha, I. (2013) Metabolic responses to recombinant bioprocesses in *Escherichia coli*. *Journal of Biotechnology*, 164, 396–408.

Castellanos-Huerta, I. *et al.* (2016) Recombinant hemagglutinin of avian influenza virus H5 expressed in the chloroplast of *Chlamydomonas reinhardtii* and evaluation of its immunogenicity in chickens. *Avian Diseases*, 60, 784–791.

Chackerian, B. (2007) Virus-like particles: Flexible platforms for vaccine development. *Expert Review of Vaccines*, 6, 381–390.

Chebolu, S. and Daniell, H. (2010) Chloroplast-derived vaccine antigens and biopharmaceuticals: Expression, folding, assembly and functionality. *Current Topics in Microbiology and Immunology*, 332, 33–54.

Cheirsilp, B. and Torpee, S. (2012) Enhanced growth and lipid production of microalgae under mixotrophic culture condition: Effect of light intensity, glucose concentration and fed-batch cultivation. *Bioresource Technology*, 110, 510–516.

Chen, F. and Johns, M. R. (1996) Heterotrophic growth of *Chlamydomonas reinhardtii* on acetate in chemostat culture. *Process Biochemistry*, 31, 601–604.

Chisti, Y. (2007) Biodiesel from microalgae. *Biotechnology Advances*, 25, 294–306.

Chojnacka, K. and Marquez-Rocha, F.-J. (2004) Kinetic and stoichiometric relationships of the energy and carbon metabolism in the culture of microalgae. *Biotechnology*, 3, 21–34.

Chu, L. and Robinson, D. K. (2001) Industrial choices for protein production by large-scale cell culture. *Current Opinion in Biotechnology*, 12, 180–187.

Clarke, B. E. *et al.* (1987) Improved immunogenicity of a peptide epitope after fusion to hepatitis B core protein. *Nature*, 330, 381–384.

Coll, J. M. (2006) Review. Methodologies for transferring DNA into eukaryotic microalgae. *Spanish Journal of Agricultural Research*, 4, 316–330.

Cronodon (no date) *Algae*. Available at: http://cronodon.com/BioTech/Algal_Bodies.html (Accessed: 16 July 2018).

Demurtas, O. C., Massa, S., Ferrante, P., Venuti, A., Franconi, R. and Giuliano, G. (2013) A *Chlamydomonas*-derived Human Papillomavirus 16 E7 vaccine induces specific tumor protection. *PLoS ONE*, 8, e61473.

Diels, A. M. J. and Michiels, C. W. (2006) High-pressure homogenization as a non-thermal technique for the inactivation of microorganisms. *Critical Reviews in Microbiology*, 32, 201–216.

Doran, P. M. (1995) *Bioprocess Engineering Principles*. *GB: Academic Press*.

Doran, P. M. (2006) Foreign protein degradation and instability in plants and plant tissue cultures. *Trends in Biotechnology*, 24, 426–432.

Dreesen, I. A. J., Charpin-El Hamri, G. and Fussenegger, M. (2010) Heat-stable oral alga-based vaccine protects mice from *Staphylococcus aureus* infection. *Journal of Biotechnology*, 145, 273–280.

Dryden, K. A., Wieland, S. F., Whitten-Bauer, C., Gerin, J. L., Chisari, F. V. and Yeager, M. (2006) Native hepatitis B virions and capsids visualized by electron cryomicroscopy. *Molecular Cell*, 22, 843–850.

Dyo, Y. M. and Purton, S. (2018) The algal chloroplast as a synthetic biology platform for production of therapeutic proteins. *Microbiology*, 164, 113–121.

Dyson, M. R. and Murray, K. (1995) Selection of peptide inhibitors of interactions involved in complex protein assemblies: Association of the core and surface antigens of hepatitis B virus. *Proceedings of the National Academy of Sciences of the United States of America*, 92, 2194–2198.

Eberhard, S., Drapier, D. and Wollman, F. A. (2002) Searching limiting steps in the

expression of chloroplast-encoded proteins: Relations between gene copy number, transcription, transcript abundance and translation rate in the chloroplast of *Chlamydomonas reinhardtii*. *Plant Journal*, 31, 149–160.

Economou, C., Wannathong, T., Szaub, J. and Purton, S. (2014) A simple, low-cost method for chloroplast transformation of the green alga *Chlamydomonas reinhardtii*. in *Chloroplast Biotechnology*, 401–411.

Erickson, E., Wakao, S. and Niyogi, K. K. (2015) Light stress and photoprotection in *Chlamydomonas reinhardtii*. *Plant Journal*, 82, 449–465.

Ferrer-Miralles, N., Domingo-Espín, J., Corchero, J., Vázquez, E. and Villaverde, A. (2009) Microbial factories for recombinant pharmaceuticals. *Microbial Cell Factories*, 8, 1–8.

Fiers, W. *et al.* (2009) M2e-based universal influenza A vaccine. *Vaccine*, 27, 6280–6283.

Fifis, T. *et al.* (2004) Size-dependent immunogenicity: therapeutic and protective properties of nano-vaccines against tumors. *The Journal of Immunology*, 173, 3148–3154.

Filette, M. De *et al.* (2008) Universal influenza A M2e-HBc vaccine protects against disease even in the presence of pre-existing anti-HBc antibodies. *Vaccine*, 26, 6503–6507.

Fischer, B. B., Wiesendanger, M. and Eggen, R. I. L. (2006) Growth condition-dependent sensitivity, photodamage and stress response of *Chlamydomonas reinhardtii* exposed to high light conditions. *Plant and Cell Physiology*, 47, 1135–1145.

Francis, D. M. and Page, R. (2010) Strategies to optimize protein expression in *E. coli*. in *Current Protocols in Protein Science*, 5.24.1-5.24.29.

Franklin, S., Ngo, B., Efuet, E. and Mayfield, S. P. (2002) Development of a GFP reporter gene for *Chlamydomonas reinhardtii* chloroplast. *The Plant Journal*, 30, 733–744.

Freivalds, J., Dislers, A., Ose, V., Pumpens, P., Tars, K. and Kazaks, A. (2011) Highly efficient production of phosphorylated hepatitis B core particles in yeast *Pichia pastoris*. *Protein Expression and Purification*, 75, 218–224.

Gerde, J. A., Yao, L., Lio, J., Wen, Z. and Wang, T. (2014) Microalgae flocculation: Impact of flocculant type, algae species and cell concentration. *Algal Research*, 3, 30–35.

Ghag, S. B., Adki, V. S., Ganapathi, T. R. and Bapat, V. A. (2016) Heterologous protein production in plant systems. *GM Crops & Food*, 5698, 1–48.

Gibson, D. G., Young, L., Chuang, R.-Y., Venter, J. C., Hutchison, C. A. and Smith, H. O. (2009) Enzymatic assembly of DNA molecules up to several hundred kilobases. *Nature Methods*, 6, 343–345.

Gibson, D. G., Smith, H. O., Hutchison, C. A., Venter, J. C. and Merryman, C. (2010) Chemical synthesis of the mouse mitochondrial genome. *Nature Methods*, 7, 901–903.

Gimpel, J. A., Hyun, J. S., Schoepp, N. G. and Mayfield, S. P. (2015) Production of recombinant proteins in microalgae at pilot greenhouse scale. *Biotechnology and Bioengineering*, 112, 339–345.

Glazyrina, J. *et al.* (2010) High cell density cultivation and recombinant protein production with *Escherichia coli* in a rocking-motion-type bioreactor. *Microbial Cell Factories*, 9, 1–11.

Gregory, J. A., Topol, A. B., Doerner, D. Z. and Mayfield, S. (2013) Alga-produced cholera toxin-Pfs25 fusion proteins as oral vaccines. *Applied and Environmental*

Microbiology, 79, 3917–3925.

Grgacic, E. V. L. and Anderson, D. A. (2006) Virus-like particles: Passport to immune recognition. *Methods*, 40, 60–65.

Groot, N. S. de and Ventura, S. (2006) Effect of temperature on protein quality in bacterial inclusion bodies. *FEBS Letters*, 580, 6471–6476.

Gustafsson, C., Govindarajan, S. and Minshull, J. (2004) Codon bias and heterologous protein expression. *Trends in Biotechnology*, 22, 346–353.

Harris, E. H. (1989) *The Chlamydomonas sourcebook. A Comprehensive Guide to Biology and Laboratory Use*. *Science*.

Harun, R., Singh, M., Forde, G. M. and Danquah, M. K. (2010) Bioprocess engineering of microalgae to produce a variety of consumer products. *Renewable and Sustainable Energy Reviews*, 14, 1037–1047.

He, D.-M., Qian, K.-X., Shen, G.-F., Zhang, Z.-F., Li, Y.-N., Su, Z.-L. and Shao, H.-B. (2007) Recombination and expression of classical swine fever virus (CSFV) structural protein E2 gene in *Chlamydomonas reinhardtii* chroloplasts. *Colloids and Surfaces*, 55, 26–30.

Heasman, M., Diemar, J., O'Connor, W., Sushames, T. and Foulkes, L. (2000) Development of extended shelf-life microalgae concentrate diets harvested by centrifugation for bivalve molluscs - a summary. *Aquaculture Research*, 31, 637–659.

Hempel, F., Lau, J., Klingl, A. and Maier, U. G. (2011) Algae as protein factories: Expression of a human antibody and the respective antigen in the diatom *Phaeodactylum tricornutum*. *PLoS ONE*, 6, e28424.

Hirschman, S. Z., Price, P., Garfinkel, E., Christman, J. and Acs, G. (1980) Expression

of cloned hepatitis B virus DNA in human cell cultures. *Proceedings of the National Academy of Sciences of the United States of America*, 77, 5507–5511.

Hitzeman, R. A., Hagie, F. E., Levine, H. L., Goeddel, D. V., Ammerer, G. and Hall, B. D. (1981) Expression of a human gene for interferon in yeast. *Nature*, 293, 717–722.

Ho, S.-H., Huang, S.-W., Chen, C.-Y., Hasunuma, T., Kondo, A. and Chang, J.-S. (2013) Bioethanol production using carbohydrate-rich microalgae biomass as feedstock. *Bioresource Technology*, 135, 191–198.

Holmes, K., Shepherd, D. A., Ashcroft, A. E., Whelan, M., Rowlands, D. J. and Stonehouse, N. J. (2015) Assembly pathway of hepatitis B core virus-like particles from genetically fused dimers. *Journal of Biological Chemistry*, 290, 16238–16245.

Hong, W., Zeng, J. and Xie, J. (2014) Antibiotic drugs targeting bacterial RNAs. *Acta Pharmaceutica Sinica B*, 4, 258–265.

Howe, C. J., Barbrook, A. C., Nisbet, R. E. R., Lockhart, P. J. and Larkum, A. W. D. (2008) The origin of plastids. *Philosophical Transactions of the Royal Society of London. Series B, Biological Sciences*, 363, 2675–2685.

Huang, A., Sun, L., Wu, S., Liu, C., Zhao, P., Xie, X. and Wang, G. (2017) Utilization of glucose and acetate by *Chlorella* and the effect of multiple factors on cell composition. *Journal of Applied Phycology*, 29, 23–33.

Huang, Z., Santi, L., LePore, K., Kilbourne, J., Arntzen, C. J. and Mason, H. S. (2006) Rapid, high-level production of hepatitis B core antigen in plant leaf and its immunogenicity in mice. *Vaccine*, 24, 2506–2513.

James, G. O., Hocart, C. H., Hillier, W., Price, G. D. and Djordjevic, M. A. (2013) Temperature modulation of fatty acid profiles for biofuel production in nitrogen

deprived *Chlamydomonas reinhardtii*. *Bioresource Technology*, 127, 441–447.

Janssen, M., Bresser, L. De, Baijens, T., Tramper, J., Mur, L. R., Snel, F. H. and Wijffels, H. (2000) Scale-up aspects of photobioreactors : effects of mixing-induced light / dark cycles. *Journal of Applied Phycology*, 12, 225–237.

Jones, C. S. *et al.* (2013) Heterologous expression of the C-terminal antigenic domain of the malaria vaccine candidate Pfs48/45 in the green algae *Chlamydomonas reinhardtii*. *Applied Microbiology and Biotechnology*, 97, 1987–1995.

Josefsberg, J. O. and Buckland, B. (2012) Vaccine process technology. *Biotechnology and Bioengineering*, 109, 1443–1460.

Kindle, L. K. (1990) High-frequency nuclear tranformation of *Chlamydomonas reinhardtii*. *Methods in Enzymology*, 297, 27–38.

Kleid, D. *et al.* (1981) Cloned viral protein vaccine for foot-and-mouth disease: responses in cattle and swine. *Science*, 214, 1125–1129.

Kong, Q., Richter, L., Yang, Y. F., Arntzen, C. J., Mason, H. S. and Thanavala, Y. (2001) Oral immunization with hepatitis B surface antigen expressed in transgenic plants. *Proceedings of the National Academy of Sciences of the United States of America*, 98, 11539–11544.

Kong, Q. X., Li, L., Martinez, B., Chen, P. and Ruan, R. (2010) Culture of microalgae chlamydomonas *reinhardtii* in wastewater for biomass feedstock production. *Applied Biochemistry and Biotechnology*, 160, 9–18.

Lanford, R. E. and Notvall, L. (1990) Expression of hepatitis B virus core and precore antigens in insect cells and characterization of a core-associated kinase activity. *Virology*, 176, 222–233.

Leu, S. and Boussiba, S. (2014) Advances in the production of high-value products by

microalgae. *Industrial Biotechnology*, 10, 169–183.

Li, F., Vijayasankaran, N., Shen, A. Y., Kiss, R. and Amanullah, A. (2010) Cell culture processes for monoclonal antibody production. *mAbs*, 2, 466–479.

Li, X., Xu, H. and Wu, Q. (2007) Large-scale biodiesel production from microalga *Chlorella protothecoides* through heterotrophic cultivation in bioreactors. *Biotechnology and Bioengineering*, 98, 764–771.

Li, Z. X., Hong, G. Q., Hu, B., Liang, M. J., Xu, J. and Li, L. (2007) Suitability of yeast- and *Escherichia coli*-expressed hepatitis B virus core antigen derivatives for detection of anti-HBc antibodies in human sera. *Protein Expression and Purification*, 56, 293–300.

Liang, T. J. (2009) Hepatitis B: The virus and disease. *Hepatology*, 49, 13–21.

Lisitsky, I., Rott, R. and Schuster, G. (2001) Insertion of polydeoxyadenosine-rich sequences into an intergenic region increases transcription in *Chlamydomonas reinhardtii* chloroplasts. *Planta*, 212, 851–857.

Lorenz, T. C. (2012) Polymerase chain reaction: Basic protocol plus troubleshooting and optimisation strategies. *Journal of Visualized Experiments*, 1–15.

Lu, Y., Chan, W., Ko, B. Y., VanLang, C. C. and Swartz, J. R. (2015) Assessing sequence plasticity of a virus-like nanoparticle by evolution toward a versatile scaffold for vaccines and drug delivery. *Proceedings of the National Academy of Sciences*, 112, 12360–12365.

Lua, L. H. L., Connors, N. K., Sainsbury, F., Chuan, Y. P., Wibowo, N. and Middelberg, A. P. J. (2014) Bioengineering virus-like particles as vaccines. *Biotechnology and Bioengineering*, 111, 425–440.

Majekodunmi, S. O. (2015) A review on centrifugation in the pharmaceutical industry.

American Journal of Biomedical Engineering, 5, 67–78.

Mamedov, T. and Yusibov, V. (2011) Green algae *Chlamydomonas reinhardtii* possess endogenous sialylated N-glycans. *FEBS Open Bio*, 1, 15–22.

Manuell, A. L. *et al.* (2007) Robust expression of a bioactive mammalian protein in *Chlamydomonas* chloroplast. *Plant Botechnology Journal*, 5, 402–412.

Mata, T. M., Martins, A. A. and Caetano, N. S. (2010) Microalgae for biodiesel production and other applications: A review. *Renewable and Sustainable Energy Reviews*, 14, 217–232.

Mayfield, S. P. and Franklin, S. E. (2005) Expression of human antibodies in eukaryotic micro-algae. *Vaccine*, 23, 1828–1832.

Mayfield, S. P. and Schultz, J. (2004) Development of a luciferase reporter gene, luxCt , for *Chlamydomonas reinhardtii* chloroplast. *The Plant Journal*, 37, 449–458.

Miao, X. and Wu, Q. (2006) Biodiesel production from heterotrophic microalgal oil. *Bioresource Technology*, 97, 841–846.

Michel, M. L. and Tiollais, P. (2010) Hepatitis B vaccines: Protective efficay and therapeutic potential. *Pathologie Biologie*, 58, 288–295.

Michelet, L., Lefebvre-Legendre, L., Burr, S. E., Rochaix, J. D. and Goldschmidt-Clermont, M. (2011) Enhanced chloroplast transgene expression in a nuclear mutant of *Chlamydomonas*. *Plant Biotechnology Journal*, 9, 565–574.

Millán, A. F.-S. *et al.* (2008) Human papillomavirus L1 protein expressed in tobacco chloroplasts self-assembles into virus-like particles that are highly immunogenic. *Plant Biotechnology Journal*, 6, 427–441.

Molina Grima, E., Belarbi, E. H., Acién Fernández, F. G., Robles Medina, a. and Chisti,

Y. (2003) Recovery of microalgal biomass and metabolites: Process options and economics. *Biotechnology Advances*, 20, 491–515.

Moon, M., Kim, C. W., Park, W. K., Yoo, G., Choi, Y. E. and Yang, J. W. (2013) Mixotrophic growth with acetate or volatile fatty acids maximizes growth and lipid production in *Chlamydomonas reinhardtii*. *Algal Research*, 2, 352–357.

Murbach, T. S., Glávits, R., Endres, J. R., Hirka, G., Vértesi, A., Béres, E. and Szakonyiné, I. P. (2018) A toxicological evaluation of *Chlamydomonas reinhardtii* , a green algae. *International Journal of Toxicology*, 37, 53–62.

Murtey, M. Das (2016) Immunogold techniques in electron microscopy. in *Modern Electron Microscopy in Physical and Life Sciences*, 143–160.

Mussgnug, J. H. (2015) Genetic tools and techniques for *Chlamydomonas reinhardtii*. *Applied Microbiology and Biotechnology*, 99, 5407–5418.

Nair, J. S. and Ramaswamy, N. K. (2004) Chloroplast proteases. *Biologia Plantarum*, 48, 321–326.

Nakamura, Y., Gojobori, T. and Ikemura, T. (2000) Codon usage tabulated from international DNA sequence databases : status for the year 2000. *Nucleic Acids Research*, 28, 292.

Nassal, M., Skamel, C., Vogel, M., Kratz, P. A., Stehle, T., Wallich, R. and Simon, M. M. (2008) Development of hepatitis B virus capsids into a whole-chain protein antigen display platform : New particulate Lyme disease vaccines. *International Journal of Medical Microbiology*, 298, 135–142.

Newman, M., Suk, F.-M., Cajimat, M., Chua, P. K. and Shih, C. (2003) Stability and morphology comparisons of self-assembled virus-like particles from wild-type and mutant human hepatitis B virus capsid proteins. *Journal of Virology*, 77, 12950–12960.

Ng, M. Y. T., Tan, W. S., Abdullah, N., Ling, T. C. and Tey, B. T. (2006) Heat treatment of unclarified *Escherichia coli* homogenate improved the recovery efficiency of recombinant hepatitis B core antigen. *Journal of Virological Methods*, 137, 134–139.

Nishimura, K., Kato, Y. and Sakamoto, W. (2016) Chloroplast proteases : Updates on proteolysis within and across suborganellar compartments. *Plant Physiology*, 171, 2280–2293.

Nishimura, K., Kato, Y. and Sakamoto, W. (2017) Essentials of proteolytic machineries in chloroplasts. *Molecular Plant*, 10, 4–19.

Oey, M., Lohse, M., Kreikemeyer, B. and Bock, R. (2009) Exhaustion of the chloroplast protein synthesis capacity by massive expression of a highly stable protein antibiotic. *Plant Journal*, 57, 436–445.

Ojo, E. O., Auta, H., Baganz, F. and Lye, G. J. (2014) Engineering characterisation of a shaken, single-use photobioreactor for early stage microalgae cultivation using *Chlorella sorokiniana*. *Bioresource Technology*, 173, 367–375.

Ojo, E. O., Auta, H., Baganz, F. and Lye, G. J. (2015) Design and parallelisation of a miniature photobioreactor platform for microalgal culture evaluation and optimisation. *Biochemical Engineering Journal*, 103, 93–102.

Patchett, M. L., Neal, T. L., Schofield, L. R., Strange, R. C., Daniel, R. M. and Morgan, H. W. (1989) Heat treatment purification of thermostable cellulase and hemicellulase enzymes expressed in *E. coli*. *Enzyme and Microbial Technology*, 11, 113–115.

Petrusevski, B., Bolier, G., Van Breemen, A. N. and Alaerts, G. J. (1995) Tangential flow filtration: A method to concentrate freshwater algae. *Water Research*, 29, 1419–1424.

Peyret, H. (2015) A protocol for the gentle purification of virus-like particles produced in plants. *Journal of Virological Methods*, 225, 59–63.

Peyret, H. *et al.* (2015) Tandem fusion of hepatitis B core antigen allows assembly of virus-like particles in bacteria and plants with enhanced capacity to accommodate foreign proteins. *PLoS ONE*, 10, e0120751.

Porro, D., Sauer, M., Branduardi, P. and Mattanovich, D. (2005) Recombinant protein production in yeasts. *Molecular Biotechnology*, 31, 245–260.

Potvin, G. and Zhang, Z. (2010) Strategies for high-level recombinant protein expression in transgenic microalgae: A review. *Biotechnology Advances*, 28, 910–918.

Prasad, B. V. V. and Schimid, M. F. (2012) Principles of virus structural organization. in *Viral Molecular Machines*, 17–47.

Preiss, S., Schrader, S. and Johanningmeier, U. (2001) Rapid, ATP-dependent degradation of a truncated D1 protein in the chloroplast. *European Journal of Biochemistry*, 268, 4562–4569.

Pumpens, P. and Grens, E. (2001) HBV core particles as a carrier for B cell/T cell epitopes. *Intervirology*, 44, 98–114.

Rai, M. and Padh, H. (2001) Expression systems for production of heterologous proteins. *Current Science*, 80, 1121–1128.

Rasala, B. A., Muto, M., Sullivan, J. and Mayfield, S. P. (2011) Improved heterologous protein expression in the chloroplast of *Chlamydomonas reinhardtii* through promoter and 5' untranslated region optimisation. *Plant Biotechnology Journal*, 9, 674–683.

Rasala, B. a *et al.* (2010) Production of therapeutic proteins in algae, analysis of

expression of seven human proteins in the chloroplast of *Chlamydomonas reinhardtii*. *Plant Biotechnology Journal*, 8, 719–733.

Roach, T., Sedoud, A. and Krieger-Liszkay, A. (2013) Acetate in mixotrophic growth medium affects photosystem II in *Chlamydomonas reinhardtii* and protects against photoinhibition. *Biochimica et Biophysica Acta*, 1827, 1183–90.

Roldão, A., Mellado, M. C. M., Castilho, L. R., Carrondo, M. J. T. and Alves, P. M. (2010) Virus-like particles in vaccine development. *Expert Review of Vaccines*, 9, 1149–1176.

Roldão, A., Silva, A. C., Mellado, M. C. M., Alves, P. M. and Carrondo, M. J. T. (2011) Viruses and virus-Like particles in biotechnology: Fundamentals and applications. in *Comprehensive Biotechnology*, 625–649.

Rolland, D. *et al.* (2001) Purification of recombinant HBc antigen expressed in *Escherichia coli* and *Pichia pastoris*: Comparison of size-exclusion chromatography and ultracentrifugation. *Journal of Chromatography B: Biomedical Sciences and Applications*, 753, 51–65.

Roose, K., De Baets, S., Schepens, B. and Saelens, X. (2013) Hepatitis B core-based virus-like particles to present heterologous epitopes. *Expert Review of Vaccines*, 12, 183–198.

Rosales-Mendoza, S., Paz-Maldonado, L. M. T. and Soria-Guerra, R. E. (2012) *Chlamydomonas reinhardtii* as a viable platform for the production of recombinant proteins: current status and perspectives. *Plant Cell Reports*, 31, 479–94.

Rosano, G. L. and Ceccarelli, E. A. (2014) Recombinant protein expression in *Escherichia coli*: advances and challenges. *Frontiers in Microbiology*, 5, 172.

Rosenberg, J. N., Oyler, G. a, Wilkinson, L. and Betenbaugh, M. J. (2008) A green light

for engineered algae: redirecting metabolism to fuel a biotechnology revolution. *Current Opinion in Biotechnology*, 19, 430–6.

Sanchez-Garcia, L., Martín, L., Mangues, R., Ferrer-Miralles, N., Vázquez, E. and Villaverde, A. (2016) Recombinant pharmaceuticals from microbial cells: A 2015 update. *Microbial Cell Factories*, 15, 1–7.

Saper, C. B. (2009) A guide to the perplexed on the specificity of antibodies. *Journal of Histochemistry & Cytochemistry*, 57, 1–5.

Schembri, L., Dalibart, R., Tomasello, F., Legembre, P., Ichas, F. and De Giorgi, F. (2007) The HA tag is cleaved and loses immunoreactivity during apoptosis. *Nature Methods*, 4, 107–108.

Schillberg, S., Fischer, R. and Emans, N. (1999) Molecular farming of recombinant antibodies in plants. *Cellular and Molecular Life Sciences*, 60, 433–445.

Schlesinger, A., Eisenstadt, D., Bar-Gil, A., Carmely, H., Einbinder, S. and Gressel, J. (2012) Inexpensive non-toxic flocculation of microalgae contradicts theories; overcoming a major hurdle to bulk algal production. *Biotechnology Advances*, 30, 1023–1030.

Schmidt, T. G. M. *et al.* (2013) Development of the Twin-Strep-tag® and its application for purification of recombinant proteins from cell culture supernatants. *Protein Expression and Purification*, 92, 54–61.

Schodel, F. *et al.* (1992) The position of heterologous epitopes inserted in hepatitis B virus core particles determines their immunogenicity. *Journal of Virology*, 66, 106–114.

Scholz, M., Hoshino, T., Johnson, D., Riley, M. R. and Cuello, J. (2011) Flocculation of wall-deficient cells of *Chlamydomonas reinhardtii* mutant *cw15* by calcium and methanol. *Biomass and Bioenergy*, 35, 4835–4840.

Schroda, M., Hemme, D. and Mühlhaus, T. (2015) The *Chlamydomonas* heat stress response. *The Plant Journal*, 82, 466–480.

Severes, A., Hegde, S., D'Souza, L. and Hegde, S. (2017) Use of light emitting diodes (LEDs) for enhanced lipid production in micro-algae based biofuels. *Journal of Photochemistry and Photobiology B: Biology*, 170, 235–240.

Shen, Y., Yuan, W., Pei, Z. and Mao, E. (2010) Heterotrophic culture of *Chlorella protothecoides* in various nitrogen sources for lipid production. *Applied Biochemistry and Biotechnology*, 160, 1674–84.

Shepard, C. W., Simard, E. P., Finelli, L., Fiore, A. E. and Bell, B. P. (2006) Hepatitis B virus infection: Epidemiology and vaccination. *Epidemiologic Reviews*, 28, 112–125.

Sivashanmugam, A., Murray, V., Cui, C., Zhang, Y., Wang, J. and Li, Q. (2009) Practical protocols for production of very high yields of recombinant proteins using *Escherichia coli*. *Protein Science*, 18, 936–948.

Soletto, D., Binaghi, L., Ferrari, L., Lodi, a., Carvalho, J. C. M., Zilli, M. and Converti, a. (2008) Effects of carbon dioxide feeding rate and light intensity on the fed-batch pulse-feeding cultivation of *Spirulina platensis* in helical photobioreactor. *Biochemical Engineering Journal*, 39, 369–375.

Sominskaya, I. *et al.* (2013) A VLP library of C-terminally truncated hepatitis B core proteins: Correlation of RNA encapsidation with a Th1/Th2 switch in the immune responses of mice. *PLoS ONE*, 8, 1–13.

Soria-Guerra, R. E. *et al.* (2013) Expression of an HBcAg-based antigen carrying angiotensin II in *Chlamydomonas reinhardtii* as a candidate hypertension vaccine. *Plant Cell, Tissue and Organ Culture*, 116, 133–139.

Specht, E. A. and Mayfield, S. P. (2014) Algae-based oral recombinant vaccines.

Frontiers in Microbiology, 5, 60.

Specht, E., Miyake-Stoner, S. and Mayfield, S. (2010) Micro-algae come of age as a platform for recombinant protein production. *Biotechnology Letters*, 32, 1373–83.

Stahl, S. J. and Murray, K. (1989) Immunogenicity of peptide fusions to hepatitis B virus core antigen. *Proceedings of the National Academy of Sciences of the United States*, 86, 6283–6287.

Stoffels, L. (2015) *Microalgae as a novel production platform for antibacterial proteins. Ph.D thesis*. *University College London*.

Stoffels, L., Taunt, H. N., Charalambous, B. and Purton, S. (2017) Synthesis of bacteriophage lytic proteins against *Streptococcus pneumoniae* in the chloroplast of *Chlamydomonas reinhardtii*. *Plant Biotechnology Journal*, 15, 1130–1140.

Su, Z.-L., Qian, K.-X., Tan, C.-P., Meng, C.-X. and Qin, S. (2005) Recombination and heterologous expression of allophycocyanin gene in the chloroplast of *Chlamydomonas reinhardtii*. *Acta Biochimica et Biophysica Sinica*, 37, 709–712.

Sun, M., Qian, K., Su, N., Chang, H., Liu, J., Shen, G. and Chen, G. (2003) Foot-and-mouth disease virus VP1 protein fused with cholera toxin B subunit expressed in *Chlamydomonas reinhardtii* chloroplast. *Biotechnology Letters*, 25, 1087–1092.

Surzycki, R. *et al.* (2009) Factors effecting expression of vaccines in microalgae. *Biologicals*, 37, 133–138.

Tagliamonte, M., Tornesello, M. L., Buonaguro, F. M. and Buonaguro, L. (2017) Virus-like particles. in *Micro- and Nanotechnology in Vaccine Development*, 205–219.

Tan, W. S., McNae, I., Ho, K. L. and Walkinshaw, M. (2007) Crystallization and X-ray analysis of the T = 4 particle of hepatitis B capsid protein with an N-terminal extension. *Acta Crystallographica Section F Structural Biology and*

Crystallization Communications, 63, 642–647.

Tan, W. S., Dyson, M. R. and Murray, K. (2003) Hepatitis B virus core antigen: Enhancement of its production in *Escherichia coli*, and interaction of the core particles with the viral surface antigen. *Biological Chemistry*, 384, 363–371.

Terpe, K. (2003) Overview of tag protein fusions : from molecular and biochemical fundamentals to commercial systems. *Literature Review in Applied Microbiology and Biotechnology*, 60, 523–533.

Tey, B. T., Chua, M. I., Chua, G. S., Tan Ng, M. Y., Awang Biak, D. R., Tan, W. S. and Ling, T. C. (2006) Production of hepatitis B core antigen in a stirred tank bioreactor: The influence of temperature and agitation. *Biotechnology and Bioprocess Engineering*, 11, 164–167.

Thompson, C. M., Petiot, E., Lennaertz, A., Henry, O. and Kamen, A. A. (2013) Analytical technologies for influenza virus-like particle candidate vaccines: challenges and emerging approaches. *Virology Journal*, 10, 1–14.

Thomson, T. M. *et al.* (2011) Scaffold number in yeast signaling system sets tradeoff between system output and dynamic range. *Proceedings of the National Academy of Sciences of the United States of America*, 108, 20265–20270.

Touze, A., Enogat, N., Buisson, Y. and Coursaget, P. (1999) Baculovirus expression of chimeric hepatitis B virus core particles with hepatitis E virus epitopes and their use in a hepatitis E immunoassay. *Journal of Clinical Microbiology*, 37, 438–441.

Tran, M., Zhou, B., Pettersson, P. L., Gonzalez, M. J. and Mayfield, S. P. (2009) Synthesis and assembly of a full-length human monoclonal antibody in algal chloroplasts. *Biotechnology and Bioengineering*, 104, 663–673.

Tran, M., Van, C., Barrera, D. J., Pettersson, P. L., Peinado, C. D., Bui, J. and Mayfield, S. P. (2013) Production of unique immunotoxin cancer therapeutics in algal

chloroplasts. *Proceedings of the National Academy of Sciences of the United States of America*, 110, 15–22.

Uduman, N., Qi, Y., Danquah, M. K., Forde, G. M. and Hoadley, A. (2010) Dewatering of microalgal cultures: A major bottleneck to algae-based fuels. *Journal of Renewable and Sustainable Energy*, 2, 1–15.

Vandamme, D., Foubert, I., Fraeye, I., Meesschaert, B. and Muylaert, K. (2012) Flocculation of *Chlorella vulgaris* induced by high pH: role of magnesium and calcium and practical implications. *Bioresource Technology*, 105, 114–9.

Vandamme, D., Foubert, I. and Muylaert, K. (2013) Flocculation as a low-cost method for harvesting microalgae for bulk biomass production. *Trends in Biotechnology*, 31, 233–239.

Várnai, A., Tang, C., Bengtsson, O., Atterton, A., Mathiesen, G. and Eijsink, V. G. H. (2014) Expression of endoglucanases in *Pichia pastoris* under control of the GAP promoter. *Microbial Cell Factories*, 13, 1–10.

Vicente, T. *et al.* (2007) Anion-exchange membrane chromatography for purification of rotavirus-like particles. *Journal of Membrane Science*, 434, S103–S110.

Vicente, T., Roldão, A., Peixoto, C., Carrondo, M. J. T. and Alves, P. M. (2011) Large-scale production and purification of VLP-based vaccines. *Journal of Invertebrate Pathology*, 107, S42–S48.

Vogel, M., Diez, M., Eisfeld, J. and Nassal, M. (2005) In vitro assembly of mosaic hepatitis B virus capsid-like particles (CLPs): Rescue into CLPs of assembly-deficient core protein fusions and FRET-suited CLPs. *FEBS Letters*, 579, 5211–5216.

Walker, T. L., Purton, S., Becker, D. K. and Collet, C. (2005) Microalgae as bioreactors. *Plant Cell Reports*, 24, 629–641.

Wang, B., Li, Y., Wu, N. and Lan, C. Q. (2008) CO_2 bio-mitigation using microalgae. *Applied Microbiology and Biotechnology*, 79, 707–18.

Wang, Y. V, Wade, M., Wong, E., Li, Y.-C., Rodewald, L. W. and Wahl, G. M. (2007) Quantitative analyses reveal the importance of regulated Hdmx degradation for p53 activation. *Proceedings of the National Academy of Sciences of the United States of America*, 104, 12365–12370.

Wannathong, T., Waterhouse, J. C., Young, R. E. B., Economou, C. K. and Purton, S. (2016) New tools for chloroplast genetic engineering allow the synthesis of human growth hormone in the green alga *Chlamydomonas reinhardtii*. *Applied Microbiology and Biotechnology*, 100, 1–11.

Widdel, F. (2007) *Theory and measurement of bacterial growth*. *Di dalam Grundpraktikum Mikrobiologie*.

Wingfield, P. T., Stahl, S. J., Williams, R. W. and Steven, A. C. (1995) Hepatitis core antigen produced in *Escherichia coli*: subunit composition, conformational analysis, and in vitro capsid assembly. *Biochemistry*, 34, 4919–4932.

Wood, D. W. (2014) New trends and affinity tag designs for recombinant protein purification. *Current Opinion in Structural Biology*, 26, 54–61.

Wooi, K. and Siang, W. (2008) Recombinant hepatitis B virus core particles : Association , dissociation and encapsidation of green fluorescent protein. *Journal of Virological Methods*, 151, 172–180.

World Health Organization (2017) *Hepatitis B*. Available at: http://www.who.int/news-room/fact-sheets/detail/hepatitis-b (Accessed: 16 July 2018).

Wynne, S. A., Crowther, R. A. and Leslie, A. G. (1999) The crystal structure of the human hepatitis B virus capsid. *Molecular cell*, 3, 771–780.

Yan, N., Fan, C., Chen, Y. and Hu, Z. (2016) The potential for microalgae as bioreactors to produce pharmaceuticals. *International Journal of Molecular Sciences*, 17, 1–24.

Yang, Z. *et al.* (2006) Expression of human soluble TRAIL in *Chlamydomonas reinhardtii* chloroplast. *Chinese Science Bulletin*, 51, 1703–1709.

Yap, B. H. J., Dumsday, G. J., Scales, P. J. and Martin, G. J. O. (2015) Energy evaluation of algal cell disruption by high pressure homogenisation. *Bioresource Technology*, 184, 280–285.

Young, R. E. B. and Purton, S. (2014) Cytosine deaminase as a negative selectable marker for the microalgal chloroplast: a strategy for the isolation of nuclear mutations that affect chloroplast gene expression. *The Plant Journal*, 80, 915–925.

Zborowski, M. and Chalmers, J. J. (1988) Chapter 3: Centrifugation. in *Laboratory Techniques in Biochemistry and Molecular Biology*, 18–69.

Zedler, J. A. Z., Gangl, D., Hamberger, B., Purton, S. and Robinson, C. (2014) Stable expression of a bifunctional diterpene synthase in the chloroplast of *Chlamydomonas reinhardtii*. *Journal of Applied Phycology*, 27, 2271–2277.

Zedler, J. A. Z., Gangl, D., Guerra, T., Santos, E., Verdelho, V. V. and Robinson, C. (2016) Pilot-scale cultivation of wall-deficient transgenic *Chlamydomonas reinhardtii* strains expressing recombinant proteins in the chloroplast. *Applied Microbiology and Biotechnology*, 100, 7061–7070.

Zeltins, A. (2013) Construction and characterization of virus-like particles: A review. *Molecular Biotechnology*, 53, 92–107.

Zhao, Q. *et al.* (2014) Characterization of virus-like particles in GARDASIL® by cryo transmission electron microscopy. *Human Vaccines and Immunotherapeutics*, 10,

734–739.

Zheng, Y., Li, T., Yu, X., Bates, P. D., Dong, T. and Chen, S. (2013) High-density fed-batch culture of a thermotolerant microalga *Chlorella sorokiniana* for biofuel production. *Applied Energy*, 108, 281–287.

Zhu, L. D., Li, Z. H. and Hiltunen, E. (2016) Strategies for lipid production improvement in microalgae as a biodiesel feedstock. *BioMed Research International*, 2016, 1–8.

Zou, Z., Eibl, C. and Koop, H.-U. (2003) The stem-loop region of the tobacco psbA 5'UTR is an important determinant of mRNA stability and translation efficiency. *Molecular Genetics and Genomics*, 269, 340–349.

Appendix 1 (A1): Composition of buffers and stock solutions

Table A1. 1: Composition of 5X Beijerincks stock solution.

For preparation of 1L 5 x Beijerincks stock solution	Mass (g)	Molar concentration (mM)
NH_4Cl	40.0	7.5
$CaCl_2 \cdot 2H_2O$	5.0	0.3
$MgSO_4 \cdot 7H_2O$	10.0	0.4

Table A1. 2: Composition of phosphate stock solution.

For preparation of 1L stock phosphate solution stock	Mass (g)	Molar concentration (mM)
K_2HPO_4 (anhydrous)	14.3	0.7
KH_2PO_4 (anhydrous)	7.3	0.5

Table A1. 3: Composition of tris-acetate stock solution.

For preparation of 1L Tris-acetate stock solution	Amount	Molar concentration (mM)
Tris base	242.0 g	20.0 mM
Glacial acetic acid	100.0 mL	17.0 mM

Table A1. 4: Composition of trace element stock solution.

For preparation of 1L trace elements solution	Mass (g)
EDTA-Na_2	50.0
H_3BO_3	11.1
$ZnSO_4 \cdot 7H_2O$	22.0
$MnCl_2 \cdot 4H_2O$	5.1
$FeSO_4 \cdot 7H_2O$	5.0
$CoCl_2 \cdot 6H_2O$	1.6
$CuSO_4 \cdot 5H_2O$	1.6

Appendix 2 (A2): Primer sequences for PCR

Check for GOI insert by sequencing:

RY-psaSEQ = AACTATTTGTCTAATTTAATAACC (Tm: 53 °C)

rbcL.R = CAAACTTCACATGCAGCAGC (Tm: 67 °C)

Check for chloroplast homoplasmy:

FLANK1 = GTCATTGCGAAAATACTGGTGC (Tm: 67 °C)

rbcL.Fn = CGGATGTAACTCAATCGGTAG (Tm: 63 °C)

RY-psaR = ataggctcttctCATGGATTTCTCCTTATAATAAC (*binding region in capital*) (Tm: 57 °C)

Appendix 3 (A3): DCW vs. OD calibration curves

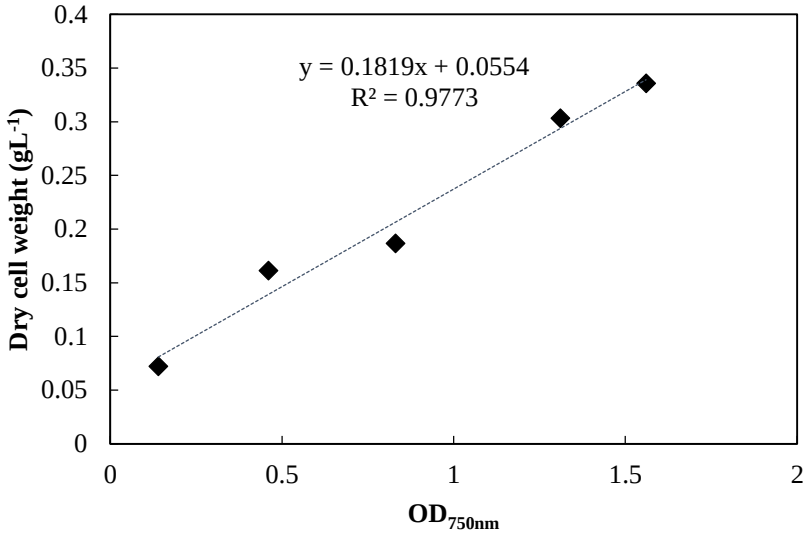

Figure A3. 1: The correlation between DCW (gL^{-1}) and OD_{750nm} for the *psaA* transgenic strain under standard mixotrophic conditions. Experiments performed as described in Section 2.3.3. Error bars represent the range of duplicate points (n=2). Dashed line fitted by linear regression.

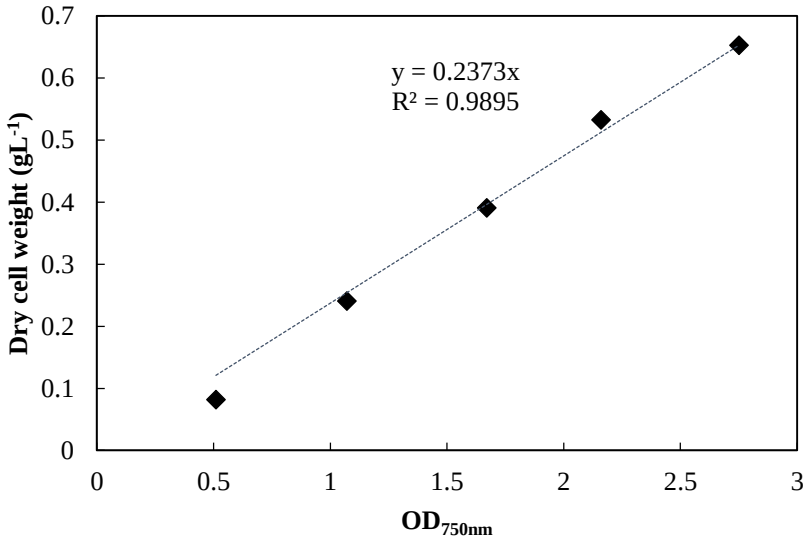

Figure A3. 2: The correlation between DCW (gL^{-1}) and OD_{750nm} for the 16S fusion transgenic strain under standard mixotrophic conditions. Experiments performed as described in Section 2.3.3. Error bars represent the range of duplicate points (n=2). Dashed line fitted by linear regression.

Appendix 4 (A4): Transgene sequences

Gene sequence of *HBc183*:

ATGGATATTGATCCATACAAAGAATTCGGTGCTTCTGTTGAATTATTATCT
TTCTTACCATCTGATTTCTTCCCATCTGTTCGTGACTTATTAGATACTGCTT
CAGCTTTATACCGTGAAGCTTTAGAATCTCCAGAACACTGTTCACCACACC
ACACTGCTTTACGTCAAGCTATTTTATGTTGGGTTGAATTAATGAACTTAG
CTACTTGGGTAGGTTCTAACTTAGAAGATCCAGCTTCACGTGAATTAGTTG
TTTCTTACGTAAACGTAAACATGGGTTTAAAAATTCGTCAATTATTATGGT
TCCACATTAGCTGTTTAACATTCGGTCGTGAAACAGTATTAGAATACTTAG
TTTCTTTCGGTGTTTGGATTCGTACTCCACCAGCTTACCGTCCACAAAACG
CTCCAATTTTATCAACTTTACCAGAAACAACTGTTGTACGTCGTCGTTGTC
GTTCACCACGTCGTCGTACTCCATCTCCACGTCGTCGTCGTTCACAATCTC
CACGTCGTCGTCGTTCACAATCTCGTGAATCACAATGT

Gene sequence of *HBc150_Strep*:

ATGGTGGATATTGATCCGTATAAAGAATTTGGCGCGACCGTGGAACTGCTG
AGCTTTCTGCCGAGCGATTTTTTTCCGAGCGTGCGCGATCTGCTGGATACCG
CGAGCGCGCTGTATCGCGAAGCGCTGGAAAGCCCGGAACATTGCAGCCCG
CATCATACCGCGCTGCGCCAGGCGATTCTGTGCTGGGGCGAACTGATGACC
CTGGCGACCTGGGTGGGCAACAACCTGGAAGATGGCGGCTTTAAAGGCAG
CGCGTGGAGCCATCCGCAGTTTGAAAAAGGCGGCGGCAGCGGCGGCGGC
AGCGGCGGCAGCGCGTGGAGCCATCCGCAGTTTGAAAAAGGCGGCAGCG
GCGAATTTGGCGGCCCGGCGAGCCGCGATCTGGTGGTGAACTATGTGAAC
ACCAACGTGGGCCTGAAAATTCGCCAGCTGCTGTGGTTTCATATTAGCTGC
CTGACCTTTGGCCGCGAAACCGTGCTGGAATATCTGGTGAGCTTTGGCGTG
TGGATTCGCACCCCGCCGGCGTATCGCCCGCCGAACGCGCCGATTCTGAGC
ACCCTGCCGGAAACCACCGTGGTGTGC

Gene sequence of *HBc150_HA*:

ATGGTGTATCCGTATGATGTGCCGGATTATGCGGGCGGCGGCGGCGGCGATA
TTGATCCGTATAAAGAATTTGGCGCGACCGTGGAACTGCTGAGCTTTCTGC
CGAGCGATTTTTTTCCGAGCGTGCGCGATCTGCTGGATACCGCGAGCGCGC
TGTATCGCGAAGCGCTGGAAAGCCCGGAACATTGCAGCCCGCATCATACCG
CGCTGCGCCAGGCGATTCTGTGCTGGGGCGAACTGATGACCCTGGCGACC
TGGGTGGGCAACAACCTGGAAGATCCGGCGAGCCGCGATCTGGTGGTGAA
CTATGTGAACACCAACGTGGGCCTGAAAATTCGCCAGCTGCTGTGGTTTCA
TATTAGCTGCCTGACCTTTGGCCGCGAAACCGTGCTGGAATATCTGGTGAG
CTTTGGCGTGTGGATTCGCACCCCGCCGGCGTATCGCCCGCCGAACGCGCC
GATTCTGAGCACCCTGCCGGAAACCACCGTGGTGTGC

Gene sequence of Δ*HBc150_HA*:

ATGGTGTACCCTTATGATGTTCCTGATTATGCTGGCGGTGGTGGTGGTGATAT
TGACCCGTACAAAGAATTTGGCGCGACCGTTGAGCTGCTGTCGTTCCTGCC
GAGCGACTTCTTTCCGTCTGTGCGCGACTTGCTGGACACCGCAAGCGCGCT
GTATCGCGAAGCGCTGGAGAGCCCAGAGCATTGTAGCCCGCACCATACGGC
CCTGCGTCAAGCGATCCTGTGCTGGGGCGAGCTGATGACCCTGGCGACTTG
GGTGGGCAATAACCTGGAAGATCCGGCCTCCCGTGACTTGGTTGTTAACTA
CGTCAATACGAATGTCGGTCTGAAGATTCGCCAGCTGCTGTGGTTCCACAT
CAGCTGCCTGACCTTCGGTCGTGAAACGGTGTTGGAGTACCTGGTGAGCTT
TGGTGTTTGGATTCGTACCCCACCGGCATATCGTCCGCCGAACGCTCCGATC
CTGAGCACCCTGCCGGAAACCACGGTCGTCTGT

Appendix 5 (A5): 16S rRNA promoter sequence and primers used during Gibson assembly

Sequence of 16S rRNA promoter:

GGCAGGCAACAAATTTATTTATTGTCCCGTAAGGGGAAGGGGAAAACAATT
ATTATTTTACTGCGGAGCAGCTTGTTATTGAAATTTTATTAAAAAAAAAATA
AAAATTTGACAAAAAAAAATAAAAAAGTTAAATTAAAAACACTGGGAATG
TTCTACATCATAAAAATCAAAAGGGTTTAAAATCCCGACAAAATTTAAACTT
TAAAGAGT

Primers used during Gibson assembly (Figure 4.11):

d: GGCAGGCAACAAATTTATTT (Tm: 63 °C)

c': ACTCTTTAAAGTTTAAATTTTGTCGG (Tm: 62 °C)

a: AAAGTGAGCTATTAACGCGT (Tm: 63 °C)

b': AATAGTTTTTTTTACATCAT (Tm: 49 °C)

b+c: AAATTTAAACTTTAAAGAGTATGATGTAAAAAAAACTATTTGTCTAATT (Tm: 69 °C)

d'+a': AAATAAATTTGTTGCCTGCCACGCGTTAATAGCTCACTTT (Tm: 79 °C)

e': ACTTTCACCAGCGTTTCTG (Tm: 63 °C)

e: GCCTTCCTGTTTTTGCTCA (Tm: 65 °C)

Appendix 6 (A6): Calculations of the specific product yield and % TSB

Given that the correlation between NIR (y) and protein accumulation (x) was y = 10.93x-2466, when the NIR was 2650 at one-fold dilution, the amount of HBc150_HA accumulated was $468 \times 10^{-6}\ mg$.

10 ml cell culture was harvested. Since the OD_{750nm} at harvest was 1, the volume of resuspension buffer added during SDS-PAGE was 500 µL. Each well was loaded with 20 µL of protein sample. In addition, since the correlation between DCW (y) and OD_{750nm} (x) was y=0.2373x, DCW was 0.2373 g/L when the OD_{750nm} was 1. Therefore, the amount of cells within 10 ml cell culture was 2.373×10^{-3} g.

$$specific\ product\ yield = \frac{amount\ of\ HBc150\_HA\ in\ the\ SDS-PAGE\ well}{amount\ of\ cells\ loaded\ in\ the\ SDS-PAGE\ well}$$

$$= \frac{468 \times 10^{-6}\ mg}{2.373 \times 10^{-3} g \times \frac{20\mu L}{500\mu L}} \approx 4.9 \frac{mg}{g} DCW$$

It was estimated that the TSP of the crude algal extract was 1mg mL^{-1}.

$$\%\ TSP = \frac{HBc15\_HA\ \ concentration}{TSP\ of\ crude\ algal\ extract} = \frac{\frac{468 \times 10^{-6}\ mg}{20 \times 10^{-3}\ mL}}{1\ mg/mL} \approx 2.34\ \%\ TSP$$